Designed and Evolved Nucleic Acid Nanotechnology

A Dissertation

Presented in Partial Fulfillment of the Requirements for the

Degree of Doctorate of Philosophy

with a

Major in Chemistry

in the

College of Graduate Studies

University of Idaho

Tulsi Ram Damase

Major Professor: Peter B. Allen, Ph.D.

Committee Members: I. Francis Cheng, Ph.D.; Patrick J. Hrdlicka, Ph.D.;

Christine E. Parent, Ph.D.

Department Administrator: Ray von Wandruszka, Ph.D.

December 2018

Authorization to Submit Dissertation

This dissertation of Tulsi Ram Damase, submitted for the degree of Doctor of Philosophy with a Major in Chemistry and titled "Designed and Evolved Nucleic Acid Nanotechnology," has been reviewed in final form. Permission, as indicated by the signatures and dates below, is now granted to submit final copies to the College of Graduate Studies for approval.

Major Professor: _____ Date:_____
Peter B. Allen, Ph.D.

Committee members: _____ Date:_____
I. Francis Cheng, Ph.D.

_____ Date:_____
Patrick J. Hrdlicka, Ph.D.

_____ Date:_____
Christine E. Parent, Ph.D.

Department

Administrator: _____ Date:_____
Ray von Wandruszka, Ph.D.

Abstract

The overall goal of this thesis is to present designed DNA circuits for amplification and localized detection plus progress toward expanding DNA circuits with aptamers' unique recognition ability. DNA is an attractive molecule in nanotechnology to construct nanodevices, nanostructures and dynamic circuits. DNA circuits are designed dynamic DNA-based molecular machines with diverse biotechnological applications, such as detection of DNA analytes and signal amplification. We used DNA circuits to make release and detector particles. We developed a label-free strategy to report DNA circuits using G-rich sequence and thioflavin-T (TFT) dye. DNA aptamers can evolve using systematic evolution of ligands by exponential enrichment (SELEX) process. DNA aptamers are molecular recognition elements made of single-stranded DNA (ssDNA) with the potential to interact with proteins, small molecules, viruses and even cells. We selected DNA aptamers against epidermal growth factor receptors (EGFR) and *Drosophila* C virus (DCV). This thesis includes five original research articles and one review.

Acknowledgements

When I started to write my thesis, I had no idea how anything I did would fit in the Designed and Evolved Nucleic Acid Nanotechnology. For me, as a Ph.D. student, a good day is to get reproducible data that agree with my model or hypothesis. I figured out a trick to be a successful graduate student; work, think and again work till you get data. It wasn't easy to work and write the thesis without invaluable advice, inspiration and support of my PI. So, I first give thanks to my PI, Dr. Peter B Allen with great appreciation and humbleness. I sincerely appreciate him for pushing me to dream big and pursue my goals.

I thank my committee members: Dr. I. Francis Cheng, Dr. Patrick J. Hrdlicka, and, Dr. Christine E. Parent, for their great academic support, time and invaluable knowledge.

I am very grateful for the faculty and staff and all other graduate students in the Chemistry Department, University of Idaho who have created such a friendly research environment.

Dedication

This dissertation is dedicated to my parents (Tikaram Damase and Kamala Damase), wife (Srijana Pandey Damase) and brother (Basanta Damase). And it is also dedicated to all my great friends. Without your support, I will not be able to make this far.

Table of Contents

List of Figures

List of Tables

List of Abbreviations

Acryd	Acrydite
APS	Ammonium persulphate
CE	Capillary electrophoresis
CHA	Catalytic hairpin assembly
Chol	Cholesterol
denat.	Denature
DCV	*Drosophila* C virus
DNA	Deoxyribonucleic acid
ds	Double-stranded
DXV	*Drosophila* X virus
EDA	Entropy driven amplifier
EDC	1-Ethyl-3-(3-dimethylaminopropyl)carbodiimide
EGFR	Epidermal growth factor receptor
H	Holo-Aptamer
HTS	High throughput sequencing
IBEST	Institute for Bioinformatics and Evolutionary Studies
IgG1-FC	Immunoglobulin gamma-1 heavy chain constant region
K_d	Dissociation constant
LOD	Limit of detection
nt	Nucleotide

NUPACK	Nucleic Acid Package
OSD	One-step strand displacement
PAGE	Polyacrylamide gel electrophoresis
PCR	Polymerase Chain Reaction
Q	Quencher
SELEX	Systematic evolution of ligands by exponential enrichment
ss	Single-stranded
SSG	Single-strand generation
SNP	Single nucleotide polymorphism
TBE	Tris/Borate/EDTA
TEMED	Tetramethylethylenediamine
TFA	Thermofluorimetric Analysis
TFT	Thioflavin-T
TR	Texas red
TRA	Texas red A
TRB	Texas red B
TRC	Texas red C
UV-Vis	Ultra Violet Visible

CHAPTER 1: DESIGNED AND EVOLVED NUCLEIC ACID NANOTECHNOLOGY: CONTRAST AND COMPLEMENTARITY

In this Chapter, we explore progress on DNA aptamers (evolved DNA), DNA circuits (designed DNA), and the newest projects that integrate both. Designed DNA nanotechnology includes static nanostructures, dynamic nanodevices, and reaction networks (sometimes called DNA circuits). DNA circuits are dynamic DNA reactions that perform computations and sequence-specific amplification of signal. Directed evolution can be used to produce DNA that can recognize specific targets. Aptamers are evolved nucleic acids; they are produced artificially with an *in vitro* selection process. DNA aptamers are molecular recognition elements made of single-stranded DNA (ssDNA) with the potential to interact with proteins, small molecules, viruses, and even cells. Designed molecular structures can incorporate aptamers for applications with immediate practical impact.

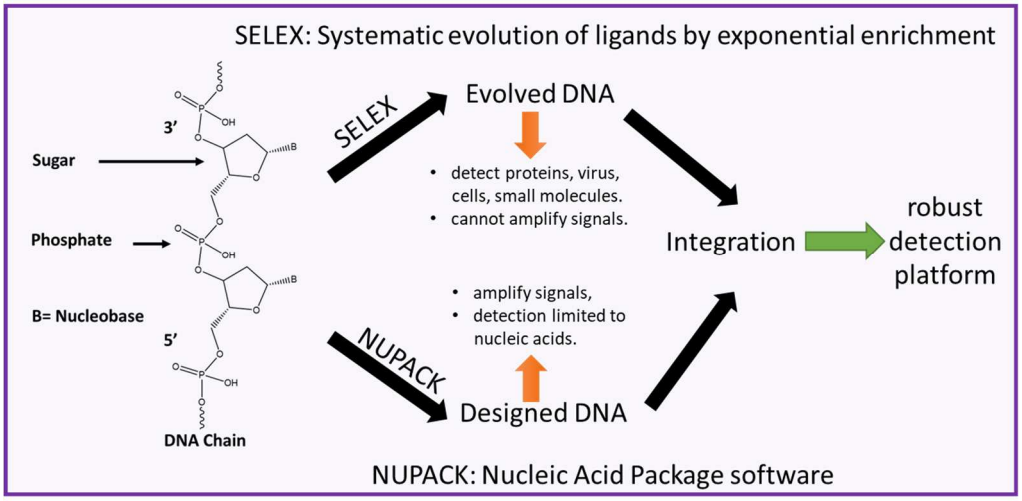

Keywords: DNA, DNA circuits, Aptamer, Aptamer-based DNA circuits.

1-1. Introduction

DNA aptamers (evolved DNA), DNA circuits (designed DNA), and the newest projects that integrate both all rely on the specific properties of DNA. The structure of DNA is predictable: Watson-Crick base pairing is strong, specific, and well characterized thermodynamically. Synthetic DNA binds with high affinity to its reverse complement DNA (synthetic or natural). This forms the famous double-stranded, double-helical structure. Single-stranded nucleic acid (DNA and RNA) molecules fold on themselves according to the same base pair rules. This can form wildly diverse structures[1,2]. Natural and artificial selection can drive the evolution of nucleic acid molecules to useful structures. However,

humans can also design machines that use these rules to perform tasks. The integration of evolved and designed DNA will allow for more practical application of both.

We review examples of evolved nucleic acid structures including natural, folded RNA (e.g., ribosomal RNA) and aptamers. Aptamers are evolved, single-stranded oligonucleotides that bind to a target with high specificity and affinity[3,4]. We contrast these with designed DNA such as DNA circuits. DNA circuits are used in recognition and signal amplification for DNA and RNA analytes. Non-biological applications of designed DNA also include structural DNA based nano-devices. Finally, we show examples of the work integrating evolved and designed elements. The first step to integrate these approaches is to extend designed DNA circuits to recognize various biomarkers using evolved DNA aptamers.

1-2. Nucleic acid structure

1-2.1. Deoxyribonucleic acid (DNA)

DNA (deoxyribonucleic acid) is a biomolecule that carries genetic information for all living organisms. The genetic information flows from DNA to RNA to protein. This is the concept of 'central dogma of molecular biology'. DNA is a polynucleotide chain composed of phosphodiester groups, five-membered carbon sugar and nitrogen-containing aromatic bases. The sugar in DNA is deoxyribose. The bases are adenine(A), cytosine(C), guanine(G) and thymine(T). Adenine and guanine are examples of bicyclic nucleobases called purines. Cytosine and thymine are examples of monocyclic nucleobase called pyrimidines. The nucleobases interact with each other, following Watson-Crick base-pairing rules. 'A' pairs with 'T' and 'G' pairs with 'C'. DNA polynucleotide chain has alternating sugar phosphate backbone[5].

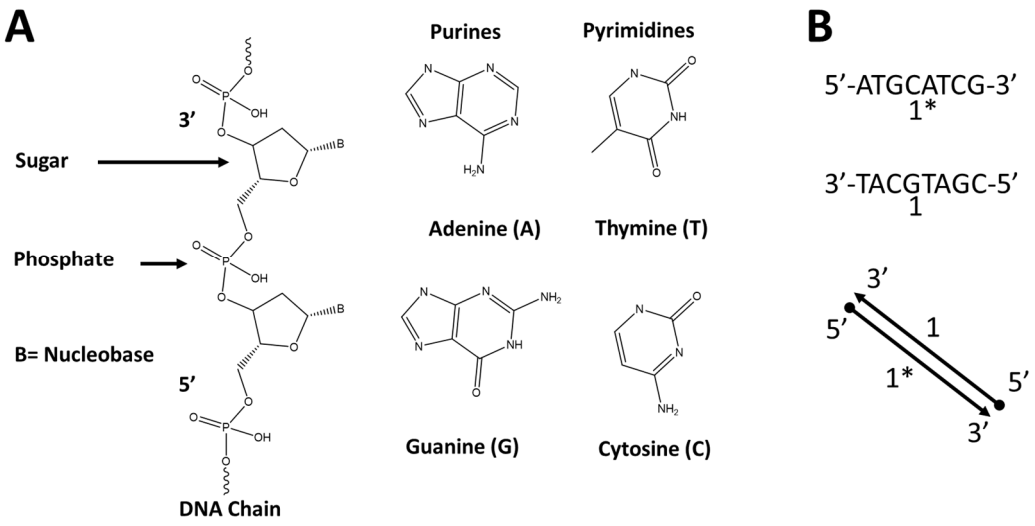

Figure 1- 1: DNA structure and representation. (A) Single-stranded DNA chain and four nucleobases of DNA. B indicates base[5]. (B) Letter codes and circle-arrow representation of DNA (5'-circle and 3'-arrow). Diagram also shows domain convention where domain 1 is an 8-nucleotide sequence and domain 1* is the reverse complementary sequence.

1-2.2. DNA hybridization

DNA is an asymmetric chiral and directional molecule. By convention, DNA sequences are written by convention from 5' to 3' (see Figure 1- 1B) though sometimes 3' to 5' to make it easier to see complementarity. In this thesis, we represent the 3' end of a DNA with an arrow (see Figure 1- 1B). Two strands that are complementary to each other in an antiparallel fashion can hybridize with each other. For instance, 5'-GGCATTCCG-3' hybridizes to 5'-CGGAATGCC-3' (see Figure 1- 2A) but not to 5'-CCGTAAGGC-3' (see Figure 1- 2B) [6]. Base stacking also contributes to the thermodynamic stability of DNA duplexes. Two complementary strands of ssDNA hybridize to form base pairs and base stacks. If the complementary length is ~18 nucleotides or higher, the interaction is thermodynamically favored at room temperature. If the interaction is complementary over ~56 base pairs, then the interaction is comparable in strength to a covalent bond[7]. In solution, associated DNA molecules "breathe" such that any given base pair may be temporarily unbound (see Figure 1- 2C). Base breathing or "fraying" is more prominent at the termini of helices and plays an essential role in DNA circuit reactions (strand displacement and branch migration)[6].

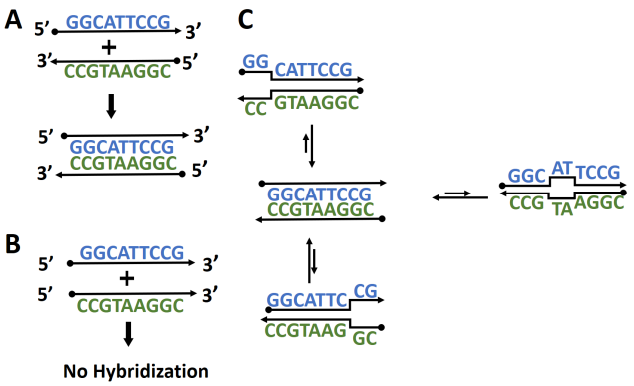

Figure 1- 2: Schematic showing hybridization and base breathing (A) DNA hybridization between two complementary strands. (B) No DNA hybridization between non-complementary strands. (C) DNA base breathing or fraying.

1-2.3. Folded nucleic acid structures

The double helix is very famous, but nucleic acids can form many other structures. RNA is well known to fold into a wide range of 3D shapes to perform its biological roles. All eukaryotic and prokaryotic ribosomes contain ribosomal ribonucleic acid (rRNA) with structural and catalytic functions. The so called secondary structure of 5S rRNA consists of RNA helices, loops, and a three-way junction[8]. Figure 1- 3A shows the tertiary structure from cryo-electron microscopy[9]. Figure 1- 3B shows a computer model predicted secondary structure based on the thermodynamics of base pairing. Many other folded RNA structures exist in nature. The Shine-Dalgarno (SD) sequence[10] is a purine-rich sequence found in many mRNAs of bacteria. The 3D structure of this RNA helps ribosomes bind to the mRNA.

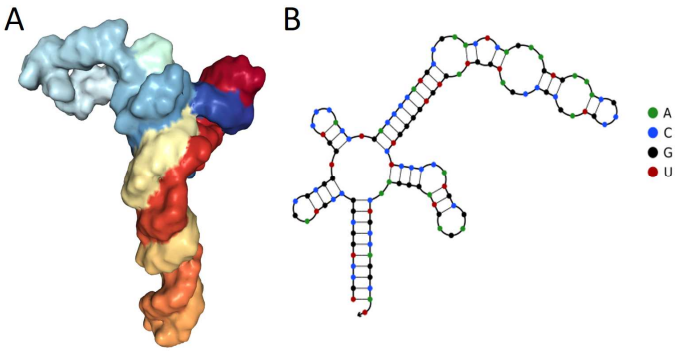

Figure 1- 3: Structure of 5S rRNA (A) 3D view of 1C2X 5S rRNA structure fitted to a cryo-electron microscopic map at 7.5 angstroms resolution[9] visualized using NGL Viewer[11]. (B) Secondary structure of 5S rRNA predicted and visualized with NUPACK(Nucleic Acid Package)[12].

DNA is chemically synthesized as single0stranded oligonucleotides that can also fold into complex structures. Single-stranded DNA assembles with its complementary sequence to form double helices.

This predictability allows DNA to be "programmed" to form complex multidimensional nanostructures. Nadrian Seeman (1982)[13] demonstrated the earliest designed DNA structures. Paul Rothemund (2006)[14] developed the modern approach to scaffolded DNA origami at the 100 nm scale. He introduced the principle of constructing discrete DNA nanostructures from a long ssDNA scaffold guided by short DNA strands called staples. DNA origami is one promising assembly techniques in the DNA nanotechnology field, but other strategies have been demonstrated. Shih et al. (2004)[15] reported the creation of DNA-based octahedra using a long (1669nt) ssDNA and five short oligonucleotides (40nt). Hao Yan (2005)[16] presented the construction of finite size DNA nanoarrays. Zheng et al.[17] designed tensegrity triangles to assemble without a long ssDNA scaffold. The crystal structure from Ducani et al.[18] and domain level schematic of a tensegrity triangle are shown in Figure 1- 4. Peng Yin (2017)[19] introduced unimolecular ssDNA origami. ssDNA can fold like proteins into programmed nanostructures and may have more practical uses than multicomponent DNA folding[1,2,19,20].

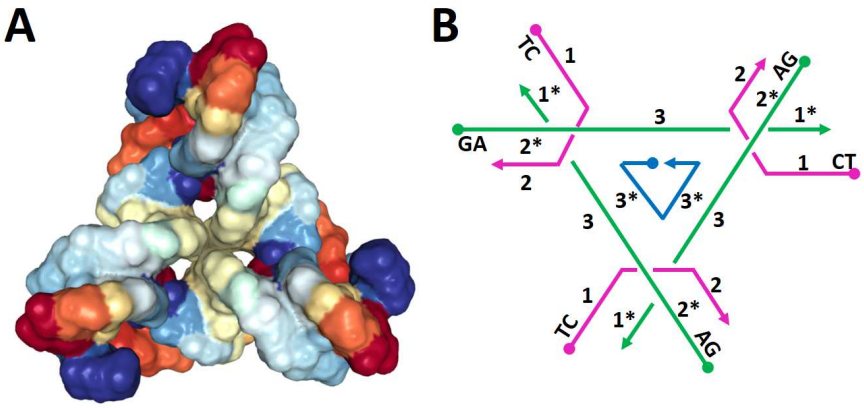

Figure 1- 4: Early example of DNA origami. (A) Self-assembled 3D DNA crystal (4B8D Tensegrity triangle[18] visualized with NGL Viewer[11]) . (B) Schematic representation of tensegrity triangle adapted from Zheng et al.[17]. Numbers represent short, complementary domains. T, G, A and C represent unpaired bases.

1-3. Evolved structures

1-3.1. Aptamers

Aptamers have gained significant attention since 1990. Aptamers are evolved by SELEX (Systematic Evolution of Ligand by Exponential Enrichment) technique[3,4]. Aptamers are short single-stranded DNA or RNA molecules that uniquely fold and bind target molecules. Aptamers bind to targets with high specificity and affinity (picomolar to micromolar range dissociation constants). Aptamers have a complementary range of targets when compared with antibodies. For example, antibodies don't recognize

toxins because they do not cause strong immune responses (or kill their host) whereas aptamers recognize toxins because aptamer selection is not tied to the immune system[21,22].

Aptamers bind to target molecules, and in some cases have affinities approaching that of monoclonal antibodies. Many antibody-based drugs are in clinical use and hundreds of antibody-based drugs are currently in clinical trials. Although monoclonal antibodies can bind to target molecules with high specificity and affinity, they have many limitations. The high production cost of monoclonal antibodies makes them less available for research. Monoclonal antibodies show less penetration into tumor tissues than aptamers because they are large in size[21,23].

Aptamers are generally non-toxic and non-immunogenic. The production cost of aptamers is low because of chemical synthesis (rather than recombinant expression in cells). They have high penetration power into tissues due to their small size. They have few side effects because the immune system does not directly recognize them. Their storage and transportation are robust because of their thermal stability. Chemical modifications are easily incorporated into aptamers without affecting their target specificity renders them attractive therapeutic probes in medical applications[24–26].

1-3.2. SELEX technology

Aptamers are generated through an *in vitro* process called SELEX, developed in 1990[3,4]. See schematic outline in Figure 1- 5. In this process, a randomized DNA library is exposed to target (for example, proteins, small molecules, viruses, and cells). The single-stranded DNA library contains a 30-80 base random sequence region flanked by primer binding sites. Those sequences that are bound to the target are retained, enriched through amplification and utilized in a further round of selection. After multiple rounds of selection, individual aptamer candidates are cloned and sequenced revealing high-affinity aptamers from the pool. The overall *in vitro* selection process is time-consuming. At each round of selection, the pool should be characterized and purified. Unwanted amplification products must be removed: primer dimers (where the random region is lost to produce an undesired, short product) are a common problem; background binders that bind the target's support are also a pernicious source of impurities. Without advanced techniques, it may take months to move from a random pool to the identification of a highly specific and high-affinity aptamer. Modern selections can be much faster[27].

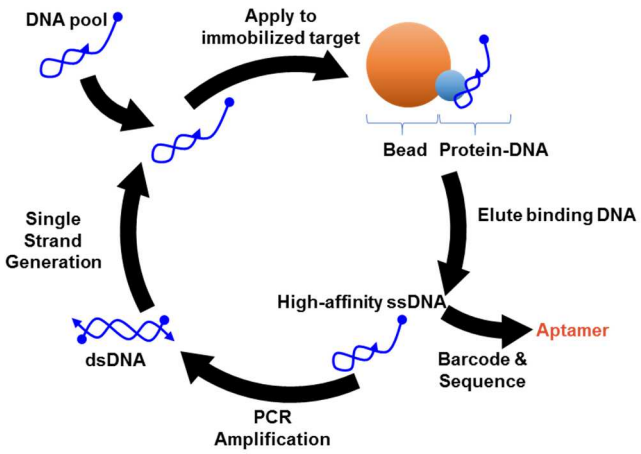

Figure 1- 5: Different steps of a typical SELEX process. A random pool is applied to an immobilized target. Undesired DNA is removed. Desired DNA that binds to target is recovered, amplified with PCR, and the pool is regenerated. After several rounds of this cycle, the pool converges on DNA with high-affinity to the target. This DNA is then sequenced, re-synthesized, and characterized.

Since 1990, many innovations have improved the SELEX process. Cell-SELEX has been used to generate aptamers[28–31] against whole living cells as targets. Next-generation sequencing has made SELEX less time-consuming and has improved the success rate[32–34]. Aptamers with chemically modified DNA have shown promise as affinity generally is increased relative to unmodified aptamers. Concerns over safety of chemically-modified nucleotides have limited the use of modified aptamers as therapeutics[35,36].

1-3.3. Evolved deoxyribozymes

Deoxyribozymes are DNA oligonucleotides that catalyze RNA cleavage and/or ligation. Deoxyribozymes are evolved and obtained through an *in vitro* selection process similar to SELEX. Breaker and Joyce (1994)[37] reported a specific DNA sequence that catalyzes the cleavage of RNA. The selection was designed such that catalytically active oligonucleotides were physically separated from the inactive pool. Diverse DNA molecules were synthesized with a RNA linker terminated with a biotin[38]. The pool was then immobilized on an avidin coated solid support. Molecules capable of self-cleavage of the RNA linker were recovered by elution. The isolated DNA was then amplified and enriched in further rounds. A similar approach was used to select DNA ligating ribozymes. Successful deoxyribozymes self-ligate an RNA, generating a longer product. These ligated products are separable by PAGE. Purtha et al. selected such a ligating ribozyme[39] which was then crystalized by Ponce-Salvatierra et al.[40] (see Figure 1- 6). Artificially evolved deoxyribozymes with defined catalytic activities have potential future *in vitro* diagnosis applications and *in vivo* therapeutic applications[41–43].

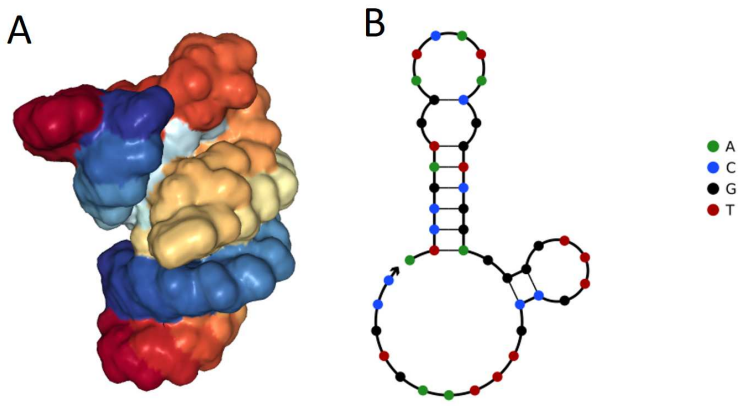

Figure 1- 6: Deoxyribozyme structure (A)3D view of 5CKK Crystal structure of 9DB1* deoxyribozyme[40] visualized using NGL Viewer[11]. (B) Predicted secondary structure of 9DB1* deoxyribozyme from NUPACK[12].

1-3.4. Aptamers as diagnostics

Many preclinical studies have revealed that DNA aptamers show promise as diagnostics tools for disease related detection. DNA aptamers can be evolved for developing diagnosis tools.

Bruno et al. (1999)[44] developed a DNA aptamer-based diagnostic sandwich assay to detect anthrax spores. The diagnostic assay which is based on electrochemiluminescence detection, was made by attaching DNA aptamer (selected against anthrax spores) on magnetic beads. The aptamer coated magnetic beads were used to capture the target spores. A biotinylated aptamer was used as the reporter component of this sandwich assay. The signal was finally transduced through the streptavidin-$Ru(bpy)_3^{2+}$ electrochemilumiscence.

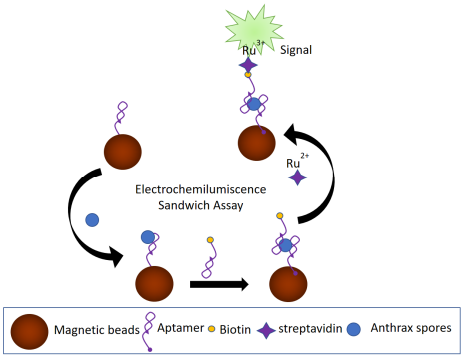

Figure 1- 7: Schematic illustrations of anthrax spores detection sandwich assay[44].

Ghosh et al. (2017)[45]developed an aptamer-based diagnosis tool to detect the level of Glycated Albumin (GA) in serum samples. The sensor consists a DNA aptamer, semiconductor quantum dot (QDs) and

gold nanoparticles (AuNPs). In this study, the 5' end of DNA aptamers was attached to QDs while the 3' ends of the aptamer was attached to AuNPs. The DNA aptamer has a hairpin like structure in absence of target. In presence of target the hairpin loop opens pushing up, quantum dot and gold nanoparticles apart. This results in an increase in photoluminescence as the fluorescence of QD is dequenched. This assay has been used for efficient diagnosis of diabetes mellitus patients.

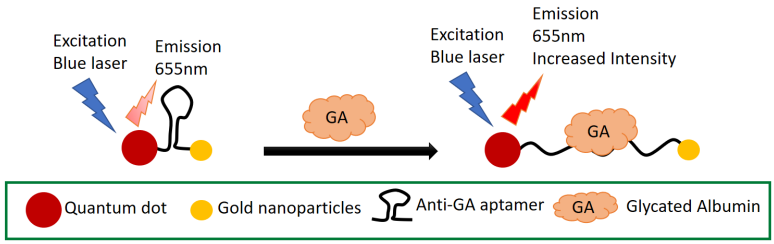

Figure 1- 8: Schematic illustrations of aptamer based Glycated Albumin detection tool[45].

1-3.5. Aptamers as therapeutics

Aptamers have shown sporadic promise as therapeutics. There is only one US Food and Drug Administration (FDA) approved aptamer-based drug (Macugen / Pegaptanib, 2004) along with a few aptamer-based drug candidates (for instance, AS1411, NOX-A12, ARC183, etc.) in clinical trials after 28 years of research. Macugen is an aptamer-based drug targeting vascular endothelial growth factor (VEGF). The Macugen is a 27 nucleotide RNA aptamer selected against VEGF. Macugen is a drug to treat age-related macular degeneration (AMD) which damages retina of older adults resulting in vision loss[23–26,46].

Although aptamers have many advantages over monoclonal antibodies, the technical challenges of aptamers and the SELEX process have resulted in suboptimal bioavailability of aptamers for *in vivo* clinical applications. The technical obstacles of aptamers are insufficient nuclease sensitivity and rapid discretion due to filtration via the kidneys. The SELEX techniques suffer from slow success rates and are a time-consuming process[47,48].

1-4. Designed DNA Reactions

Biology uses regulatory networks to control cellular behavior[49]. These networks are highly complex and hard to reproduce. Designed DNA reaction networks (i.e., DNA circuits) with the potential to detect and regulate nucleic acids and proteins could be a powerful tool in biology. Construction of synthetic

DNA circuits that mimic biological circuits is challenging. Over the last 18 years, the field has exploded with the advent of robust design elements and access to inexpensive synthetic DNA.

Designed DNA circuits rely on the ideas and concepts of computation and logic gates. The field grew from simple roots to highly complex systems from 2000 to 2018. Lee et al. (1970)[50] discovered "branch migration" and "strand displacement". In 2000, Yurke et al.[51] used the phenomenon of strand displacement and branch migration to construct a DNA based molecular machine. This proved to be a highly designable reaction that could function with almost any sequence. The field has progressed rapidly, using this basic reaction to tackle ever more difficult tasks. Benenson et al. (2004)[52] designed a DNA-based biomolecular computer to diagnose disease related messenger RNA *in vitro* and release an ssDNA drug as output. Seelig et al. (2006)[53] designed hybridization-based digital logic circuits. Designed circuits implement AND, OR, and NOT gates using oligonucleotides as input and output. Signal restoration (i.e. amplification) renders circuits sensitive enough to detect target in the presence of noise. Yin et al. (2008)[54] demonstrated diverse bimolecular self-assembly pathways including triggered assembly of quantized binary molecular trees. Zhang and Winfree (2009)[55] characterized the kinetics of DNA strand displacement reactions using toehold exchange. Quian et al. (2011)[56] demonstrated multilayer circuits using reversible strand displacement processes and computed responses to a complex series of inputs. This work integrated ~100 different designed oligonucleotides into a single circuit. Chen et al. (2013)[57] did a detailed study of circuit leakage in amplification cascades and developed unique protocols to designed DNA amplifier circuits with minimal leakage. Srinivas et al. (2017)[58] demonstrated an enzyme free, dynamic chemical oscillator using DNA strand displacement cascades. The result was an oscillating reaction analogous to the Belousov–Zhabotinsky and related chemical oscillators[59]. Thubagere et al. (2017)[60] demonstrated an autonomous, cargo-sorting, DNA-based molecular robot. This achievement was widely reported by the popular press. The design of dynamic DNA-DNA reaction networks is a growing and dynamic field.

1-4.1. DNA Strand Displacement

The diverse achievements of DNA circuits rely on the DNA strand displacement reaction. The DNA strand displacement is a process in which two strands hybridize with each other and displace a third strand[1,55]. In toehold-mediated strand displacement reactions, a prehybridized duplex is composed of an output strand and a substrate strand with an unpaired single-stranded region (see Figure 1- 9A)[55]. The short single-stranded region is known as a toehold. An input strand initiates binding in the toehold region and initiates branch migration. Branch migration is a non-biased, random walk of DNA base pairs breaking and reforming[50,51,53,61]. In a strand displacement reaction, the input strand displaces an

output strand irreversibly from the prehybridized duplex. In toehold exchange strand displacement reactions, both the reactant and product have toeholds to initiate branch migration (see Figure 1- 9B)[55]. This allows for continuous equilibration of reactants and products. The formation of products is thermodynamically possible because products have more base pairs and stacking energy. The formation of products is kinetically possible because of the toehold and molecular breathing.

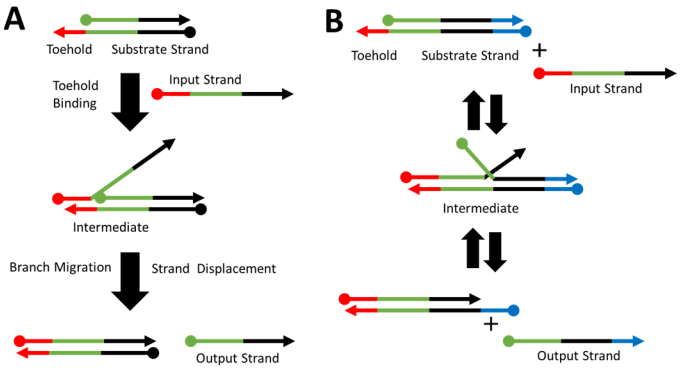

Figure 1- 9: Schematic showing DNA strand displacement via 3-way branch migration. (A)Toehold mediated strand displacement reaction[1,55,61]. (B) Strand displacement using toehold exchange[1,55,61].

1-4.2. DNA circuits

DNA circuits are dynamic DNA devices composed of DNA strands. DNA circuits can be built from a collection of DNA strand displacement reactions. The output of one reaction can be the input of another reaction. This network of connected reactions can amplify signals, perform computations and Boolean logic, and produce a detectable output.

DNA circuits can amplify a DNA or RNA input signal. In catalytic DNA amplifier circuits, the input is recycled multiple times for catalytic generation of output. In some cases, exponential amplifiers catalytically generate further catalyst. The entropy driven amplifier (EDA) circuits and catalytic hairpin assembly (CHA) are good examples of non-enzymatic DNA amplifier circuits.

Zhang et al.[62] initially designed the EDA circuits (see Figure 1- 10A). The addition of each input molecule generates more than one output molecule. The input strand first binds to the toehold of a spine strand displacing a blocker, whereby a toehold for a fuel strand is exposed. The fuel strand binds to the toehold and displaces the input strand and signal strand. The total number of base pairs before and after the reaction is unchanged in this reaction, as one free input strand releases two free output strands and double-stranded product effectively increasing system entropy. In 2017, Damase and Allen[63] adapted

the EDA circuits to generate release and sensor particles. Release particles release signal oligonucleotides and the released DNA is captured by sensor particles. This is an analogy of cell-to-cell communication.

Pierce and Yin[54] initially developed the catalytic hairpin assembly (CHA) circuit (see Figure 1- 10B). In this reaction, a pair of hairpins are designed to be complementary to each other. Spontaneous hybridization between two hairpins (H1 and H2) is kinetically unfavorable as the complementary regions are kinetically trapped as double-stranded species. The input strand binds to the toehold of H1 and exposes a single-stranded region. The exposed single-stranded region binds the toehold of H2 triggering branch migrations. The thermodynamically favorable duplex H1/H2 is formed displacing the input oligonucleotide (catalyst) allowing for another cycle to occur, further amplifying signal[61].

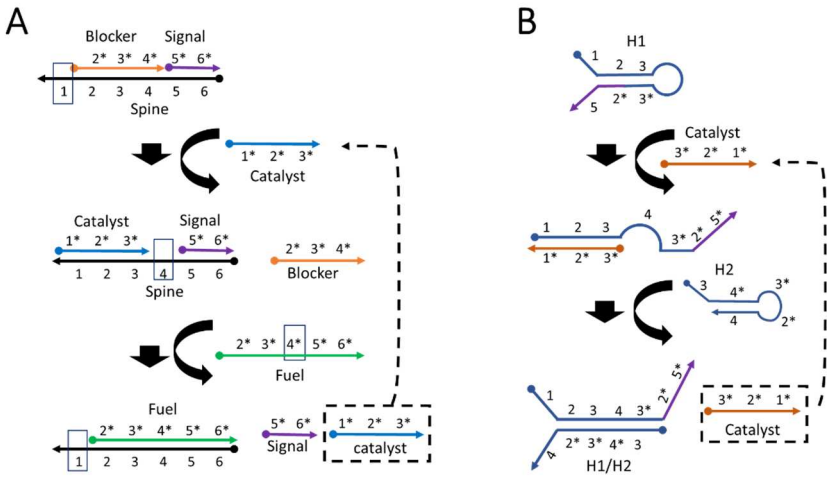

Figure 1- 10: Schematic of DNA circuits. (A) Entropy driven Amplifier circuits[61,62].(B) Catalytic Hairpin Assembly reaction[54,61,64].

The hybridization chain reaction (HCR)[54,65] is a designed, enzyme-free alternative for detection of DNA analytes, developed in the Pierce lab. The reaction is based on recognition and hybridization between two kinetically trapped hairpins in the presence of an initiator. Two hairpins are designed to hybridize with each other in presence of initiator. They form long concatemers (see Figure 1- 11). The long concatemers can be used as reporters for detection. The initiator opens one hairpin and exposes a single-stranded region. This single-stranded region is a toehold for a second hairpin. The second hairpin then binds to the toehold forming a nicked double-stranded DNA. The double-stranded DNA has an exposed toehold that is identical to the initiator. The chain reaction continues until hairpins are exhausted. Pierce (2014) reported that HCR amplifiers can detect five different mRNAs targets simultaneously in zebrafish embryos[66].

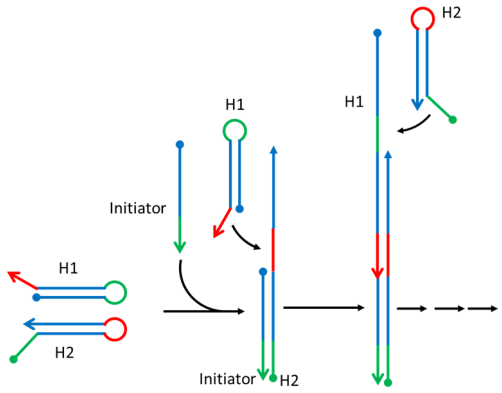

Figure 1- 11: Schematic of Hybridization Chain Reaction based on work by Evanko et al.[67]

1-4.3. Nanomachines, Walkers and "DNA nanorobots"

Inspired by biological motor proteins, scientists around the world are building synthetic motors made of designed nucleic acids. Researchers have demonstrated the beauty of DNA walkers in mimicking cell transportation systems. Proof-of-concept studies have demonstrated that the technology might be used for drug transportation and release. Potential future biomedical applications of walkers encompass biomarker detection and signal amplification. Futurists imagine such nanomachines walking inside the human body, finding molecular targets and tagging them for intervention.

DNA walkers are autonomous DNA nanomachines propelled by strand displacement reactions (or other DNA-DNA reactions). Sherman et al. (2004)[68] demonstrated DNA-based molecular walkers similar to the protein "walkers" kinesin and myosin V. The walker advances on a track using strand displacement reaction. The hybridization of the input DNA strand provides the driving force of the molecular walker. Shin et al. (2004)[69] also demonstrated a molecular walker composed of two partially complementary ssDNA strands. Kinesin movement along a tubule inspired the development of this example molecular machine. The Shin walker walks on a predefined track with the help of attachment fuel strands and detachment fuel strands. Jung et al. (2016) developed a stochastic DNA walker that autonomously traversed the surface of DNA coated microparticles driven by the CHA reaction[70]. In 2017, Damase and Allen[63] adapted the EDA circuit to develop DNA based molecular walker that could transfers from one particle to another. The DNA walker was released from "release particles" with the addition of fuel strand. "Sensor particles" then captured the walker which then walked randomly on the surface of sensor particles. The sensor particles reported this activity through an increase in fluorescence emission (see schematic in Figure 1- 12).

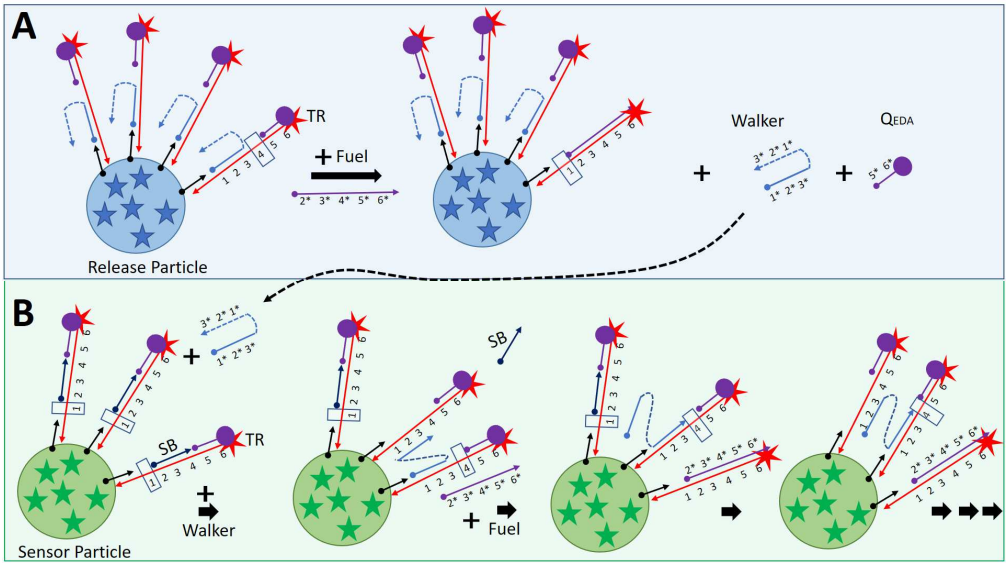

Figure 1- 12: Schematic of DNA walker release and capture. (A) Release particles release walker on addition of the fuel strand. (B) Sensor particle captures the displaced walker. The captured walker then walks on the surface of sensor particles using the EDA reaction. The fuel strand displaces one leg of a catalyst. The displaced leg hybridizes with a second substrate before the remaining leg is displaced by fuel.

1-5. Integration of evolved and designed DNA structures

Although the philosophies of evolved and designed DNA are very different, both are made of DNA and there are advantages in the combination of the two approaches. Designed structures can 1) assemble objects in space at the nanoscale and 2) perform dynamic and computational tasks. Both can be expanded with the capabilities of evolved DNA. In the first case, DNA can be designed to link nanoscale objects together. Nanostructures such as DNA origami can be used as an addressable scaffold to arrange non-designed elements like aptamers, antibodies, or protein. In the second case, DNA reactions can integrate with aptamers to interact with non-nucleic acids. There is not yet a method to design DNA to bind to a non-nucleic acid target; that interaction must be evolved in a process like SELEX. Aptamers can guide DNA circuits and extend their ability to interact with various analytes such as small molecules, proteins, and other biological entities.

1-5.1. Aptamer Nanostructure Colocalization

Designed nucleic acid structures can hold multiple aptamers. In some cases, the spacing and orientation can be precisely controlled. Likewise, other nanostructures can be held together by designed DNA-DNA interactions[71] including superlattices of gold nanoparticles[72]. This field has become quite mature,

with dozens of examples and applications in photonics and optical detection. We give a few highlights here.

Borghei et al. (2016)[73] developed a cancer cell detection method based on simple, designed hybridization between aptamers and two types of gold nanoparticles functionalized with ssDNA (DNA-AuNPs). Both designed DNA probes bind to the aptamer in absence of target. Designed DNA binding induces nanoparticle aggregation and produces a color change. Target cells bind to aptamers and remove them from the solution. The result is no self-assembly and an unchanged, red color (see Figure 1- 13).

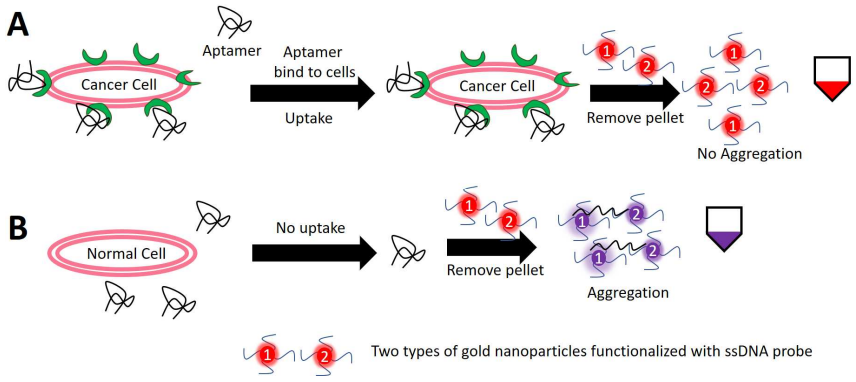

Figure 1- 13: Schematic of aptamer-based aggregation of gold nanoparticles functionalized with ssDNA to detect cancer cells based on work by Borghei et al. The aggregation is induced by designed DNA hybridization of aptamer and ssDNA of gold nanoparticles[73].

Aptamers can be linked to nanostructures by designed hybridization. In one example from 2018, Zhao et al.[74] demonstrated a nanostructure that held three aptamers, a drug (doxorubicin), and an siRNA therapeutic (against anaplastic lymphoma kinase). They used this assembly to treat a model of anaplastic large cell lymphoma(ALCL). The aptamer-nanomedicine bound to ALCL cells via the aptamer. The cells internalized the aptamer-linked nanostructure and the cargo (doxorubicin and siRNA) were released.

There are many examples of designed hybridization linking aptamers to nanostructures. A designed DNA origami held dozens of aptamers in order to spatially organize thrombin and platelet derived growth factor (PDGF)[75]. Zhu et al. (2013) reported the integration of designed DNA called nanoflowers and cancer targeting aptamers to selectively recognize cancer cells[76]. Norouzi et al. (2018) presented aptamer-integrated DNA assembly to detect cancer cells[77]. The DNA assembly consisted of a concatemer linked with three-way junctions. The integrated aptamer guided the assembly to detect cancer cells. DNAzymes embedded in the aptamer-functionalized DNA assembly produced a colorimetric signal.

1-5.2. Aptamers at the interface between DNA circuits and biology

Aptamers can be integrated with more dynamic DNA nanotechnology and DNA circuits. While there are fewer examples (see Table 1- 1), it is an exciting field with growing possibilities. Bompiani et al. (2012)[78] reported an excellent example to show the beauty of integration of evolved DNA and designed DNA. Thrombin-aptamer is an anticoagulant drug while its reverse complement acts as an "antidote." This contrasts with warfarin, a small molecule anticoagulant. The effect of warfarin is continuous until the drug leaves the body. With the thrombin aptamer, the drug's effect can be shut off with the addition of the reverse complement antidote. This designed, DNA-based antidote modulates the anticoagulant property of the aptamer and improves its safety[78].

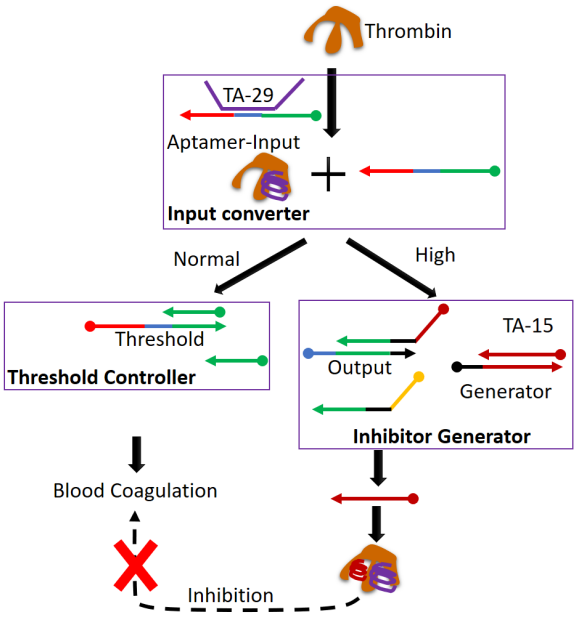

Figure 1- 14: Schematic illustrations of regulation of thrombin using aptamer-based DNA circuits based on Han et al.[79]

The modulation of the thrombin aptamer was extended to include dynamic control using a DNA circuit (see Figure 1- 14). The DNA circuit was designed using two different aptamers (TA-29 and TA-15). TA-29 binds to heparin exosite without inhibitory function. TA-15 binds to the fibrinogen exosite with strong inhibitory function. The thrombin input displaces TA-29 from duplex. The displaced DNA input is consumed by the threshold controller. The additional, displaced TA-29 also binds to the heparin exosite without inhibition. When the threshold controller DNA is depleted, DNA input will generate TA-15. TA-15 will bind to fibrinogen exosite and inhibit blood coagulation[79]. This means that inhibition only occurs when the activity exceeds the desired level encoded into the circuit.

Table 1- 1: Integration of DNA Circuits and Evolved DNA

Authors	**Evolved DNA**	**Designed DNA**	**Year**
Fan et al.[80]	Thrombin aptamer, TBA15	DNA circuit	2018
Borghei et al.[73]	AS 1411 for cancer cells	DNA hybridization	2016
Ang et al.[81]	Thrombin binding aptamer	DNA circuit	2016
Martini et al.[82]	Thiamine pyrophosphate (TPP) aptamer	Strand displacement	2015
Zhu et al.[83]	ATP aptamer	DNA circuit	2014
Zhu et al.[84]	sgc8 & TDO5 aptamers	HCR (DNA nanotrain)	2013
Li et al.[85]	Aptamer against homodimer BB of platelet derived growth factor (PDGF-BB)	Strand Displacement	2013
You et al. [86]	Sgc8c, Sgc4f, and TC01 for cancer cells	Strand Displacement	2014
Li et al.[87]	Two thrombin binding aptamers	Strand Displacement	2013
Han et al. [79]	TA-29 and TA-15 for thrombin	DNA circuit	2012
Bompiani et al. [78]	Thrombin aptamer	DNA hybridization	2012

In the thrombin activity regulator, the output was an inhibitory aptamer TA-15. In the same system, an aptamer acted as an input to the DNA circuit as well. The non-inhibitory aptamer, TA-29, detected the target. This regulated the DNA circuit based on a concentration triggered threshold. Aptamer TA-29 might be considered a transducer to convert thrombin concentration to an oligonucleotide input to which the circuit could respond.

Aptamer transducers have also been used for small molecule targets. Zhu et al. (2014) reported a DNA circuit integrated with an aptamer to detect the small molecule adenosine triphosphate (ATP)[83]. The principle is outlined in Figure 1- 15. In the presence of target (ATP), an aptamer (M) binds to the ATP. The bound ATP-aptamer complex then undergoes a conformational change, exposing a toehold that is complementary to a region of a second DNA oligonucleotide (R). M and R react to produce an output strand, S. Two guanosine-rich oligonucleotides bind output S to form a G-Quadruplex structure. The split G-Quadruplex structure binds to protoporphyrin IX (PPIX), resulting in increased fluorescence emission.

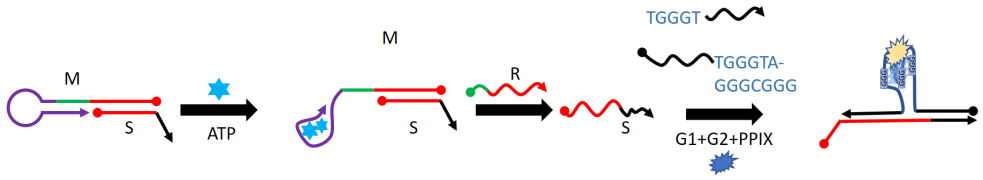

Figure 1- 15: Schematic illustrations of aptamer-based DNA circuit to detect ATP based on Zhu et al.[83]

In summary, integration of aptamers and DNA circuits allows nucleic acid nanomachines to manipulate and respond to proteins and small molecules. Given the diverse aptamers in the literature, this might be expanded to viruses and cells as well. Aptamers provide specific biorecognition and DNA circuits provide precise and autonomous control. Integration of aptamers as inputs to a DNA logic circuit could compute a response based on multiple biomarkers. When a circuit generates an active aptamer as a product, the aptamer can act on biology as a regulation element. These two approaches have complementary applications in synthetic biology and biomedicine.

1-6. Conclusions

The DNA nanotechnology field has produced impressive and beautiful achievements including precisely designed nanostructures and nanodevices. Few practical examples yet exist of utilizing DNA nanotechnology to meet biological needs in basic or biomedical science. The design of DNA to interact with other DNA is well understood, but the design of DNA to interact with protein or small molecules remains beyond the current capacity of computational prediction. If dynamic DNA technology could respond to protein analytes, it could be applied to analytical and diagnostic problems. The newest demonstrations in the literature show the integration of DNA circuits with biological regulatory networks. The interface between these two worlds of constructed and natural molecules is evolved DNA.

Aptamers are evolved DNA that bind to specific targets such as proteins. They can bind with strong affinity and specificity, but, like antibodies, often require further amplification to act as detectors for

low-concentration analytes. DNA circuits can be integrated with aptamers to solve this problem. Unlike enzymatic reactions, DNA-DNA reaction components can be easily dried, stored, transported and operated under harsh conditions. An aptamer can generate a signal in response to a specific target, and DNA circuits can amplify the signal. This integration strategy suggests a robust detection platform. This strategy could be significant in developing point-of-care devices.

DNA circuits and aptamers might eventually be used to interact with biological regulatory networks. This could be applied to provide side about internal dynamic regulation of cells as well as to modify disease states. Aptamers can act as the "output" of a DNA circuit to affect a biological system according to an internal program. Thrombin aptamers have been demonstrated as anticoagulant drugs[78]. The DNA circuit for regulating thrombin[79] set thresholds for activating and deactivating a thrombin aptamer. This represents a first step towards self-regulating therapeutics. The system could continuously maintain an active concentration high enough to derive therapeutic benefit but not so high as to cause side-effects.

Aptamers on both the input and output side of NA circuits might allow for a more complete integration of these non-natural networks with biological regulation. The Saito lab[88] and Aldaye lab[89] used intracellular RNA circuits with the stated goal of applying these reactions within cells for synthetic biology applications. Integration with evolved elements may allow designed regulatory networks to respond to expression patterns rather than transcription patterns. Ultimately, evolved and designed reaction patterns may help to enable synthetic regulation.

This all shows that integrated DNA-aptamer-circuits have powerful applications. However, it will be challenging to integrate the underlying philosophies. The abstract principles of DNA circuits (i.e. base pairing and known, non-canonical structures) must be expanded to include the diverse and idiosyncratic properties of aptamers.

1-7. Acknowledgments

Research reported in this publication was supported by the National Institute of General Medical Sciences of the National Institutes of Health under Award Number P20GM104420. The content is solely the responsibility of the authors and does not necessarily represent the official views of the National Institutes of Health.

1-8. References

(1) Zhang, D. Y.; Seelig, G. Dynamic DNA Nanotechnology Using Strand-Displacement Reactions. *Nature Chemistry* **2011**, *3* (2), 103–113. https://doi.org/10.1038/nchem.957.

(2) Seeman, N. C. Structural DNA Nanotechnology: An Overview. *Methods Mol Biol* **2005**, *303*, 143–166. https://doi.org/10.1385/1-59259-901-X:143.

(3) Ellington, A. D.; Szostak, J. W. In Vitro Selection of RNA Molecules That Bind Specific Ligands. *Nature* **1990**, *346* (6287), 818–822. https://doi.org/10.1038/346818a0.

(4) Tuerk, C.; Gold, L. Systematic Evolution of Ligands by Exponential Enrichment: RNA Ligands to Bacteriophage T4 DNA Polymerase. *Science* **1990**, *249* (4968), 505–510. https://doi.org/10.1126/science.2200121.

(5) Alberts, B.; Johnson, A.; Lewis, J.; Raff, M.; Roberts, K.; Walter, P. The Structure and Function of DNA. *Molecular Biology of the Cell. 4th edition* **2002**.

(6) Amano, R.; Takada, K.; Tanaka, Y.; Nakamura, Y.; Kawai, G.; Kozu, T.; Sakamoto, T. Kinetic and Thermodynamic Analyses of Interaction between a High-Affinity RNA Aptamer and Its Target Protein. *Biochemistry* **2016**, *55* (45), 6221–6229. https://doi.org/10.1021/acs.biochem.6b00748.

(7) Breslauer, K. J.; Frank, R.; Blocker, H.; Marky, L. A. Predicting DNA Duplex Stability from the Base Sequence. *Proceedings of the National Academy of Sciences* **1986**, *83* (11), 3746–3750. https://doi.org/10.1073/pnas.83.11.3746.

(8) Woodson, S. A.; Leontis, N. B. Structure and Dynamics of Ribosomal RNA. *Current Opinion in Structural Biology* **1998**, *8* (3), 294–300. https://doi.org/10.1016/S0959-440X(98)80061-4.

(9) Mueller, F.; Sommer, I.; Baranov, P.; Matadeen, R.; Stoldt, M.; Wöhnert, J.; Görlach, M.; van Heel, M.; Brimacombe, R. The 3D Arrangement of the 23 S and 5 S RRNA in the Escherichia Coli 50 S Ribosomal Subunit Based on a Cryo-Electron Microscopic Reconstruction at 7.5 Å Resolution11Edited by D. E. Draper. *Journal of Molecular Biology* **2000**, *298* (1), 35–59. https://doi.org/10.1006/jmbi.2000.3635.

(10) Kaminishi, T.; Wilson, D. N.; Takemoto, C.; Harms, J. M.; Kawazoe, M.; Schluenzen, F.; Hanawa-Suetsugu, K.; Shirouzu, M.; Fucini, P.; Yokoyama, S. A Snapshot of the 30S Ribosomal Subunit Capturing MRNA via the Shine-Dalgarno Interaction. *Structure* **2007**, *15* (3), 289–297. https://doi.org/10.1016/j.str.2006.12.008.

(11) Rose, A. S.; Bradley, A. R.; Valasatava, Y.; Duarte, J. M.; Prlić, A.; Rose, P. W.; Valencia, A. NGL Viewer: Web-Based Molecular Graphics for Large Complexes. *Bioinformatics*. https://doi.org/10.1093/bioinformatics/bty419.

(12) Zadeh, J. N.; Steenberg, C. D.; Bois, J. S.; Wolfe, B. R.; Pierce, M. B.; Khan, A. R.; Dirks, R. M.; Pierce, N. A. NUPACK: Analysis and Design of Nucleic Acid Systems. *Journal of Computational Chemistry* **2011**, *32* (1), 170–173. https://doi.org/10.1002/jcc.21596.

(13) Seeman, N. C. Nucleic Acid Junctions and Lattices. *Journal of Theoretical Biology* **1982**, *99* (2), 237–247. https://doi.org/10.1016/0022-5193(82)90002-9.

(14) Rothemund, P. W. K. Folding DNA to Create Nanoscale Shapes and Patterns. *Nature* **2006**, *440* (7082), 297–302. https://doi.org/10.1038/nature04586.

(15) Shih, W. M.; Quispe, J. D.; Joyce, G. F. A 1.7-Kilobase Single-Stranded DNA That Folds into a Nanoscale Octahedron. *Nature* **2004**, *427* (6975), 618–621. https://doi.org/10.1038/nature02307.

(16) Liu, Y.; Ke, Y.; Yan, H. Self-Assembly of Symmetric Finite-Size DNA Nanoarrays. *J. Am. Chem. Soc.* **2005**, *127* (49), 17140–17141. https://doi.org/10.1021/ja055614o.

(17) Zheng, J.; Birktoft, J. J.; Chen, Y.; Wang, T.; Sha, R.; Constantinou, P. E.; Ginell, S. L.; Mao, C.; Seeman, N. C. From Molecular to Macroscopic via the Rational Design of a Self-Assembled 3D DNA Crystal. *Nature* **2009**, *461* (7260), 74–77. https://doi.org/10.1038/nature08274.

(18) Ducani, C.; Kaul, C.; Moche, M.; Shih, W. M.; Högberg, B. Enzymatic Production of Monoclonal Stoichiometric Single-Stranded DNA Oligonucleotides. *Nat Methods* **2013**, *10* (7). https://doi.org/10.1038/nmeth.2503.

(19) Han, D.; Qi, X.; Myhrvold, C.; Wang, B.; Dai, M.; Jiang, S.; Bates, M.; Liu, Y.; An, B.; Zhang, F.; et al. Single-Stranded DNA and RNA Origami. *Science* **2017**, *358* (6369), eaao2648. https://doi.org/10.1126/science.aao2648.

(20) Nangreave, J.; Han, D.; Liu, Y.; Yan, H. DNA Origami: A History and Current Perspective. *Current Opinion in Chemical Biology* **2010**, *14* (5), 608–615. https://doi.org/10.1016/j.cbpa.2010.06.182.

(21) Ashrafuzzaman, M. Aptamers as Both Drugs and Drug-Carriers. *BioMed Research International* **2014**, *2014*, e697923. https://doi.org/10.1155/2014/697923.

(22) Blind, M.; Blank, M. Aptamer Selection Technology and Recent Advances. *Mol Ther Nucleic Acids* **2015**, *4* (1), e223. https://doi.org/10.1038/mtna.2014.74.

(23) Ireson, C. R.; Kelland, L. R. Discovery and Development of Anticancer Aptamers. *Mol Cancer Ther* **2006**, *5* (12), 2957–2962. https://doi.org/10.1158/1535-7163.MCT-06-0172.

(24) Keefe, A. D.; Pai, S.; Ellington, A. Aptamers as Therapeutics. *Nat Rev Drug Discov* **2010**, *9* (7), 537–550. https://doi.org/10.1038/nrd3141.

(25) Sundaram, P.; Kurniawan, H.; Byrne, M. E.; Wower, J. Therapeutic RNA Aptamers in Clinical Trials. *European Journal of Pharmaceutical Sciences* **2013**, *48* (1–2), 259–271. https://doi.org/10.1016/j.ejps.2012.10.014.

(26) Lee, J. W.; Kim, H. J.; Heo, K. Therapeutic Aptamers: Developmental Potential as Anticancer Drugs. *BMB Rep* **2015**, *48* (4), 234–237. https://doi.org/10.5483/BMBRep.2015.48.4.277.

(27) Darmostuk, M.; Rimpelova, S.; Gbelcova, H.; Ruml, T. Current Approaches in SELEX: An Update to Aptamer Selection Technology. *Biotechnology Advances* **2015**, *33* (6, Part 2), 1141–1161. https://doi.org/10.1016/j.biotechadv.2015.02.008.

(28) Civit, L.; Taghdisi, S. M.; Jonczyk, A.; Haßel, S. K.; Gröber, C.; Blank, M.; Stunden, H. J.; Beyer, M.; Schultze, J.; Latz, E.; et al. Systematic Evaluation of Cell-SELEX Enriched Aptamers Binding to Breast Cancer Cells. *Biochimie* **2018**, *145*, 53–62. https://doi.org/10.1016/j.biochi.2017.10.007.

(29) Morris, K. N.; Jensen, K. B.; Julin, C. M.; Weil, M.; Gold, L. High Affinity Ligands from in Vitro Selection: Complex Targets. *Proc Natl Acad Sci U S A* **1998**, *95* (6), 2902–2907.

(30) Homann, M.; Göringer, H. U. Combinatorial Selection of High Affinity RNA Ligands to Live African Trypanosomes. *Nucleic Acids Res* **1999**, *27* (9), 2006–2014.

(31) Ulrich, H.; Magdesian, M. H.; Alves, M. J. M.; Colli, W. In Vitro Selection of RNA Aptamers That Bind to Cell Adhesion Receptors of *Trypanosoma Cruzi* and Inhibit Cell Invasion. *Journal of Biological Chemistry* **2002**, *277* (23), 20756–20762. https://doi.org/10.1074/jbc.M111859200.

(32) Schütze, T.; Wilhelm, B.; Greiner, N.; Braun, H.; Peter, F.; Mörl, M.; Erdmann, V. A.; Lehrach, H.; Konthur, Z.; Menger, M.; et al. Probing the SELEX Process with Next-Generation Sequencing. *PLOS ONE* **2011**, *6* (12), e29604. https://doi.org/10.1371/journal.pone.0029604.

(33) Kahvejian, A.; Quackenbush, J.; Thompson, J. F. What Would You Do If You Could Sequence Everything? *Nature Biotechnology* **2008**, *26* (10), 1125–1133. https://doi.org/10.1038/nbt1494.

(34) Zimmermann, B.; Gesell, T.; Chen, D.; Lorenz, C.; Schroeder, R. Monitoring Genomic Sequences during SELEX Using High-Throughput Sequencing: Neutral SELEX. *PLoS ONE* **2010**, *5* (2), e9169. https://doi.org/10.1371/journal.pone.0009169.

(35) Agrawal, S. Importance of Nucleotide Sequence and Chemical Modifications of Antisense Oligonucleotides. *Biochim Biophys Acta* **1999**, *1489* (1), 53–68. https://doi.org/10.1016/S0167-4781(99)00141-4.

(36) Tanaka, M.; Nyce, J. W. Respirable Antisense Oligonucleotides: A New Drug Class for Respiratory Disease. *Respir Res* **2001**, *2* (1), 5–9. https://doi.org/10.1186/rr32.

(37) Breaker, R. R.; Joyce, G. F. A DNA Enzyme That Cleaves RNA. *Chem. Biol.* **1994**, *1* (4), 223–229.

(38) Silverman, S. K. In Vitro Selection, Characterization, and Application of Deoxyribozymes That Cleave RNA. *Nucleic Acids Res* **2005**, *33* (19), 6151–6163. https://doi.org/10.1093/nar/gki930.

(39) Purtha, W. E.; Coppins, R. L.; Smalley, M. K.; Silverman, S. K. General Deoxyribozyme-Catalyzed Synthesis of Native 3‘–5‘ RNA Linkages. *J. Am. Chem. Soc.* **2005**, *127* (38), 13124–13125. https://doi.org/10.1021/ja0533702.

(40) Ponce-Salvatierra, A.; Wawrzyniak-Turek, K.; Steuerwald, U.; Höbartner, C.; Pena, V. Crystal Structure of a DNA Catalyst. *Nature* **2016**, *529* (7585), 231–234. https://doi.org/10.1038/nature16471.

(41) Baum, D. A.; Silverman, S. K. Deoxyribozymes: Useful DNA Catalysts in Vitro and in Vivo. *Cellular and Molecular Life Sciences* **2008**, *65* (14), 2156–2174. https://doi.org/10.1007/s00018-008-8029-y.

(42) Silverman, S. K. Catalytic DNA: Scope, Applications, and Biochemistry of Deoxyribozymes. *Trends Biochem Sci* **2016**, *41* (7), 595–609. https://doi.org/10.1016/j.tibs.2016.04.010.

(43) Eckhoff, G.; Codrea, V.; Ellington, A. D.; Chen, X. Beyond Allostery: Catalytic Regulation of a Deoxyribozyme through an Entropy-Driven DNA Amplifier. *Journal of Systems Chemistry* **2010**, *1* (1), 13. https://doi.org/10.1186/1759-2208-1-13.

(44) Bruno, J. G.; Kiel, J. L. In Vitro Selection of DNA Aptamers to Anthrax Spores with Electrochemiluminescence Detection. *Biosensors and Bioelectronics* **1999**, *14* (5), 457–464. https://doi.org/10.1016/S0956-5663(99)00028-7.

(45) Ghosh, S.; Datta, D.; Cheema, M.; Dutta, M.; Stroscio, M. A. Aptasensor Based Optical Detection of Glycated Albumin for Diabetes Mellitus Diagnosis. *Nanotechnology* **2017**, *28* (43), 435505. https://doi.org/10.1088/1361-6528/aa893a.

(46) Macugen New FDA Drug Approval | CenterWatch https://www.centerwatch.com/drug-information/fda-approved-drugs/drug/872/macugen-pegaptanib (accessed Sep 3, 2018).

(47) Damase, T. R.; Miura, T. A.; Parent, C. E.; Allen, P. B. Application of the Open QPCR Instrument for the in Vitro Selection of DNA Aptamers against Epidermal Growth Factor Receptor and Drosophila C Virus. *ACS Comb. Sci.* **2018**, *20* (2), 45–54. https://doi.org/10.1021/acscombsci.7b00138.

(48) Damase, T. R.; Ellington, A. D.; Allen, P. B. Purification of Single-Stranded DNA by Co-Polymerization with Acrylamide and Electrophoresis. *BioTechniques* **2017**, *62* (6). https://doi.org/10.2144/000114557.

(49) Emmert-Streib, F.; Dehmer, M.; Haibe-Kains, B. Gene Regulatory Networks and Their Applications: Understanding Biological and Medical Problems in Terms of Networks. *Front Cell Dev Biol* **2014**, *2*. https://doi.org/10.3389/fcell.2014.00038.

(50) Lee, C. S.; Davis, R. W.; Davidson, N. A Physical Study by Electron Microscopy of the Terminally Repetitious, Circularly Permuted DNA from the Coliphage Particles of Escherichia Coli 15. *Journal of Molecular Biology* **1970**, *48* (1), 1–22. https://doi.org/10.1016/0022-2836(70)90215-9.

(51) Yurke, B.; Turberfield, A. J.; Jr, A. P. M.; Simmel, F. C.; Neumann, J. L. A DNA-Fuelled Molecular Machine Made of DNA. *Nature* **2000**, *406* (6796), 605–608. https://doi.org/10.1038/35020524.

(52) Benenson, Y.; Gil, B.; Ben-Dor, U.; Adar, R.; Shapiro, E. An Autonomous Molecular Computer for Logical Control of Gene Expression. *Nature* **2004**, *429* (6990), 423–429. https://doi.org/10.1038/nature02551.

(53) Seelig, G.; Soloveichik, D.; Zhang, D. Y.; Winfree, E. Enzyme-Free Nucleic Acid Logic Circuits. *Science* **2006**, *314* (5805), 1585–1588. https://doi.org/10.1126/science.1132493.

(54) Yin, P.; Choi, H. M. T.; Calvert, C. R.; Pierce, N. A. Programming Biomolecular Self-Assembly Pathways. *Nature* **2008**, *451* (7176), 318–322. https://doi.org/10.1038/nature06451.

(55) Zhang, D. Y.; Winfree, E. Control of DNA Strand Displacement Kinetics Using Toehold Exchange. *J. Am. Chem. Soc.* **2009**, *131* (47), 17303–17314. https://doi.org/10.1021/ja906987s.

(56) Qian, L.; Winfree, E. Scaling Up Digital Circuit Computation with DNA Strand Displacement Cascades. *Science* **2011**, *332* (6034), 1196–1201. https://doi.org/10.1126/science.1200520.

(57) Chen, X.; Briggs, N.; McLain, J. R.; Ellington, A. D. Stacking Nonenzymatic Circuits for High Signal Gain. *PNAS* **2013**, *110* (14), 5386–5391. https://doi.org/10.1073/pnas.1222807110.

(58) Srinivas, N.; Parkin, J.; Seelig, G.; Winfree, E.; Soloveichik, D. Enzyme-Free Nucleic Acid Dynamical Systems. *Science* **2017**, *358* (6369), eaal2052. https://doi.org/10.1126/science.aal2052.

(59) Zhabotinsky, A. M. A History of Chemical Oscillations and Waves. *Chaos: An Interdisciplinary Journal of Nonlinear Science* **1991**, *1* (4), 379–386. https://doi.org/10.1063/1.165848.

(60) Thubagere, A. J.; Li, W.; Johnson, R. F.; Chen, Z.; Doroudi, S.; Lee, Y. L.; Izatt, G.; Wittman, S.; Srinivas, N.; Woods, D.; et al. A Cargo-Sorting DNA Robot. *Science* **2017**, *357* (6356), eaan6558. https://doi.org/10.1126/science.aan6558.

(61) Jung, C.; Ellington, A. D. Diagnostic Applications of Nucleic Acid Circuits. *Acc Chem Res* **2014**, *47* (6), 1825–1835. https://doi.org/10.1021/ar500059c.

(62) Zhang, D. Y.; Turberfield, A. J.; Yurke, B.; Winfree, E. Engineering Entropy-Driven Reactions and Networks Catalyzed by DNA. *Science* **2007**, *318* (5853), 1121–1125. https://doi.org/10.1126/science.1148532.

(63) Damase, T. R.; Spencer, A.; Samuel, B.; Allen, P. B. Biomimetic Molecular Signaling Using DNA Walkers on Microparticles. *Scientific Reports* **2017**, *7* (1), 4081. https://doi.org/10.1038/s41598-017-04316-1.

(64) Zang, Y.; Lei, J.; Ling, P.; Ju, H. Catalytic Hairpin Assembly-Programmed Porphyrin–DNA Complex as Photoelectrochemical Initiator for DNA Biosensing. *Anal. Chem.* **2015**, *87* (10), 5430–5436. https://doi.org/10.1021/acs.analchem.5b00888.

(65) Dirks, R. M.; Pierce, N. A. Triggered Amplification by Hybridization Chain Reaction. *PNAS* **2004**, *101* (43), 15275–15278. https://doi.org/10.1073/pnas.0407024101.

(66) Choi, H. M. T.; Beck, V. A.; Pierce, N. A. Next-Generation *in Situ* Hybridization Chain Reaction: Higher Gain, Lower Cost, Greater Durability. *ACS Nano* **2014**, *8* (5), 4284–4294. https://doi.org/10.1021/nn405717p.

(67) Evanko, D. Hybridization Chain Reaction. *Nature Methods* **2004**, *1*, 186–187. https://doi.org/10.1038/nmeth1204-186a.

(68) Sherman, W. B.; Seeman, N. C. A Precisely Controlled DNA Biped Walking Device. *Nano Letters* **2004**, *4* (7), 1203–1207. https://doi.org/10.1021/nl049527q.

(69) Shin, J.-S.; Pierce, N. A. A Synthetic DNA Walker for Molecular Transport. *Journal of the American Chemical Society* **2004**, *126* (35), 10834–10835. https://doi.org/10.1021/ja047543j.

(70) Jung, C.; Allen, P. B.; Ellington, A. D. A Stochastic DNA Walker That Traverses a Microparticle Surface. *Nature Nanotechnology* **2016**, *11* (2), 157–163. https://doi.org/10.1038/nnano.2015.246.

(71) Rosi, N. L.; Mirkin, C. A. Nanostructures in Biodiagnostics. *Chemical Reviews* **2005**, *105* (4), 1547–1562. https://doi.org/10.1021/cr030067f.

(72) Lin, Q.-Y.; Mason, J. A.; Li, Z.; Zhou, W.; O'Brien, M. N.; Brown, K. A.; Jones, M. R.; Butun, S.; Lee, B.; Dravid, V. P.; et al. Building Superlattices from Individual Nanoparticles via Template-Confined DNA-Mediated Assembly. *Science* **2018**, *359* (6376), 669–672. https://doi.org/10.1126/science.aaq0591.

(73) Borghei, Y.-S.; Hosseini, M.; Dadmehr, M.; Hosseinkhani, S.; Ganjali, M. R.; Sheikhnejad, R. Visual Detection of Cancer Cells by Colorimetric Aptasensor Based on Aggregation of Gold Nanoparticles Induced by DNA Hybridization. *Analytica Chimica Acta* **2016**, *904*, 92–97. https://doi.org/10.1016/j.aca.2015.11.026.

(74) Zhao, N.; Zeng, Z.; Zu, Y. Self-Assembled Aptamer-Nanomedicine for Targeted Chemotherapy and Gene Therapy. *Small* **2018**, *14* (4), 1702103. https://doi.org/10.1002/smll.201702103.

(75) Chhabra, R.; Sharma, J.; Ke, Y.; Liu, Y.; Rinker, S.; Lindsay, S.; Yan, H. Spatially Addressable Multiprotein Nanoarrays Templated by Aptamer-Tagged DNA Nanoarchitectures. *J. Am. Chem. Soc.* **2007**, *129* (34), 10304–10305. https://doi.org/10.1021/ja072410u.

(76) Zhu, G.; Hu, R.; Zhao, Z.; Chen, Z.; Zhang, X.; Tan, W. Noncanonical Self-Assembly of Multifunctional DNA Nanoflowers for Biomedical Applications. *J. Am. Chem. Soc.* **2013**, *135* (44), 16438–16445. https://doi.org/10.1021/ja406115e.

(77) Norouzi, A.; Ravan, H.; Mohammadi, A.; Hosseinzadeh, E.; Norouzi, M.; Fozooni, T. Aptamer–Integrated DNA Nanoassembly: A Simple and Sensitive DNA Framework to Detect Cancer Cells. *Analytica Chimica Acta* **2018**, *1017*, 26–33. https://doi.org/10.1016/j.aca.2018.02.037.

(78) Bompiani, K. M.; Monroe, D. M.; Church, F. C.; Sullenger, B. A. A High Affinity, Antidote-Controllable Prothrombin and Thrombin-Binding RNA Aptamer Inhibits Thrombin Generation and Thrombin Activity. *Journal of Thrombosis and Haemostasis* **2012**, *10* (5), 870–880. https://doi.org/10.1111/j.1538-7836.2012.04679.x.

(79) Han, D.; Zhu, Z.; Wu, C.; Peng, L.; Zhou, L.; Gulbakan, B.; Zhu, G.; Williams, K. R.; Tan, W. A Logical Molecular Circuit for Programmable and Autonomous Regulation of Protein Activity Using DNA Aptamer–Protein Interactions. *Journal of the American Chemical Society* **2012**, *134* (51), 20797–20804. https://doi.org/10.1021/ja310428s.

(80) Fan, D.; Fan, Y.; Wang, E.; Dong, S. A Simple, Label-Free, Electrochemical DNA Parity Generator/Checker for Error Detection during Data Transmission Based on "Aptamer-Nanoclaw"-Modulated Protein Steric Hindrance. *Chem. Sci.* **2018**, *9* (34), 6981–6987. https://doi.org/10.1039/C8SC02482K.

(81) Ang, Y. S.; Tong, R.; Yung, L.-Y. L. Engineering a Robust DNA Split Proximity Circuit with Minimized Circuit Leakage. *Nucleic Acids Res* **2016**, *44* (14), e121–e121. https://doi.org/10.1093/nar/gkw447.

(82) Martini, L.; Meyer, A. J.; Ellefson, J. W.; Milligan, J. N.; Forlin, M.; Ellington, A. D.; Mansy, S. S. In Vitro Selection for Small-Molecule-Triggered Strand Displacement and Riboswitch Activity. *ACS Synth. Biol.* **2015**, *4* (10), 1144–1150. https://doi.org/10.1021/acssynbio.5b00054.

(83) Zhu, J.; Zhang, L.; Zhou, Z.; Dong, S.; Wang, E. Molecular Aptamer Beacon Tuned DNA Strand Displacement to Transform Small Molecules into DNA Logic Outputs. *Chemical Communications* **2014**, *50* (25), 3321. https://doi.org/10.1039/c3cc49833f.

(84) Zhu, G.; Zhang, S.; Song, E.; Zheng, J.; Hu, R.; Fang, X.; Tan, W. Building Fluorescent DNA Nanodevices on Target Living Cell Surfaces. *Angewandte Chemie International Edition* **2013**, *52* (21), 5490–5496. https://doi.org/10.1002/anie.201301439.

(85) Li, F.; Zhang, H.; Wang, Z.; Li, X.; Li, X.-F.; Le, X. C. Dynamic DNA Assemblies Mediated by Binding-Induced DNA Strand Displacement. *J. Am. Chem. Soc.* **2013**, *135* (7), 2443–2446. https://doi.org/10.1021/ja311990w.

(86) You, M.; Peng, L.; Shao, N.; Zhang, L.; Qiu, L.; Cui, C.; Tan, W. DNA "Nano-Claw": Logic-Based Autonomous Cancer Targeting and Therapy. *Journal of the American Chemical Society* **2014**, *136* (4), 1256–1259. https://doi.org/10.1021/ja4114903.

(87) Li, F.; Lin, Y.; Le, X. C. Binding-Induced Formation of DNA Three-Way Junctions and Its Application to Protein Detection and DNA Strand Displacement. *Analytical Chemistry* **2013**, *85* (22), 10835–10841. https://doi.org/10.1021/ac402179a.

(88) Karagiannis, P.; Fujita, Y.; Saito, H. RNA-Based Gene Circuits for Cell Regulation. *Proc. Jpn. Acad., Ser. B* **2016**, *92* (9), 412–422. https://doi.org/10.2183/pjab.92.412.

(89) Delebecque, C. J.; Lindner, A. B.; Silver, P. A.; Aldaye, F. A. Organization of Intracellular Reactions with Rationally Designed RNA Assemblies. *Science* **2011**, 1206938. https://doi.org/10.1126/science.1206938.

CHAPTER 2: BIOMIMETIC MOLECULAR SIGNALING USING DNA WALKERS ON MICROPARTICLES

Published in: "Damase, T. R.; Spencer, A.; Samuel, B.; Allen, P. B. Biomimetic Molecular Signaling Using DNA Walkers on Microparticles. Scientific Reports 2017, 7 (1), 4081."

We report the release of catalytic DNA walkers from hydrogel microparticles and the detection of those walkers by substrate-coated microparticles. This might be considered a synthetic biology analog of molecular signal release and reception. One type of particles was coated with components of a DNA one-step strand displacement (OSD) reaction to release the walker. A second type of particle was coated with substrate (or "track") for the molecular walker. We distinguish these particle types using fluorescence barcoding: we synthesized and distinguished multiple particle types with multicolor fluorescence microscopy and automated image analysis software. This represents a step toward amplified, multiplex, and microscopically localized detection based on DNA nanotechnology.

2-1. Introduction

DNA nanotechnology has demonstrated the ability to build static objects and dynamic machines at the nanometer scale with molecular precision. Designed DNA reaction-diffusion systems have performed feats of biomimetic computation: they have recapitulated oscillating patterns in a reaction diffusion system[1] and are moving toward biomimetic regulatory and signaling pathways[2]. DNA origami[3] has been used to build 3D objects[4] from DNA that move and react to stimuli[5]. However, these systems are not practical for observing chemical information exchange among microscale objects. We hope to move toward tools that could be used to explore biological phenomena within the cellular microenvironment such as cytokines and extracellular miRNA. These species are important biomarkers for nerve injury and cancer[6–8]. We present one step toward more practical bioanalytical applications of DNA nanotechnology. This paper describes a system that can release a molecular walker from one particle type and detect that walker using a second particle type.

DNA circuits are DNA-DNA reactions in which base-pairing rules are used to construct specific reactions and reaction networks. The field of DNA computation has demonstrated a remarkable array of such DNA circuits for performing logical operations and amplification. One simple and robust DNA-DNA reaction is the one step strand displacement (OSD) reaction[9]. In this reaction, an input single-stranded DNA (ssDNA) oligonucleotide binds to a 2-part DNA complex. The interaction is initiated using a short single-stranded "toehold." The input ssDNA displaces an output strand and forms a longer and more stable duplex. The displaced ssDNA strand can then serve as an input for further such OSD

reactions. Complex pathways can be designed. In one example, a set of more than 30 OSD reactions were integrated to compute the square root of a four-bit binary number[10]. Arrays of DNA-bearing particles have also been used to execute complex communication. DNA polymerase was used to drive rationally designed DNA circuits on particle surfaces[11].

Enzyme-free DNA circuits can also amplify a molecular signal. In catalytic amplifiers, one input can produce many output molecules. One example is the catalytic hairpin assembly (CHA) reaction[12]. The CHA reaction starts with unstable, kinetically trapped DNA hairpins which in presence of catalyst strand assembled into a more stable double-stranded DNA (dsDNA) duplex. Many detection methods can report the amplified output[13]. Enzyme-free signal amplification using DNA circuits offer advantages over enzymatic amplification: they can be dehydrated, are robust to temperature change and are more easily re-designed for new targets[14]. Our work has shown that these circuits can also be immobilized on particles; the output of the reaction can then be measured using fluorescence microscopy[15].

Microparticle-based sensing offers advantages in terms of multiplexing[16], simplicity[17] and automation[18]. Other labs have demonstrated particle multiplexing using lithographically generated shapes[19], size[20] and fluorescence spectrum[16]. Microparticles have been used as affinity capture as well as for sandwich assays read out by flow cytometry or microscopy. The use of a fluorogenic assay simplifies the experiment further as it alleviates the need to wash the particles[20].

We set out to immobilize an amplifying DNA circuit on the surfaces of hydrogel microparticles. We used a molecular walker based on the entropically driven amplifier (EDA)[21] from the Zhang lab's. The EDA is designed so that two input molecules react to generate three product molecules. The resulting gain in entropy drives the reaction. One of the reaction products is a regenerated catalytic domain. (see **Supporting Information Online** Figure A- S1 for a detailed circuit comparison between our design and that by Zhang et. al.[21]). By incorporating two catalytic domains on the same molecule (a divalent DNA strand displacement catalyst), we bias the molecule to remain persistently on a single particle bearing the substrate. Previous work has shown that this basic approach produces catalytic activity that is constrained to the surface of a particle[22]. We refer to this divalent catalyst as a DNA walker. It takes a "step" when one catalytic domain completes a reaction and is released, but the other domain remains bound to substrate. As long as one leg re-binds before the other leg is released, the walker will crawl over the surface of the particle, leaving behind a trail of fluorescent reaction product.

We made particles that released walker molecules and other particles that detected the walkers. We use fluorescence barcoding to identify the two particle types. We released a DNA walker from blue "release microparticles," whereas the DNA walker was detected using with green "detector microparticles." Different particle types were generated with barcoded fluorescence intensity ratios in the green (λ_{ex} 490 nm) and blue (λ_{ex} 400 nm) channels in order to identify the specific particle type in a multiplex analysis. The detector particles were generated with the EDA substrate (TR-SB-Q_{EDA}) immobilized on their surface. The molecular walker persisted on the surface of the detector particles and generated significant fluorescence despite extremely low average concentration. In our design, a fluorogenic DNA reaction product is detected in the red channel (λ_{ex} 580 nm). We demonstrate that the multiplex capability can be extended further. We generated three particle types and used custom automated image analysis to selectively quantify the red fluorescence response among blue green and teal particles.

2-2. Results

2-2.1. Generation of hydrogel particles

We synthesized fluorescent hydrogel microparticles coated with DNA. We generated these polyacrylamide hydrogel particles by emulsion and radical polymerization. We synthesized our own particles rather than using commercially available particles because commercial fluorescent particles are too bright. Even a small amount of bleed-through into the red channel distorts the quantification.

Acrylamide/bis-acrylamide prepolymer was dispersed into microdroplets by extrusion or homogenization in mineral oil. The microdroplets were polymerized into microparticles. DNA was included in the prepolymer mixture. This DNA complex was synthesized with a cholesterol and an acrydite modification. The hydrophobic cholesterol caused the DNA to associate with the aqueous/oil interface when the water was dispersed in the oil. When the hydrogel polymerized, it incorporated the acrydite into the polymer. This locked the DNA in place at the surface of the particle (see **Methods**). In our previous work[15], we compared the cases with and without the cholesterol-modified DNA. Fluorescence microscopy showed localization of the fluorescent DNA to the margin of the particle only in the case where the cholesterol was added. We applied Texas Red modified DNA complex (TR-Q_{OSD} or TR-SB-Q_{EDA}). We used an OSD reaction to remove the cholesterol-DNA and add the TR complex.

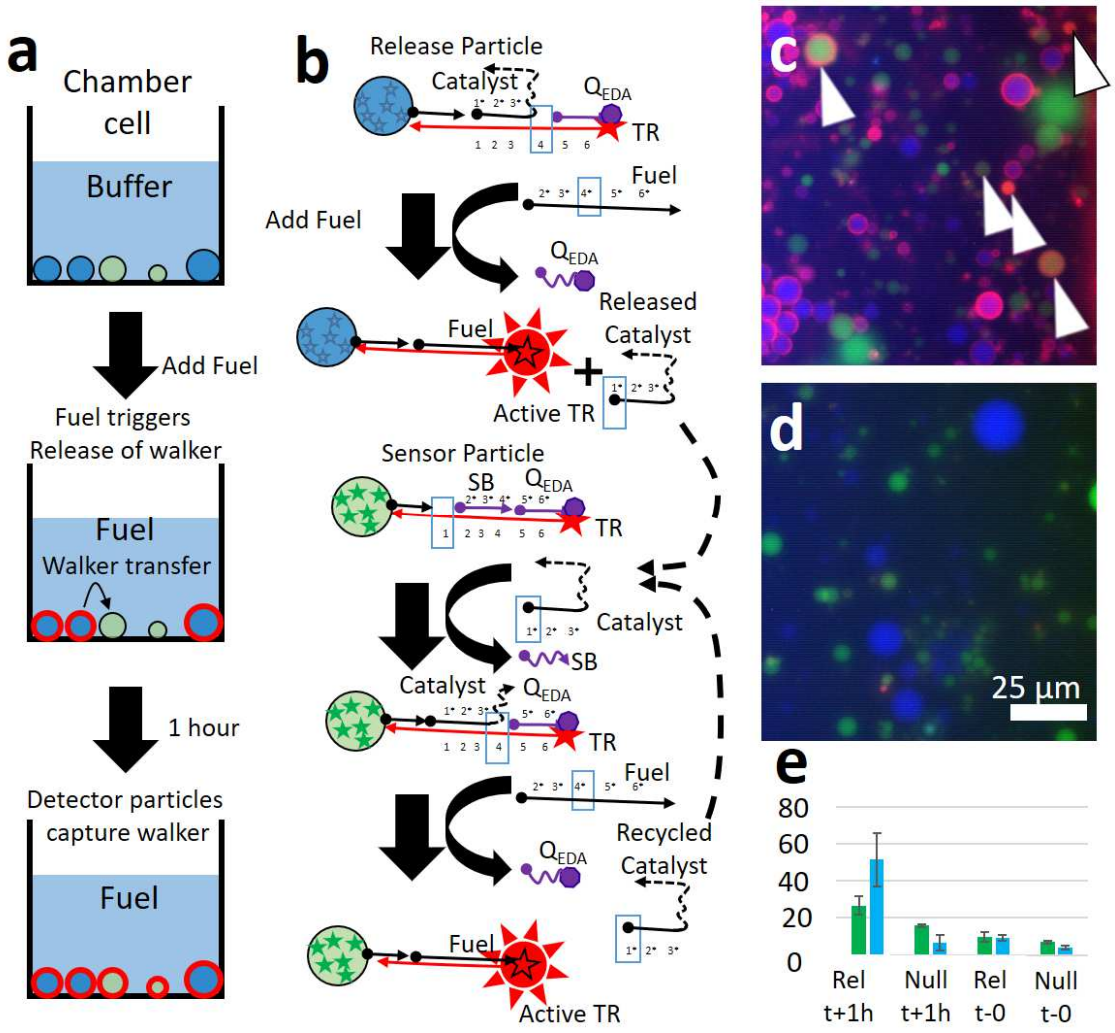

Figure 2- 1: Demonstration of molecular walker release and capture. (a) A schematic showing the experimental steps for walker release and detection. (b) A schematic showing how Cascade Blue dyed (blue) particles released the DNA walker in response to fuel; the DNA walker diffused to fluorescein-dyed (green) sensor particles and acted to de-quench Texas Red on their surfaces (arrows). (c) Fluorescence micrograph shows fluorescein dyed sensor particles and cascade blue release particles after incubation for 1 hour with fuel. (d) Fluorescence micrographs of the control system with blue particles bearing SB instead of the DNA walker after incubation for 1 hour with fuel. (e) Bar graph shows the average red fluorescence of the blue and green particles before and after addition of fuel from 8 or more images. Error bars represent the standard deviation of the particle intensities.

2-2.2. Microscopically localized detection of diffusing DNA walker

We released DNA walker molecules from release particles and detected these walkers using a set of detector particles. The detector particles were assembled with an immobilized substrate for the entropy driven amplifier (EDA) circuit on their surfaces. The mechanism of the EDA is shown in Figure 2-1(b). This circuit was adapted from the EDA published by Zhang et al[21]. The functionality of the circuit

in free solution was also verified by gel electrophoresis (see Figure A- S1). The walkers were a bivalent version of the EDA catalyst.

Release and detector particles were settled on the surface of a chamber slide and viewed with a fluorescence microscope. The walkers were released from blue-dyed particles. Green-dyed detector particles captured and reported the walkers. The walker catalyzed a fluorogenic EDA reaction, causing the green particles to display red fluorescence. Figure 2- 1(c) shows representative initial and final fluorescence state of the release (blue) and detector (green) particles. Initially, no particles were fluorescent in the red channel. A single-stranded DNA molecule was added to the system (denoted "fuel"). This fuel molecule served two purposes: 1. it released the molecular walkers from the blue-dyed particles by an OSD reaction; 2. it participated in the catalytic reaction of the molecular walker on the surface of the green particles.

The fluorescent rings around some particles correspond to many fluorophores within the focal plane of the microscope. Because our particles have a wide size distribution, some particles are not in focus. These do not show clear rings of fluorescence and sometimes appear as a solid spot. Other particles may contain fewer DNA molecules. We compensate for this by averaging data from many particles using an automated image analysis system as described below.

We collected 8-14 images before and after adding the fuel molecule. We processed these images using automated image analysis software to extract average responses from the blue particles and green particles. The results show that the blue particles become highly fluorescent after adding fuel. The green particles also become fluorescent after adding fuel; this only occurs when DNA walker is present and so we can infer that the DNA walker was transferred to the green particles. The negative control case (Figure 2- 1(d)) shows that when the release particles lack the DNA walker (blue particles are coated with TR-SB-Q_{osd} instead), neither the blue nor the green particles show strong red fluorescence. Gray-scale fluorescence intensity images for the components of the false-colored micrographs are included in **Supporting Information Online** as Figure A- S2.

As shown in the schematic in Figure 2- 1(a), 1 µl of dilute particles were added to 40 µl of reaction buffer in a well slide on the microscope. At most, the particles carried 1 pMol of immobilized catalyst (assuming zero losses during particle synthesis, washing, and dilution). This gives a maximal bound of 2.5 nM final average concentration. This is already lower than the LOD for bulk concentrations of catalyst (as described below in Figure 2- 2). In fact, most (>90%) of the particles were removed by the subsequent washing (to leave only a scattering of particles adhered to the surface). A more reasonable

estimate of the average concentration is less than 0.3 nM. Therefore, we conclude that the transient, high concentration after release produced the response on the green particles.

2-2.3. Mechanism and performance of DNA walker

The green particles detect the walker only because the walker is persistently associated with the particle surface. Our detector particles responded to catalytic walker at a concentration that was transiently high (immediately after release) but which decreased to sub-nanomolar concentrations after diffusion. The detector particles are not sensitive enough to detect the walker at these low concentrations. We tested the limit of detection of the DNA walker in order to interpret the release-and-capture experiment.

We first tested the limit of detection for the detector circuit in solution (without particles) against DNA walker in solution. The DNA walker permits the rearrangement of the other DNA species into a more stable conformation. In our designed reaction, the product is fluorescent. The rate of rearrangement into the fluorescent product configuration is very slow without the DNA walker; the reaction rate increases by several orders of magnitude in the presence of the DNA walker.

We adapted a catalytic circuit originally published by David Zhang et. al.[21] Our circuit design is shown in Figure 2- 1(b). We made three changes to the original design: 1) we simplified the circuit to include the fluorogenic reporter in the substrate; 2) we reoriented the design to allow for the key chemical modifications in the appropriate positions (e.g. the acrydite is only available as a 5' modification); 3) our version of the catalyst was divalent with two catalytic domains. This divalent catalyst is called a DNA walker because it remains persistently bound to the particles over multiple turnovers. The use of polyvalency to allow for walking behavior has been presented elsewhere[12,22,23]. The release-and-catch experiment shown in Figure 2- 1 highlights the best performance of the system. For a detailed comparison of our circuit to the original, see **Supporting Information Online**, Figure A- S1**.** Figure 2- 2 shows the operation of this circuit and that it was immobilized on the surface of the microparticles. The particles become fluorescent when the DNA walker was added.

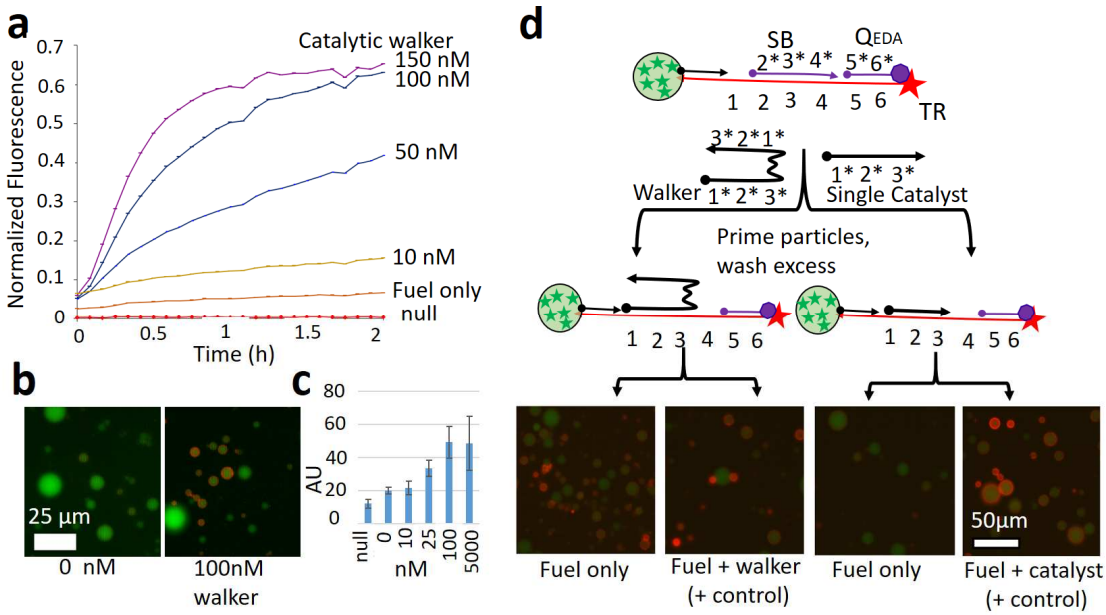

Figure 2- 2: Demonstration of the catalytic circuit in solution. (a) Graph of fluorescence over time shows how the fluorescence of the DNA increases with increasing DNA walker concentrations. (b) End-point fluorescence micrographs of detector particles after incubation with DNA walker for one hour. (c) Average particle fluorescence as observed in the fluorescence microscope (error bars are the standard deviation of the averages of three images) (d) Schematic and end-point fluorescence micrographs showing the high persistence of the walker.

Individually, fuel or DNA walker are unable to displace the quencher from the Texas Red complex. Once the DNA walker displaces the SB (blocker) strand, the fuel can displace the quencher and DNA walker (so that the catalytic domain is recycled). We combined substrate (TR-SB-Q_{EDA}) and fuel in a 384 well plate with various concentrations of the DNA walker. The resulting increase in fluorescence is shown in Figure 2- 2(a). The plate reader data (solution phase) suggests that we are able to detect a presence of 10 nM initiator.

We performed the catalytic EDA reaction with TR-SB-Q_{EDA} on the surface of detector particles. We allowed a range of DNA walker concentrations to react with the particles for 1 hour. We examined the results using fluorescence microscopy. Fluorescence micrographs are shown in Figure 2- 2(b). The data show a clear increase in the endpoint fluorescence as the quantity of DNA walker increases. We analyzed image data from six conditions. We measured the average particle fluorescence over all of the particles in a given image. The results are shown in Figure 2- 2(c). Microscopy data (on particles) suggest a limit of detection of 16 nM with the LumaView LED-based microscope. The LOD in terms of the average solution phase walker concentration is not adequate to detect the ~0.3 nM average concentration of walker in the release-and-catch experiment. The transiently high concentration after release accounts for the detection of walker by the detector particles.

2-2.4. Divalent walker is necessary to detect transient exposure

We performed controls to show that the double catalyst is a persistent walker on the surfaces of micro-particles. We also show that the walker (with two catalytic domains) is necessary for high persistence and strong response to transient exposure to catalyst. A non-walker catalyst (with only a single catalytic domain) has lower persistence on the particle surface. We transiently exposed substrate particles to 25 nM double catalyst or 50 nM single catalyst (equivalent number of catalytic domains). After one minute, the unbound catalyst was removed by centrifugation and resuspension in buffer. Even the single catalyst binds to the substrate with 22 bases of hybridization. This has a binding energy of 27 kcal/mol and the dissociation constant of 1×10^{-20} (per OligoCalc[24]). This is essentially a permanent association (without fuel to provide the energy to displace the catalyst). The double catalyst interacts even more strongly. The resulting "primed" particles were then incubated with fuel for one hour (See Figure 2-2(d)). Only the double catalyst had significant response. The persistence of the double catalyst allowed it to 'walk' through multiple catalytic turnovers while the single catalyst was essentially immediately released.

2-2.5. Mechanism and performance of the OSD reaction

To show the advantages of amplification with the walker, we also characterized the sensitivity of a simple strand displacement reaction. The sensitivity of the one-step strand displacement (OSD) reaction was lower than that achieved by amplification with the DNA walker. This characterization also demonstrates the reactions used to build and operate our detector particles. OSD reactions were used to immobilize the molecular walker substrate complex on the particles and to release the molecular walker from the release particles. OSD reactions are not catalytic but are simple and reliable. We demonstrate the functionality of the OSD reaction in Figure 2- 3. A simple fluorogenic complex on particles is activated using an OSD reaction. Particles were generated containing fluorescein-modified poly-T (without cholesterol, to visualize the particles in green fluorescence prior to surface detection). Figure 2- 3(a) shows how green microparticles were coated with the fluorogenic DNA complex and how the cholesterol-modified strand was removed. The particle is initially coated with the acrydite and cholesterol DNA. When this particle encounters its complementary ssDNA, it hybridizes to the surface-bound complex and displaces the cholesterol DNA.

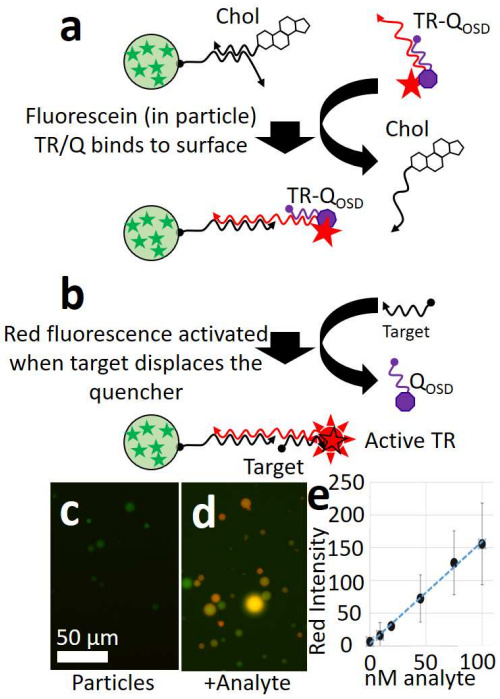

Figure 2- 3: Demonstration of OSD reaction on particle surface. (a) schematic shows how sensor particles are prepared. Cholesterol DNA is displaced by the quenched detector complex (TR-QOSD). (b) A schematic shows how the presence of TR-QOSD was verified. A specific ssDNA displaces the quencher molecule (QOSD). This results in increased Texas Red fluorescence on the microparticle surface. (c) Fluorescence micrograph shows initial green fluorescence of the sensor microparticles. (d) Fluorescence micrograph shows the increased red fluorescence after addition of ssDNA. (e) Calibration curve shows the mean fluorescence and standard deviation among several images at various concentrations of ssDNA.

A second OSD reaction can also remove the quencher (see Figure 2- 3(b)). The displacement of the quencher results in the activation of the fluorophore on the microparticle surface. This shows that the TR complex was added and is available to react further. Figure 2- 3(c) shows the initial green fluorescence of the particles; Figure 2- 3(d) shows the results after the ssDNA displacer was added to the mixture. The particles show a clear increase in red fluorescence. The red fluorescence intensity was quantified using automated image analysis software (see below).

The calibration curve in Figure 2- 3(e) shows the average intensity of the particles in 4-6 images. The standard deviation from image to image is shown as the error bars. The results indicate that we can achieve a limit of detection (LOD) of approximately 25 nM with the OSD reaction and the Lumaview LED microscope. Using a more sophisticated and sensitive confocal microscope, the limit of detection was <10 nM for a ssDNA displacer (as shown in **Supporting Information Online**, Figure A- S3).

2-2.6. Blue/green fluorescence barcoding

Our image analysis software required a clear distinguishing feature between release and detector particles. We used the fluorescence response in green and blue to identify the two particle types. We generated particles with very different fluorescence emission profiles. We performed controls and characterizations to show that we could detect specific reactions on barcoded particles using OSD reactions. We generated three different types of particles containing different ratios of green and blue fluorophores. By immobilizing different fluorogenic sensors on the surfaces of each type of particle, we were able to detect three different DNA species.

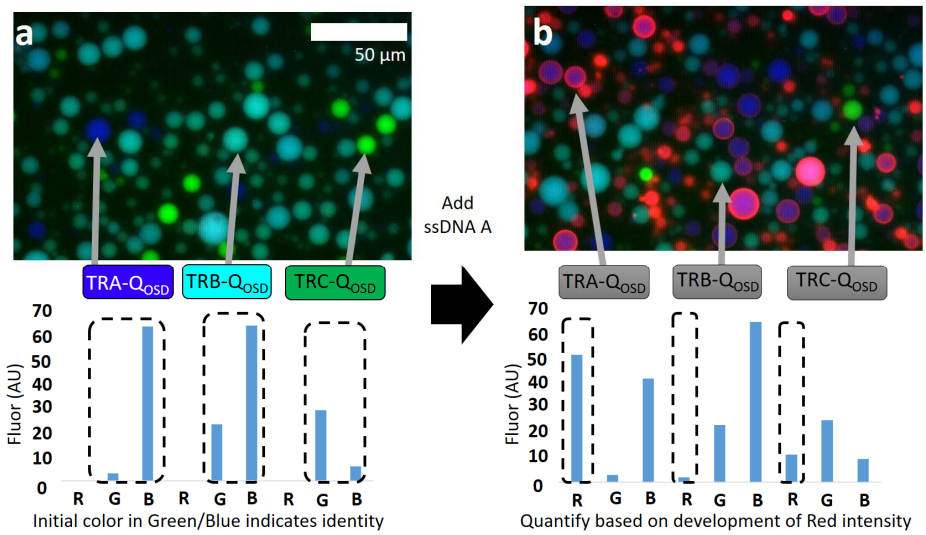

Figure 2- 4: Multiplex particles using blue and green fluorescence. (a) fluorescence micrograph and bar graph show the microparticles and corresponding fluorescence intensities in the red, green and blue channels before addition of ssDNA A. (b) Fluorescence micrograph and bar graph show resulting fluorescence intensities of the microparticles after addition of ssDNA A.

Each immobilized DNA complex bears a quenched Texas Red fluorophore and a toehold sequence specific for one ssDNA displacer. As a consequence, the three particle types display red fluorescence in response to the addition of a particular ssDNA. Figure 2- 4 shows fluorescence micrographs before and after adding ssDNA A which is specifically reported by TR_A-Q_{OSD}. The OSD reaction proceeded as outlined above (and shown in Figure 2- 4(a)). Green, blue, and teal particle types can be identified by the specific ratio of red and green fluorescence. The concentration of ssDNA A could be inferred by the red fluorescence immobilized on the blue particle type (Figure 2- 4(b)). Grayscale fluorescence intensity images for the components of the false-colored micrographs are included in **Supporting Information Online** as Figure A- S4.

This simple case shows that the particles respond specifically despite the fact that the sequences of the three ssDNA displacers are the same over two thirds of their length. Strand displacement probes of this kind in solution have high specificity[25]. Our particle-based application of this system shows a strong signal in the red channel. The use of fluorescein, pacific blue and Texas Red dyes at these low concentrations did not produce bleed through of the blue and green fluorescence into the red channel (which would complicate quantification).

2-2.7. Multiplex fluorescent data analysis with Python

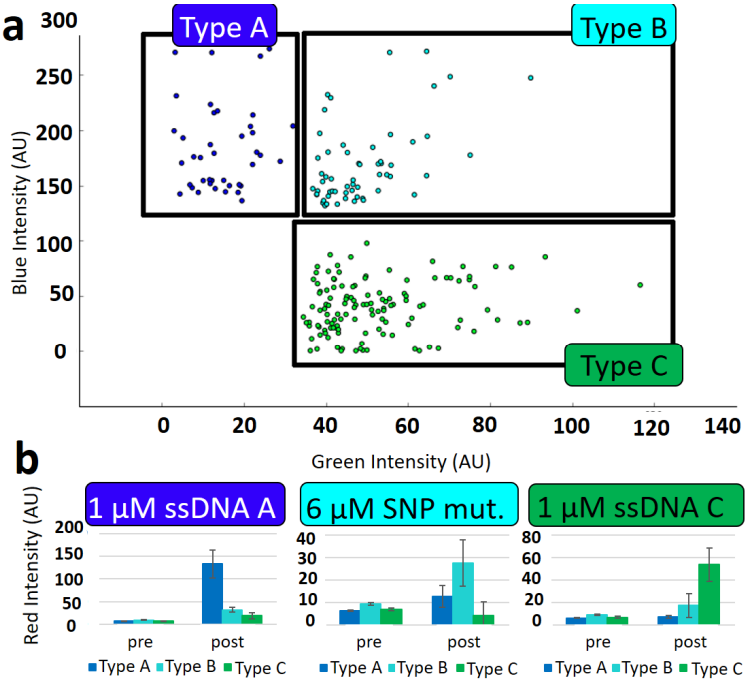

Figure 2- 5: Results of automated image analysis using Python. (a) Images of particles are sorted according to their blue/green fluorescence. A scatter plot shows how the blue, green and teal particle data are sorted. (b) Red fluorescence intensity is graphed before and after adding the respective ssDNA. Error bars are the standard deviation of the mean of 9 images.

To process many images of release and detector particles, we used automated image analysis software (see **Supporting Information Online**). We show that this software can discriminate three different particle types and quantify their red fluorescence. Blue, teal, and green particles were generated as above to respond to ssDNA A, B, and C, respectively. Experimental samples of a mix of all three particle types were exposed to high concentrations of ssDNA A, and C. We also exposed the particle mix to a single nucleotide polymorphism (SNP) mutant of ssDNA B. This was designed to differ by one base from ssDNA B. The resulting fluorescence micrographs were processed using our software. That program examines the images and finds bright objects in the blue and green channels. The program

sorted the objects according to their green and blue fluorescence as shown in the scatter plot in Figure 2- 5(a). For example, objects showing strong blue fluorescence and low green fluorescence were designated as Type A particles. Teal and green objects were processed similarly.

Type A and C particles responded specifically to their respective ssDNA. No particles responded strongly to ssDNA B SNP. Type B particles responded at less than 50% maximum intensity even at extremely high concentration of 6 μM. The highest crosstalk was between the ssDNA B SNP and the blue (Type A) particles. This may be due to the two bases of sequence similarity between ssDNA A and B. Based on these results, we chose the Type C acrydite DNA to attach the TR complex for the release particles and detection particles (the TR complexes in Figure 2- 1).

The software was able to discriminate the response of the three particle types to three different ssDNA species. Despite potential issues surrounding the OSD reaction specificity, the software reliably found and sorted particles in the image data. Red fluorescence from blue, green and teal particles was measured with no significant interference from the green or blue barcoding channels.

2-3. Discussion

We set out to show that a DNA circuit could amplify a molecular signal exchanged between microparticles. We achieved this using a DNA walker released from blue-dyed hydrogel microparticles and captured by green-dyed hydrogel microparticles. The green-dyed detector particles were synthesized with the walker's fluorogenic substrate on their surfaces. This was meant to be similar to the exchange of soluble chemical signals among cells.

Hydrogel particles with a similar size to cells were synthesized by dispersion polymerization. The DNA was self-organized on the particle surfaces with a cholesterol modification. The particles can be identified by a fluorescence barcode in the blue and green wavelengths with simultaneous quantification by red fluorescence. Simple OSD reactions that de-quench Texas Red fluorophores showed a limit of detection of 25 nM (limited by the sensitivity of our microscope). The DNA walker reaction can also de-quench Texas Red fluorophores. The DNA walker reaction could be detected with a LOD of 16 nM with the LED-based epifluorescence microscope. It also allowed for capture and detection of a DNA walkers released from particles on the surface of the chamber slide.

The walker enabled detection by its persistent association with the detector particle. The walker was a divalent catalyst for the EDA circuit. The immobilized OSD and non-walker EDA reactions are both insufficiently sensitive to detect the DNA released from other particles. When DNA is released, it is

rapidly diluted. The total quantity of release particles was limited to the small number retained on the microscope slide (and thus, the total quantity of DNA walker was very small). We conservatively estimate that the final concentration of DNA walker in the sample was sub-nanomolar. Without some way to retain the molecules at the initial concentration, the final concentration would be far below the limits of detection. The polyvalent DNA walker was retained by the detector particles through multiple turnovers of the EDA reaction. The released DNA walkers were thus successfully reported by the detector particles because of the high transient concentration upon release.

This work shows the utility of a particle platform to report the activity of DNA reactions. As this technology matures, it may help to enable the detection of diffusing analytes locally around cells. This would require a "transducer" such as a conformation changing aptamer[26] that could activate the walker upon binding.

2-4. Methods

2-4.1. Generation of hydrogel particles

DNA was purchased from IDT (Integrated DNA Technologies Coralville, IA) and was used without further purification unless otherwise noted. See **Supporting Information Online** for sequence information. Our technique for generating hydrogel particles has been described in detail elsewhere[15]. Briefly, we prepared 100 µl of a prepolymer mixture containing 10µM cholesterol/acrylamide-modified DNA complex, 20% w/v acrylamide (Research Products International Corp, IL 60056 USA), fluorescently labeled poly-T DNA (fluorescein and/or Pacific Blue conjugated acrydite-modified DNA as described below), 10% w/v ammonium persulfate (Bio-Rad Laboratories, Hercules, CA), and phosphate buffer (pH 6.8, 50 mM sodium phosphate, 50 mM sodium chloride, both from EMD Chemicals, Gibbstown, Germany). This mixture was homogenized in 1 ml a solution of 1% Span-80 (Sigma-Aldrich, St Louis) in mineral oil (Cococare Products, Dover, New Jersey) by shearing with a 2 mm steel shear mixer in a rotary tool for 4 min at 10,000 rpm. To this solution we added 8 µl of TEMED (Bio-Rad Laboratories, Hercules, CA) to initiate polymerization. The suspension was placed in a nitrogen atmosphere and shaken to remove oxygen. The suspension was allowed to polymerize for 60 minutes (see Figure 2- 6). The suspension was then washed free from oil by repeated centrifugation and resuspension in 70% ethanol (Pharmco-AAPER, Brookfield CT). After all oil was removed, the suspension was dried in a gentle stream of air for ~30 min. The particles were then resuspended in the working buffer. The fluorogenic DNA complex (the appropriate version of TR and Q) was annealed by heating to 85 °C for 2 min then cooling at 0.1 °C per min to room temperature in working buffer and then

incubated with the particles. The TR strand was designed with a toehold and complementary region to the acrydite-modified DNA. It displaced the cholesterol-modified DNA by an OSD reaction. The particles were then washed three times with working buffer and refrigerated until use. The resulting range in size from 1 to 10 microns (easily visible with light microscopy).

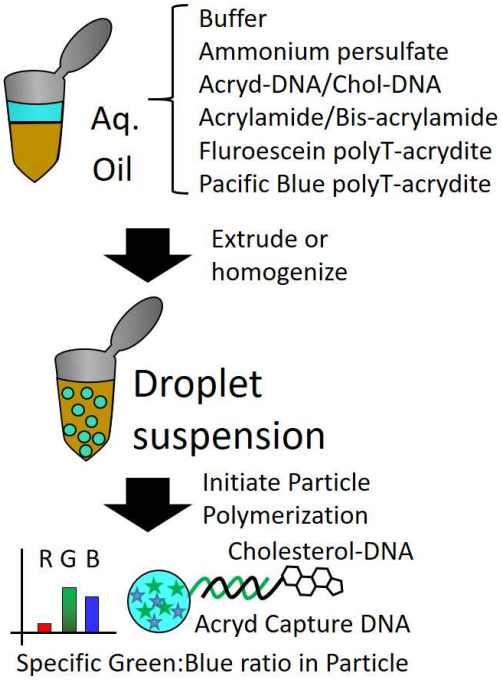

Figure 2- 6: Schematic of procedure for generating DNA-decorated, polyacrylamide hydrogel microparticles.

2-4.2. Demonstration of fluorogenic DNA assay

We show that the DNA immobilized on the surface can be designed to increase in fluorescence in response to an unlabeled oligonucleotide. We prepared a fluorogenic reporter complex for ssDNA C (see **Supporting Information Online** for sequences). This was made of a final concentration of 1 µM TRC (HPLC purified), 1 µM Q_{OSD} (HPLC purified) in phosphate buffer. This was annealed as above. We incubated the particles (as generated above) with the DNA reporter complex. The particles were allowed to settle on a chamber slide and then incubated with various concentrations unlabeled ssDNA C (AnaC) oligonucleotide for 30 minutes. Samples of the particles before and after the addition of various concentrations of the ssDNA were observed on the fluorescent microscope (LumaScope 620, EtaLuma, Carlsbad, CA). This microscope uses 3 LED illumination sources to illuminate different fluorophores. False color images are generated by combining a red channel (λ_{ex} 580nm), green channel (λ_{ex} 490nm) and blue channel (λ_{ex} 400nm).

2-4.3. Generation of fluorescein- and Cascade Blue-labeled poly-T

Dual-modified acrydite/fluorescein poly-T DNA was acquired from IDT and used without further purification. Dual-modified 5'-acrydite and 3'-amine poly-T DNA was acquired from IDT and derivatized with Cascade Blue succinimidyl ester (Thermo-Fisher, Waltham, MA) according to manufacturer's instructions. The resulting product was then purified using size exclusion columns (Thermo-Fisher, Waltham, MA). The product was stored at -20°C in water until needed.

2-4.4. Multiplexed red-fluorescent detection with blue/green fluorescence barcoding

Three different versions of the Texas Red DNA (denoted TRA, TRB and TRC) were designed with three corresponding oligonucleotides (denoted ssDNA A, ssDNA B, and ssDNA C). The designs differed only in their toehold regions and so shared a common quencher (denoted Q_{OSD}). The three reporter complexes were immobilized onto three different particle batches as described above. In order to differentiate the particle types, the particles were generated with different ratios of fluorescently-labeled polyT DNA. Particles bearing TRA were dyed blue by including 2 μM pacific blue conjugated acrydite-DNA. Particles bearing TRB were dyed teal by including 6 μM fluorescein conjugated acrydite-DNA and 2 μM pacific blue conjugated acrydite-DNA. Particles bearing TRC were dyed green by including 1 μM fluorescein conjugated acrydite-DNA. These particles were added to a chamber slide and allowed to settle. The chamber was then gently rinsed with reaction buffer. Particles were then observed with a fluorescence microscope and their fluorescence quantified using automated image analysis software (see **Supporting Information Online**). Data representing strong blue, green, or blue/green fluorescence were sorted into appropriate categories (Figure 2- 5(a)). The appropriate ssDNA was then added (ssDNA A, 1 μM; ssDNA B SNP, 6 μM; ssDNA C, 1 μM) and the samples were incubated for 15 minutes. The particles were again observed with a fluorescence microscope and their fluorescence quantified.

2-4.5. PAGE analysis of catalytic assembly circuit

We ran native PAGE analysis of our adapted Zhang EDA circuit. We made a 10% polyacrylamide gel with sodium borate running buffer. We loaded 2 μl of NEB low molecular weight ladder in lanes 1 and 8. We assembled reactions and controls as follows: Lane 2, Negative Control: TR-SB-Q_{EDA} complex at 2 μM. Lane 3, Intermediate control: TR-SB-Q_{EDA} complex at 2 μM and mono-valent catalyst extended with 10 bases of poly-T at 2uM. Lane 4, No-catalyst (reaction leakage) control: TR-SB-Q_{EDA} complex at 2 μM and Fuel extended with 10 bases of poly T at 10 μM. Lane 5, Positive Control: TR at 2 μM and Fuel extended with 10 bases of poly T at 20 μM. Lane 6, Experimental: TR-SB-Q_{EDA} complex at 2 μM,

catalyst at 2uM and Fuel extended with 10 bases of poly T at 10 μM. Lane 7, Experimental with extended catalyst: TR-SB-Q_{EDA} complex at 2 μM, catalyst extended by 10 bases of poly T at 2uM, and Fuel extended with 10 bases of poly T at 10 μM.

2-4.6. Amplification of fluorescent signal using catalytic DNA circuit

DNA circuit components were assembled in circuit buffer (50 mM phosphate, 500 mM NaCl, pH 6.8). TR and a slight excess of Q were annealed. A slight excess of SB was added and the mixture was allowed to react for 30 min. The final concentration of the TR-SB-Q_{EDA} complex was 1000 nM and the final concentration of fuel was 1000 nM (in all cases except negative control from which fuel was omitted). A 384 well plate was blocked with superblock (Thermo-Fisher, Waltham, MA) for 1 hour at room temperature then washed with circuit buffer. Catalyst DNA/DNA walker or buffer was then added to the TR-SB-Q_{EDA} solution achieve the final concentration shown in Figure 2- 2(a). The samples were then transferred to the prepared 384 well plate. The plate was read with a fluorescence plate reader (Beckman-Coulter, Pasadena, CA).

2-4.7. Detection of global DNA walker by particles

We prepared green particles bearing the TR-SB-Q_{EDA} DNA. The complex was assembled as described above. The particles were prepared with capture DNA on their surface also as described above. The TR-SB-Q_{EDA} complex was incubated with the particles for 1 hour then excess complex was washed away. The particles were then refrigerated until use. We suspended these particles in 18 μl of circuit buffer and allowed the particles to settle to the bottom of a chamber slide. We then added 1 μl of 5 μM fuel and 1 μl of the appropriate 20x concentration of DNA walker (to a final concentration shown in Figure 2- 2(c)). We acquired fluorescence data after incubating for 1 hour at 37 °C. The red fluorescence intensity was quantified using automated image analysis software (see **Supporting Information Online**) and is shown in Figure 2- 2.

2-4.8. Microscopically localized detection of diffusing DNA walker

Blue particles were prepared as above bearing the TR-Q_{EDA} complex; the SB was omitted, and DNA walker was substituted. We denote these particles “release particles” as fuel can directly displace the DNA walker (see detailed schematic in **Supporting Information**, Figure -A S3). We prepared green particles bearing the TR-SB-Q_{EDA} complex as “detector particles” for the DNA walker as described above. We mixed 1 μl of each particle type and 18 μl of circuit buffer and allowed the particles to settle to the bottom of a chamber slide. We then added 1 μl of 5 μM Fuel (but did not add additional DNA

walker). We added more 20 µl circuit buffer before incubating. We acquired fluorescence data after incubating for 1 hour at 37 °C. The red fluorescence intensity of the green and blue particles was quantified using automated image analysis software (see **Supporting Information Online**) and is shown in Figure 2- 2(b).

We tested the persistence of the non-walker catalyst and the walker catalyst on Green particles bearing the TR-SB-Q_{EDA} complex. The particles were prepared in the same way as detector particles as described above. 50nM single-domain catalyst (non-walker) was added to 10µl of particles in order to "prime" the particles with catalyst. The particles were washed three times with circuit buffer to remove excess, unbound catalyst. 1 µl of washed, primed particles were added to 18 µl of circuit buffer followed by 1 µl of 5 µM of fuel. Incubation was carried out at 37 °C for 1 hour. The results were viewed using an epifluorescence microscope. We added additional 100nM of single catalyst in the positive control case. The equivalent experiment was for double catalyst with 25 nM priming catalyst (equivalent number of active domains). An additional 50nM of double catalyst was added for the positive control case.

2-5. Acknowledgments
This publication was made possible by an Institutional Development Award (IDeA) from the National Institute of General Medical Sciences of the National Institutes of Health under Grant #P20GM103408.

2-6. Author Contributions Statement
P.B.A. and T.R.D wrote the main manuscript text and prepared figures. P.B.A. T.R.D and A.S. contributed to the automated image analysis code. T.R.D. performed microscopy and plate-reader experiments. All authors helped develop particle generation techniques. All authors reviewed the manuscript.

2-7. Competing interests
The authors have declared that no competing interests exist.

2-8. References

(1) Montagne, K.; Plasson, R.; Sakai, Y.; Fujii, T.; Rondelez, Y. Programming an in Vitro DNA Oscillator Using a Molecular Networking Strategy. *Molecular Systems Biology* **2011**, *7* (1), 466.

(2) Padirac, A.; Fujii, T.; Rondelez, Y. Nucleic Acids for the Rational Design of Reaction Circuits. *Current Opinion in Biotechnology* **2013**, *24* (4), 575–580.

(3) Rothemund, P. W. K. Folding DNA to Create Nanoscale Shapes and Patterns. *Nature* **2006**, *440* (7082), 297–302.

(4) Han, D.; Pal, S.; Nangreave, J.; Deng, Z.; Liu, Y.; Yan, H. DNA Origami with Complex Curvatures in Three-Dimensional Space. *Science* **2011**, *332* (6027), 342–346.

(5) Andersen, E. S.; Dong, M.; Nielsen, M. M.; Jahn, K.; Subramani, R.; Mamdouh, W.; Golas, M. M.; Sander, B.; Stark, H.; Oliveira, C. L. P.; et al. Self-Assembly of a Nanoscale DNA Box with a Controllable Lid. *Nature* **2009**, *459* (7243), 73–76.

(6) Genemaras, A. A.; Ennis, H.; Kaplan, L.; Huang, C.-Y. Inflammatory Cytokines Induce Specific Time- and Concentration-Dependent MicroRNA Release by Chondrocytes, Synoviocytes, and Meniscus Cells. *J. Orthop. Res.* **2016**, *34* (5), 779–790.

(7) Tsai, M.-C.; Wei, C.-P.; Lee, D.-Y.; Tseng, Y.-T.; Tsai, M.-D.; Shih, Y.-L.; Lee, Y.-H.; Chang, S.-F.; Leu, S.-J. Inflammatory Mediators of Cerebrospinal Fluid from Patients with Spinal Cord Injury. *Surgical Neurology* **2008**, *70*, *Supplement 1*, S19–S24.

(8) Raig, E. T.; Jones, N. B.; Varker, K. A.; Benniger, K.; Go, M. R.; Biber, J. L.; Lesinski, G. B.; Carson, W. E. VEGF Secretion Is Inhibited by Interferon-Alpha in Several Melanoma Cell Lines. *Journal of Interferon & Cytokine Research* **2008**, *28* (9), 553–562.

(9) Srinivas, N.; Ouldridge, T. E.; Šulc, P.; Schaeffer, J. M.; Yurke, B.; Louis, A. A.; Doye, J. P. K.; Winfree, E. On the Biophysics and Kinetics of Toehold-Mediated DNA Strand Displacement. *Nucl. Acids Res.* **2013**, *41* (22), 10641–10658.

(10) Qian, L.; Winfree, E. Scaling Up Digital Circuit Computation with DNA Strand Displacement Cascades. *Science* **2011**, *332* (6034), 1196–1201.

(11) Gines, G.; Zadorin, A. S.; Galas, J.-C.; Fujii, T.; Estevez-Torres, A.; Rondelez, Y. Microscopic Agents Programmed by DNA Circuits. *Nat Nano* **2017**, *advance online publication*.

(12) Yin, P.; Choi, H. M. T.; Calvert, C. R.; Pierce, N. A. Programming Biomolecular Self-Assembly Pathways. *Nature* **2008**, *451* (7176), 318–322.

(13) Li, B.; Ellington, A. D.; Chen, X. Rational, Modular Adaptation of Enzyme-Free DNA Circuits to Multiple Detection Methods. *Nucl. Acids Res.* **2011**.

(14) Allen, P. B.; Arshad, S. A.; Li, B.; Chen, X.; Ellington, A. DNA Circuits as Amplifiers for the Detection of Nucleic Acids on a Paperfluidic Platform. *Lab Chip* **2012**, *12*, 2951–2958.

(15) Damase, T. R.; Stephens, D.; Spencer, A.; Allen, P. B. Open Source and DIY Hardware for DNA Nanotechnology Labs. *Journal of Biological Methods* **2015**, *2* (3), 24.

(16) Dunbar, S. A. Applications of Luminex® XMAP™ Technology for Rapid, High-Throughput Multiplexed Nucleic Acid Detection. *Clinica Chimica Acta* **2006**, *363* (1–2), 71–82.

(17) England, E.; Newton, P.; Neal, F.; Kitching, L.; Colley, C.; Rossant, C. J. Application of the Mirrorball High-Sensitivity Cytometer to Multiplexed Assays for Antibody Drug Discovery. *J Biomol Screen* **2015**, *20* (4), 536–544.

(18) Berensmeier, S. Magnetic Particles for the Separation and Purification of Nucleic Acids. *Appl Microbiol Biotechnol* **2006**, *73* (3), 495–504.

(19) Meiring, J. E.; Schmid, M. J.; Grayson, S. M.; Rathsack, B. M.; Johnson, D. M.; Kirby, R.; Kannappan, R.; Manthiram, K.; Hsia, B.; Hogan, Z. L.; et al. Hydrogel Biosensor Array Platform Indexed by Shape. *Chem. Mater.* **2004**, *16* (26), 5574–5580.

(20) Horejsh, D.; Martini, F.; Poccia, F.; Ippolito, G.; Di Caro, A.; Capobianchi, M. R. A Molecular Beacon, Bead-Based Assay for the Detection of Nucleic Acids by Flow Cytometry. *Nucleic Acids Res* **2005**, *33* (2), e13.

(21) Zhang, D. Y.; Turberfield, A. J.; Yurke, B.; Winfree, E. Engineering Entropy-Driven Reactions and Networks Catalyzed by DNA. *Science* **2007**, *318* (5853), 1121–1125.

(22) Jung, C.; Allen, P. B.; Ellington, A. D. A Stochastic DNA Walker That Traverses a Microparticle Surface. *Nat Nanotechnol* **2016**, *11* (2), 157–163.

(23) Lund, K.; Manzo, A. J.; Dabby, N.; Michelotti, N.; Johnson-Buck, A.; Nangreave, J.; Taylor, S.; Pei, R.; Stojanovic, M. N.; Walter, N. G.; et al. Molecular Robots Guided by Prescriptive Landscapes. *Nature* **2010**, *465* (7295), 206–210.

(24) Kibbe, W. A. OligoCalc: An Online Oligonucleotide Properties Calculator. *Nucl. Acids Res.* **2007**, *35* (suppl 2), W43–W46.

(25) Yurke, B. Using DNA to Power the Nanoworld. In *Controlled Nanoscale Motion*; Linke, H., Månsson, A., Eds.; Springer Berlin Heidelberg: Berlin, Heidelberg; Vol. 711, pp 331–347.

(26) Zhu, J.; Zhang, L.; Zhou, Z.; Dong, S.; Wang, E. Molecular Aptamer Beacon Tuned DNA Strand Displacement to Transform Small Molecules into DNA Logic Outputs. *Chem. Commun.* **2014**, *50* (25), 3321–3323.

CHAPTER 3: PURIFICATION OF SINGLE-STRANDED DNA BY CO-POLYMERIZATION WITH ACRYLAMIDE AND ELECTROPHORESIS

Published in: "Damase, T. R.; Ellington, A. D.; Allen, P. B. Purification of Single-Stranded DNA by Co-Polymerization with Acrylamide and Electrophoresis. BioTechniques 2017, 62 (6), 275–282."

Single-stranded DNA (ssDNA) oligonucleotides are useful as aptamers, hybridization probes and for emerging applications in DNA nanotechnology. Current methods to purify ssDNA require both strand separation and a separate size separation step and may still leave double-stranded DNA impurities in the sample. We use commercially-available acrydite DNA primers to immobilize one strand of a PCR product within a polyacrylamide matrix. Electrophoresis moves the non-crosslinked DNA into the gel where the single-stranded, size-appropriate product can be recovered. We show that this produces a high yield of pure ssDNA.

3-1. Introduction

Single-stranded DNA (ssDNA) is useful for aptamers[1], self-assembly[2], DNA origami[3], DNA circuits[4], hybridization probes[5], and DNA robotics[6]. Chemically synthesized DNA is single-stranded by default.

We present a method to produce single-stranded DNA from a PCR product. The use of a PCR product may be advantageous over synthetic DNA because PCR introduces fewer mutations than chemical synthesis and is not limited to ~120 bases. Starting from a clonal sample, PCR products can have significantly higher sequence purity than chemically synthesized DNA. High sequence purity is critical for high performance in DNA circuit technology[7].

Our single-strand generation (SSG) method is scalable and requires only one purification step for the removal of the unwanted complementary strand as well as size-based removal of residual primer and unwanted PCR products. SSG by co-polymerization and electrophoresis may be applied to the product of advanced PCR protocols such as Gibson assembly[8] to create long, single-stranded products of arbitrary sequence. This may be of use for DNA origami and other self-assembly applications.

SSG takes advantages of a commercially available DNA modification known as an acrydite. This modification adds a polymerizable vinyl group which incorporates into a growing acrylamide polymer chain[9]. Acrydite modified DNA has been used for a number of applications including a switchable hydrogel [10], capture of mercury [11] or PDGF [12], and for modifying the rate of electrophoresis of specific

sequences [13]. Our technique is superficially similar to the method by which the Church group immobilized polymerase colonies within thin polyacrylamide gels[14]. The acrydite is critical for the formation of clonal PCR products ('polonies') in some forms of DNA sequencing[14].

In cases when significant quantities of pure, single-stranded DNA are required, our approach using acrydite modified primers and polyacrylamide immobilization is a worthwhile option. We also show that this technique can integrate SSG, size separation and electro-elution into a single step.

3-2. Method Summary

Commercially-available 5'-acrydite modified DNA primers to purify ssDNA by immobilizing one strand of a PCR product within a polyacrylamide matrix.

3-3. Results and Discussion

3-3.1. Acrydite modified DNA is immobile under electrophoresis

Of the two strands of the dsDNA PCR product, the acrydite strand is trapped in the co-polymer while the complementary strand is mobile. To demonstrate this, PCR was performed with one primer modified with both acrydite and red fluorescent dye (Cy5). The reverse primer was modified with fluorescein. The PCR product was polymerized into a denaturing PAGE gel (5%). A schematic diagram of the process is presented in Figure 3- 1. Initially, both the green-fluorescent and red-fluorescent strands were co-localized (yellow-colored gel). Upon application of voltage, only the fluorescein-labeled product (green) migrates into the gel. The acrydite and Cy5 co-labeled strand (red) is fixed. This is shown in the final gel image in Figure 3- 1B. Additionally, residual primer from the PCR reaction is clearly visible as a second green band. After electrophoresis, the pure, single-stranded product can be cut and eluted per standard gel purification protocols.

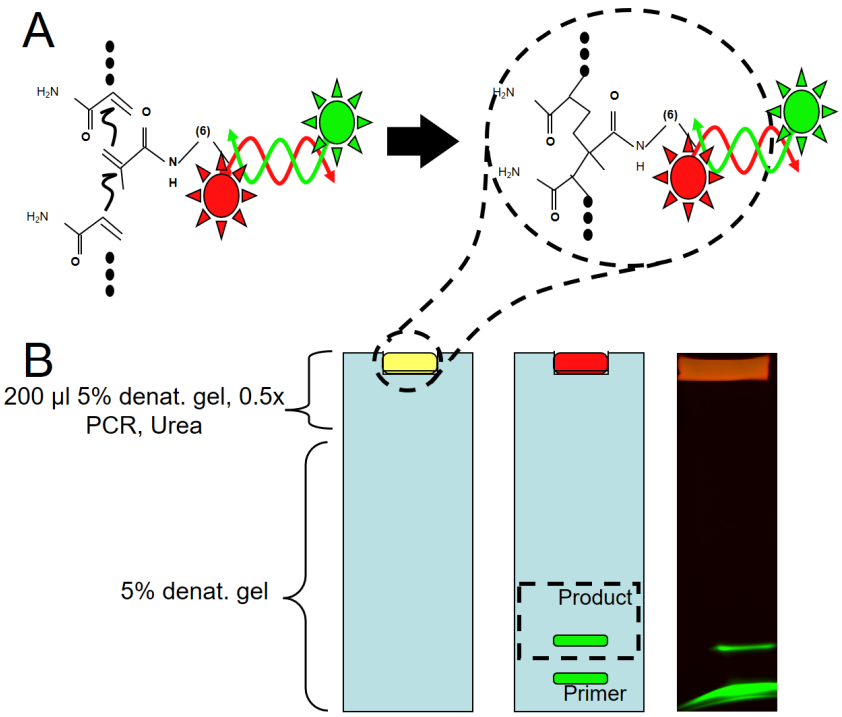

Figure 3- 1: Outline of the single-strand generation (SSG) technique. (A) The schematic shows how double-stranded DNA (dsDNA) is produced from a primer modified with the acrydite and Cy5 at its 5' terminus and a reverse primer modified with fluorescein. These primers produce a double-stranded product. When co-polymerized with acrylamide, this product is immobilized within the polymer matrix. (B) Fluorescence gel image (right) shows that Cy5-modified, co-polymerized strand remains at the top of the gel, while the single-stranded product and primer migrate separately.

3-3.2. Single-stranded DNA verification

We isolated single-stranded, fluorescein-modified DNA by cutting and eluting the band of interest. To show that the product recovered by this method is single-stranded, we used two orthogonal methods. The first method was native gel analysis. Figure 3- 2A shows an image of a native gel of the primer, PCR product (dsDNA), and ssDNA purified by this method. The native gel shows clear separation between the dsDNA and ssDNA. After the single-strand generation with the acrydite primer (followed by cutting the gel and eluting the product) most of the result is single-stranded.

We corroborated with a quencher-modified hybridization probe (see Figure 3- 2B). The probe was designed to bring a quencher into proximity to the fluorescein moiety on the ssDNA product. Upon hybridization, the quencher molecule reduces the fluorescence intensity by ~90%. The probe only hybridizes to ssDNA and so this demonstrates that the fluorescein modified product was single-stranded. As a negative control, we also tested the dsDNA PCR product. The double-stranded PCR product was unable to hybridize to the quencher probe. Its fluorescence remained virtually unchanged.

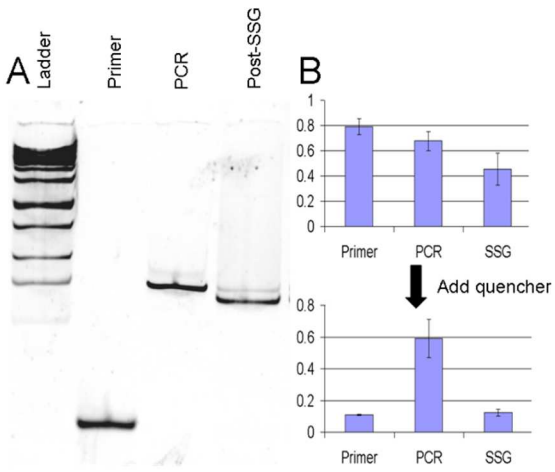

Figure 3- 2: Verification of single-stranded DNA (ssDNA) purification. (A) Native gel image shows clear resolution of single-strand generation (SSG) product as compared with a double-stranded DNA (dsDNA) PCR product. (B) Fluorescence intensity shows the result of FRET-based quenching using a hybridization probe to bind ssDNA.

3-3.3. Aptamers synthesized PCR and purified by co-polymerization and electrophoresis

High purity ssDNA is produced by our SSG technique. We purified the single-stranded DNA product from PCR by two methods: SSG by co-polymerization and electrophoresis, and the biotin-avidin immobilization technique described elsewhere (i.e. Ploysciences Technical data sheet 753) [15,16]. Single-stranded aptamer was also generated by chemical synthesis. Figure 3- 3A shows ssDNA aptamer generated by 3 methods. Lane 1 is a ladder for size comparison. Lane 2 shows the ssDNA generated by PCR with an acrydite primer followed by co-polymerization with acrylamide and electrophoresis. Only one band is visible at the correct size for ssDNA. Lane 3 is the ssDNA generated by PCR with a biotinylated primer followed by purification with avidin-coated magnetic beads. Lane 4 is chemically synthesized DNA with the same sequence. Purified ssDNA aptamer from SSG by co-polymerization and electrophoresis shows high ssDNA purity.

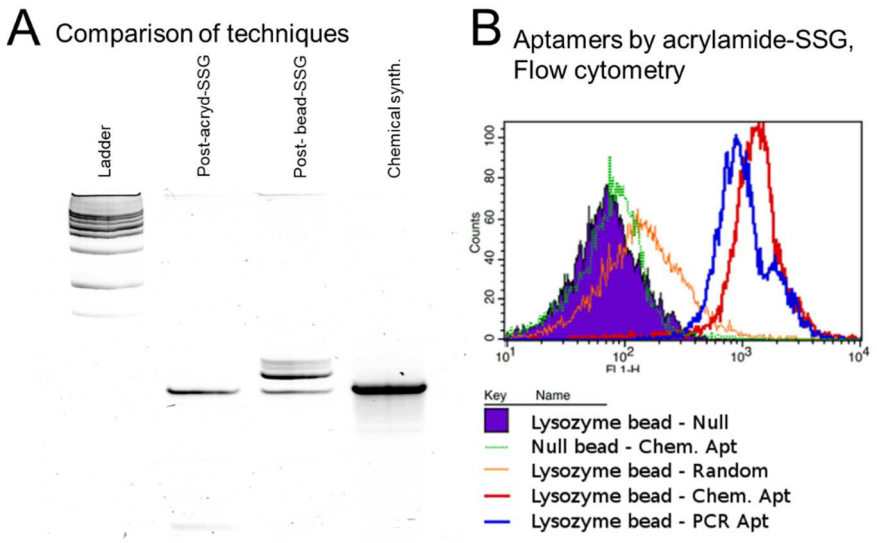

Figure 3- 3: Purity and functionality of aptamers derived from this and other techniques**.** (A) Native gel analysis shows the purity of SSG by co-polymerization and electrophoresis. SSG using avidin coated beads, and chemical synthesis. (B) Flow cytometry analysis shows relative fluorescence of lysozyme beads (purple) lysozyme beads with random DNA (orange), uncoated beads mixed with synthetic aptamer (green), lysozyme beads mixed with synthetic aptamer (red), and lysozyme beads mixed with aptamer derived from PCR and SSG by co-polymerization and electrophoresis (blue).

We next sought to test if this procedure produced functional aptamers. To do so, we generated a previously described aptamer against lysozyme by PCR with modified primers. The "Clone 1" anti-lysozyme aptamer was originally produced in the Ellington laboratory. It was originally selected in RNA[17]. Other groups report that the DNA sequence also acts as an aptamer[18,19]. In this study, both PCR and chemically synthesized DNA resulted in functional aptamer. Based on these and other experiments in our hands, we can conclude that this is one of the few, exceptional cases where RNA and its parent DNA sequence both bind the target. This is a strange and coincidental result; most aptamers do not function when translated directly to a different chemistry. These results corroborate the many instances in the literature that indicate that the Clone 1 anti-lysozyme aptamer is a special case.

Flow cytometry analysis showed that the generated ssDNA aptamer is functional. Figure 3- 4B shows lysozyme-coated beads exposed to random DNA, the chemically synthesized aptamer against lysozyme or the PCR-generated aptamer against lysozyme. Both the PCR and chemically synthesized aptamers show strong binding to the lysozyme-coated beads. The random DNA shows no significant association to the lysozyme beads. This indicates that the interaction is specific for the aptamer sequence. Uncoated beads show no fluorescence with or without the aptamer. This indicates that the binding is specific to the protein.

3-3.4. Heating releases DNA from wells

When purifying the ssDNA aptamer from the PCR product, it was necessary to heat the gel to allow the DNA to electrophorese (see **Materials and Methods**). We used horizontal PAGE to investigate why this was necessary. Without the application of heat, the desired ssDNA PCR product was retained in the well, despite 7M urea and the voltage gradient.

Our first hypothesis was that the retention was due to the 80 bp of hybridization in the PCR product. To test this, we reduced the complementarity to 23 bp by annealing the fluorescein-labeled Clone 1 aptamer DNA[17] (denoted F-Aptamer in Figure 3- 4) to a 23-nucleotide-long acrydite-modified primer (denoted AC-Clone1-P_2 in Figure 3- 4A-B) and performed SSG by co-polymerization and electrophoresis. Despite the relatively short 23 bases of hybridization, significant quantities of the aptamer DNA were retained in the well (see Figure 3- 4A, bottom lane). This indicated that our hypothesis was incorrect since the shorter hybridization stretch of 23bp, which should be easily denatured in 7M urea, did not allow the release of the desired ssDNA from the well.

We next tested the hypothesis that this retention phenomenon was dependent on length. Here, we annealed a 5'-acrydite modified 19nt long oligonucleotide (denoted AC-DNA in Figure 3- 4A-B) to a 19nt long, fully complementary, fluorescein-modified strand (denoted F-DNA* in Figure 3- 4A-B). Despite similar hybridization length, the short DNA was easily purified from its complement in a denaturing gel without application of heat. Virtually all of the 19nt, fluorescein-modified mobile strand enters the gel (Figure 3- 4A, middle lane). In order to show that the acrydite-modified 19-mer was retained, a strand modified with both fluorescein and acrydite (denoted AC-DNA-F in Figure 3- 4A-B) was also co-polymerized into the well (top lane) and was successfully retained. (see materials and methods, Supplementary Table B- S1 for sequence and nomenclature details).

After the first 20 minutes of electrophoresis (without heating), it was clear that much of the aptamer-length DNA was not mobile (despite a short hybridization length). In order to release aptamer-length DNA from the polyacrylamide, it was necessary to heat the gel. We heated running buffer to near boiling in a microwave and then poured it over the gel in the region of the wells. Electrophoresis was then continued for 20 more minutes (see Figure 3- 4B). The aptamer band became mobile. This new band had the same mobility as the first, indicating that this was the same species. Likewise, this was the same sample of DNA that yielded only a single band in Figure 3- 3A. This experiment demonstrates the necessity of heating the gel in order to release all long ssDNA from the polymer. The retention of DNA in the well is not due to hybridization, but likely due to entanglement in the polymer matrix.

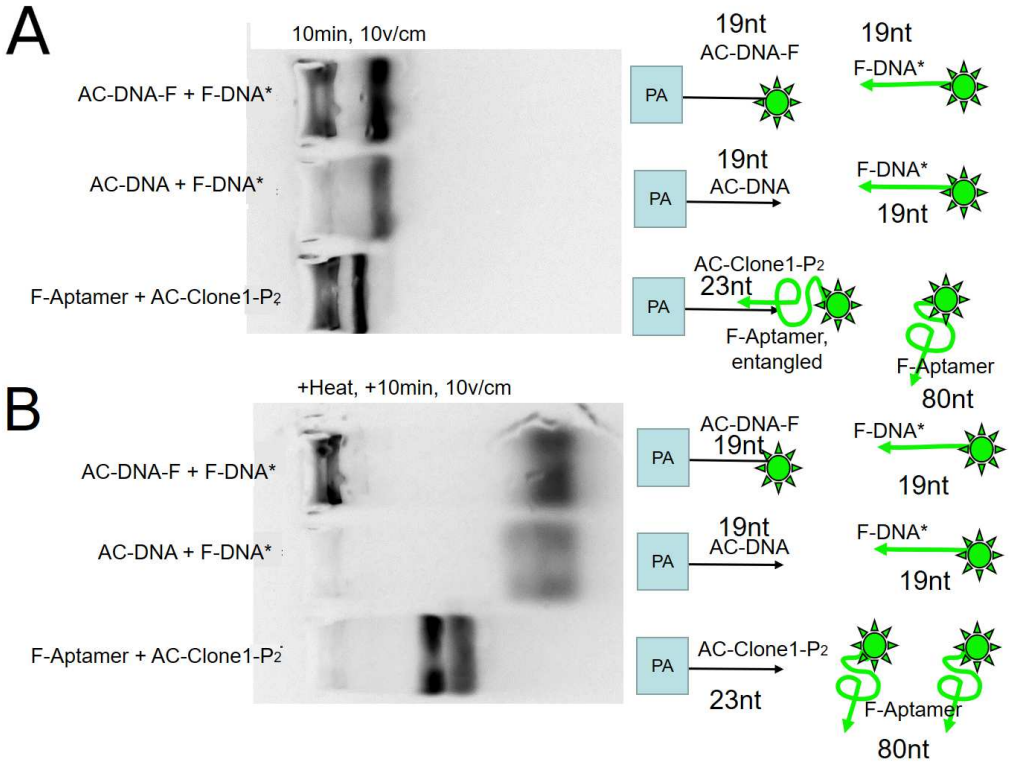

Figure 3- 4: PAGE analysis shows that added heat is required for successful single-strand generation (SSG). (A) Fluorescence image shows the gel after 10 min of electrophoresis. Schematic at right shows the contents of each well and the corresponding bands. (B) Fluorescence images of the same gel after applying heat followed by 20 min of further electrophoresis. Heat released all of the long DNA (third lane).

3-3.5. Horizontal PAGE for SSG and integrated electroelution

Use of a horizontal gel allows for electroelution to be carried out rather than cutting and extracting the product band. The use of a second "extraction" comb (for additional wells for electroelution and extraction) in horizontal PAGE made SSG and electroelution of DNA faster. We used Inkscape software to design a separate comb for electroelution that was deeper and wider than the loading comb. The design was laser cut in acrylic with a CO_2 laser cutter (see Figure 3- 5A-B).

Typically, PAGE is carried out in vertical gels. It is not possible to cast extraction wells in a vertical gel because of the glass plates. Vertical gels are cast between glass plates to exclude oxygen during polymerization. To cast a horizontal PAGE gel, it was necessary to exclude oxygen during polymerization by other means. We carried out the polymerization in a bag filled with nitrogen gas (or argon) to exclude oxygen. The gel was cast with the two combs and electrophoresis was carried out per standard horizontal gel electrophoresis procedures.

Figure 3- 5C shows a horizontal gel for SSG by copolymerization and electrophoresis with electroelution. Lanes 1-4 (from top) contain an aptamer pool. Lane 5 was left empty to avoid any inadvertent cross contamination; primer standard in Lane 6 was present too distinguish the undesired band. The pool was amplified using acrydite-modified primer and fluorescein-labeled primer. The acrydite-modified strand was retained in the well. The fluorescein labeled product is clearly visible under blue LED illumination. We allowed the primer to run through the extraction wells and out the other side of the gel (see Figure 3- 5D). The product bands could then be observed approaching the extraction wells under a blue light transilluminator in real time. When the product bands entered the wells, they were aspirated with a pipette. The process takes approximately 1 hour. Precipitation and recovery then proceeded as per published aptamer selection protocols. This eliminated the need for a separate strand separation step or an overnight extraction of the gel.

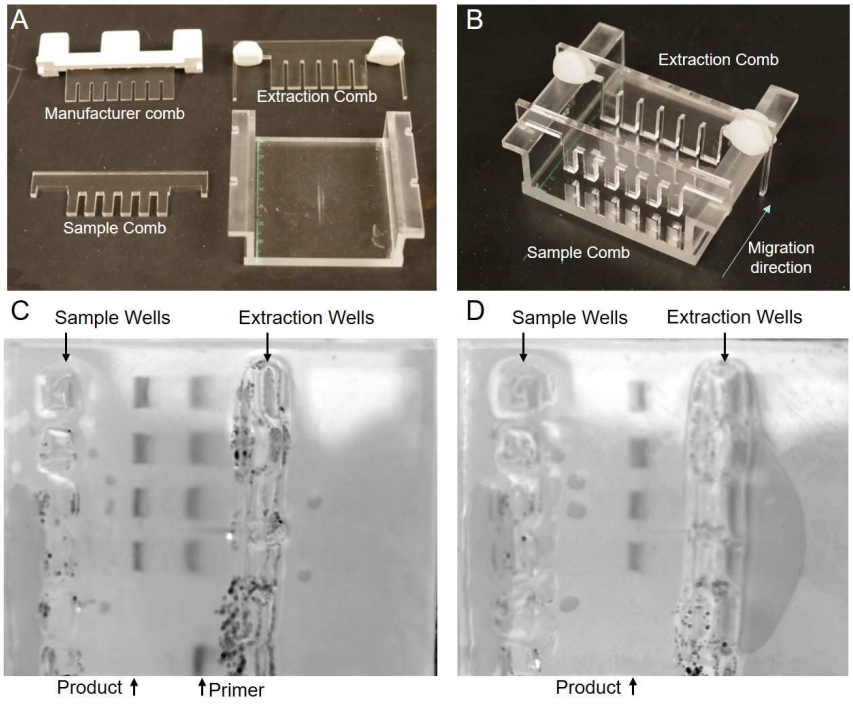

Figure 3- 5: Demonstration of electro-elution technique using a set of “extraction wells” molded into the horizontal polyacrylamide gel. (A) Photograph showing the original sample comb and our adapted injection and extraction combs, as well as the Bio-Rad gel tray for which they were designed. (B) Photograph shows the extraction and injection combs in the tray for molding. (C) Fluorescence image showing the separation of product and primer from a PCR-amplified aptamer pool. (D) Fluorescence image showing the same gel after further separation, with the product poised to enter the extraction wells and be recovered.

3-4. Conclusions

There are several methods by which one can isolate ssDNA from dsDNA. Methods for purifying ssDNA from PCR products include induced mobility shift[20], biotin-avidin bead immobilization[16], selective digestion with a DNase[21], and asymmetric addition of PCR primers[22]. These methods vary in cost, purity and scalability. An induced mobility shift[20] in one primer can cause problems in amplification (e.g. PEG-modified primers may perform less well in PCR) enzymatic digestion with a DNase[21] or chemical breakage of one strand will leave impurities (as well as introducing another step to the overall process). Asymmetric addition of PCR primers[22] will leave a significant quantity of dsDNA in the product and is highly prone to amplification errors. The most popular method is to extract the unwanted, biotinylated strand using avidin-coated microspheres[16]. This method has several pitfalls. Unreacted primer occupies the avidin sites on the beads. The biotin-avidin interaction will break down at the melting temperature of long, double-stranded DNA[23]. This contributes to significant dsDNA impurities. Bead based methods have significant costs: $1.8/nMol for avidin beads plus $.50/nMol for the biotin primer. SSG by co-polymerization and electrophoresis requires only acrydite primer which costs $.8 per nMol. The immobile phase, polyacrylamide, is very inexpensive and scalable. Electrophoretic mobility is a second dimension of purification inherent in the technique. Both the acrydite-modified strand and any residual primer are removed from a PCR reaction in a single step.

We have shown that SSG can be used to purify a functional aptamer. The technique could also be used to purify an ssDNA pool in the course of DNA aptamer selection. In addition, SSG may also find application for generating ssDNA for affinity probes or the backbone for DNA origami[3]. It's important to note that compared with chemical synthesis, PCR production of DNA has much higher sequence fidelity, which is crucial for applications such as DNA computation/DNA circuitry[24].

3-5. Materials and methods

3-5.1. Materials

Unless otherwise stated, materials were acquired from Sigma Aldrich (St. Louis, MO) and used without further purification. DNA was acquired from IDT, Integrated DNA Technologies (Coralville, IA), and used without further purification (for sequence information, see Supplementary Table B- S1).

3-5.2. Demonstration of capture of acrydite strand

For the initial demonstration of single-strand generation byco-polymerization with Acrylamide and Electrophoresis, we modified one primer with acrydite and Cy5 red-fluorescent dye. The other primer

was purchased with a green fluorescent 5' fluorescein modification. Figure 3- 1 shows how the DNA sample was prepared by mixing 100µl of 10% denaturing gel (prepolymer before initiation of polymerization) with 100µl PCR product + appropriate mass of dry urea (5% final acrylamide concentration, 7M final urea concentration). The DNA/prepolymer was loaded into the dry well of 5% denaturing PAGE gel. The gel was heated as described below and electrophoresis was performed to separate the green-fluorescent strand from the immobilized red-fluorescent strand. The result was imaged using a standard gel imaging system with LED illumination (FluorChem Imaging System, ProteinSimple, San Jose, CA).

3-5.3. Single-strand generation and purification (vertical gel electrophoresis)

PCR was performed in all cases with the Accuprime Pfx reaction kit (Life Technologies, Grand Island, NY) using 50 nM template, 10 µM concentration of each primer, and 8 thermal cycles. The PCR product was encouraged to denature by adding solid urea to a final concentration of 7M in a 100 µl reaction. Polyacrylamide was prepared from a commercially prepared stock solution of 40% acrylamide in water with a 19:1 ratio of acrylamide: bis-acrylamide (Bio-Rad, Hercules, CA). Denaturing polyacrylamide was prepared with final concentrations of 7M urea, 20% acrylamide, and 0.25x TBE buffer. Polymerization was initiated by adding 1 µl of TEMED (N,N,N′,N′-tetramethylethylenediamine) and 10 µl 10% ammonium persulfate to an aliquot of 1 mL of denaturing acrylamide prepolymer. A portion of this mixture (prepolymer before initiation of polymerization) was rapidly mixed 1:1 with 100 µl of PCR product (five 20 µl PCR reactions per manufacturer's instructions, pooled) with 7M urea (10% acrylamide, final concentration). The PCR/polymerizing acrylamide mixture was added to a dry well in a standard vertical denaturing PAGE gel. Full polymerization of the PCR/denaturing acrylamide was ensured by flushing the space above the well with a gentle stream of argon or 99.97% nitrogen (to displace any oxygen that inhibits the polymerization). After ~ 30 min of polymerization, we set up the electrophoresis rig. Crushing the polyacrylamide and loading the macerated pieces into the well produced a very broad, irregularly shaped band and this approach was discarded (data not shown). Polymerization within the well was a superior approach. We heated running buffer in a microwave to boiling and added the hot (~80-90 °C) buffer to the cathode reservoir (by pouring the hot buffer over the filled wells) in order to encourage release of the DNA from the well. The addition of the hot buffer was continued until the gel rig was full to the necessary volume for electrophoresis. The DNA-containing gel was in direct contact with hot buffer as voltage was applied. The hot buffer should be applied promptly and not allowed to cool. We then electrophoresed according to the diagram shown in Figure 3- 1.

SB (5 mM sodium borate) and TBE buffers can be used as running buffers. SB and TBE were prepared at RT at pH 8.42 and 8.36 respectively. At 80 °C, these pH values change to 8.21 and 7.47 respectively. This pH change is transient. The gel cools to 30-40 °C during electrophoresis. This change in pH did not noticeably cause degradation of the DNA.

In order to visualize the separation of the two strands, we used primers modified with two different fluorophores. The mobile strand was generated from a fluorescein-modified primer. The immobile (acrydite) primer was prepared with an internal Cy5 modification. Using these two dyes, we could visualize the progress of the separation. We scanned this gel with a gel imager (FluorChem Q, Protein-Simple, Santa Clara, CA) after 45 min of electrophoresis at 500 V.

As an alternative approach, the PCR product can be pre-concentrated by standard ethanol precipitation. The pellet can then be dissolved in a smaller volume of acrylamide prepolymer. In our hands, the increased concentration in the well was offset by losses during precipitation. In some cases (e.g. for a faint product band) this approach may be preferred.

The fluorescent band bearing the single-stranded, fluorescein-modified product was cut from the gel under blue LED illumination at ~475nm (Bulldog Bio, Portsmouth, NH). The DNA was eluted by the standard crush and soak method[25]. When the eluted (recovered) DNA was too dilute for efficient ethanol precipitation, we concentrated by extracting with butanol. The product was then precipitated with ethanol and analyzed further as per below.

3-5.4. PAGE analysis

The fluorescein-labeled single-stranded products (ssDNA released by denaturing PAGE) were analyzed for purity using native PAGE. We resuspended the single-stranded product in 10 µl. We quantified with UV-Vis spectroscopy. We made equal molar concentration of primer and single-stranded product and electrophoresed these samples and a 25 bp green fluorescent ladder (Jena Bioscience, Jena, Germany) on a 15% native PAGE gel and visualized with the Storm scanner for the fluorescent signal.

3-5.5. Quencher analysis

To further establish that the product was in fact single-stranded, we tested for the hybridization of a complementary oligonucleotide (quench probe) with a 3’ quencher modification. When properly hybridized, the quench probe positions an Iowa Black quencher within a few nanometers of the 5’ fluorescein modification on the complementary strand. This causes a sharp decrease in fluorescence inten-

sity. The quench probe will only hybridize to ssDNA. If the product is double-stranded, then hybridization will be blocked, and fluorescence will remain. Triplicate 10 µl samples of 100 nM fluorescein-modified product (PCR product, SSG product and primer control) were prepared in PCR tubes. These were measured with a QuantiFluor fluorometer (Promega, Madison, WI) for their initial fluorescence values. 1.1 equivalents of quench probe DNA were then added, vortexed to mix, and centrifuged and allowed to incubate for approximately 1 min. The quenched fluorescence was then recorded.

3-5.6. Comparison of single-strand generation techniques for aptamer production

In order to ascertain the effectiveness of this method for generating functional aptamers, we purchased a template for PCR amplification of a known aptamer sequence binding lysozyme. We amplified this template with a fluorescein modified primer and a acrydite modified reverse primer. We performed the single-stranded generation protocol as described above. We conjugated lysozyme to 5.8 µm carboxylate modified beads (Bangs Labs, Fishers, IN) by the standard EDC (1-ethyl-3-(3-dimethylaminopropyl) carbodiimide) coupling protocol. These beads were incubated with the SSG product, randomized fluorescent DNA (no sequence similarity to the aptamer), and a chemically synthesized fluorescent aptamer of the same sequence. We also incubated on coated beads with the chemically synthesized fluorescent aptamer as a negative control. Incubation's are carried out for 30 min and then the beads were washed 3 times. Flow cytometry was performed on these particles with a FACScalibur (BD Bioscience San Jose, CA). The distribution of fluorescence intensities with excitation by 488 nm light was recorded.

3-5.7. Single-strand generation and purification (horizontal gel electrophoresis)

A 7 M urea denaturing polyacrylamide gel was cast horizontally as described in a previous work[26]. Briefly, 25 ml prepolymer solution (7M urea, 6% acrylamide/bis, SB buffer) was initiated with 84 µl of APS and 20 µl TEMED. The gel prepolymer was then poured into a horizontal mold. The mold was then placed in a plastic bag which was purged with nitrogen. The gel was allowed to polymerize for 30 min. Fluorescein-labeled and acrylamide-labeled DNA were assembled in 1 M sodium phosphate at pH 8 and annealed by raising the temperature to 80 °C and cooling slowly at 0.1 °C per second to RT. The mixture was cooled slowly to promote intermolecular hybridization between two strands. The prepolymer mixture (2.5 mL) was initiated by adding 8.4 µL of APS and 2 µL of TEMED. Once mixed, 20 µL of this solution were added to the 5 µL of DNA solution. This was then transferred to a dry well in the polyacrylamide gel. In order to avoid distortions in the electric field lines, the remaining wells were also filled with non-DNA-containing acrylamide. The loaded gel was placed in a plastic bag and purged with nitrogen. The gel was run at 10 V/cm for 10 min. It was then imaged using a blue LED

transilluminator and a digital camera. In order to release the ssDNA from the cross-linked gel in the well, 25 mL of SB buffer for heated to boiling in a microwave. This hot water was then poured over the gel. Electrophoresis was continued at 10 V/cm for 10 min. The gel was imaged again as described above for comparison.

Initial association between the fluorescein and acrydite labeled DNA was promoted using 1M sodium phosphate buffer. If the DNA were only held together by hybridization, 7M urea and the exchange of buffer into 5mM SB during electrophoresis would be adequate to release the DNA into the gel. Instead, heat was required. This demonstrated that the mobile DNA is associated or entangled with the gel rather than with its complementary DNA strand.

3-6. Acknowledgments

This work was funded by the National Institutes of Health (EUREKA, 1-R01-GM094933), The Welch Foundation (F-1654), a National Security Science and Engineering Faculty Fellowship (FA9550-10-1-0169), and support from the National Institute of General Medical Sciences (P20-GM104420).

3-7. Author Contributions

P.B.A. and T.R.D wrote the main manuscript text, prepared figures and conducted experiments. A.D.E. advised on aptamer applications and verification and helped to prepare and edit the manuscript.

3-8. Competing interests statement

The authors have declared that no competing interests exist.

3-9. Correspondence

Address correspondence to Peter B Allen, University of Idaho, Dept. of Chemistry, 001 Renfrew Hall, 875 Perimeter Dr, Moscow, ID 83844-2343, USA. E-mail: pballen@uidaho.edu

3-10. References

(1) Cho, E. J.; Lee, J.-W.; Ellington, A. D. Applications of Aptamers as Sensors. *Annu. Rev. Anal. Chem.* **2009**, *2* (1), 241–264.

(2) Tang, H.; Deschner, R.; Allen, P.; Cho, Y.; Sermas, P.; Maurer, A.; Ellington, A. D.; Willson, C. G. Analysis of DNA-Guided Self-Assembly of Microspheres Using Imaging Flow Cytometry. *J. Am. Chem. Soc.* **2012**, 15245–15248.

(3) Rothemund, P. W. K. Folding DNA to Create Nanoscale Shapes and Patterns. *Nature* **2006**, *440* (7082), 297–302.

(4) Allen, P. B.; Arshad, S. A.; Li, B.; Chen, X.; Ellington, A. DNA Circuits as Amplifiers for the Detection of Nucleic Acids on a Paperfluidic Platform. *Lab. Chip* **2012**, *12*, 2951–2958.

(5) Iida, K.; Nishimura, I. Gene Expression Profiling by DNA Microarray Technology. *Crit. Rev. Oral Biol. Med.* **2002**, *13* (1), 35–50.

(6) Olah, M. J.; Stefanovic, D. Multivalent Random Walkers — A Model for Deoxyribozyme Walkers. In *DNA Computing and Molecular Programming*; Cardelli, L., Shih, W., Eds.; Lecture Notes in Computer Science; Springer Berlin Heidelberg, 2011; pp 160–174.

(7) Chen, X.; Briggs, N.; McLain, J. R.; Ellington, A. D. Stacking Nonenzymatic Circuits for High Signal Gain. *Proc. Natl. Acad. Sci.* **2013**, *110* (14), 5386–5391.

(8) Gibson, D. G.; Benders, G. A.; Andrews-Pfannkoch, C.; Denisova, E. A.; Baden-Tillson, H.; Zaveri, J.; Stockwell, T. B.; Brownley, A.; Thomas, D. W.; Algire, M. A.; et al. Complete Chemical Synthesis, Assembly, and Cloning of a Mycoplasma Genitalium Genome. *Science* **2008**, *319* (5867), 1215–1220.

(9) Kenney, M.; Ray, S.; Boles, T. C. Mutation Typing Using Electrophoresis and Gel-Immobilized Acrydite Probes. *BioTechniques* **1998**, *25* (3), 516–521.

(10) Liedl, T.; Dietz, H.; Yurke, B.; Simmel, F. Controlled Trapping and Release of Quantum Dots in a DNA-Switchable Hydrogel. *Small* **2007**, *3* (10), 1688–1693.

(11) MacLean, J. L.; Morishita, K.; Liu, J. DNA Stabilized Silver Nanoclusters for Ratiometric and Visual Detection of Hg2+ and Its Immobilization in Hydrogels. *Biosens. Bioelectron.* **2013**, *48*, 82–86.

(12) Soontornworajit, B.; Zhou, J.; T. Shaw, M.; Fan, T.-H.; Wang, Y. Hydrogel Functionalization with DNA Aptamers for Sustained PDGF-BB Release. *Chem. Commun.* **2010**, *46* (11), 1857–1859.

(13) Kenney, M.; Ray, S.; Boles, T. C. Mutation Typing Using Electrophoresis and Gel-Immobilized Acrydite Probes. *BioTechniques* **1998**, *25* (3), 516–521.

(14) Mitra, R. D.; Church, G. M. In Situ Localized Amplification and Contact Replication of Many Individual DNA Molecules. *Nucleic Acids Res.* **1999**, *27* (24), e34.

(15) Liang, C.; Li, D.; Zhang, G.; Li, H.; Shao, N.; Liang, Z.; Zhang, L.; Lu, A.; Zhang, G. Comparison of the Methods for Generating Single-Stranded DNA in SELEX. *The Analyst* **2015**, *140* (10), 3439–3444.

(16) Kuo, T.-C. Streamlined Method for Purifying Single-Stranded DNA from PCR Products for Frequent or High-Throughput Needs. *BioTechniques* **2005**, *38* (5), 700, 702.

(17) Kirby, R.; Cho, E. J.; Gehrke, B.; Bayer, T.; Park, Y. S.; Neikirk, D. P.; McDevitt, J. T.; Ellington, A. D. Aptamer-Based Sensor Arrays for the Detection and Quantitation of Proteins. *Anal. Chem.* **2004**, *76* (14), 4066–4075.

(18) Rodriguez, M. C.; Kawde, A.-N.; Wang, J. Aptamer Biosensor for Label-Free Impedance Spectroscopy Detection of Proteins Based on Recognition-Induced Switching of the Surface Charge. *Chem. Commun. Camb. Engl.* **2005**, No. 34, 4267–4269.

(19) Cheng, A. K. H.; Ge, B.; Yu, H.-Z. Aptamer-Based Biosensors for Label-Free Voltammetric Detection of Lysozyme. *Anal. Chem.* **2007**, *79* (14), 5158–5164.

(20) Pagratis, N. C. Rapid Preparation of Single Stranded DNA from PCR Products by Streptavidin Induced Electrophoretic Mobility Shift. *Nucleic Acids Res.* **1996**, *24* (18), 3645–3646.

(21) Avci-Adali, M.; Paul, A.; Wilhelm, N.; Ziemer, G.; Wendel, H. P. Upgrading SELEX Technology by Using Lambda Exonuclease Digestion for Single-Stranded DNA Generation. *Molecules* **2009**, *15* (1), 1–11.

(22) Gyllensten, U. B.; Erlich, H. A. Generation of Single-Stranded DNA by the Polymerase Chain Reaction and Its Application to Direct Sequencing of the HLA-DQA Locus. *Proc. Natl. Acad. Sci. U. S. A.* **1988**, *85* (20), 7652–7656.

(23) Holmberg, A.; Blomstergren, A.; Nord, O.; Lukacs, M.; Lundeberg, J.; Uhlén, M. The Biotin-Streptavidin Interaction Can Be Reversibly Broken Using Water at Elevated Temperatures. *ELECTROPHORESIS* **2005**, *26* (3), 501–510.

(24) Yin, P.; Choi, H. M. T.; Calvert, C. R.; Pierce, N. A. Programming Biomolecular Self-Assembly Pathways. *Nature* **2008**, *451* (7176), 318–322.

(25) Chen, Z.; Ruffner, D. E. Modified Crush-and-Soak Method for Recovering Oligodeoxynucleotides from Polyacrylamide Gel. *BioTechniques* **1996**, *21* (5), 820–822.

(26) Damase, T. R.; Stephens, D.; Spencer, A.; Allen, P. B. Open Source and DIY Hardware for DNA Nanotechnology Labs. *J. Biol. Methods* **2015**, *2* (3), 24.

CHAPTER 4: APPLICATION OF THE OPEN QPCR INSTRUMENT FOR THE *IN VITRO* SELECTION OF DNA APTAMERS AGAINST EPIDERMAL GROWTH FACTOR RECEPTOR AND *DROSOPHILA* C VIRUS

Published in: "Damase, T. R.; Miura, T. A.; Parent, C. E.; Allen, P. B. Application of the Open QPCR Instrument for the in Vitro Selection of DNA Aptamers against Epidermal Growth Factor Receptor and Drosophila C Virus. ACS Comb. Sci. 2018, 20 (2), 45–54."

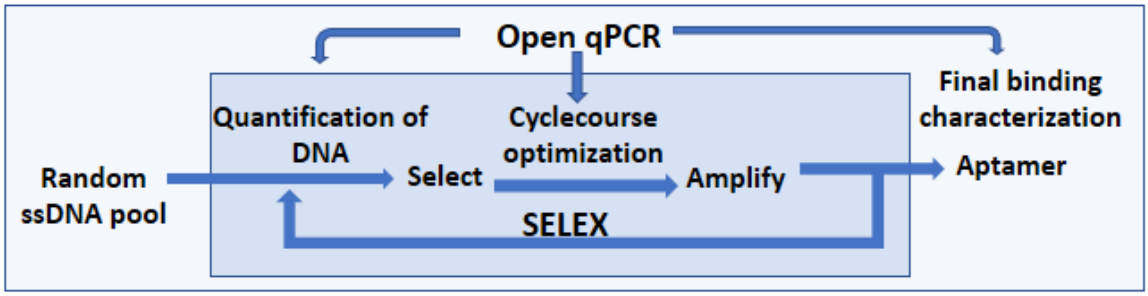

The low-cost Open qPCR instrument can be used for different tasks in the aptamer selection process: quantification of DNA, cyclecourse optimization, screening and final binding characterization. We have selected aptamers against whole *Drosophila* C virus (DCV) particles and recombinant Epidermal Growth Factor Receptor (EGFR). We performed systematic evolution of ligands by exponential enrichment (SELEX) using the Open qPCR to optimize each amplification step. The Open qPCR instrument identified the best aptamer candidate. The Open qPCR has the capacity to perform melt curves, and we used this function to perform thermofluorimetric analysis (TFA) to quantify target-aptamer binding. We confirmed target-aptamer binding using flow cytometry. A sandwich type luminescence bioassay based on our anti-DCV aptamer was sensitive to DCV and did not respond to a related virus, demonstrating that our selected anti-DCV aptamer can be used to specifically detect DCV.

Keywords: SELEX, aptamers, *Drosophila* C virus, EGFR, high throughput sequencing, thermofluorimetric analysis, binding curve

4-1. Introduction

We set out to show that a qPCR technique could be used to simplify and reduce the expense and improve the efficiency of aptamer selection and characterization (e.g. relative to P-32 detection). The Open qPCR is a qPCR instrument for performing quantitative PCR with real time monitoring of fluorescence. Chai Biotechnologies used "open source" principles to design the instrument (as in open

source software). Examples of open source scientific software include Python, R, and ImageJ. Applying the open source approach to hardware has benefits relative to fully proprietary hardware. Open source scientific hardware (OSSH) design provides complete information to reconstruct an instrument[1]. This disclosure makes instruments cheaper and more customizable and reproducible. Open hardware is an emerging field with examples in 3D printing (RepRap) and single board computers (Raspberry Pi)[2]. The Open qPCR instrument operates with closed PCR tube strips (2 strips of 8 samples each). The tubes contain the sample and reagents. A Blue LED illuminates the top of each tube through a heated lid. Fluorescence is measured from the side of the bottom of the tube.

Aptamers are single-stranded (ss) DNA or RNA molecules that bind to a target with high affinity and specificity[3]. In the past two decades, researchers have generated aptamers for the detection of proteins[4], small molecules[5], whole cells[6], and whole viruses[7], among other targets. The specific binding ability of aptamers to diverse targets make them important reagents for clinical detection, bio-imaging, and therapeutics[8,9]. We performed aptamer selections against *Drosophila* C virus (DCV) and Epidermal Growth Factor Receptor (EGFR). DCV is a positive-sense RNA viral pathogen affecting the widely-studied model organism *Drosophila melanogaster.* The study of this virus is important to the investigation of antiviral host defense in fruit flies[10–12]. An aptamer against DCV can be used for rapid and cost-effective detection of infected flies to help researchers study the effects of DCV on its host; this is the first instance of an anti-DCV aptamer. EGFR is overexpressed in many cancer cells and is a biomarker for early cancer detection and a target for cancer therapeutics[13]. An RNA aptamer against EGFR was selected in 2011[14].

SELEX (Systematic Evolution of Ligands by Exponential Enrichment) is the method for generating aptamers. Ellington[11] and Tuerck[15,16] first introduced SELEX in 1990. In brief, the process starts with a ssDNA library consisting of a 30-80bp random sequence region flanked by primer binding sites. Some members of this randomized DNA library bind to a target. A target immobilized on a solid support separates bound DNA from unbound DNA. After elution and amplification with PCR, the pool contains a higher proportion of binding DNA. After multiple rounds of binding and amplification, the pool converges on high-affinity aptamers. The overall SELEX process is time-consuming with classical SELEX experiments taking months to move from a pool to the identification of a highly specific and high-affinity binding aptamer[3].

Since 1990, many groups have built upon SELEX. Cell-SELEX is a technique that generates aptamers against cell surface biomarkers[6,17,18]. This technique uses whole living cells as targets to select aptamers. Whole-virus SELEX is the analogous technique that generates virus-specific aptamers[19]. Next-

generation sequencing improved the speed and success rate of aptamer selections[3,20]. Integration of SELEX on microfluidic chips also made SELEX faster[21,22]. Rapid-SELEX[23] used multiple rounds of selection without amplification. CE-SELEX[24] used the rapid mode of capillary electrophoresis to separate binding DNA. All of these methods can benefit from a method to optimize the number of PCR cycles and quantify the DNA pool at each step.

In the present study, we performed eight rounds of classical selection using whole virus immobilized on magnetic microparticles to generate an anti-DCV aptamer. We performed four rounds of classical selection using recombinant EGFR immobilized on magnetic particles to generate an anti-EGFR aptamer. We characterized the pool with high throughput sequencing (HTS)[25]. Each round required only two days of effort. We chose to select DNA aptamers because they are more stable than RNA aptamers, which have a 2'-OH group that can attack the phosphodiester linkage leading to hydrolysis of RNA aptamers[3,26]. DNA aptamers also have the advantage of being more easily synthesized with modifications for various immobilization and detection schemes.

We have demonstrated the use of the low cost Open qPCR in many aspects of *in vitro* aptamer selection including quantification of ssDNA after each round of selection, optimization, screening and characterization. Optimization with Open qPCR will make aptamer generation more efficient and reduce failure due to over- or under-amplification (traditionally, PCR and gel electrophoresis must be run at a range of cycles to optimize amplification for each round of selection). The use of the Open qPCR will bring SELEX to more laboratories including undergraduate serving institutions where high cost capital equipment may be a limiting factor. We also present three novel findings: 1) Thermofluorimetry analysis can build a binding curve and determine a binding constant even in the presence of interference from endogenous fluorescence; 2) We selected the first anti-DCV aptamer with micromolar range dissociation constant (K_d of 0.3 ± 0.1 μM); and 3) we selected a new DNA aptamer against EGFR with a K_d of 9 ± 3 nM which is stronger by a significant margin than previously published DNA aptamers against EGFR[27].

4-2. Results and Discussion

4-2.1. Aptamer Selection Procedure with Open qPCR

We generated aptamers, using our *in vitro* selection technique with Open qPCR, as molecular recognition elements to detect the presence of target (DCV or EGFR). Figure 4- 1 shows an outline of the SELEX procedure. We used magnetic microspheres coated with target for positive selection (denoted "positive selection microspheres"). We coated magnetic microspheres with non-target (a related virus,

DXV, or a related recombinant protein, IgG1-FC) for negative selection (denoted “negative selection microspheres”).

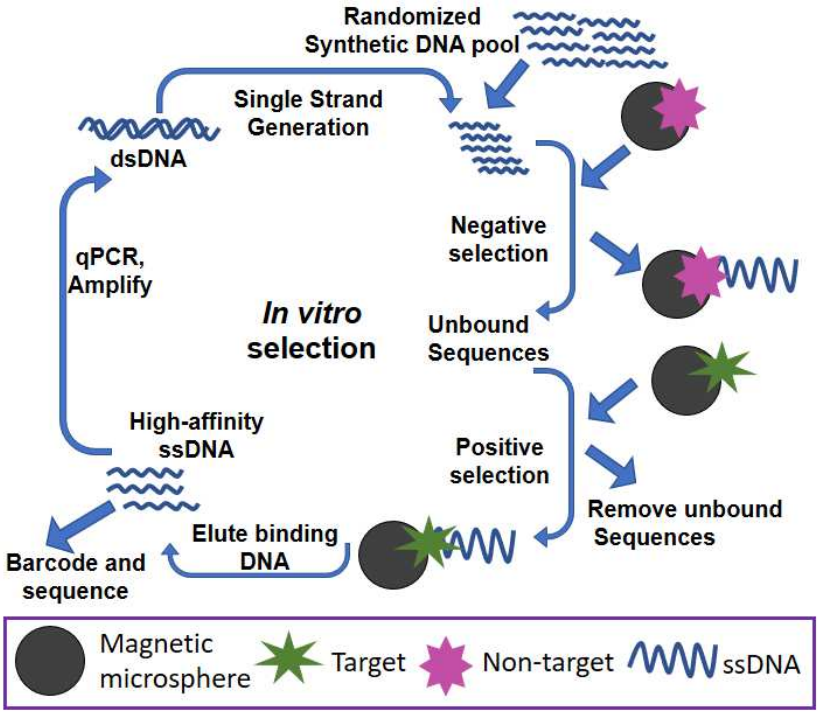

Figure 4- 1: Schematic illustration of SELEX.

We used the Open qPCR to optimize the number of cycles for PCR amplification. If PCR is not optimized, the yield will be prohibitively low (too few cycles) or contaminated with unwanted product (too many cycles). Very small amounts of parasitic amplicons (especially primer dimers) carried through from round to round can poison a selection. These amplicons can amplify much more efficiently and consume primer and NTP, reducing the yield of desired product. After several rounds of contaminated selection, the whole laboratory can become contaminated with these efficient replicators, rendering a pool useless. Reducing parasitic amplicon formation in the first place is a very valuable practice. We used the number of cycles that produced 50-75% of maximal fluorescence by the Open qPCR. Although contamination is a significant concern for any qPCR application, it can be minimized by careful handling of samples and immediate disposal of qPCR samples. We take the additional precaution of never opening qPCR samples. Samples carried through for further use are amplified by conventional PCR with an optimal number of cycles. After amplification, we carried out single-strand generation using copolymerization and electrophoresis[27] to regenerate the pool.

4-2.2. Choice of aptamer candidates from HTS data with *k*-mer analysis

Following the SELEX process, we identified aptamer candidates by *k*-mer analysis. HTS returned approximately 300,000 reads. We identified aptamer sequences in the HTS data based on overrepresentation of short 12-mer sequences for DCV and 15-mer sequences for EGFR *(k*-mer analysis[25]). A program written in Python determined the frequency with which each unique *k*-mer sequence appeared in the data. The Institute for Bioinformatics and Evolutionary Studies (IBEST) sequencing core acquired and provided sequence data in FASTA format. The Python program filtered the data according to three quality requirements: 1) each sequence must begin with a primer binding site (as identified by Illumina software); 2) the next 30 nucleotides must not contain more than 9 bases of homology with either primer sequence (to exclude primer dimers); 3) the final 22 nucleotides must contain the second primer binding site sequence with no more than 4 mismatched bases. From these data, we derived all possible *k*-mer sub-sequences (where *k*=12 for DCV and *k*=15 for EGFR). We then filtered the data to remove all duplicates. For each item in the list of unique *k*-mers, we counted the total number of occurrences in each round of the data. We selected the most abundant *k*-mers for experimental characterization. We have included the Python source used to process the DCV data as **Supporting Information Online**. We processed EGFR data similarly.

In the case of DCV, the two most highly represented 12-mer sequences appeared six and four times in the data. We chose four aptamer candidates for further study (aptamer candidates include the randomized region plus primer binding sites). We chose two from the set of six that contained the first over-represented 12-mer. We chose two more from the set of four containing the second over-represented 12-mer. We named these aptamer candidates DCVKM1 through DCVKM4 (for sequence information see Table C- S1, **Supporting Information Online)**. We found two *k*-mers (LINN and FINNI) represented 4 times each in the data from round 4 of the selection against EGFR. FINNI was also represented in round 3. We chose 9 candidates (with random and conserved regions). We named these candidates LINN1 through LINN4 and FINNI1 through FINNI5. We ordered synthetic oligonucleotides for these sequences and tested the affinity of the aptamer candidates using the Open qPCR instrument and fluorescence microscopy.

4-2.3. Determination of Affinity and Specificity for DCV

We screened DCV aptamer candidates for their affinity for DCV by incubating them with positive selection microspheres. We used the Open qPCR to quantify each aptamer candidate that bound the positive selection microspheres. We found that the aptamer candidate DCVKM3 required the fewest

number of cycles to produce significant fluorescence (above a threshold of 10% maximal fluorescence, as calculated by the Open qPCR software). The Open qPCR instrument reported the lowest Cq value (8.8) for DCVKM3. This suggested that DCVKM3 had the highest binding affinity for the target (see Figure 4- 2(A)). Therefore, we chose aptamer DCVKM3 for further study.

We next tested the specificity of aptamer-target binding with a capture assay. We coated microspheres with DCVKM3 and MUT (a scrambled mutant version of DCVKM3). We incubated these microspheres with DCV and then incubated with fluorescein-labeled aptamer Apt-F (annealed complex of DCVKM3 and a short, fluorescein-conjugated, complementary oligonucleotide, P2-F; see **Supporting Information Online** for sequence information). The particles coated with DCVKM3 showed strong fluorescence (Figure 4- 2(C)). The particles coated with MUT did not show significant fluorescence. This indicated that the binding of DCV to DCVKM3 was specific to the aptamer sequence.

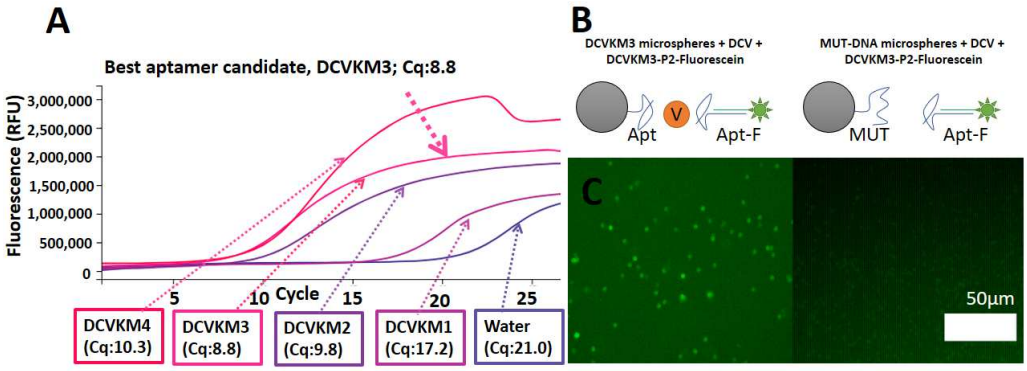

Figure 4- 2: Affinity and specificity test of aptamer DCVKM3. (A) Affinity test of aptamer candidates via Open qPCR. (B) Schematic of the design of the experimental conditions with DCVKM3 (Apt) and control nonspecific DNA (MUT). Orange circle labeled 'V' represents DCV. (C) Fluorescence micrographs show the difference in fluorescence capture by aptamer-coated microspheres as compared to MUT-coated microspheres.

4-2.3. Determination of Affinity and Specificity for EGFR

We screened EGFR aptamer candidates for their affinity for EGFR by incubating them along with control (P2-F) with positive selection microparticles. We then observed the microparticles in a fluorescence microscope and measured mean particle fluorescence using Image J. The mean particle fluorescence (calculated using 10 particles) was high for LINN2 indicating that LINN2 has more binding affinity towards target as shown in Figure 4- 3(B). To identify specificity of LINN2, we incubated the LINN2 aptamer with positive selection microparticles and negative selection microparticles and ob-

served in the fluorescence microscope. The LINN2 aptamer incubated with positive selection microparticles showed strong fluorescence while the negative control showed significantly less fluorescence as shown in Figure 4- 3(A). We took this to indicate that the LINN2 aptamer is specific.

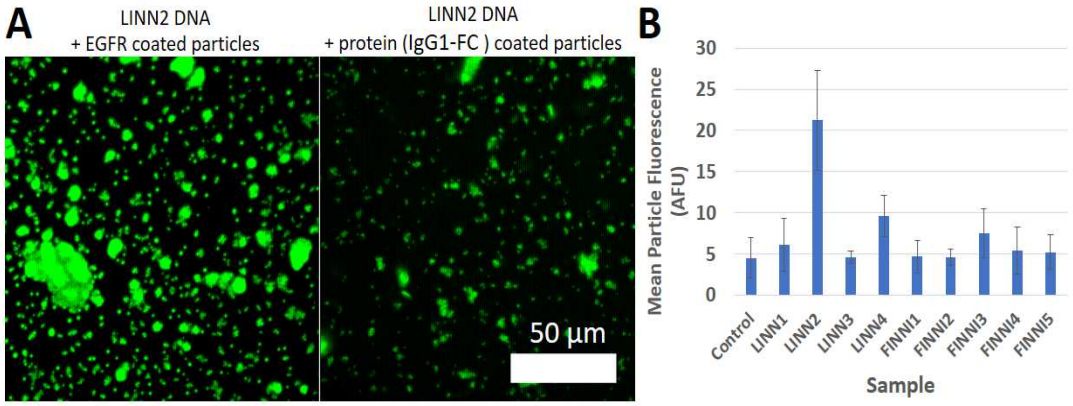

Figure 4- 3: Affinity and specificity test of aptamer LINN2. (A) Fluorescence micrographs show specificity test of aptamer LINN2 with positive (left) and negative (right) selection microparticles. (B) Affinity test of EGFR aptamer candidates by observing in Fluorescence microscope and measuring mean particle fluorescence using Image J.

4-2.4. Thermofluorimetric Analysis (TFA) using Open qPCR

The Open qPCR instrument can be used to obtain a binding isotherm and quantify the aptamer-target dissociation coefficient (K_d) by thermofluorimetric analysis (TFA)[4]. This low-cost technique can be used in place of more expensive techniques like surface plasmon resonance or flow cytometry. Thermofluorimetry measures the fluorescence of a mixture of DNA and intercalating dye as a function of temperature. Intercalating dyes are only highly fluorescent when bound to double-stranded DNA. At high temperatures, double-stranded DNA melts and the fluorescence decreases. The melting temperature of an oligonucleotide is the temperature of the maximum rate of change of fluorescence as a function of temperature (dF/dT). The same principle can report aptamer binding. The Easley research group at Auburn University has reported the use of TFA for aptamer binding assays[4,28] with a more expensive qPCR instrument (Bio-Rad CFX96). We confirmed that this technique can validate aptamers and that it can be performed with the Open qPCR.

TFA can detect aptamer binding because binding changes the stability of the aptamer. Aptamers are typically structured and have dsDNA regions. These regions bind to intercalating dye and show fluorescence. The bound aptamer-protein complex will melt at a different (usually higher) temperature relative to the unbound aptamer. As such, it will display a unique feature in the thermofluorimetric curve.

By measuring this unique feature as a function of protein concentration, we can establish a binding isotherm.

4-2.5. TFA on aptamer LINN2-EGFR complex

We performed TFA on samples of the LINN2 aptamer with variable concentrations of EGFR. TFA allowed us to measure a signal specific to the EGFR- LINN2 complex. We held the aptamer concentration constant at 50 nM. The most dilute EGFR samples are nearly equivalent to an aptamer-only control. The aptamer-only controls are provided as Figure C- S3. For pure proteins like EGFR, the change in the background as a function of target concentration can be neglected (see Figure C- S5 Supporting Information Online for EGFR only control). We found a strong and specific signal for the EGFR-LINN2 complex in the dF/dT data when we added 500 nM of the target. This indicates that a high concentration of the target increases the thermal stability of the target-bound aptamer complex. We averaged the dF/dT signal over a range of 3 °C (from 35-37 °C) to generate a binding curve. We described the binding equilibrium of the aptamer and target with a simple equilibrium model assuming that the number of aptamer binding sites is one. This reduces to Equation 1:

$$[AT]^2 + (-[A]_t - [T]_t - K_d)[AT] + [A]_t[T]_t = 0 \qquad (1)$$

We solved Equation 1 in Excel to generate a predicted value for the concentration of aptamer-target complex, [AT], as a function of the experimental value of the total aptamer ($[A]_t$) and total target ($[T]_t$) for a given value of K_d. We then applied a linear relationship (signal, S = m[AT] +b) to generate a predicted signal. We used Excel's nonlinear solver to minimize the deviation between the predicted signal values of S and experimental data. We allowed Excel to adjust the parameters K_d, slope (m), intercept (b). We applied this non-linear regression analysis to the aptamer-EGFR complex data and found K_d was 9 ± 3 nM (standard deviation of four replicates, see **Supporting Information Online**, Figure C- S6).

4-2.6. TFA on aptamer DCVKM3-DCV complex

To perform TFA on the aptamer-DCV complex, we had to perform background subtraction. The fluorescence of DNA intercalating dyes does not usually increase in the presence of protein. The change in the background as a function of target concentration can be neglected for most pure protein targets. For whole-virus selections, the situation is more complicated. Because of the structure and accessibility of its nucleic acid content, the virus contributed significant background in the dF/dT data. This background must be subtracted.

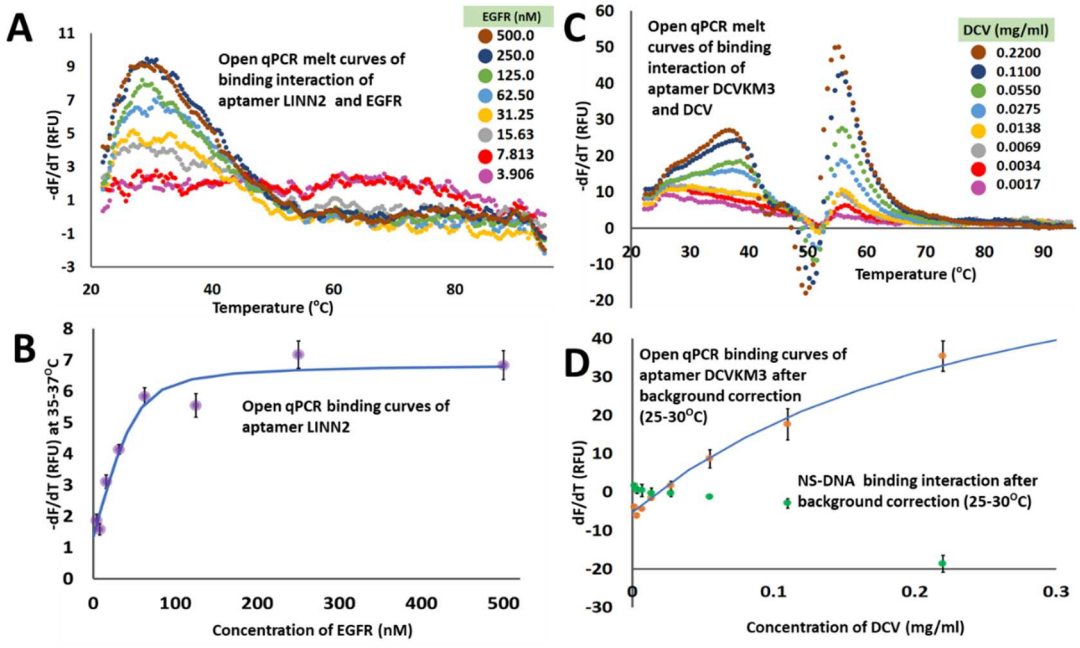

Figure 4- 4: Aptamer-target binding studies via TFA using Open qPCR. (A) TFA melt curves of aptamer LINN2 with target EGFR. (B) Graph shows dF/dT data as a function of EGFR concentration. The blue line is the best fit binding isotherm used to determine dissociation constant (K_d) between LINN2 and EGFR. (C) TFA melt curves of aptamer DCVKM3 with target DCV. (D) Graph shows background-subtracted dF/dT data as a function of DCV concentration for DCVKM3 (orange dots) and nonspecific DNA (NS-DNA, green dots). The blue line is the best fit binding isotherm used to determine dissociation constant (K_d) between DCVKM3 and DCV.

To specifically measure the aptamer-virus complex signal, we took the dF/dT data from the DCV-only sample (see Figure C- S1 **Supporting Information Online**) and subtracted it from the equivalent aptamer+DCV data (Figure 4- 4(C)). The most dilute cases are nearly equivalent to an aptamer-only control. The aptamer only controls are provided in **Supporting Information Online** (Figure C- S4). The temperature of 25-30 °C was chosen as it gives the largest difference between DCV-only and DCV-plus-DCVKM3 as a function of virus concentration (see **Supporting Information Online,** Figure C- S1). As an example of the calculation: at 0.055 mg/ml of DCV and 50 nM of DCVKM3 (Figure 4C, green trace), the average -dF/dT signal at 25-30 °C was 13 RFU; the average -dF/dT of the virus only sample at the same temperature range was 21 RFU; the difference of -8 RFU was taken as the virus-specific signal and plotted in Figure 4- 4D at 0.055 mg/ml. Full experimental and background data for specific and nonspecific analysis are shown in **Supporting Information Online,** Figure C- S2. We applied a nonlinear regression analysis to fit a binding isotherm to the data. We determined the K_d of

the aptamer with DCV which shows clear binding. We also calculated the equivalent values for non-specific DNA, NS-DNA, and overlaid them for comparison in Figure 4- 4 (see also Figure C- S2). NS-DNA did not show binding. Error bars are the standard deviation of the 9 fluorescence readings used to measure the aptamer-complex signal in the thermofluorimetry curve. The average and standard deviation of the four replicates of the binding assay K_d was 0.18 ± 0.06 mg/ml.

4-2.7. Flow Cytometric Analysis of Binding Isotherm

We verified the Open qPCR binding assay results using flow cytometry. Flow cytometry uses laser scattering and fluorescence to characterize microspheres or cells in a fluid[29]. To measure the dissociation constant, we labeled target-coated clear microspheres with a fluorescein-modified aptamer at a range of concentrations. We used forward scattering (FS) and side scattering (SS) to threshold for high scattering events (which appeared only when we added microspheres). This high scattering population is denoted **P1** in Figure 4- 5(A) and Figure 4- 5(D). We chose this population as corresponding to single microparticle events (as opposed to higher scattering aggregates). We then measured the fluorescence intensity of the selected microspheres (Figure 4- 5(B) and Figure 4- 5(E)). Figure 4- 5(C) and Figure 4- 5(F) shows the median fluorescence intensity of the high-scattering microspheres as a function of aptamer concentration. We applied a nonlinear regression as in the TFA analysis with the exception that we also used excel to fit the total protein parameter, $[T]_t$ (we did not have a precise value for the coupling efficiency between target and microparticles). Nonlinear fitting revealed that the dissociation constant,K_d, of DCVKM3 binding DCV was 300 ± 100 nM (average and standard deviation of the three replicates). For EGFR, K_d was 10 ± 7 nM (average and standard deviation of the three replicates). This result supports the conclusion that DCVKM3 does bind DCV and LINN2 binds EGFR. This is independent confirmation of the general conclusion obtained by TFA using the Open qPCR.

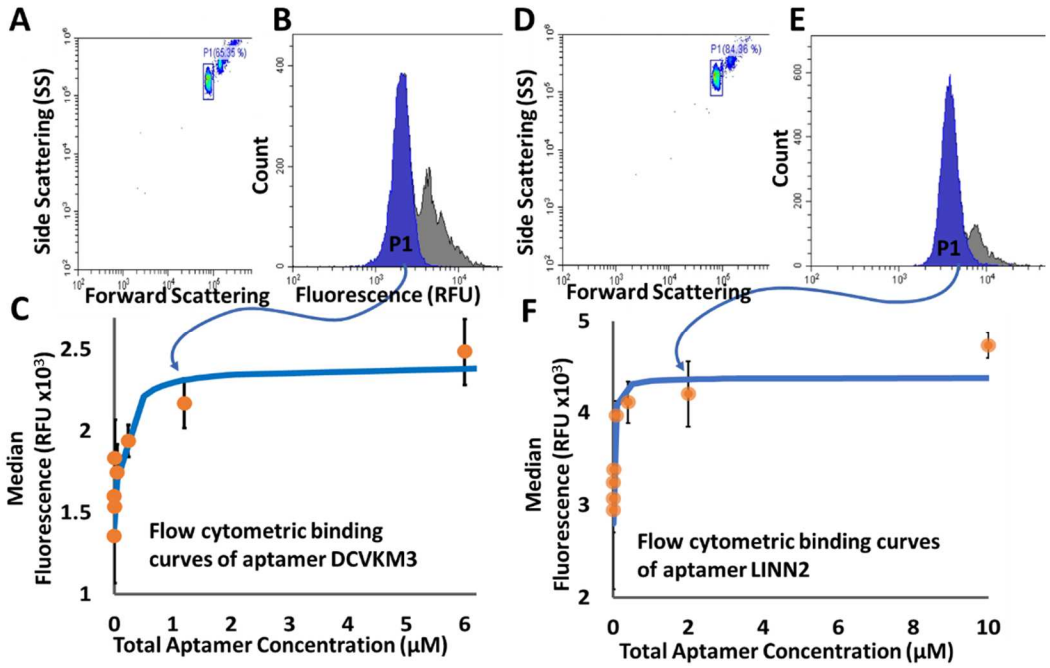

Figure 4- 5: Binding assay by flow cytometry. (A) Flow cytometric scatter plot of particles bearing DCV bound to DCVKM3 aptamer. We chose and analyzed the high scattering events (population P1, blue box) for FITC fluorescence. (B) A histogram shows the FITC fluorescence (RFU) of all events (grey) with population P1 highlighted (blue). We used the median of P1 FITC fluorescence to construct the binding curve of aptamer DCVKM3. (C) A binding curve of aptamer DCVKM3 shows median fluorescence (average and standard deviation of triplicates) as a function of aptamer concentration; best fit binding isotherm is shown in blue. (D) Flow cytometric scatter plot of particles bearing EGFR bound to LINN2 aptamer. We chose and analyzed the high scattering events (population P1, blue box) for FITC fluorescence. (E) A histogram shows the FITC fluorescence of all events (grey) with population P1 highlighted-(blue). We used the median of P1 FITC fluorescence to construct the binding curve of aptamer LINN2. (F) A binding curve of aptamer LINN2 shows median fluorescence (average and standard deviation of triplicates) as a function of aptamer concentration; best fit binding isotherm is shown in blue.

4-2.8. Virus Assay with Aptamer Biorecognition

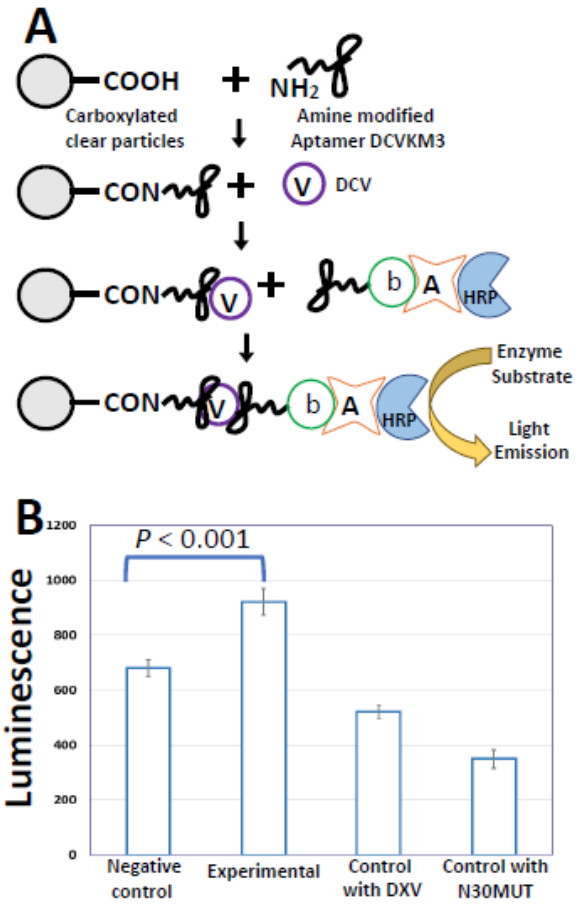

Figure 4- 6: Sandwich assay to detect DCV. (A) Schematic illustrations show the design of the luminescence assay for DCV (V = virus, b = biotin, A = avidin, HRP = horseradish peroxidase). (B) Average (n=69) luminescence values (arbitrary units) are shown for the assay with experimental (DCV) and control samples (null, non-target virus DXV, unrelated DNA sequence N30MUT).

To show the utility of aptamer-based virus detection, we developed an enzyme linked chemiluminescence sandwich assay[30,31]. This is a proof-of-concept demonstration of the use of aptamers in the rapid and sensitive detection of DCV. Such an assay could be used for screening infected flies. We used purified whole virus as our analyte in Figure 4- 5. DCV is a ~10 MD particle with many copies of each capsid protein[32]. The sandwich complex presented in Figure 4- 2B and Figure 4- 5A should work for large viral target, but will likely not work for EGFR; we did not attempt the same technique with EGFR. This assay is similar to enzyme linked aptamer sorbent assay (ELASA)[20,21]. Aptamers replace the antibodies used in traditional ELISA. We conducted the luminescence assay by immobilizing amine-modified aptamer DCVKM3 on the surface of clear carboxylate-coated microspheres (Figure 4- 6(A)). After exposure to sample, the resulting aptamer-DCV microspheres captured biotin-modified DCVKM3

labeled with avidin horseradish peroxidase (HRP) for luminescence detection. We averaged 69 luminescence readings at different locations in the well (Figure 4- 6(B)) to compensate for heterogeneities arising from particle settling. The best test for the specificity of the aptamer-based assay was to measure response to a high concentration of a very similar analyte. We tested the response of the aptamer-based sandwich assay to a sample of a related fly virus, DXV. The luminescence was significantly higher in the case of the DCV sample as compared to a sample containing DXV (the non-target virus). This is a very stringent test of the specificity of this aptamer. We also showed that the scrambled sequence, N30MUT, did not capture the target (we used N30MUT coated microspheres instead of aptamer-coated microspheres). The luminescence of the experimental sample significantly exceeded that of the non-target control ($P < 0.0001$, t-test). Based on this signal and standard deviation, we calculate a limit of detection (3 standard deviations of the average of 69 measurements) to be 0.7 μg of virus.

4-3. Conclusion

We report the use of the Open qPCR instrument in aptamer selection. The resulting aptamers specifically bound our targets. We chose our aptamers from a set of aptamer candidates because they showed adequate affinity and high specificity for our targets as determined with the Open qPCR instrument. The Open qPCR instrument measured the target-aptamer binding using thermofluorimetric analysis (TFA) using the melt curve analysis function (rather than quantitative PCR). Only one other group has performed aptamer binding curve analysis with thermofluorimetry[4]. We have shown that 1) the technique works reliably in a second lab; 2) that the technique can be corroborated with an unrelated technique, flow cytometry; and 3) that thermofluorimetry works with difficult samples like whole virus. The use of thermofluorimetry to measure aptamer-virus binding is a wholly novel result.

Flow cytometry confirmed binding and the DCV-aptamer complex had a dissociation constant (K_d) of 0.3 μM ± 0.1 μM. According to Jousset et. al.[32], DCV virus particles have a total molecular weight of 10 MD and (based on the total protein and constituent molecular weights) have tens of each protein per virus particle. According to Hedges et. al.[33], DCV has a $T = 3$ icosahedral structure. If the aptamer binds to an epitope that occurs 60 times per virus particle, this would suggest that our K_d by TFA (0.18 mg/ml) is equivalent to 1 μM, which is qualitatively similar to the value recovered with flow cytometry.

Furthermore, we developed a proof-of-concept method for the detection of DCV based on aptamer DCVKM3-coated microspheres. The use of a particle surface may enhance binding by presenting multiple aptamers (i.e., avidity effects). The assay was rapid, taking <2 hours for the detection of DCV. The aptamer was specific and did not cross react with a second fly virus, DXV. This methodology has

the potential to contribute to the development of rapid and sensitive detection methods for other viruses. The selected aptamer against DCV is the first aptamer against this target. We developed this aptamer for application in research on DCV infected flies. These results stand as a unique contribution to the field.

The unified use of a single instrument (the Open qPCR) to optimize amplification, screen candidates, and characterize binding is a unique result. We did not use qPCR to replace PCR entirely, however; large scale amplification was carried out with conventional PCR. This work shows that the Open qPCR instrument can be used for multiple tasks during aptamer selection. The instrument is economically priced (~$3,000) and can be used to rapidly optimize a PCR reaction in place of a cyclecourse. It can also quantify DNA obtained after single-strand generation, and screen and characterize aptamer candidates. We measured a binding isotherm with the Open qPCR and TFA; we used flow cytometry to validate the results. TFA is a new technique for aptamer binding assays and has not yet gained popularity. It could become more common as equipment becomes more widely available. TFA is promising as a relatively simple and low-cost binding assay (as compared to radiolabeled dot blots or surface plasmon resonance). Background issues associated with the DCV made the measurement of the DCV-aptamer binding challenging. Nonetheless, TFA identified and characterized the binding. TFA does not require fluorescently-modified DNA or radioisotopes. As such, we anticipate that it will prove generally useful in aptamer research.

4-4. Experimental procedures

4-4.1. Aptamer Library

A single-stranded DNA oligonucleotide pool (N30 pool) was purchased as a gel-purified oligonucleotide from IDT (Integrated DNA Technologies, Coralville, IA, USA) and was used as received. The pool consisted of 30 mer randomized sequence region flanked by two primer-binding sites. The primers used in the selection (P1, P1-f, P2-F and P2-acryd) were also synthesized by IDT. See **Supporting Information Online** for sequence information in Table C- S1.

4-4.2. Preparation of Positive and Negative Selection Microspheres for anti-DCV aptamer selection

DCV, *Drosophila* C virus, (Charolles strain) was originally obtained from Dr. Luis Teixeira, Instituto Gulbenkian de Ciencia, Oeiras, Portugal. DCV was grown in *Drosophila* S2 cells and purified by density gradient ultracentrifugation as described in detail elsewhere[34]. Incubation of 40 µl of pre-washed

and activated magnetic microspheres (ProMag TM Magnetic Microspheres, 1 HC. COOH, solids 2.53% 0.78 µM, Bangs Laboratories Inc., IN, USA) was carried out with 40 µl of DCV (0.44 mg/ml) for 2 hours at room temperature by vortexing, followed by washing in selection buffer (1X phosphate buffer, pH 8, 50 mM Na_2HPO_4, 50 mM NaH_2PO_4, both from EMD Chemicals, Gibbstown, Germany). The microspheres were resuspended in 40 µl of selection buffer. Five µl were then used for each round of aptamer selection (denoted "positive selection microspheres"). Negative selection microspheres were treated as above with the presence of *Drosophila* X virus (DXV, 0.43 mg/ml, prepared by the same methods as DCV). DXV source material was kindly provided by Dr. Louisa Wu, University of Maryland.

4-4.3. Preparation of Positive and Negative Selection Microspheres for anti-EGFR aptamer selection

EGFR, Human Protein, Recombinant (hIgG1-Fc Tag, Active, Sino Biological Life Technologies, CA, USA) was diluted in 80 µl of 2.5X Py modified buffer (pH 6.8, 125 mM Na_2HPO_4, 125 mM NaCl, both from EMD Chemicals, Gibbstown, Germany) resulting a concentration 0.625 µM. Incubation of 40 µl of pre-washed and activated magnetic microspheres (ProMag TM Magnetic Microspheres, 1 HC. COOH, solids 2.53% 0.78 µm, Bangs Laboratories Inc., IN, USA) was carried out with 40 µl of EGFR solution (0.625 µM) for 2 hours at room temperature by vortexing, followed by washing in selection buffer (1X phosphate buffer, pH 8, 50 mM Na_2HPO_4, 50 mM NaH_2PO_4, both from EMD Chemicals, Gibbstown, Germany). The microspheres were resuspended in 40 µl of selection buffer. Five µl were then used for each round of aptamer selection (denoted "positive selection microspheres"). Negative selection microspheres were treated as above with the presence of IgG1-FC Recombinant Human Protein (Sino Biological Life Technologies, CA, USA).

4-4.4. Aptamer Selection

Approximately 500 pmol (10^{14} molecules) of DNA library was annealed in 45 µl of selection buffer. Five µl of negative selection microspheres were then added to the annealed pool and incubated for 30 minutes by rotating at room temperature. This was denoted "negative selection". Magnets were then used to immobilize magnetic microspheres and the supernatant buffer containing the unbound pool was transferred to another vial containing positive selection microspheres. Aptamers were incubated 30 minutes at room temperature with slow mixing at room temperature. This was denoted "positive selection". Unbound DNA was then removed and fresh buffer was added to the tube. Washing was done four times in selection buffer. Microspheres were then resuspended in water and bound aptamers were

eluted after heat treatment (90 °C) for five minutes. The number of PCR cycles required for amplification was then optimized in Open qPCR and the eluted DNA was amplified by PCR. Single-strand generation was carried out in 5% denaturing 7M urea PAGE gel. For EGFR, gel was cast in vertical gel rig. For DCV, the gel was cast with two sets of combs, i.e. loading and extraction combs[27]. The round one (R1) ssDNA pool was generated by aspirating sample from extraction wells followed by ethanol precipitation. Approximately 50 pmol of R1 ssDNA pool was used as pool for second round. Using the same methodology, selection was carried out up to four rounds (anti-EGFR aptamer selection) and eight rounds (anti-DCV aptamer selection).

4-4.5. Library Preparation for anti-DCV aptamer selection

The eluted DNA from rounds 2, 4, 6 and 8 was amplified first with CS1-P1 and CS2-P2 and then with barcoded primers. The amplified product was finally purified by 4% non-denaturing PAGE gel and submitted to the Institute for Bioinformatics and Evolutionary Studies sequencing core facility at the University of Idaho for MiSeq sequencing (MiSeq, Illumina, San Diego, CA, USA).

4-4.6. Library Preparation for anti-EGFR aptamer selection

The eluted DNA of each round (rounds 1, 2, 3 and 4) was amplified first with CS1. P1 and CS2. P2 and then with barcoded primers. The amplified product was finally purified by 4% non-denaturing PAGE gel and submitted to the Institute for Bioinformatics and Evolutionary Studies sequencing core facility at the University of Idaho for MiSeq sequencing (MiSeq, Illumina, San Diego, CA, USA).

4-4.7. Candidate Screening and Affinity Test of anti-DCV Aptamer Candidates

Affinity testing was carried out with four possible aptamer candidates (DCVKM1, DCVKM2, DCVKM3, and DCVKM4) obtained by *k*-mer analysis. Each aptamer candidate (50 pmol) was incubated with 5 µl of positive selection microspheres separately for 30 minutes at 37 °C. This process was followed by washing with 100 µl selection buffer five times. Incubation with 100 µl selection buffer was then carried out for one hour at 37 °C. The supernatant buffer was then removed and 50 µl of water was added. The bound DNA was then eluted by heating the sample at 90 °C in a water bath. The qPCR analysis of eluted DNA was carried out to find the best aptamer candidate. For this, reaction mixtures were made by taking 100 µl of 2X Taq master mix (Thermo Scientific, Waltham, MA, USA), 1 µl of P1(100 µM), 1 µl of P2-acryd (100 µM), 10 µl of evagreen (Evagreen Dye, 20X in water, Biotium, CA, USA) and 78 µl of water (for sequence information see Table C- S1, **Supporting Information Online**). The reaction mixtures were then aliquoted into five vials of 19 µl each. One µl eluted DNA

of each aptamer candidate and 1 µl water were added to vials. Then qPCR was performed with the Open qPCR (CHAI Bio, CA, USA) with the following parameters: denaturation 15 seconds at 95 °C, annealing 15 seconds at 60 °C, and elongation 30 seconds at 68 °C.

4-4.8. Candidate Screening and Affinity Test of anti-EGFR Aptamer Candidates

Affinity testing was carried out with nine possible aptamer candidates (LINN1 through LINN4 and FINNI1 through FINNI5) obtained by *k*-mer analysis. The positive selection microspheres (EGFR coated magnetic microspheres) were blocked and diluted by five times in superblock for 1 hour. The blocked microspheres were washed one time in selection buffer. Two µl of 200 nM of each aptamer candidate (prepared in selection buffer followed by annealed fast and then diluted to 200 nM) was incubated with 2 µl of blocked positive selection microspheres separately for 2 hours at 37 °C. This process was followed by washing, resuspending in 10 µl selection buffer and then observed on the fluorescent microscope (LumaScope 620, EtaLuma, Carlsbad, CA) in the green channel (λ_{ex} 490 nm). The control sample was prepared in the same way by incubating P2-F (instead of aptamer candidates) and performed scoping on the fluorescent microscope.

4-4.9. Specificity Test of anti-DCV aptamer with Fluorescence Microscopy

Specificity test was performed with nonspecific DNA (MUT, a scrambled sequence variant of DCVKM3). To do so, aptamer DCVKM3 was labeled by annealing 40 pmol DCVKM3 with 50 pmol P2-F (a short, fluorescein-conjugated, complementary oligonucleotide; for sequence information see Table C- S1, **Supporting Information Online**) in 20 µl selection buffer. The labeled aptamer was named DCVKM3-F. The amine-modified aptamer DCVKM3 was conjugated with clear carboxylate-coated microspheres (Uniform Microspheres, 2.19 µm, Bangs Laboratories Inc., IN, USA) to make DCVKM3 microspheres. Ten µl aptamer DCVKM3 microspheres incubated with target DCV were further incubated for 30 minutes with 20 pmol of DCVKM3-F. The incubation was followed by washing six times with selection buffer, resuspending in 100 µl selection buffer and then observed on the fluorescent microscope (LumaScope 620, EtaLuma, Carlsbad, CA) in the green channel (λ_{ex} 490 nm). The control sample was prepared in the same way by conjugating amine modified nonspecific DNA (MUT instead of aptamer DCVKM3), with the clear carboxylate-coated microspheres to make control microspheres. The resulting control microspheres were incubated initially with target DCV and then further incubated with DCVKM3-F for 30 minutes. This step was followed by washing and resuspending in 100 µl selection buffer and imaging by fluorescence microscopy.

4-4.10. Specificity Test of anti-EGFR aptamer with Fluorescence Microscopy

To do specificity test, the positive selection microparticles (EGFR coated magnetic microparticles) were blocked and diluted by five times in superblock for 1 hour. The blocked microparticles were washed one time in selection buffer. Two µl of 200 nM of LINN2 aptamer candidate (annealed fast in selection buffer) was incubated at room temperature for 2 hours with 2 µl blocked positive selection microparticles (EGFR coated magnetic microparticles). The incubation was followed by washing, re-suspending in 10 µl selection buffer and then observed on the fluorescent microscope. Similarly, incubation of LINN2 aptamer candidate with blocked negative selection microparticles (IgG1Fc coated magnetic microparticles) was carried out.

The control of P2-F was prepared in the same way as LINN2 aptamer candidate and incubated with positive and negative selection microparticles separately and observed in Fluorescence microscope respectively.

4-4.11. Binding Assay by Thermofluorimetric Analysis (anti-EGFR Aptamer)

Binding of aptamer to target was tested with melting curve analysis. To do so, protein buffer was made. Protein buffer is a 1:4 mixture of 5X Py buffer (pH 6.8, 250 mM Na_2HPO_4, 250 mM NaCl, both from EMD Chemicals, Gibbstown, Germany) and 1X phosphate buffer (pH 8, 50 mM Na_2HPO_4, 50 mM NaH_2PO_4, both from EMD Chemicals, Gibbstown, Germany). Then master solution containing 1X EvaGreen, and 1X LINN2 (50 nM) was made in protein buffer. Then stock sample containing 1X EvaGreen, 1X LINN2 and EGFR (500 nM as shown in Figure 4- 4, and 250 nM as shown in Figure C-S6) was made. This was serially diluted eight times with 2-fold dilutions in master solution. The control experiment was carried out similarly without aptamer LINN2 as shown in Figure C- S5 in **Supporting Information Online**. One more control experiment was carried out similarly without target EGFR as shown in Figure C- S3 in **Supporting Information Online**. All samples were placed in the Open qPCR and melt curve data was acquired at 1.2 °C per min with data collection at 30 seconds intervals. A unique feature in the dF/dT curve at in the aptamer+EGFR samples was noted. This signal increased in magnitude as a function of EGFR concentration.

4-4.12. Binding Assay by Thermofluorimetric Analysis (anti-DCV Aptamer)

Binding of aptamer to target was tested with melting curve analysis. To do so, master solution containing 1X EvaGreen, and 1X DCVKM3 (50 nM) was made in selection buffer. Then stock sample containing 1X EvaGreen, 1X DCVKM3 and DCV (concentration in mg/ml as shown in Figure 4- 4, 0.22

mg/ml and Figure C- S7, 0.15 mg/ml) was made. This was serially diluted eight times with 2-fold dilutions in master solution. The control experiment was carried out similarly without aptamer DCVKM3 for background correction contributed by virus, DCV itself. The aptamer only control experiment was carried out similarly without target as shown in Figure C- S4 in **Supporting Information Online**. One more control experiment was performed by taking non-specific DNA "NS-DNA" instead of aptamer DCVKM3 in a similar way as with aptamer DCVKM3 as shown in Figure C- S2 in **Supporting Information Online**. All sets of samples were placed in the Open qPCR and melt curve data was acquired at 1.2 °C per min with data collection at 30 seconds intervals. A unique feature in the dF/dT curve at in the aptamer+DCV samples relative to the DCV-only samples was noted. This feature appeared as a decrease in the melting rate for the aptamer-DCV complex at 25-30 °C (for a direct comparison of the controls and experimental, see Figure C- S1 in **Supporting Information Online**). The difference in melting rate between DCV only and aptamer+DCV at 25-30 °C was taken as a signal. This signal increased in magnitude as a function of DCV concentration.

4-4.13. Binding Assay by Flow Cytometric Analysis

To do flow cytometric analysis of DCVKM3 aptamer, target DCV-coated clear microspheres were made by conjugating DCV with clear carboxylate-coated microspheres by the same procedure as above. DCVKM3-am, an amine modified aptamer, was conjugated with FITC (Sigma-Aldrich, MO, USA) to yield DCVKM3-FITC (12 µM, analyzed by Quick drop, Molecular Devices, CA, USA). DCVKM3-FITC (25 µl) was added to the first PCR tube containing 25 µl of selection buffer and then 5-fold serial dilution was carried out across eight tubes in selection buffer. Five µl of DCV-coated clear microspheres were added to each tube and incubated for 30 minutes. Ten µl incubated sample was taken in a vial and 200 µl selection buffer was added to wash. After removing supernatant, particles were finally resuspended in 200 µl of the selection buffer to perform flow cytometric analysis using a Beckman Coulter CytoFLEX S.

In case of LINN2 aptamer, we carried out whole experiments in similar way as DCVKM3 aptamer, by taking EGFR coated clear microspheres and 3'-fluorescein modified LINN2 aptamer (LINN2-F, ~10 µM). LINN2-F (50 µl) was added to the first PCR tube and then 5-fold serial dilution was carried out across eight tubes in selection buffer. Five µl of EGFR-coated clear microspheres were added to each tube and incubated for 30 minutes. Ten µl incubated sample was taken in a vial and 200 µl selection buffer was added to wash. After removing supernatant, particles were finally resuspended in 200 µl of the selection buffer to perform flow cytometric analysis using a Beckman Coulter CytoFLEX S.

4-4.14. Aptamer Sandwich Assay to Detect Virus

To perform the aptamer-based detection assay for DCV, DCVKM3 microspheres were made by conjugating amine modified aptamer DCVKM3 with clear carboxylate-coated microspheres. Ten µl of DCVKM3 microspheres were incubated with 4 µl of DCV (2 ug) for 1 hour at room temperature. The resulting microspheres (obtained by incubating DCVKM3 microspheres with DCV) were blocked by washing (centrifugation, supernatant removal and resuspension) three times in commercial, protein-based blocking buffer (1% Superblock, Thermo Scientific, IL, USA in selection buffer). One hundred µl of 200 nM complex of biotinylated aptamer DCVKM3 conjugated with avidin HRP (Thermo Fisher Scientific, CA, USA) was added followed by incubation for 30 minutes at room temperature by shaking. Washing was then carried out two times with 100 µl of the selection buffer and finally resuspended in 20 µl of the selection buffer. Five µl of the resuspended sample was loaded in a well of 384-well plates (Microplate, 384 well, PS, F-Bottom, Black, Non-Binding, Germany) followed by addition of 45 µl of 1:1 mixture of supersignal (Enhancer solution and stable peroxide solution, Thermo Scientific, USA). The absorbance value was measured at 450 nm and 25 °C in multi-mode microplate reader (SpectraMax iD3, Molecular Devices, CA, USA). The experiment was carried out in triplicate. Three control experiments were carried out in a similar way. The negative control was carried out without adding target DCV whereas the non-target control was carried out by adding DXV instead of DCV. A third control (MUT) was carried out using MUT microspheres instead of DCVKM3 microspheres.

4-5. Acknowledgments

This publication was made possible by an Institutional Development Award (IDeA) from the National Institute of General Medical Sciences of the National Institutes of Health under Grant P20GM103408. Research reported in this publication was supported by the National Institute of General Medical Sciences of the National Institutes of Health under Award Number P20GM104420. This published work was supported by an Institutional Development Award (IDeA) from the National Institute of General Medical Sciences of the National Institutes of Health under grant number P30 GM103324.The content is solely the responsibility of the authors and does not necessarily represent the official views of the National Institutes of Health.

AUTHOR INFORMATION

Corresponding Author

Email: *pballen@uidaho.edu

Notes

The authors declare no competing financial interest.

4-6. References

(1) Zhang, C.; Wijnen, B.; Pearce, J. M. Open-Source 3-D Platform for Low-Cost Scientific Instrument Ecosystem. *J. Lab. Autom.* **2016**, 2211068215624406.

(2) Pearce, J. M. Emerging Business Models for Open Source Hardware. *J. Open Hardw.* **2017**, *1* (1).

(3) Darmostuk, M.; Rimpelova, S.; Gbelcova, H.; Ruml, T. Current Approaches in SELEX: An Update to Aptamer Selection Technology. *Biotechnol. Adv.* **2015**, *33* (6, Part 2), 1141–1161.

(4) Hu, J.; Kim, J.; Easley, C. J. Quantifying Aptamer-Protein Binding via Thermofluorimetric Analysis. *Anal. Methods Adv. Methods Appl.* **2015**, *7* (17), 7358–7362.

(5) Nguyen, V.-T.; Kwon, Y. S.; Gu, M. B. Aptamer-Based Environmental Biosensors for Small Molecule Contaminants. *Curr. Opin. Biotechnol.* **2017**, *45*, 15–23.

(6) Tang, Z.; Shangguan, D.; Wang, K.; Shi, H.; Sefah, K.; Mallikratchy, P.; Chen, H. W.; Li, Y.; Tan, W. Selection of Aptamers for Molecular Recognition and Characterization of Cancer Cells. *Anal. Chem.* **2007**, *79* (13), 4900–4907.

(7) Woo, H.-M.; Kim, K.-S.; Lee, J.-M.; Shim, H.-S.; Cho, S.-J.; Lee, W.-K.; Ko, H. W.; Keum, Y.-S.; Kim, S.-Y.; Pathinayake, P.; et al. Single-Stranded DNA Aptamer That Specifically Binds to the Influenza Virus NS1 Protein Suppresses Interferon Antagonism. *Antiviral Res.* **2013**, *100* (2), 337–345.

(8) Ashrafuzzaman, M. Aptamers as Both Drugs and Drug-Carriers. *BioMed Res. Int.* **2014**, *2014*, e697923.

(9) Meng, H.-M.; Liu, H.; Kuai, H.; Peng, R.; Mo, L.; Zhang, X.-B. Aptamer-Integrated DNA Nanostructures for Biosensing, Bioimaging and Cancer Therapy. *Chem. Soc. Rev.* **2016**, *45* (9), 2583–2602.

(10) Chtarbanova, S.; Lamiable, O.; Lee, K.-Z.; Galiana, D.; Troxler, L.; Meignin, C.; Hetru, C.; Hoffmann, J. A.; Daeffler, L.; Imler, J.-L. Drosophila C Virus Systemic Infection Leads to Intestinal Obstruction. *J. Virol.* **2014**, *88* (24), 14057–14069.

(11) Kapun, M.; Nolte, V.; Flatt, T.; Schlötterer, C. Host Range and Specificity of the Drosophila C Virus. *PLOS ONE* **2010**, *5* (8), e12421.

(12) Unckless, R. L. A DNA Virus of Drosophila. *PLOS ONE* **2011**, *6* (10), e26564.

(13) Baselga, J. The EGFR as a Target for Anticancer Therapy--Focus on Cetuximab. *Eur. J. Cancer* **2001**, *37* (Supplement 4), 16–22.

(14) Li, N.; Nguyen, H. H.; Byrom, M.; Ellington, A. D. Inhibition of Cell Proliferation by an Anti-EGFR Aptamer. *PLoS ONE* **2011**, *6* (6), e20299.

(15) Ellington, A. D.; Szostak, J. W. In Vitro Selection of RNA Molecules That Bind Specific Ligands. *Nature* **1990**, *346* (6287), 818–822.

(16) Tuerk, C.; Gold, L. Systematic Evolution of Ligands by Exponential Enrichment: RNA Ligands to Bacteriophage T4 DNA Polymerase. *Science* **1990**, *249* (4968), 505–510.

(17) Kim, E.; Dua, P.; Kim, S. Cell-Based Aptamer Selection for Diagnosing Cancer and Predicting Cancer Progression. *Toxicol. Environ. Health Sci.* **2009**, *1* (2), 140–143.

(18) Cao, B.; Hu, Y.; Duan, J.; Ma, J.; Xu, D.; Yang, X.-D. Selection of a Novel DNA Aptamer for Assay of Intracellular Interferon-Gamma. *PLOS ONE* **2014**, *9* (5), e98214.

(19) Nitsche, A.; Kurth, A.; Dunkhorst, A.; Pänke, O.; Sielaff, H.; Junge, W.; Muth, D.; Scheller, F.; Stöcklein, W.; Dahmen, C.; et al. One-Step Selection of Vaccinia Virus-Binding DNA Aptamers by MonoLEX. *BMC Biotechnol.* **2007**, *7*, 48.

(20) Schütze, T.; Wilhelm, B.; Greiner, N.; Braun, H.; Peter, F.; Mörl, M.; Erdmann, V. A.; Lehrach, H.; Konthur, Z.; Menger, M.; et al. Probing the SELEX Process with Next-Generation Sequencing. *PLOS ONE* **2011**, *6* (12), e29604.

(21) Blind, M.; Blank, M. Aptamer Selection Technology and Recent Advances. *Mol. Ther. — Nucleic Acids* **2015**, *4* (1), e223.

(22) Cho, M.; Soo Oh, S.; Nie, J.; Stewart, R.; Eisenstein, M.; Chambers, J.; Marth, J. D.; Walker, F.; Thomson, J. A.; Soh, H. T. Quantitative Selection and Parallel Characterization of Aptamers. *Proc. Natl. Acad. Sci. U. S. A.* **2013**, *110* (46), 18460–18465.

(23) Szeto, K.; Latulippe, D. R.; Ozer, A.; Pagano, J. M.; White, B. S.; Shalloway, D.; Lis, J. T.; Craighead, H. G. RAPID-SELEX for RNA Aptamers. *PLOS ONE* **2013**, *8* (12), e82667.

(24) Mosing, R. K.; Mendonsa, S. D.; Bowser, M. T. Capillary Electrophoresis-SELEX Selection of Aptamers with Affinity for HIV-1 Reverse Transcriptase. *Anal. Chem.* **2005**, *77* (19), 6107–6112.

(25) Hoon, S.; Zhou, B.; Janda, K. D.; Brenner, S.; Scolnick, J. Aptamer Selection by High-Throughput Sequencing and Informatic Analysis. *BioTechniques* **2011**, *51* (6), 413–416.

(26) Keefe, A. D.; Pai, S.; Ellington, A. Aptamers as Therapeutics. *Nat. Rev. Drug Discov.* **2010**, *9* (7), 537–550.

(27) Damase, T. R.; Ellington, A. D.; Allen, P. B. Purification of Single-Stranded DNA by Co-Polymerization with Acrylamide and Electrophoresis. *BioTechniques* **2017**, *62* (6), 275–282.

(28) Kim, J.; Hu, J.; Bezerra, A. B.; Holtan, M. D.; Brooks, J. C.; Easley, C. J. Protein Quantification Using Controlled DNA Melting Transitions in Bivalent Probe Assemblies. *Anal. Chem.* **2015**, *87* (19), 9576–9579.

(29) Meyer, M.; Scheper, T.; Walter, J.-G. Aptamers: Versatile Probes for Flow Cytometry. *Appl. Microbiol. Biotechnol.* **2013**, *97* (16), 7097–7109.

(30) Moore, M. D.; Escudero-Abarca, B. I.; Jaykus, L.-A. An Enzyme-Linked Aptamer Sorbent Assay to Evaluate Aptamer Binding. *Methods Mol. Biol. Clifton NJ* **2017**, *1575*, 291–302.

(31) Toh, S. Y.; Citartan, M.; Gopinath, S. C. B.; Tang, T.-H. Aptamers as a Replacement for Antibodies in Enzyme-Linked Immunosorbent Assay. *Biosens. Bioelectron.* **2015**, *64*, 392–403.

(32) Jousset, F.-X.; Bergoin, M.; Revet, B. Characterization of the Drosophila C Virus. *J. Gen. Virol.* **1977**, *34* (2), 269–283.

(33) Hedges, L. M.; Johnson, K. N. Induction of Host Defence Responses by Drosophila C Virus. *J. Gen. Virol.* **2008**, *89* (6), 1497–1501.

(34) Osborne, S. E.; Leong, Y. S.; O'Neill, S. L.; Johnson, K. N. Variation in Antiviral Protection Mediated by Different Wolbachia Strains in Drosophila Simulans. *PLOS Pathog.* **2009**, *5* (11), e1000656.

CHAPTER 5: IDIOSYNCRASIES OF THERMOFLUORIMETRIC APTAMER BINDING ASSAYS

Forthcoming in: Biotechniques.

To explore thermofluorimetric analysis (TFA) in detail, we compared two related aptamers. The first, LINN2, is a DNA aptamer previously selected against EGFR recombinant protein. In this work, we selected a second aptamer, KM4, against EGFR-overexpressing A549 cells. The two aptamers were derived from the same pool and bind the same target but behave differently in TFA. Our results suggest four overall conclusions about TFA of aptamers: 1. some aptamers show reduced fluorescence upon target binding suggesting that target-bound aptamer is not always fluorescent; 2. many aptamers do not obey the intuitive assumptions that aptamer-target interactions stabilize a folded conformation; 3. TFA may be most appropriate for aptamers with significant double-stranded structure; 4. kinetic effects may be significant and the order of operations in preparing samples should be carefully optimized.

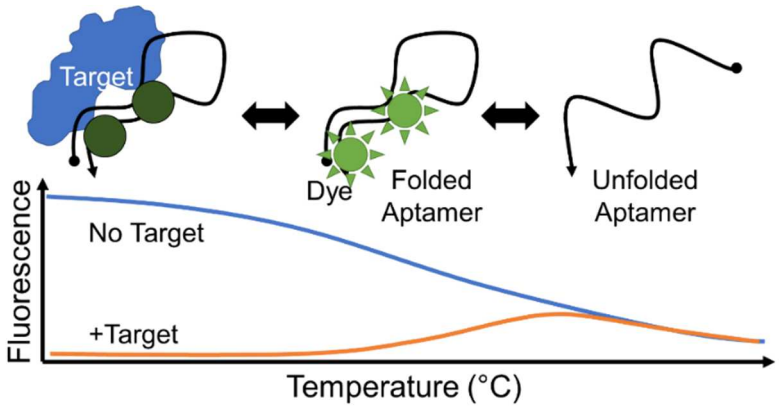

Keywords: Aptamer, EGFR, Thermofluorimetric Analysis, Cell-SELEX, Hybrid SELEX, Binding assay, melt curve analysis, fluorescence, Open qPCR, EvaGreen.

5-1. Introduction

Thermofluorimetry is an accessible technique for measuring aptamer-target equilibrium [1]. Aptamers are single-stranded DNA (ssDNA) or RNA that bind a target molecule. Aptamers have been generated using an in vitro process called SELEX (systematic evolution of ligands by exponential enrichment) since 1990 [2,3]. In SELEX, DNA that binds a target is isolated from a pool of DNA with random sequences and structures. Measuring the binding strength of the resulting aptamers is often either slow (e.g., gel shift analysis [4,5]) or are very complex and expensive (e.g., surface plasmon resonance analysis [6,7], flow cytometry [8–12]). Thermofluorimetry (or melt curve analysis) can be performed with most qPCR

instruments (including the inexpensive Open qPCR instrument) and can make sensitive measurements without separation of bound and unbound DNA. However, thermofluorimetry has several caveats which we explore in this work through a comparison of a published aptamer against EGFR [8] and a new aptamer from an identical parent pool.

Thermofluorimetry measures the loss of fluorescence as a dye (like EvaGreen, EG, or SYBR Green) dissociates from DNA during thermal melting of double-stranded structure. It might be assumed that target-bound DNA structures should melt at a higher temperature than the unbound aptamer. However, the shape of the melt curve is dependent on the specific properties of the individual aptamer. The perturbation of this melting process by target can generate a binding isotherm. However, the interpretation of these features in terms of specific thermodynamic properties is difficult.

We have analyzed two aptamers from an identical pool to compare the thermofluorimetric properties. To select the new aptamer, we pre-selected the pool against recombinant Epidermal Growth Factor Receptor (EGFR) for 4 rounds (after which the pool displayed high diversity as determined by high throughput sequencing). We then continued the selection using A549 cells overexpressing EGFR. This is a version of "hybrid SELEX" [13–15] and, to the best of our knowledge, represents the first cell-SELEX DNA aptamer against wild-type EGFR. EGFR is overexpressed in many cancer cells. Currently, EGFR diagnosis is based on anti-EGFR antibodies[9]. DNA is more easily synthesized with modifications like fluorophores and attachment chemistry for diagnostic applications.

Aptamers generated against soluble, purified, cell-surface proteins in non-physiological conditions will often not recognize the same protein in its native conformation. This problem can be overcome by selecting aptamers for their ability to bind whole living cells under native conditions. Esposito et al. (2011) reported RNA aptamers against EGFR using cell-SELEX [16]. Tan et al. (2013) reported DNA aptamers against target human glioblastoma multiforme (GBM) cells overexpressing epidermal growth factor receptor variant III (EGFRvIII), the most common form of EGFR mutation, using cell-SELEX[17]. Unlike the published DNA aptamer against EGFR recombinant target protein[8] the new aptamer presented here does bind to cells overexpressing EGFR.

We tested the ability of our new aptamer to bind EGFR with three methods: qPCR, flow cytometry, and thermofluorimetry. Thermofluorimetry (melt curve analysis) is a relatively new method with several surprising caveats. We present data showing the importance of annealing and the order of operations as well as careful interpretation of the melting curve signal. The method of thermofluorimetry for binding assays is relatively new and has many advantages. A simple model predicts changes in the TFA

signal on target binding but is too simplistic: it ignores kinetics and the perturbations of binding by dye. We discuss the simple model and its limitations of this model in light of our data.

5-2. Method Summary

We compare two aptamers generated from identical pools against EGFR to explore the advantages and limitations of thermofluorimetric analysis (TFA).

5-3. Materials & Methods

5-3.1. Specificity test using the real-time Apta-PCR

KM4 aptamer candidate (generated by hybrid cell-SELEX see Supplementary Data Figure D- S1) was incubated at room temperature for 2 hours with 2 µl blocked positive microspheres (EGFR coated clear microspheres). The incubation was followed by washing, resuspending in selection buffer and then amplification (95°C-15secs, 64°C-15secs, 69°C-30secs) on the Open qPCR. Similarly, blocked positive microspheres were incubated with scrambled DNA, "MUT-DNA" (flanked with primer binding sites) and the same amplification analysis was performed with the Open qPCR.

5-3.2. Binding Assay by Thermofluorimetric Analysis

Master solution containing 1X EvaGreen (EG), and 1X KM4 (50 nM) was made in protein buffer (see Supplementary Data for details) and then annealed (80°C-30 secs, rapidly cool to 4°C). Sample containing 1X EG, 1X KM4 and EGFR was serially diluted eight times with 2-fold dilutions in master solution containing 1X EG and 1X KM4 such that only target (EGFR) was diluted. The control experiment was carried out similarly without a target. Samples were placed in the Open qPCR and melt curve data were acquired at 1.2 °C per min with data collection every 30 seconds. We noted a unique feature in the dF/dT curve (first derivative of fluorescence with respect to temperature) in the aptamer+EGFR samples. This signal increased as a function of EGFR concentration. The importance of annealing was tested with melting curve analysis. To do so, the experiment was carried out similarly as above skipping an annealing step. A further control experiment was performed by taking non-specific DNA "NS-DNA" instead of aptamer KM4 in a similar way as with aptamer KM4.

5-4. Results and Discussion

5-4.1. Screening of selected aptamers with EGFR cells

We selected a second aptamer KM4 from same pool to explore thermofluorimetric analysis (TFA) in detail. To do so, we performed hybrid-SELEX with recombinant protein and EGFR-positive cells (see Supplementary Data Figure D- S1). We evaluated our hybrid SELEX candidates with qPCR (see Supplementary Data Figure D- S2), fluorescence microscopy (see Supplementary Data Figure D- S3), and flow cytometry (see Supplementary Data Figure D- S4). We found a candidate comparable to published aptamer LINN2 (see Supplementary Data Figure D- S5). We concluded that KM4 binds to the A431 cells. We chose the KM4 sequence for further analysis.

5-4.2. Recombinant EGFR binding using the qPCR

Prior to comparison of thermofluorimetric properties in detail, we needed to characterize our second aptamer, KM4. We tested binding of cell-SELEX aptamer KM4 against recombinant EGFR using real-time Apta-PCR analysis. We found that KM4 binds to recombinant EGFR-coated microspheres (see Figure 5- 1). The KM4 aptamer was synthesized with primer binding regions. We also acquired a scrambled aptamer which also included primer binding regions. We incubated blocked, positive microspheres (EGFR coated clear microspheres) with the KM4 aptamer. We varied the concentration of the KM4 from 0 to 10 µM. We tested the negative control DNA at the high concentration of 10 µM. The Open qPCR computes a Ct (cycle at which fluorescence exceeds a threshold value) for each sample. We computed ΔCt by comparison to a water-only control (where water was added to the qPCR master mix instead of template). The results revealed the selected aptamer KM4 could bind to recombinant EGFR as well as EGFR-overexpressing cells.

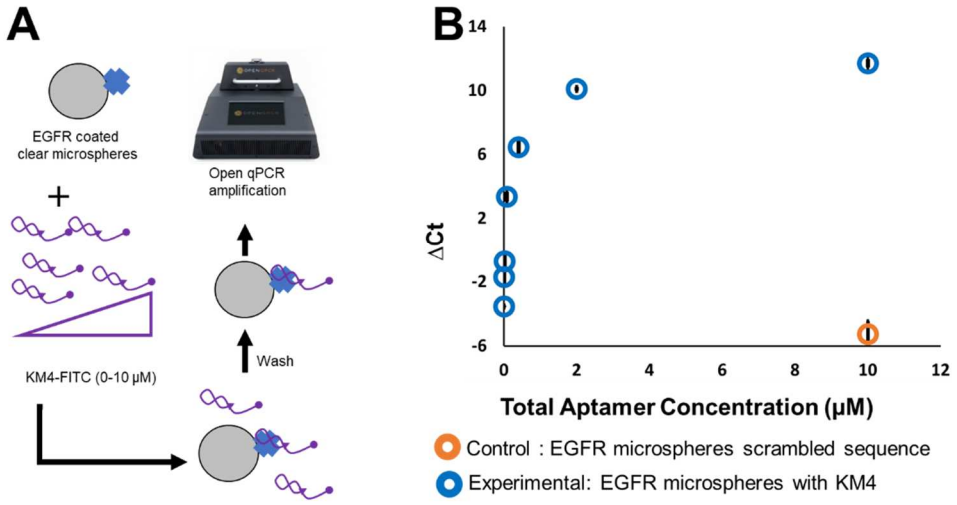

Figure 5- 1: Real-time Apta-PCR to confirm binding of aptamer KM4 to recombinant EGFR. (A) Schematic of the steps of Apta-PCR analysis. (B) qPCR ΔCt is plotted as a function of total aptamer concentration. ΔCt was calculated as the difference between the cycle threshold of the sample and negative control. Error bars are standard deviations of triplicates.

5-4.3. Thermofluorimetric Analysis (TFA)

We used KM4 to explore the differences in TFA response as compared to LINN2. Having confirmed that aptamer KM4 binds to A431 cells and recombinant EGFR, we measured the binding using thermofluorimetry (as shown in Figure 5- 2A). These results show a melting transition that represents an analytical signal at 30-32°C. The analytical signal corresponds to the interaction between the aptamer and target. We chose the average value of the dF/dT signal at 30-32°C and plotted against EGFR concentration to create a binding curve. Depending on the aptamer, we use a temperature from 22-60°C. Within this temperature range, we look for a distinct, changing signal as a function of target concentration. We excluded temperatures above 60°C (as such temperatures will likely denature aptamer and/or protein structure). In the case of the TFA shown in Figure 5- 2, 30-32°C was chosen by inspection to have a significant change as a function of protein concentration. The graph in Figure 5- 2 was calculated as follows for the 250 nM EGFR case; the other concentrations were calculated similarly. A sample containing 250 nM of EGFR concentration and 50 nM of KM4 was subjected to thermal denaturation while monitoring fluorescence. The Open qPCR reports -dF/dT or the rate of fluorescence loss as a function of temperature. Melt curve data (-dF/dT) were collected from 30-32°C at 5 temperature points and the average and standard deviation were calculated to be 315 ± 140 RFU/°C. The equivalent average -dF/dT data for the blank (0 nM EGFR plus 50 nM KM4) was calculated to be 1390 RFU/°C. We normalized the -dF/dT signal of the EGFR-containing sample to the blank (0 nM EGFR) and calculated a ratiometric signal of 0.22 ± .10 for 250 nM EGFR and 50 nM KM4. This ratiometric signal is plotted

in terms of normalized dF/dT for clarity. Seven results are displayed because the eighth experiment (the blank) was used to normalize the other seven experiments. We fitted nonlinear regression analysis and calculated K_d as ~ 1 nM as shown in Figure 5- 2B. We performed a control experiment similarly taking nonspecific DNA, NS-DNA instead of aptamer KM4 (as shown in Figure 5- 2B, blue circles). Nonspecific DNA does not show binding.

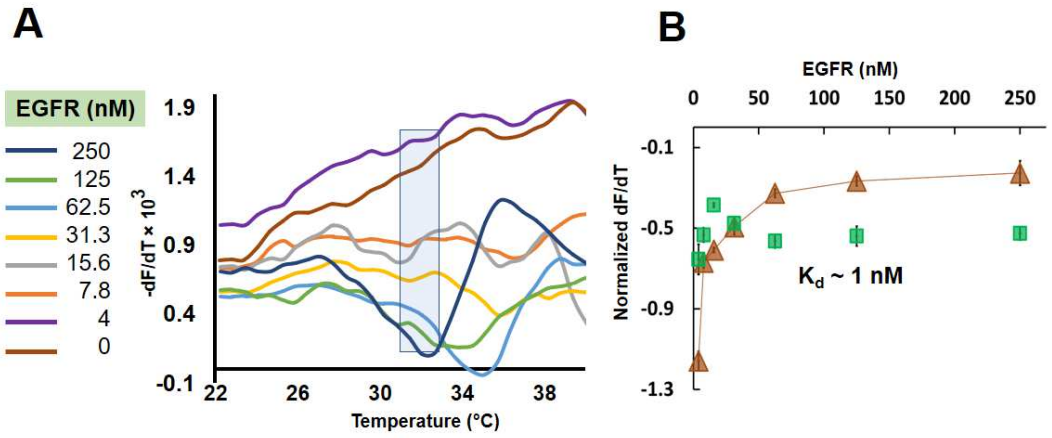

Figure 5- 2: TFA to determine the binding constant of aptamer KM4 to recombinant EGFR. (A) The derivative signal (dF/dT) is plotted as a function of temperature. The value of dF/dT changes intensity in as a function of EGFR concentration. (B) Comparison of binding isotherm of the aptamer (KM4) and nonspecific DNA (NS DNA). The binding curve was generated by plotting dF/dT vs. EGFR concentration at 30-32°C. Error bars are standard deviations of the differential signals at 30-32°C.

The measured K_d from TFA (~1 nM) differs from that derived from cytometry (K_d = 46 nM, see Supplementary Data Figure D- S4). There are multiple reasons to account for this difference: 1.) TFA is a homogeneous, one-step technique. Flow cytometric analysis is a heterogeneous technique and requires washing. Washing might reduce the observed affinity of the aptamer. 2.) In TFA, the signal-to-background ratio is aptamer-specific. Some uncertainty of the signal at low target concentrations might be the reason for the difference in K_d. 3.) Each aptamer also differs in its binding mechanism and entropically driven aptamers can show significantly higher affinity at a higher temperature [18–20]. 4.) TFA uses intercalating dyes to report the interaction of aptamer and target. EvaGreen (EG) is an intercalating dye and consists of two acridine orange moieties linked with a flexible spacer. Intercalation may affect DNA structure, and bound dye may interact with the protein as well.

5-4.4. Model of TFA

We constructed an equilibrium model to examine the thermofluorimetric behavior produced by different mechanistic assumptions. We show that an intuitive model of aptamer-target melting cannot produce the results we obtained. Under the intuitive model, a fluorescent aptamer will be stabilized by target binding. Under this model, aptamer-target complex is stabilized and will remain fluorescent at higher temperatures (compared to aptamer alone). This may be true for some aptamers but is not true for KM4 or LINN2. We suspect that the mechanism of signal generation in TFA will be specific to the aptamer sequence. To show the contrast between this predicted behavior and our observed behavior, we generated four simulated melt curves for qualitative comparison to our data.

To construct this model, we consider two simultaneous equilibria between three states: 1: target-bound, structured holo-aptamer ("H"); 2: an unbound, structured apo-aptamer ("A"); and 3: unbound, denatured, linear aptamer ("L"). The equilibrium between apo-aptamer and linear aptamer is assumed to be governed by a binding enthalpy and temperature independent entropy on the order of that derived from mFold [21]. The binding energy is derived from published aptamer calorimetric data (and so is realistic but not related to this specific aptamer) [22]. The model ignores dye-DNA equilibrium and any possible kinetic effects. This equilibrium model should be considered a qualitative exploration of overall trends.

We show our experimental melt curve data (Figure 5- 3A-B) and four simulated cases for comparison. We consider that the holo-aptamer may or may not be fluorescent. We also consider two scenarios for the thermodynamics of aptamer-target binding: 1. where the aptamer-target binding equilibrium coefficient is nearly constant over the relevant temperature range per known data[22] and; 2. where we contrive that the aptamer-target complex should also display melting behavior in the relevant range.

The model was defined by two equilibria: K_{al} is the apo-linear (melting) equilibrium coefficient, and K_{ah} is the apo-holo (binding) equilibrium coefficient:

$$\frac{A}{L} = K_{al} \tag{1}$$

$$\frac{A \times T}{H} = K_{ah} \tag{2}$$

These equilibria were constrained by the total aptamer, A_{tot}, and the total target, T_{tot}:

$$A + L + H = A_{tot} \tag{3}$$

$$H + T = T_{tot} \tag{4}$$

These four equations can be solved explicitly (see Supplementary Data, Python source code). The result is an expression for the Holo-aptamer (H) and Apo-aptamer (A) concentration as a function of K_{al}, K_{ah}, A_{tot}, and T_{tot}.

$$[H] = \frac{(A_{tot} \cdot K_{al}) + (K_{ah} \cdot K_{al}) + K_{ah} + (K_{al} \cdot T_{tot}) - \sqrt{\begin{array}{c}(A_{tot}{}^2 \cdot K_{al}{}^2) + (2A_{tot} \cdot K_{ah} \cdot K_{al}{}^2) + (2A_{tot} \cdot K_{ah} \cdot K_{al}) \\ -(2A_{tot} \cdot K_{al}{}^2 \cdot T_{tot}) + (K_{ah}{}^2 \cdot K_{al}{}^2) + (2K_{ah}{}^2 \cdot K_{al}) + K_{ah}{}^2 + \\ (2K_{ah} \cdot K_{al}{}^2 \cdot T_{tot}) + (2K_{ah} \cdot K_{al} \cdot T_{tot}) + (K_{al}{}^2 \cdot T_{tot}{}^2)\end{array}}}{2K_{al}} \quad (5)$$

$$[A] = \frac{(A_{tot} \cdot K_{al}) - (K_{ah} \cdot K_{al}) - K_{ah} - (K_{al} \cdot T_{tot}) + \sqrt{\begin{array}{c}(A_{tot}{}^2 \cdot K_{al}{}^2) + (2A_{tot} \cdot K_{ah} \cdot K_{al}{}^2) + (2A_{tot} \cdot K_{ah} \cdot K_{al}) \\ -(2A_{tot} \cdot K_{al}{}^2 \cdot T_{tot}) + (K_{ah}{}^2 \cdot K_{al}{}^2) + (2K_{ah}{}^2 \cdot K_{al}) + K_{ah}{}^2 \\ +(2K_{ah} \cdot K_{al}{}^2 \cdot T_{tot}) + (2K_{ah} \cdot K_{al} \cdot T_{tot}) + (K_{al}{}^2 \cdot T_{tot}{}^2)\end{array}}}{2(K_{al}+1)} \quad (6)$$

This equilibrium model allowed us to calculate theoretical concentrations for holo-aptamer, apo-aptamer, and linear DNA at a range of target concentrations and temperatures. The result is a simulated TFA curve that can show a variety of behaviors over a reasonable range of input parameters. Intuitive assumptions (apo- and holo-aptamer are fluorescent; K_{ah} is constant) produce the behavior shown in Figure 5- 3C. In this case, aptamer binding produces increased fluorescence and an apparent increase in melting temperature. However, this simulated curve is clearly inconsistent with the data for KM4 and LINN2. Figure 5- 3F is more qualitatively consistent and is derived from the assumption that the bound aptamer is non-fluorescent and has an independent melting event. The model shows that LINN2 and KM4 do not follow intuitive assumptions about the underlying chemistry of thermofluorimetric analysis. We suggest the following considerations when analyzing TFA melt curves:

1. Some aptamers may not obey the assumption that both the holo-aptamer and apo-aptamer are highly fluorescent. We should acknowledge that either may bind intercalating dye more efficiently depending on the specific aptamer DNA sequence.
2. Some aptamers may not obey the assumption that target is released from bound aptamer at a different temperature than the denaturation of the unbound folded structure.
3. Some aptamers may produce more fluorescence than others in the presence of fluorogenic dyes. Some aptamers will therefore perform better in TFA than others. With dyes like EG, the signal-to-background ratio is better for aptamers with significant double-stranded structure (see predicted secondary structures, Supplementary Data Figure D- S5).

We attempted to fit the simulation to experimental TFA data to determine the thermodynamic parameters. Although the data resemble the model shown in Figure 5- 3F, the fit parameters derived from that model were highly contradictory. This further indicates that the equilibrium model is not a complete description of the process. Fitting the model to the curve of the aptamer alone (0 nM EGFR) yielded a set of thermodynamic constants for the melting equilibrium. Fitting the case with 65 nM of EGFR present yielded another set of thermodynamic constants for the melting equilibrium and constants for the binding equilibrium. These constants were irreconcilable. Fitting both simultaneously failed to converge (see Supplementary Data Figure D- S6).

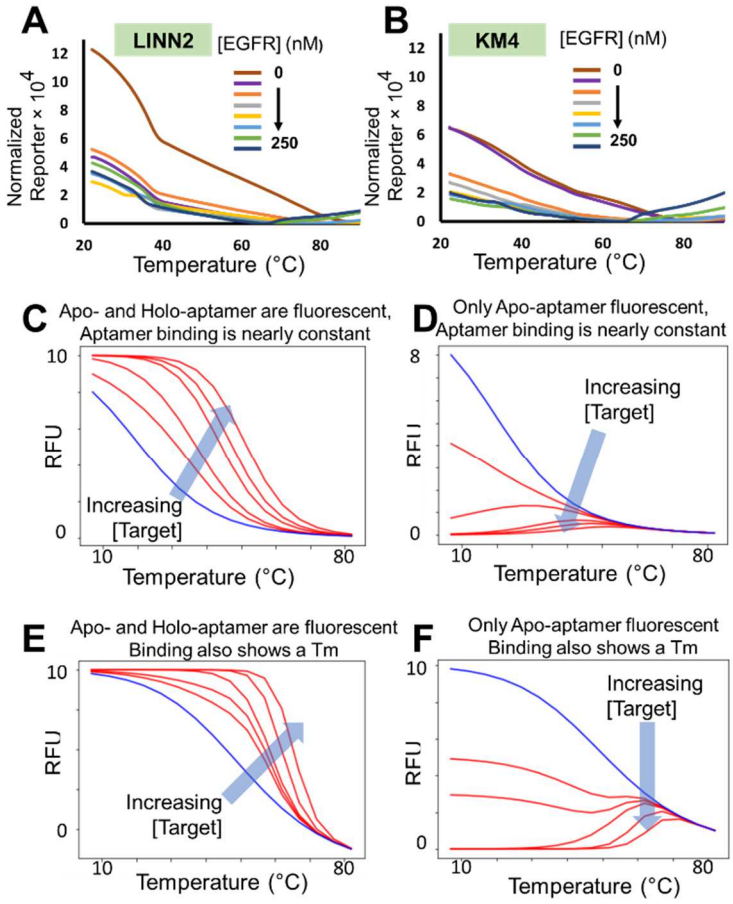

Figure 5- 3: Qualitative comparison of experimental melt curves and simulated melt curves based on equilibrium models. (A) TFA of LINN2 shows fluorescence as a function of temperature. (B) TFA of KM4 shows fluorescence as a function of temperature. (C) Model when apo-, and holo-aptamer are fluorescent, and target binding affinity is nearly constant. Blue line shows the aptamer only; red lines show a range of increasing target concentrations. (D) Model when only apo-aptamer is fluorescent, and target binding affinity is nearly constant. (E) Model when apo- and holo-aptamer are fluorescent, and target binding also shows a Tm (melting point). (F) Model when only apo-aptamer is fluorescent, and target binding shows a Tm.

5-4.5. Kinetic Effects on Thermofluorimetric Analysis

We suspect that kinetics plays a role in the fluorescence loss during TFA. The equilibrium model ignored any kinetic effects. This may account for the quantitative differences between our model and data. Kinetic effects of dye binding, aptamer-target binding, and aptamer folding could all affect the melt curve. If the kinetics were negligible, then the order of assembly of the reaction mixture would not affect the results. However, we found that annealing the aptamer with the dye present shows a very different trend compared to annealing the aptamer alone and adding the dye. This suggests that annealing the aptamer alone may generate a kinetically trapped state in which equilibrium dye binding is not obtained until the sample is heated.

We initially performed TFA by combining aptamer and EG followed by annealing. We carried out an alternate procedure by annealing prior to adding EG. We generated a binding curve from the experimental case by plotting the average of the differential signal at 30-32°C against target EGFR concentration. We also generated a binding curve for the alternative case by taking of normalized average of the differential signal at 32-35°C against target EGFR concentration. Both were normalized with respect to blank (0 nM target). Annealing with EG shows a clear binding trend while the alternative did not. We interpret this to indicate that annealing with EG might set up a kinetically trapped state. Such a trapped state could show a more dramatic dF/dT signal upon rearranging at higher temperatures. It was advantageous to anneal aptamer KM4 with the dye, but every aptamer could behave differently.

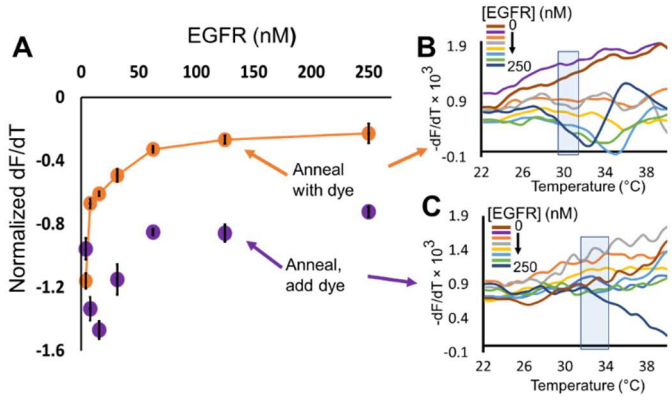

Figure 5- 4: Kinetic effects on Thermofluorimetric Analysis of aptamer KM4 with recombinant EGFR. (A) Binding curve generated by annealing 1X aptamer and EG before adding target (orange color, error bars are standard deviations of average of differential signals at 30-32°C), and by annealing aptamer without EG followed by adding EG and target (violet color, error bars are standard deviations of differential signals at 32-35°C). (B) The derivative signal (dF/dT) is plotted as a function of temperature for aptamer annealed with EG. (C) The derivative signal (dF/dT) is plotted as a function of temperature for aptamer annealed alone followed by EG addition.

5-4.6. Implications of thermodynamic and kinetic results

Thermofluorimetric analysis (TFA) technique allows for the measurement of a signal from target-aptamer complexes using an intercalating dye. Our novel DNA aptamer, KM4, was selected against EGFR overexpressing cells. This aptamer binds both cell surfaces and recombinant EGFR. The published DNA aptamer, LINN2,[8] failed to bind native cell surface EGFR.

The pair of related molecules allows for a direct comparison of aptamer idiosyncrasies when analyzed with TFA. Aptamer KM4 was not as amenable to TFA as LINN2. Its folded structure is less fluorescent in the presence of EG. Additionally, both KM4 and LINN2 show reduced EG fluorescence upon target binding. This suggests that TFA is not equally applicable to all aptamers. TFA gives a better signal-to-background ratio for aptamers having more double-stranded DNA in its folded form.

We generated a simple equilibrium model to try to explain our TFA results. The model shows that complex melting behavior is possible. Adding kinetic effects further complicates matters. Given the complexity of the melt curves, we suggest that over-interpretation of melt curves should be avoided. Some features in the melt curve correspond to the bound complex. However, the precise thermodynamic origin of the features (e.g., stabilization of the folded structure) are probably oversimplifications.

This body of work suggests several key considerations when using TFA to perform binding assays including: mechanistic uncertainty, aptamer-dye interaction, and the possibility of kinetic effects. The common mechanistic interpretation will not be true in all cases. Only in a sub-set of aptamers will the folded, fluorescent aptamer be stabilized by target binding. This mechanism should not be assumed in interpreting TFA of aptamers. Aptamers will show poor performance if they have a low double-stranded structure or if their binding activity is disrupted by the intercalating dye. If mFold, NuPACK or similar software predicts few internal base pairs, then the aptamer may be a poor candidate for TFA. Finally, we note that the order of operations in assembling the reaction may affect the outcome of the experiment. This suggests that kinetic effects may be important. In addition to target concentration and buffer choice (which are common parameters for any binding assay), the order of operations in assembling samples should be carefully optimized.

Many aptamers show double-stranded structure and will be amenable to TFA, but it should not be considered universal. Aptamers will show poor performance if they have a low double-stranded structure or if their binding activity is disrupted by the intercalating dye. It may nonetheless be preferable to fluorescence anisotropy [23], or de-quenching a fluorophore [24], which require covalently modified DNA and whose performance is also very specific to each aptamer. We validated the binding of aptamer

KM4 to the target using a known technique, flow cytometry [8–12]. Many methods exist for measuring protein-aptamer equilibria (e.g., flow cytometry, SPR, radioactive dot blot assay) [25]. These can be used to confirm TFA results. The ubiquity and simplicity of melt curve analysis and the fact that it is a homogeneous assay all make TFA an attractive option for initial characterization of a new aptamer.

5-5. Acknowledgements

We thank Prof. Samir Iqbal for the kind gift of A549 cells.

5-6. Financial Disclosure

This work is supported by the National Institute of General Medical Sciences of the National Institutes of Health under Award Number P20GM104420. This published report is supported by an Institutional Development Award (IDeA) from the National Institute of General Medical Sciences of the National Institutes of Health under grant number P30GM103324. The content is solely the responsibility of the authors and does not necessarily represent the official views of the National Institutes of Health.

5-7. Author Contributions

T.R.D. wrote the main manuscript text, prepared figures, and conducted experiments. P.B.A. supervised whole project and helped prepare and edit the manuscript.

5-8. References

(1) Hu, J.; Kim, J.; Easley, C. J. Quantifying Aptamer–Protein Binding via Thermofluorimetric Analysis. *Anal. Methods* **2015**, *7* (17), 7358–7362. https://doi.org/10.1039/C5AY00837A.

(2) Tuerk, C.; Gold, L. Systematic Evolution of Ligands by Exponential Enrichment: RNA Ligands to Bacteriophage T4 DNA Polymerase. *Science* **1990**, *249* (4968), 505–510. https://doi.org/10.1126/science.2200121.

(3) Ellington, A. D.; Szostak, J. W. In Vitro Selection of RNA Molecules That Bind Specific Ligands. *Nature* **1990**, *346* (6287), 818–822. https://doi.org/10.1038/346818a0.

(4) Pan, Y.; Duncombe, T. A.; Kellenberger, C. A.; Hammond, M. C.; Herr, A. E. High-Throughput Electrophoretic Mobility Shift Assays for Quantitative Analysis of Molecular Binding Reactions. *Anal Chem* **2014**, *86* (20), 10357–10364. https://doi.org/10.1021/ac502700b.

(5) Wang, M. S.; Reed, S. M. Direct Visualization of Electrophoretic Mobility Shift Assays Using Nanoparticle-Aptamer Conjugates. *Electrophoresis* **2012**, *33* (2), 348–351. https://doi.org/10.1002/elps.201100308.

(6) Lin, P.-H.; Chen, R.-H.; Lee, C.-H.; Chang, Y.; Chen, C.-S.; Chen, W.-Y. Studies of the Binding Mechanism between Aptamers and Thrombin by Circular Dichroism, Surface Plasmon Resonance and Isothermal Titration Calorimetry. *Colloids and Surfaces B: Biointerfaces* **2011**, *88* (2), 552–558. https://doi.org/10.1016/j.colsurfb.2011.07.032.

(7) Sypabekova, M.; Bekmurzayeva, A.; Wang, R.; Li, Y.; Nogues, C.; Kanayeva, D. Selection, Characterization, and Application of DNA Aptamers for Detection of Mycobacterium Tuberculosis Secreted Protein MPT64. *Tuberculosis* **2017**, *104*, 70–78. https://doi.org/10.1016/j.tube.2017.03.004.

(8) Damase, T. R.; Miura, T. A.; Parent, C. E.; Allen, P. B. Application of the Open QPCR Instrument for the in Vitro Selection of DNA Aptamers against Epidermal Growth Factor Receptor and Drosophila C Virus. *ACS Comb. Sci.* **2018**, *20* (2), 45–54. https://doi.org/10.1021/acscombsci.7b00138.

(9) Wang, D.-L.; Song, Y.-L.; Zhu, Z.; Li, X.-L.; Zou, Y.; Yang, H.-T.; Wang, J.-J.; Yao, P.-S.; Pan, R.-J.; Yang, C. J.; et al. Selection of DNA Aptamers against Epidermal Growth Factor Receptor with High Affinity and Specificity. *Biochemical and Biophysical Research Communications* **2014**, *453* (4), 681–685. https://doi.org/10.1016/j.bbrc.2014.09.023.

(10) Shangguan, D.; Li, Y.; Tang, Z.; Cao, Z. C.; Chen, H. W.; Mallikaratchy, P.; Sefah, K.; Yang, C. J.; Tan, W. Aptamers Evolved from Live Cells as Effective Molecular Probes for Cancer Study. *PNAS* **2006**, *103* (32), 11838–11843. https://doi.org/10.1073/pnas.0602615103.

(11) Zhang, P.; Zhao, N.; Zeng, Z.; Feng, Y.; Tung, C.-H.; Chang, C.-C.; Zu, Y. Using an RNA Aptamer Probe for Flow Cytometry Detection of CD30-Expressing Lymphoma Cells. *Laboratory Investigation* **2009**, *89* (12), 1423–1432. https://doi.org/10.1038/labinvest.2009.113.

(12) Dunaway, A. B.; Sullivan, R. S.; Siegel, K. J.; Milam, V. T. Evaluating the Dual Target Binding Capabilities of Immobilized Aptamers Using Flow Cytometry. *Biointerphases* **2015**, *10* (1), 019015. https://doi.org/10.1116/1.4915107.

(13) Parekh, P.; Kamble, S.; Zhao, N.; Zeng, Z.; Portier, B. P.; Zu, Y. Immunotherapy of CD30-Expressing Lymphoma Using a Highly Stable SsDNA Aptamer. *Biomaterials* **2013**, *34* (35), 8909–8917. https://doi.org/10.1016/j.biomaterials.2013.07.099.

(14) Hicke, B. J.; Marion, C.; Chang, Y. F.; Gould, T.; Lynott, C. K.; Parma, D.; Schmidt, P. G.; Warren, S. Tenascin-C Aptamers Are Generated Using Tumor Cells and Purified Protein. *J. Biol. Chem.* **2001**, *276* (52), 48644–48654. https://doi.org/10.1074/jbc.M104651200.

(15) Sun, H.; Zhu, X.; Lu, P. Y.; Rosato, R. R.; Tan, W.; Zu, Y. Oligonucleotide Aptamers: New Tools for Targeted Cancer Therapy. *Mol Ther Nucleic Acids* **2014**, *3* (8), e182. https://doi.org/10.1038/mtna.2014.32.

(16) Esposito, C. L.; Passaro, D.; Longobardo, I.; Condorelli, G.; Marotta, P.; Affuso, A.; Franciscis, V. de; Cerchia, L. A Neutralizing RNA Aptamer against EGFR Causes Selective Apoptotic Cell Death. *PLOS ONE* **2011**, *6* (9), e24071. https://doi.org/10.1371/journal.pone.0024071.

(17) Civit, L.; Taghdisi, S. M.; Jonczyk, A.; Haßel, S. K.; Gröber, C.; Blank, M.; Stunden, H. J.; Beyer, M.; Schultze, J.; Latz, E.; et al. Systematic Evaluation of Cell-SELEX Enriched Aptamers Binding to Breast Cancer Cells. *Biochimie* **2018**, *145*, 53–62. https://doi.org/10.1016/j.biochi.2017.10.007.

(18) Amano, R.; Takada, K.; Tanaka, Y.; Nakamura, Y.; Kawai, G.; Kozu, T.; Sakamoto, T. Kinetic and Thermodynamic Analyses of Interaction between a High-Affinity RNA Aptamer and Its Target Protein. *Biochemistry* **2016**, *55* (45), 6221–6229. https://doi.org/10.1021/acs.biochem.6b00748.

(19) Sakamoto, T.; Ennifar, E.; Nakamura, Y. Thermodynamic Study of Aptamers Binding to Their Target Proteins. *Biochimie* **2018**, *145*, 91–97. https://doi.org/10.1016/j.biochi.2017.10.010.

(20) Kanakaraj, I.; Chen, W.-H.; Poongavanam, M.; Dhamane, S.; Stagg, L. J.; Ladbury, J. E.; Kourentzi, K.; Strych, U.; Willson, R. C. Biophysical Characterization of VEGF–AHt DNA Aptamer Interactions. *International Journal of Biological Macromolecules* **2013**, *57*, 69–75. https://doi.org/10.1016/j.ijbiomac.2013.02.016.

(21) Zuker, M. Mfold Web Server for Nucleic Acid Folding and Hybridization Prediction. *Nucleic Acids Res* **2003**, *31* (13), 3406–3415.

(22) Potty, A. S. R.; Kourentzi, K.; Fang, H.; Jackson, G. W.; Zhang, X.; Legge, G. B.; Willson, R. C. Biophysical Characterization of DNA Aptamer Interactions with Vascular Endothelial Growth Factor. *Biopolymers 91* (2), 145–156. https://doi.org/10.1002/bip.21097.

(23) Li, W.; Wang, K.; Tan, W.; Ma, C.; Yang, X. Aptamer-Based Analysis of Angiogenin by Fluorescence Anisotropy. *Analyst* **2007**, *132* (2), 107–113. https://doi.org/10.1039/B614138B.

(24) Nutiu, R.; Li, Y. Structure-Switching Signaling Aptamers. *J. Am. Chem. Soc.* **2003**, *125* (16), 4771–4778. https://doi.org/10.1021/ja028962o.

(25) Jing, M.; Bowser, M. T. A Review of Methods for Measuring Aptamer-ProteinEquilibria. *Anal Chim Acta* **2011**, *686* (1–2), 9–18. https://doi.org/10.1016/j.aca.2010.10.032.

CHAPTER 6: THIOFLAVIN-T AS A FLUOROGENIC SMALL MOLECULE REPORTER FOR AN ENZYME-FREE CATALYTIC DNA AMPLIFIER

DNA binds to thioflavin-T (TFT) in a sequence-dependent manner and enhances TFT fluorescence. We discovered a novel, guanosine-rich DNA sequence that produces fluorescence upon binding with TFT. We use this sequence as a TFTSignal oligonucleotide to report the activity of several DNA circuits without covalent DNA modification. The DNA circuits conditionally sequester or liberate the TFTSignal oligonucleotide from a double-stranded DNA duplex. This strategy offers label-free, cost-effective and sensitive fluorogenic detection of multiple DNA-DNA reactions including: 1) molecular beacon reaction; 2) split reporter reaction; 3) one step strand displacement reaction; and 4) a catalytic DNA circuit called the entropy driven amplifier reaction.

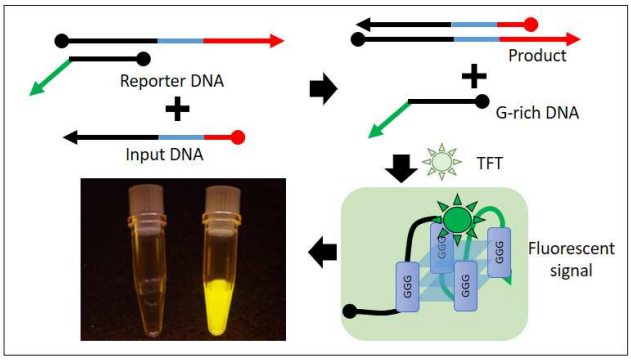

Keywords: Thioflavin-T, label-free DNA circuits, G-rich sequence, entropy driven amplifier reaction

6-1. Introduction

DNA circuits are dynamic, designed reactions that can amplify signals[1], perform computations, and interface with biology[2]. These reactions are built based on base pairing rules and the known kinetics of the one step strand displacement (OSD) reaction[3]. These reactions do not require enzymes or thermocycling and so are attractive as components of bioassays and diagnostics[4]. Many techniques can be employed to read out the activity of DNA circuits (absorbance, electrochemistry, photonic color change[5]) but the most popular is fluorescence. The most popular technique is to design the reaction with fluorophore- and quencher-functionalized oligonucleotides such that fluorescence is activated by the reactions as a result of an initial biorecognition event[1,4,6,7]. However, modified nucleic acids are expensive, the quenched reporter complex must be purified to remove residual fluorophore-modified oligonucleotide, and any degradation of the oligonucleotides produces undesired background.

Small molecule dyes can emit fluorescence when they interact with DNA. Many intercalating dyes produce fluorescence upon binding nonspecifically to double-stranded DNA. DNA circuits that produce a net increase in dsDNA content can be monitored using an intercalating dye (albeit with high background from the dsDNA content in the starting material[8]). Other small molecules will bind to oligonucleotides with specific sequences and become fluorescent. The most famous example is DFHBI, which binds to an RNA aptamer mimic of GFP. The RNA aptamer constrains the conformation of DFHBI and causes it to become fluroescent[9]. DNA aptamers have been evolved against the pro-fluorophore dapoxyl sulfonyl ethylenediamine[10] but that dye is not commercially available. A DNA aptamer against malachite green[11] only functions in the absence of salt and is hindered by the fact that double-stranded DNA also binds malachite green in a nonspecific manner. PPIX and thioflavin-T (TFT) are readily available small molecules that have been reported to bind to G-Quadruplex DNA[12–14] and increase in fluorescence (see Figure 6- 1). In the present work, we set out to develop circuits to selectively activate fluorescence by generating the appropriate sequences to interact with these small molecules.

We identified a sequence of ssDNA that is not a canonical G-Quadruplex forming sequence, but nonetheless produces bright fluorescence in the presence of TFT. This fluorescence can be deactivated by adding the reverse-complementary oligonucleotide. We applied this new oligonucleotide, TFTSignal, as a reporter of DNA circuit activity. Our starting DNA complexes sequester the TFTSignal; recognition of an ssDNA analyte (EDAAnalyte) liberates the TFTSignal oligonucleotide in its active form resulting in fluorescence.

We present three novel findings: 1) a label-free oligonucleotide reporter for fluorogenic detection in combination with the small molecule dye, TFT; 2) design considerations for integrating this oligonucleotide reporter sequence into multiple DNA circuits; and 3) demonstration of the catalytic entropy driven amplifier (EDA) with TFT readout.

6-2. Experimental Section

6-2.1. Materials and Methods

Desalted DNA oligonucleotides with standard desalting were purchased from Integrated DNA Technologies, IDT (Coralville, IA, USA). Thioflavin-T (TFT) was purchased from Arcos Organics, NJ, USA. Protoporphyrin IX disodium salt was purchased from Frontier Scientific, NJ, USA. Tris was purchased from Amresco, OH, USA. Ethylenediaminetetraacetic acid (EDTA) and sodium chloride (NaCl) were obtained from EMD Chemicals, Gibbstown, Germany. Potassium chloride was obtained from Avantor Performance Materials, PA, USA. All reagents used were of analytical grade. To measure

fluorescence, samples were loaded in black, clear-bottom, 384-well plates (Corning ME, USA). Fluorescence intensity, excitation and emission spectra were collected in the multimode microplate reader (SpectraMax iD3, Molecular Devices, CA, USA).

6-2.2. TFT fluorescence activated by G-Quadruplex DNA

Four different samples of the specific oligonucleotide, GQplex (10 µM, 4 µM, 0.4 µM and 0.04 µM) were prepared in Tris buffer (20 mM Tris, 50 mM NaCl, 10 mM EDTA, pH 7) containing 5 µM TFT (see Supporting Information for sequences). An image was taken under blue light (FastGene Blue LED Gel Illuminator, Bulldog Bio, Portsmouth, NH). The fluorescence intensity from a 20 µl sample was measured in the plate reader (SpectraMax iD3) in triplicate using an excitation wavelength of 440 nm and an emission wavelength of 510 nm.

6-2.3. Comparison of TFT with Protoporphyrin IX

Fluorescence emission spectra of TFT were measured in presence of GQplex, dsDNA and ssDNA (see Supporting Information for sequences). The final concentration of each oligo was 500 nM and TFT was 5 µM in each 20 µl sample. The control was carried out with the only TFT (no DNA). The fluorescence measurements recorded in Tris buffer containing 10 mM potassium ions using an excitation wavelength of 440 nm and emission wavelengths from 480 nm to 560 nm. Similarly, Fluorescence emission spectra of PPIX were recorded with an excitation wavelength of 410 nm and emission wavelengths from 550 nm to 750 nm.

6-2.4. Measurement of TFT fluorescence from DNA circuits

Beacon opening reactions were followed by monitoring the fluorescence emission in presence of: 1) TFTBeacon (500 nM), 2) BeaconAnalyte (500 nM), and 3) TFTBeacon (500 nM), as well as BeconAnalyte (500 nM), in the presence of 5 µM of TFT in Tris buffer using an excitation wavelength of 410 nm and an emission wavelength 510 nm. The reaction was monitored for 72 hours.

The split reporter reaction was followed by monitoring fluorescence emission of TFT in the presence of two oligonucleotides: Part A (500 nM); Part B (500 nM); and a mixture of Part A (500 nM) and Part B (500 nM). All samples contained 5 µM of TFT in Tris buffer with an excitation wavelength of 410 nm and an emission wavelength 510 nm. The reaction time for the reaction was 72 hours.

The one step strand displacement reaction was followed by monitoring fluorescence. Samples were assembled containing: 1) TFTSignal at 500 nM; 2) Fuel at 500 nM; 3) Spine at 500 nM; 4) Spine-

TFTSignal complex at 500 nM; 5) Spine-TFTSignal (500 nM) complex plus Fuel (500 nM). All were prepared with 5 µM of TFT in Tris buffer. The fluorescence was recorded using an excitation wavelength of 410 nm and emission wavelength 510 nm for one hour.

6-2.5. Entropy Driven Amplifier with TFT readout

Fluorescence measurements of entropy driven amplifier circuit reaction were measured by recording fluorescence value of Spine-TFTSignal-Block complex with 12.5%, 50%, 75% and 100% EDAAnalyte in the presence of Fuel (100%) and 5 µM of TFT in Tris buffer using an excitation wavelength of 410 nm and an emission wavelength 510 nm. The fluorescence emission associated with each oligonucleotide (Spine, TFTSignal, Block, Fuel) and Spine-TFTSignal-Block complex were measured as controls in the presence of 5 µM of TFT in Tris buffer. Spine-TFTSignal-Block plus Fuel in presence of 5 µM of TFT in Tris buffer was used as the leakage control. The final concentration of each oligo was 500 nM and, the final concentration of TFT was 5 µM. The final volume of each sample was 20 µl. The reaction kinetics were measured for 48 hours.

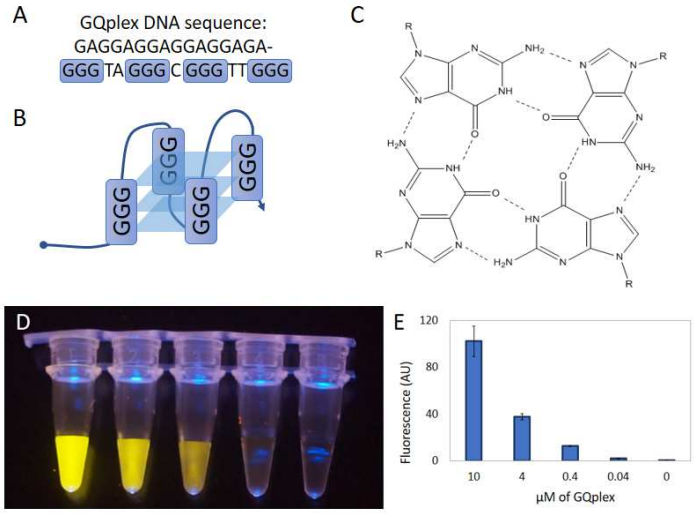

Figure 6- 1: TFT fluorescence activated by G-Quadruplex. (A) G-Quadruplex sequence. (B) G-Quadruplex structure. (C) Guanosine tetrad structure (R =polymer backbone). (D) Fluorescence emission of 5 µM TFT upon excitation with a blue transilluminator in the presence of 10 µM, 4 µM, 0.4 µM, 0.04 µM and 0 µM G-Quadruplex DNA (GQplex). (E) Fluorescence intensity of 5 µM G-Quadruplex upon excitation with a wavelength of 440 nm in the presence of 10 µM, 4 µM, 0.4 µM, 0.04 µM and 0 µM G-Quadruplex DNA.

EDA circuit reactions were carried out for 48 hours at 37°C before PAGE analysis with 10% non-denaturing gel (10 mM Mg2+). Prior to electrophoresis, EDA circuit reactions and controls were as-

sembled as follows: Lane 1, negative control: Spine-TFTSignal-Block complex at 1 µM. Lane 2, Intermediate control: Spine-TFTSignal-Block complex at 1 µM plus EDAAnalyte at 1 µM. Lane 3, Leakage control: Spine-TFTSignal-Block complex at 1 µM plus Fuel at 1 µM. Lane 4, Experimental 100% EDAAnalyte: Spine-TFTSignal-Block complex at 1 µM, Fuel at 1 µM, EDAAnalyte at 1 µM. Lane 5, Experimental 10% EDAAnalyte: Spine-TFTSignal-Block complex at 1 µM, Fuel at 1 µM and EDAAnalyte at 0.1 µM. Lane 6, Positive control: Spine-TFTSignal complex at 1 µM, Fuel at 1 µM. Lane 7, Positive control: TFTSignal at 1 µM. Lane 8, Positive control (30 X): TFTSignal at 30 µM. The electrophoresis was carried out in a refrigerator for 28 hours at 100 V in 1X Sodium Borate (5 mM sodium borate) buffer. The gel was stained first in 1X GelRed (Biotium, CA, USA) for one hour and then in 20 µM TFT for 30 minutes. The gel image was taken in blue light after each staining (FastGene Blue LED Gel Illuminator).

6-3. Results and Discussion

6-3.1. TFT fluorescence activated by G-Quadruplex DNA

Xu et al. reported that the canonical G-Quadruplex, PW17, efficiently induced TFT fluorescence[15]. To investigate the activation of thioflavin-T (TFT) fluorophore by a known G-Quadruplex structure, we designed an oligonucleotide called GQplex containing the PW17 sequence. Warious concentration of GQplex were combined with the environmentally sensitive dye, TFT. The GQplex DNA oligonucleotide interacted with the TFT dye which resulted in enhanced fluorescence. See Figure 6- 1A for the GQplex sequence. The enhanced fluorescence could result from interactions between GQplex and TFT that restrict rotation between benzothiazole and dimethylaminobenzene rings and stabilized TFT in a more fluorescent conformation. We found a 40 nM limit of detection for GQplex in the presence of 5 µM TFT.

6-3.2. TFT results in higher signal than Protoporphyrin IX

TFT[13] and protoporphyrin IX (PPIX)[16–18] were both fluorescent in the presence of G-Quadruplex DNA. We compared the enhanced fluorescence of TFT and PPIX after binding to GQplex, dsDNA and ssDNA (see Supporting Information for sequences). The increase in fluorescence was greater when the dyes bound GQPlex than when bound to dsDNA or ssDNA suggesting that background fluorescence should be low. Moreover, the results showed that binding of TFT to GQplex produces more fluorescence than the corresponding binding of PPIX (see Figure 6- 2). TFT showed a much higher signal-to-background ratio (42) than PPIX (5). TFT is also more soluble in water, inexpensive, and excitable at 410 nm. TFT has a broad absorption band and is compatible with simple blue LED excitation at ~470 nm. For those

reasons, we adopted TFT as a fluorescent reporter rather than PPIX for further development. We noted that PPIX could also function in circumstances where a far-red fluorophore is preferable. Other options such as intercalating dyes can detect increases in dsDNA concentration[8] but are not applicable to many DNA circuits such as the EDA, which have very little change in overall dsDNA content. The published malachite green aptamer[11] was not fluorogenic under our optimum conditions for DNA circuit function (i.e. 50-300 mM sodium chloride).

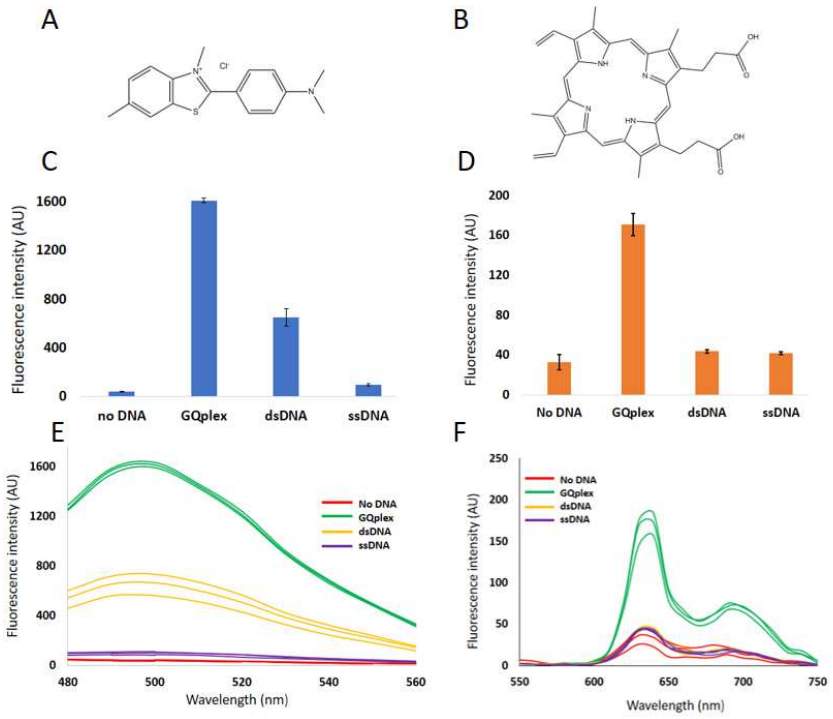

Figure 6- 2: Comparison of TFT and PPIX fluorescence in the presence of GQPlex. (A) Structure of thioflavin-T. (B) Structure of Protoporphyrin IX. (C) Fluorescence emission of 5 µM TFT upon excitation with a wavelength of 440 nm in the absence or presence of GQplex, dsDNA, ssDNA respectively. (D) Fluorescence emission of 5 µM protoporphyrin IX upon excitation with a wavelength of 410 nm in the absence or presence of GQplex, dsDNA, ssDNA respectively. (E) Fluorescence emission spectra of 5 µM TFT upon excitation with a wavelength of 440 nm in the absence or presence of GQplex, dsDNA, ssDNA respectively. (F) Fluorescence emission spectra of 5 µM protoporphyrin IX upon excitation with a wavelength of 410 nm in the absence or presence of GQplex, dsDNA, ssDNA respectively.

6-3.3. Three simple reactions followed with TFT fluorescence

We used TFT to detect the product of three basic DNA reactions. The reactions were designed to hide or reveal a TFTSignal oligonucleotide. These three reactions are representative of the final detection step in more complex DNA circuits. We found the TFTSignal sequence by serendipity (see Supporting

Information Online for sequences). TFTSignal DNA (domains 2-3-5) was originally designed to be one half of a split version of PW17[15]. Surprisingly, TFT was more fluorescent when mixed with TFTSignal than an oligonucleotide containing the full version of PW17 (domains 4-5). We characterized oligonucleotides to determine which combinations of the domains were critical for this activity and all three domains are required (See Supporting Information Online).

A molecular beacon reaction (see Figure 6- 3A) resulted in increased fluorescence emission upon the opening of a hairpin in a similar manner to that reported by Tan et al.[12] We designed TFTBeacon to sequester the TFTSignal sequence within a double-stranded duplex. Upon addition of a model analyte, BeaconAnalyte (comprising domains 10-12-2) the TFTBeacon opened to reveal the TFTSignal. The exposed TFTSignal region resulted in increased fluorescence emission of the TFT. The fluorescence of the reaction product was 2.8 times the cumulative emission from TFTBeacon and BeaconAnalyte.

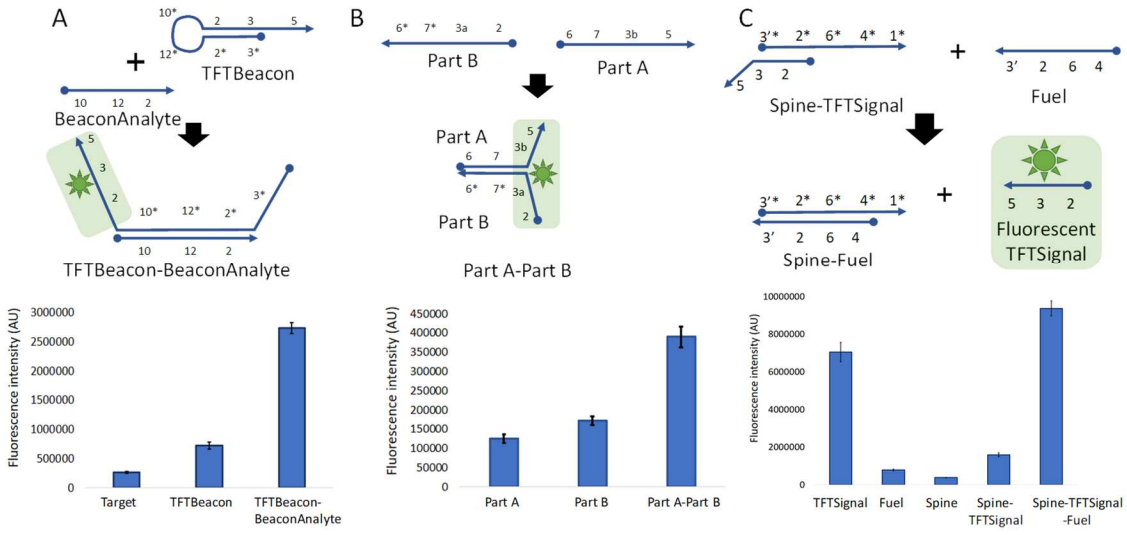

Figure 6- 3: TFT Reporter can be used to follow three DNA circuit reactions. (A) Molecular beacon reaction. (B) Split reporter reaction. (C) One step strand displacement reaction.

The TFT reporter can also be used to monitor a split reporter reaction (see Figure 6- 3B) in which hybridization brought together two halves of the TFTSignal sequence. This strategy has been successfully applied with other G-Quadruplex reporting systems[19,20]. Part A had a complementary region to Part B; each also brought half of the TFTSignal sequence into the complex. When both were introduced to a solution, they hybridized (through domains 6/6* and 7/7*) and produced the TFTSignal sequence (as 2-3a-3b-5). The emission of this product and TFT was only modestly enhanced. In this case, the emission from the product was only 1.3 times the cumulative emission from Part A and Part B.

Finally, one step strand displacement (OSD) reactions can be monitored by the TFT reporter (see Figure 6- 3C). In the OSD reaction, the TFTSignal is released from a reverse complementary oligonucleotide. OSD reactions have been used previously to generate reporter complexes including G-Quadruplex reporters[21,22]. We hybridized a TFTSignal and a reverse complementary oligonucleotide called Spine. When a third oligonucleotide, Fuel, was introduced into the reaction, Fuel hybridized to the Spine and displaced TFTSignal into solution. TFT interacts with the displaced TFTSignal oligonucleotide and produces increased fluorescence emission. The OSD reaction produced 3.9 times the cumulative emission from Fuel and the Spine-TFTSignal complex. Of these three reaction types evaluated, the OSD reaction produced the largest increase in fluorescence emission and the highest signal-to-background ratio. We selected this reaction as the key step in a catalytic circuit, the entropy driven amplifier (EDA).

6-3.4. Entropy Driven Amplifier (EDA) with TFT readout

The EDA was originally reported by Zhang et al.[23]. This circuit can report the presence of a nucleic acid analyte molecule that is orthogonal in sequence to the TFTSignal. The EDA circuit has the additional advantage that the reaction is designed to be catalyzed by the analyte. Because of this catalytic property, more than one molecule of TFTSignal is activated for each analyte molecule. The reaction scheme in Figure 6- 4A illustrates the mechanism of the EDA circuit[1,23]. We designed the Spine-TFTSignal-Block complex in such a manner that the TFTSignal oligonucleotide was sequestered in a double-stranded duplex. A second oligonucleotide, Block, prevented the interaction of Fuel and Spine until triggered. Addition of the catalytic analyte oligonucleotide, EDAAnalyte, results in hybridization of EDAAnalyte to Spine and the release of Block. Fuel then displaced both TFTSignal and Block into solution. The displaced TFTSignal enhanced the fluorescence of TFT. EDAAnalyte was then recycled to bind to another Spine-TFTSignal-Block complex. In principle, the reaction could be designed to react with an arbitrary sequence of DNA or RNA (i.e. the EDAAnalyte sequence need not be homologous or complementary to the TFTSignal sequence). This is an example of label-free, enzyme-free, DNA circuit-based detection.

We analyzed the EDA circuit and TFT reporter with native PAGE. Figure 6- 4B is a false color image of the PAGE gel. Blue color indicates the fluorescence after staining with a nonspecific intercalating dye. Yellow color indicates fluorescence after staining the same gel with TFT. New bands representing the TFTSignal oligonucleotide were visible after staining with TFT (single-stranded TFTSignal DNA did not stain with the intercalating dye).

The TFTSignal oligonucleotide appears as a new band when Fuel is provided. The reaction proceeded

in all cases for 48 hours at 37 °C followed by electrophoresis at 4 °C for 28 hours. Under these conditions, “leakage” (i.e. unwanted interaction between Fuel and Spine-TFTSignal-Block in the absence of EDAAnalyte) was sufficient to complete the reaction. To follow the time course of the reaction, we measured the fluorescence emission over time using a fluorescence plate reader at room temperature to increase the rate relative to the PAGE experiment.

Figure 6- 4C shows catalytic amplification by the EDA circuit. We recorded fluorescence intensity at the appropriate wavelengths for TFT over the course of 48 hours. The addition of EDAAnalyte allowed the EDA to produce the TFTSignal oligonucleotide which then interacted with TFT to produce fluorescence. In Figure 6- 4C, only 500 nM EDAAnalyte is shown. We also performed the reaction in the presence of 250, 125 and 65 nM as shown in Figure 6- 4D**.** A sub-stoichiometric quantity of EDAAnalyte (50% concentration relative to the Spine-TFTSignal-Block) is enough to produce maximal signal output form the reporter. This shows the catalytic activity of the system.

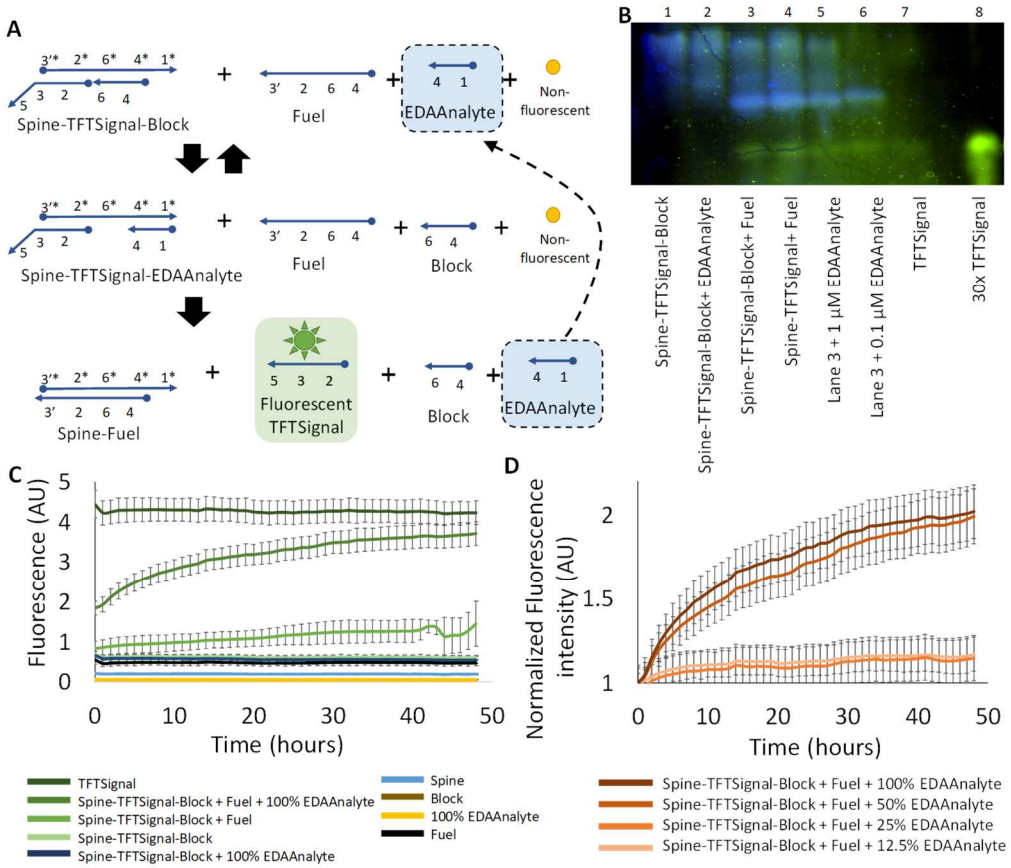

Figure 6- 4: Entropy Driven Amplifier with TFT readout. (A) Schematic of entropy driven amplifier circuit. (B) Native PAGE analysis of EDA circuit. (C) Fluorescence readout of EDA reaction. (D) Comparison of EDA catalytic performance.

6-4. Conclusion

Since the EDA was first demonstrated by Zhang et al.[23] in 2007, it has been used to detect protein analytes,[24] regulate a DNA ribozyme[25] and as the underlying mechanism for a DNA walker[1]. The design has proven highly robust to sequence changes. The EDA has been adapted to fluorescent readout by de-quenching a fluorescent reporter[26,27] and to colorimetric[25] methods. Similar reactions have used electrochemical methods[28] to detected oligonucleotide analytes. Electrochemical and fluorescence detection schemes require modification of DNA with an electroactive or fluorescent molecule, respectively. Such modification is expensive and introduces purity considerations. Synthesis impurities (e.g. branched DNA or residual fluorophore) degrade the analytical performance of the sensors. Purification of a conventional DNA reporter requires non-denaturing PAGE to recover the duplex of a fluorophore-oligonucleotide hybridized to a quencher-oligonucleotide. Any degradation after the purification produces unwanted background.

To address this issue, we demonstrated label-free, enzyme-free DNA circuits with fluorescence detection via TFT as a reporter. The circuits release a single-stranded DNA product with a novel G-rich sequence we call TFTSignal. There are several design considerations for using TFT and TFTSignal to report DNA circuit activity. To reduce background, other ssDNA in the system should be screened for interaction with TFT. Guanosine rich sequences (even those not obviously prone to form G-Quadruplex structures) tend to give high background with TFT. Sequestering such sequences in dsDNA complexes in the design reduces background. The most effective reporter design strategy was to release TFTSignal from a double-stranded state to permit interactions with TFT.

The TFTSignal oligonucleotide prompts fluorescence emission from TFT using convenient excitation and emission wavelengths. TFT has a fluorescein-like spectrum and can be excited with blue LEDs or comparable light sources. TFT is inexpensive, water-soluble, and yields a high signal-to-background ratio upon binding to TFTSignal. This makes TFT an attractive dye for monitoring the outcome of DNA circuits. The label-free strategy is a simple, rapid, and cheap alternative to covalently modified DNA. DNA circuits can activate TFT fluorescence through many means including the association of a split TFTSignal oligonucleotide or displacing TFTSignal from a double-stranded complex. This renders the reaction compatible with many possible DNA circuits (see Figure 6- 3). The TFTSignal tag could also be used to monitor a specific single-stranded DNA in PAGE analysis. We showed that TFT can be used to stain a PAGE gel, facilitating the characterization of the EDA circuit. Oligonucleotides that are similar in size but that differ in sequence could be analyzed by including the TFTSignal sequence and

staining with TFT (i.e. rather than covalently labeling the oligonucleotide with a fluorophore). An oligonucleotide with stronger and more specific interactions with TFT would allow for improved performance at lower concentrations of TFT or DNA. *In vitro* selection of an oligonucleotide that is shorter and tighter binding could produce such a result.

We hope that this work will allow for more groups to enter the field of DNA circuits by reducing the barriers to entry. DNA circuits are a vehicle for exploring biophysical principles such as thermodynamics, reaction rates, and reaction networks. With our TFT-based reporter system, all that is needed for entry are inexpensive unmodified oligonucleotides, TFT, and a blue LED.

6-5. Acknowledgment

This publication was made possible by an Institutional Development Award (IDeA) from the National Institute of General Medical Sciences of the National Institutes of Health under Grant #P20GM103408.

Author Contributions

P.B.A. and T.R.D. conceptualized experiments. T.R.D, P.B.A and M.S. optimized, carried out experiments and analyzed data. P.B.A. and T.R.D wrote the manuscript.

AUTHOR INFORMATION

Corresponding Author

*Peter B. Allen. Email: pballen@uidaho.edu.

Notes

The authors declare no competing financial interest.

6-6. References

(1) Damase, T. R.; Spencer, A.; Samuel, B.; Allen, P. B. Biomimetic Molecular Signaling Using DNA Walkers on Microparticles. *Scientific Reports* **2017**, *7* (1), 4081. https://doi.org/10.1038/s41598-017-04316-1.

(2) Han, D.; Zhu, Z.; Wu, C.; Peng, L.; Zhou, L.; Gulbakan, B.; Zhu, G.; Williams, K. R.; Tan, W. A Logical Molecular Circuit for Programmable and Autonomous Regulation of Protein Activity Using DNA Aptamer–Protein Interactions. *Journal of the American Chemical Society* **2012**, *134* (51), 20797–20804. https://doi.org/10.1021/ja310428s.

(3) Yurke, B.; Turberfield, A. J.; Jr, A. P. M.; Simmel, F. C.; Neumann, J. L. A DNA-Fuelled Molecular Machine Made of DNA. *Nature* **2000**, *406* (6796), 605–608. https://doi.org/10.1038/35020524.

(4) Allen, P. B.; Arshad, S. A.; Li, B.; Chen, X.; Ellington, A. D. DNA Circuits as Amplifiers for the Detection of Nucleic Acids on a Paperfluidic Platform. *Lab Chip* **2012**, *12* (16), 2951–2958. https://doi.org/10.1039/c2lc40373k.

(5) Li, B.; Ellington, A. D.; Chen, X. Rational, Modular Adaptation of Enzyme-Free DNA Circuits to Multiple Detection Methods. *Nucleic Acids Res* **2011**, *39* (16), e110–e110. https://doi.org/10.1093/nar/gkr504.

(6) Damase, T. R.; Stephens, D.; Spencer, A.; Allen, P. B. Open Source and DIY Hardware for DNA Nanotechnology Labs. *Journal of Biological Methods* **2015**, *2* (3), e24.

(7) Yin, P.; Choi, H. M. T.; Calvert, C. R.; Pierce, N. A. Programming Biomolecular Self-Assembly Pathways. *Nature* **2008**, *451* (7176), 318–322. https://doi.org/10.1038/nature06451.

(8) Huang, J.; Su, X.; Li, Z. Enzyme- and Label-Free Amplified Fluorescence DNA Detection Using Hairpin Probes and SYBR Green I. *Sensors & Actuators: B. Chemical* **2014**, *Complete* (200), 117–122. https://doi.org/10.1016/j.snb.2014.04.032.

(9) Paige, J. S.; Wu, K. Y.; Jaffrey, S. R. RNA Mimics of Green Fluorescent Protein. *Science* **2011**, *333* (6042), 642–646. https://doi.org/10.1126/science.1207339.

(10) Kato, T.; Shimada, I.; Kimura, R.; Hyuga, M. Light-up Fluorophore–DNA Aptamer Pair for Label-Free Turn-on Aptamer Sensors. *Chemical Communications* **2016**, *52* (21), 4041–4044. https://doi.org/10.1039/C5CC08816J.

(11) Wang, H.; Wang, J.; Sun, N.; Cheng, H.; Chen, H.; Pei, R. Selection and Characterization of Malachite Green Aptamers for the Development of Light–up Probes. *ChemistrySelect* **2016**, *1* (8), 1571–1574. https://doi.org/10.1002/slct.201600154.

(12) Tan, X.; Wang, Y.; Armitage, B. A.; Bruchez, M. P. Label-Free Molecular Beacons for Biomolecular Detection. *Analytical Chemistry* **2014**, *86* (21), 10864–10869. https://doi.org/10.1021/ac502986g.

(13) Zhang, X. F.; Xu, H. M.; Han, L.; Li, N. B.; Luo, H. Q. A Thioflavin T-Induced G-Quadruplex Fluorescent Biosensor for Target DNA Detection. *Analytical Sciences* **2018**, *34* (2), 149–153. https://doi.org/10.2116/analsci.34.149.

(14) Zhang, Z.; Sharon, E.; Freeman, R.; Liu, X.; Willner, I. Fluorescence Detection of DNA, Adenosine-5′-Triphosphate (ATP), and Telomerase Activity by Zinc(II)-Protoporphyrin IX/G-Quadruplex Labels. *Analytical Chemistry* **2012**, *84* (11), 4789–4797. https://doi.org/10.1021/ac300348v.

(15) Xu, L.; Sun, N.; Zhou, L.; Chen, X.; Wang, J.; Wang, Q.; Wang, K.; Zhang, J.; Pei, R. A Label-Free Fluorescence Assay for Potassium Ions Using Riboflavin as a G-Quadruplex Ligand. *Analyst* **2015**, *140* (10), 3352–3355. https://doi.org/10.1039/C5AN00242G.

(16) Zhou, Z.; Li, D.; Zhang, L.; Wang, E.; Dong, S. G-Quadruplex DNA/Protoporphyrin IX-Based Synergistic Platform for Targeted Photodynamic Cancer Therapy. *Talanta* **2015**, *134*, 298–304. https://doi.org/10.1016/j.talanta.2014.11.039.

(17) Li, T.; Wang, E.; Dong, S. Parallel G-Quadruplex-Specific Fluorescent Probe for Monitoring DNA Structural Changes and Label-Free Detection of Potassium Ion. *Anal. Chem.* **2010**, *82* (18), 7576–7580. https://doi.org/10.1021/ac1019446.

(18) Zhu, J.; Zhang, L.; Dong, S.; Wang, E. How to Split a G-Quadruplex for DNA Detection: New Insight into the Formation of DNA Split G-Quadruplex †Electronic Supplementary Information (ESI) Available: DNA Sequence, Fig. S1–S11, Tables S1–S4, Extended Experimental Details and Discussions. See DOI: 10.1039/C5sc01287b Click Here for Additional Data File. *Chem Sci* **2015**, *6* (8), 4822–4827. https://doi.org/10.1039/c5sc01287b.

(19) Ang, Y. S.; Tong, R.; Yung, L.-Y. L. Engineering a Robust DNA Split Proximity Circuit with Minimized Circuit Leakage. *Nucleic Acids Res* **2016**, *44* (14), e121–e121. https://doi.org/10.1093/nar/gkw447.

(20) Kikuchi, N.; Kolpashchikov, D. M. Split Spinach Aptamer for Highly Selective Recognition of DNA and RNA at Ambient Temperatures. *Chembiochem* **2016**, *17* (17), 1589–1592. https://doi.org/10.1002/cbic.201600323.

(21) Seelig, G.; Soloveichik, D.; Zhang, D. Y.; Winfree, E. Enzyme-Free Nucleic Acid Logic Circuits. *Science* **2006**, *314* (5805), 1585–1588. https://doi.org/10.1126/science.1132493.

(22) Zhang, D. Y.; Seelig, G. Dynamic DNA Nanotechnology Using Strand-Displacement Reactions. *Nature Chemistry* **2011**, *3* (2), 103–113. https://doi.org/10.1038/nchem.957.

(23) Zhang, D. Y.; Turberfield, A. J.; Yurke, B.; Winfree, E. Engineering Entropy-Driven Reactions and Networks Catalyzed by DNA. *Science* **2007**, *318* (5853), 1121–1125. https://doi.org/10.1126/science.1148532.

(24) Kim, D.; Garner, O. B.; Ozcan, A.; Di Carlo, D. Homogeneous Entropy-Driven Amplified Detection of Biomolecular Interactions. *ACS Nano* **2016**, *10* (8), 7467–7475. https://doi.org/10.1021/acsnano.6b02060.

(25) Eckhoff, G.; Codrea, V.; Ellington, A. D.; Chen, X. Beyond Allostery: Catalytic Regulation of a Deoxyribozyme through an Entropy-Driven DNA Amplifier. *Journal of Systems Chemistry* **2010**, *1*, 13. https://doi.org/10.1186/1759-2208-1-13.

(26) Zhang, D. Y.; Turberfield, A. J.; Yurke, B.; Winfree, E. Engineering Entropy-Driven Reactions and Networks Catalyzed by DNA. *Science* **2007**, *318* (5853), 1121–1125. https://doi.org/10.1126/science.1148532.

(27) Damase, T. R.; Spencer, A.; Samuel, B.; Allen, P. B. Biomimetic Molecular Signaling Using DNA Walkers on Microparticles. *Sci Rep* **2017**, *7* (1), 4081. https://doi.org/10.1038/s41598-017-04316-1.

(28) Li, B.; Ellington, A. D.; Chen, X. Rational, Modular Adaptation of Enzyme-Free DNA Circuits to Multiple Detection Methods. *Nucl. Acids Res.* **2011**. https://doi.org/10.1093/nar/gkr504.

CHAPTER 7: SUMMARY AND CONCLUSIONS

The work presented in this dissertation has focused on (1) enzyme-free dynamic DNA circuits to develop DNA-based molecular machines to detect a DNA analyte, (2) a label-free strategy to develop a simple, rapid, and cheap alternative to fluorescently modified DNA in detection, (3) development of cost-efficient and fast techniques to select aptamers and characterize aptamer-target binding and, (4) selection of DNA aptamers against various targets (EGFR and DCV). The dissertation has demonstrated an aptamer-based detection assay and explored binding assay techniques including thermofluorimetric analysis.

DNA has been used to construct precise nanodevices, nanostructures, and dynamic circuits. DNA circuits are dynamic, designed, DNA-based molecular machines with diverse biotechnological applications such as diagnosis based on nucleic acid analytes and signal amplification. Few examples exist of the application of DNA nanotechnology to biological needs in basic or biomedical science.

Our work demonstrates a step toward practical applications of DNA nanotechnology. We showed the release of catalytic DNA walkers from hydrogel microparticles and the detection of those walkers by substrate-coated microparticles in Chapter 2 using dynamic DNA circuits. These release and capture particles represent an analogy of cell-to-cell communication. Our detector particles might be considered a prototype of a localized detector for such signal molecules. We coated one type of particle with DNA circuits to release the walker and the second type of particle with DNA circuits that provide a track for the molecular walker. This strategy could be helpful to push DNA nanotechnology to do an amplification of the signal, multiplexing, and microscopically localized detection.

In chapter 6, we show the successful design of label-free, enzyme-free DNA circuits that generate free oligonucleotides with G-rich sequences. These G-rich oligonucleotides activated thioflavin-T. Thioflavin-T is soluble in water and is inexpensive and need not be chemically conjugated to the DNA. This property makes thioflavin-T an attractive dye molecule to monitor DNA circuit reactions. The label-free strategy is a simple, rapid, and cheap alternative to fluorescently modified DNA. This also shows how DNA aptamers might be integrated into DNA circuits: the G-rich oligonucleotides were derived from an aptamer against anionic porphyrins. Perhaps performance can be increased with an aptamer selected directly against thioflavin-T.

DNA aptamers are evolved DNA using the systematic evolution of ligands by exponential enrichment (SELEX) process. DNA aptamers are molecular recognition elements made of single-stranded DNA (ssDNA) with a potential to interact with proteins, small molecules, viruses, and even cells. Aptamer

generation is time consuming and suffers from a low success rate. A large number of techniques have been introduced to shorten SELEX time by improving efficiency of separation between unbound and target-bound aptamer complexes. Formation of the unwanted product during PCR amplification is another significant barrier in aptamer selection. In Chapter 3, our work demonstrates purification of ssDNA and its extraction using extraction wells. This purification and extraction techniques help to select aptamers easily and quickly. In Chapter 4, we report the SELEX using the Open qPCR to optimize each amplification step. We selected aptamers against whole *Drosophila* C virus (DCV) particles and recombinant Epidermal Growth Factor Receptor (EGFR). In Chapter 5, we explore TFA in detail. To do so, we compared two related aptamers, derived from the same pool, LINN2 (selected against EGFR recombinant protein) and KM4 (selected against EGFR-overexpressing A549 cells). The two aptamers behave differently in TFA. We compared the TFA results to a simple equilibrium model. We also noted kinetic effects on TFA.

The design of DNA to interact with other DNA is well understood, but the design of DNA to interact with proteins and small molecules remain beyond the current capacity of computational prediction. If dynamic DNA technology could respond to protein analytes, it could be applied to analytical and diagnostic applications. Aptamers are strong and specific, but (like antibodies) often require further amplification to yield a useful signal at low target concentrations. DNA circuits can be integrated with aptamers to solve this problem. Unlike enzymatic reactions, DNA-DNA reactions can be easily dried, stored, transported and operated under harsh conditions. Aptamers are specific to various targets, and DNA circuits can amplify aptamer signals.

This thesis represents a step toward future applications of DNA aptamers integrated with designed DNA circuits. Aptamers will extend the recognition capabilities of DNA from Watson-Crick base pairing to interactions with various targets. This integration strategy makes aptamer-based DNA circuits an exciting detection platform. This strategy could be significant in developing point-of-care diagnostics. With further research and optimization, aptamer-based dynamic DNA nanotechnology could be very useful in the diagnostics field. Ultimately, evolved and designed reaction patterns may help to enable synthetic regulation for synthetic biology.

APPENDIX A: CHAPTER 2 SUPPORTING INFORMATION

Biomimetic Molecular Signaling Using DNA Walkers on Microparticles

Published in: "Damase, T. R.; Spencer, A.; Samuel, B.; Allen, P. B. Biomimetic Molecular Signaling Using DNA Walkers on Microparticles. Scientific Reports 2017, 7 (1), 4081."

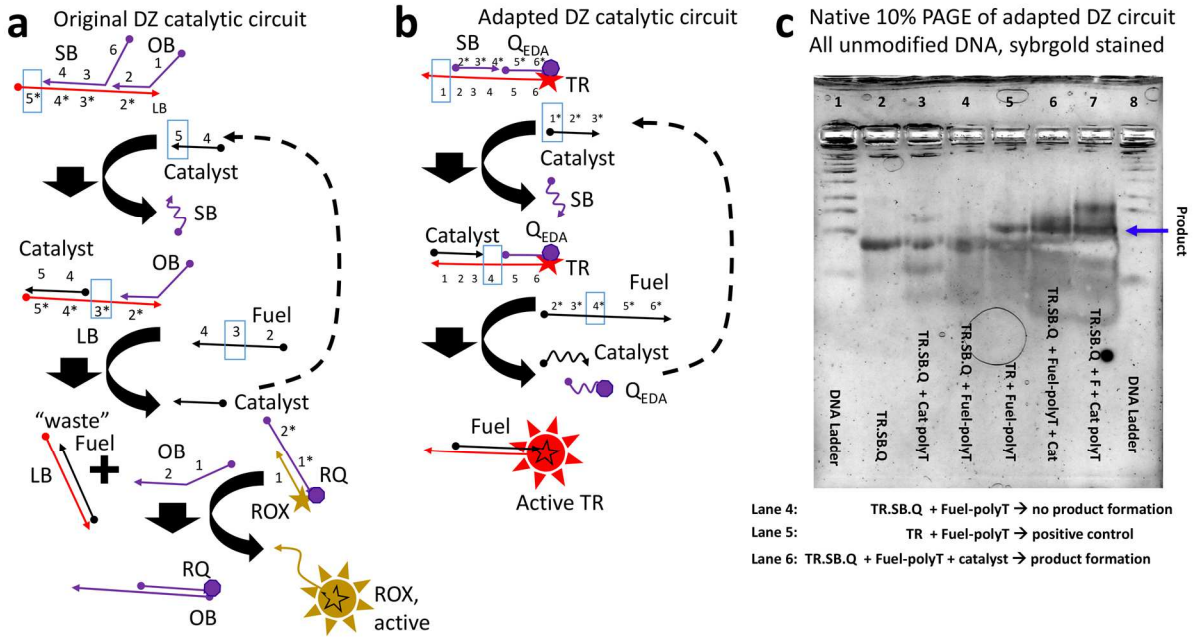

Figure A- S 1: (a) Schematic of the original EDA circuit by Zhang et. al.[1] reorganized to show the comparison to our adapted, fluorogenic reaction. Open toeholds are highlighted in blue boxes. (b) Detailed schematic our adapted reaction. (c) Native PAGE gel stained with SybrGold shows the operation of the adapted circuit.

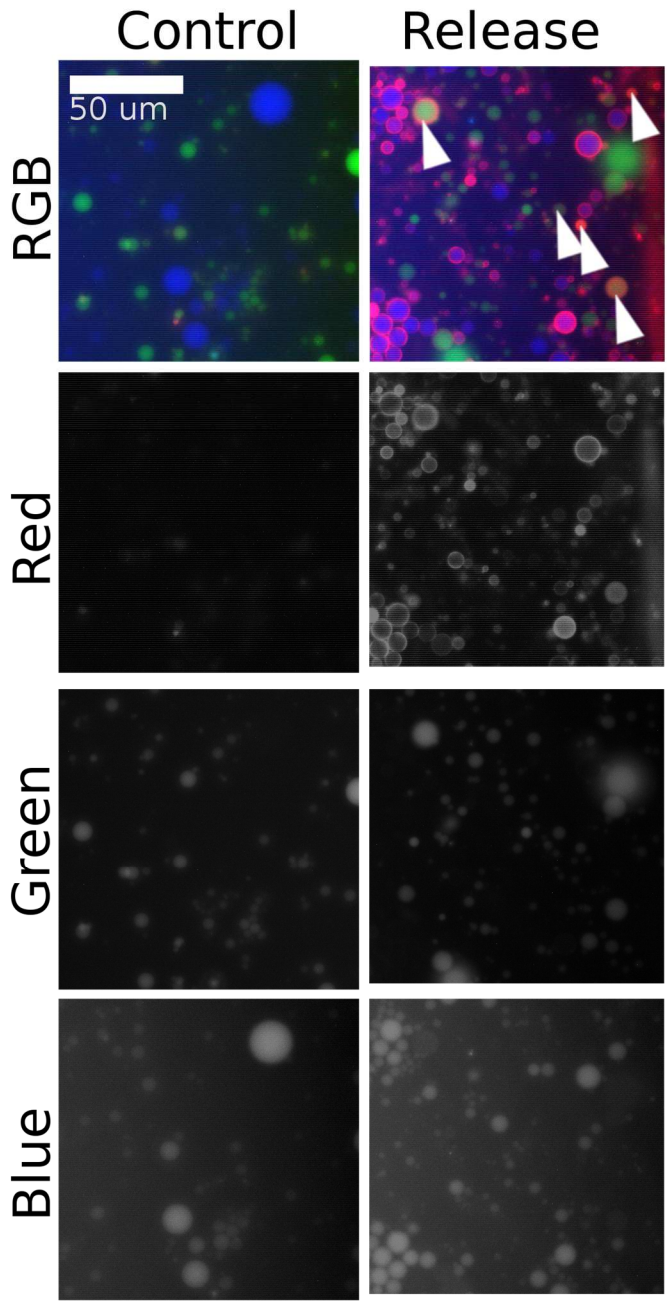

Figure A- S 2: Red, green, and blue channels of image data from Figure 2- 1.

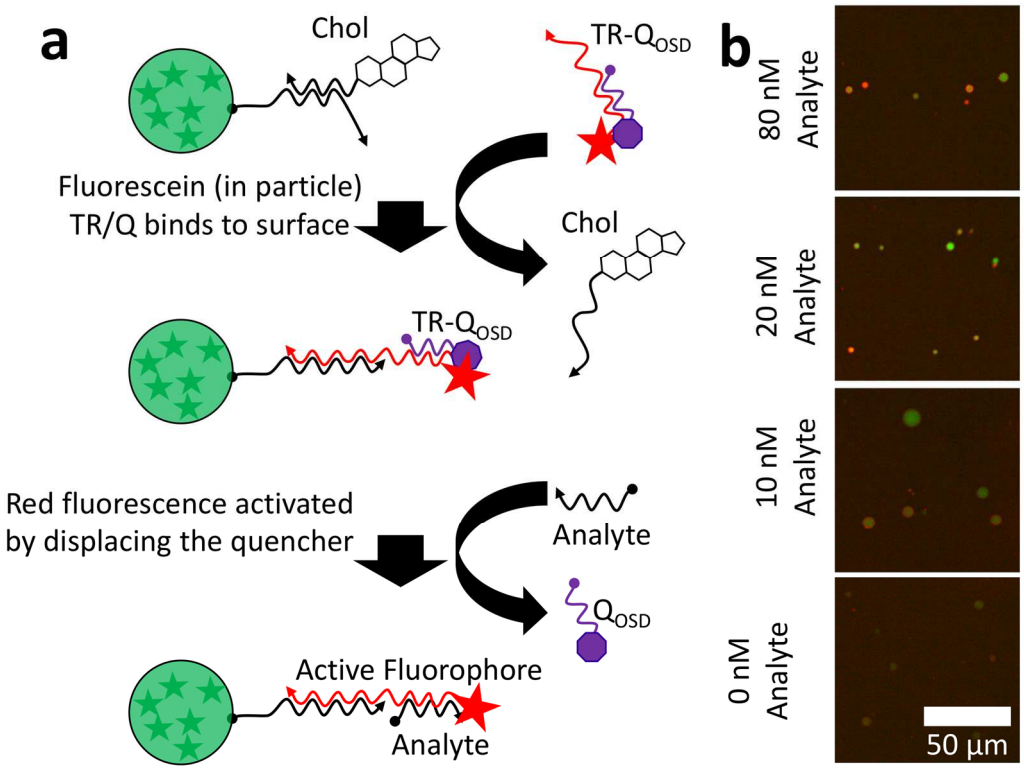

Figure A- S 3: We measured the limit of detection for the OSD reaction using a laser confocal microscope rather than a LED epifluorescence microscope. (a) A schematic shows the reaction where the fluorogenic complex displaces the cholesterol-modified DNA at the surface. The ssDNA then is able to displace the quencher and activate the Texas Red fluorophore. The particles contain fluorescein for identification. (b) The result showed fluorescence at 10 nM of the ssDNA.

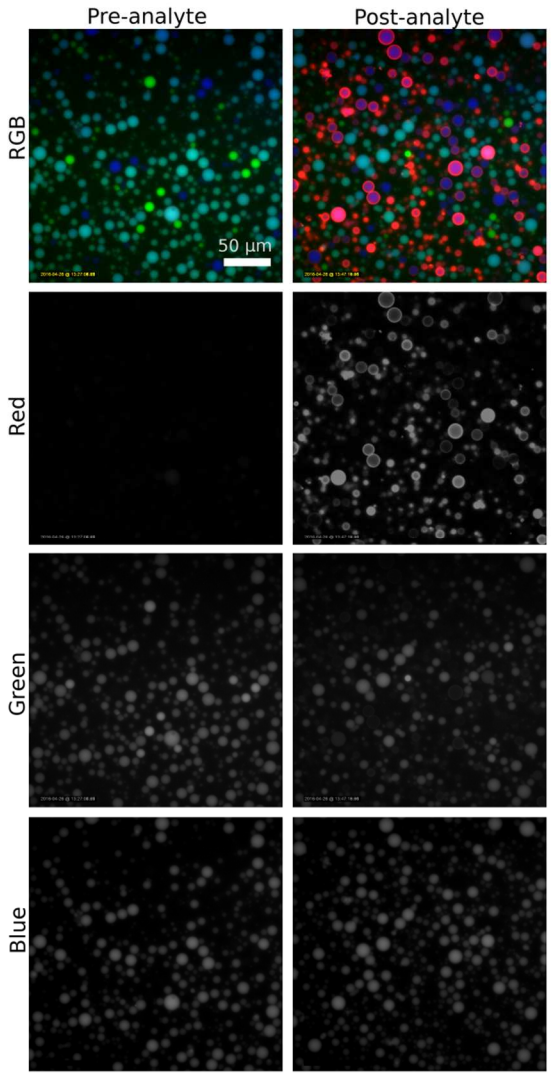

Figure A- S 4: Grayscale images corresponding to the microscopy data shown in Figure 2- 4.

Table A- S1: Sequences for all DNA.

Multiplex OSD components	
Q_{OSD}	AATTCGGCCTGGAATA 3'Iowa black Red Quencher
Chol.A	GTCTCTGTGCCGCTATAATTTT 3'Cholesterol (HPLC)
Acryd.A	5'Acrydite ATTATAGCGGCACAGAGACTAAGGTCGG (HPLC)
TRA	5'TexasRed TATTCCAGGCCGAATTAACAAACTG CCGACCTTAGTCTCTGTGCCGCTATAAT (HPLC)
Chol.B	ATCAACTA CCTACTATTTT 3'Cholesterol (HPLC)
Acryd.B	5'Acrydite ATAGTAGG TAGTTGAT ATTGGTAG (HPLC)
TRB	5'Texas Red TATTCCAG GCCGAATT CACTCCGAG CTACCAAT ATCAACTA CCTACTAT
Chol.C	AACACTCA ACGCTACCTTT 3'Cholesterol (HPLC)
Acryd.C	5'Acrydite GGTAGCGT TGAGTGTT AAAGTAGG (HPLC)
TRC	5'Texas Red TATTCCAG GCCGAATT CTCTAAATG CCTACTTT AACACTCA ACGCTACC
Pacific blue Poly-T	5'Acrydite TTTTTT 3'Pacific Blue
Fluorescein Poly-T	5'Acrydite TTTTTT 3'Fluorescein
ssDNA A	5'AGTTTGTT AATTCGGC CTGGAATA
ssDNA B	5'TCGGAGTG AATTCGGC CTGGAATA
ssDNA B SNP (SNP underlined)	5'TCGGAGTC AATTCGGC CTGGAATA
ssDNA C	5'ATTTAGAG AATTCGGC CTGGAATA
EDA circuit components	
Br	5'Texas Red TCTCCAACTAACTTACGG CCCT CATTCAATACCCTACG TCTCCA CCTACTTT AACACTCA ACGCTACC HPLC
Q_{EDA}	CCGTAAGTTAGTTGGAGA 3'Iowa black Red Quencher
Cat	TGGAGACGTAGGGTATTGAATGAGAGTGGAGATGGGAGTAGTTGGAGACGTAGGGTATTGAATG
Fuel	CGTAGGGTATTGAATG AGGG CCGTAAGTTAGTTGGAGA
SB	CGTAGGGTATTGAATG AGGG
Cat-polyT	TGGAGA CGTAGGGTATTGAATG TTTTTTTTTTTT
Fuel-polyT	CGTAGGGTATTGAATG AGGG CCGTAAGTTAGTTGGAGA TTTTTTTTTTTT

Python Source Code.

```
#Written in Anaconda, Python 2.7, iPython notebook
#Begin 160425 Local release from blue, detection by green - Fig 2- 1

# -*- coding: utf-8 -*-
# <nbformat>3.0</nbformat>

# <codecell>

#import packages to find the filenames and format the list
import numpy as np
import glob
#get a list of tiff files with green fluorescence data
numOfFiles=len(glob.glob('./160425_GreenCdetector*/*F1*'))
fileList=np.array([\
                   glob.glob('./160425_GreenCdetector*/*F3*'),\
                   glob.glob('./160425_GreenCdetector*/*F2*'),\
                   glob.glob('./160425_GreenCdetector*/*F1*'),\
                   np.zeros(numOfFiles),\
                   np.zeros(numOfFiles)])
#format the list and add a column of zeros to be replaced with average intensity value
fileList=np.transpose(fileList)
[fileList[0,0],fileList[0,1],fileList[0,2],fileList[0,3],fileList[0,4]]

# <codecell>

#PRELIMINARY LOADING OF ALL OF THE DEPENDENCIES
import skimage.io as ski
import scipy
import matplotlib.pyplot as plt
from skimage import morphology as mski
from skimage.morphology import disk
import glob
%matplotlib inline

#MAKE FUNCTIONS TO LOAD, BIN, BACKGROUND SUBTRACT THE IMAGE
def AVG_pixel(Im):
    row,col = np.shape(Im)
    x = np.floor((row-50)/2) #note that we cut off the bottom 50 pixels to remove time/date
stamp
    y = np.floor(col/2)
    new_Image = np.zeros([int(x),int(y)],dtype=float)

    for i in range(1,int(x)):
        for j in range(1,int(y)):
            new_Image[i-1,j-1] = float(Im[2*i-1,2*j-1])+float(Im[2*i-2, 2*j-2])+float(Im[2*i-
1,2*j-2])+float(Im[2*i-2,2*j-1])
    return new_Image

def loadBinBGFile(fileName, color):
    I=ski.imread(fileName)      #read in a file
    I = AVG_pixel(I[:,:,color]) #bin the file using the above function
    A = np.size(I)
    Red_list = np.reshape(I,[1,A])
    #The channel intensities are sorted in an acending list
    Red_list = np.sort(Red_list)
    #The minimum background is removed from the image by taking the first 10% value
    min_back_red = Red_list[0,np.floor(0.1*A)]
    I = I-min_back_red
    I = np.clip(I,0.,Red_list[0,-1])
    return I

#process and clean up the mask to remove small and
#very large objects also smooth edges
def processMask(mask):
    mask = mski.remove_small_objects(mask, min_size=50)
    mask = mask-mski.remove_small_objects(mask, min_size=1900)
    mask = mski.opening(mask, disk(3))
    mask = mski.closing(mask, disk(3))
    mask = mski.dilation(mask,disk(3))
```

```
    return mask

#This function takes an image and a labeled mask (created later with scipy.ndimage.label)
#it resurns a list of the average intensity of each object in the mask
def measureRedObjectsFromMask(I2, LabelMask):
    results=np.zeros(LabelMask[1])
    maxDim=len(I2[0])-1
    for j in range(1,LabelMask[1]):
        currentObject=(LabelMask[0]==j)
        currentObjectPoints=np.nonzero(currentObject)
        currentObjectPointsAdjusted=(np.clip(currentObjectPoints[0],0,maxDim),np.clip(curren-
tObjectPoints[1],0,maxDim))
        results[j]=np.mean(I2[currentObjectPointsAdjusted])
    return results

# <codecell>

#LOAD THE INITIAL GREEN/BLUE IMAGE AND VISUALLY SHOW HOW THE MASK WILL BE MADE
i=1
IR=loadBinBGFile(fileList[i,0], 0)
IG=loadBinBGFile(fileList[i,1], 1)
IB=loadBinBGFile(fileList[i,2], 2)
#MAKE THE MASK
#A mask is created by thresholding the image, all pixels above the value specified
# are set as 1 while those bellow are 0
#thresholds are set heuristically based on inspection;
#thresholds are used consistently for the remaining files
gthresh=30
bthresh=240
mask = np.logical_or((IG > gthresh),(IB > bthresh))
tealmask= np.logical_and((IG > gthresh),(IB > bthresh))
greenmask = mask-(IB > bthresh)
bluemask =  mask-(IG > gthresh)

#the masks are labeled so that each disconencted object is set to a unique value
tealmask=processMask(tealmask)
Labeltealmask=scipy.ndimage.label(tealmask)
greenmask=processMask(greenmask)
Labelgreenmask=scipy.ndimage.label(greenmask)
bluemask=processMask(bluemask)
Labelbluemask=scipy.ndimage.label(bluemask)

#SHOW THE RESULTS
fig, axes = plt.subplots(ncols=3, figsize=(10, 5), sharex=True, sharey=True, subplot_kw={'ad-
justable':'box-forced'})
axes[0].imshow(IB+IG, cmap=plt.cm.gray)
axes[0].set_title('Image')

axes[1].imshow((greenmask > 0), cmap=plt.cm.gray)
axes[1].set_title('maskG')

axes[2].imshow((bluemask > 0), cmap=plt.cm.gray)
axes[2].set_title('maskB')

for ax in axes:
    ax.axis('off')
plt.show()

# <codecell>

#DEMONSTRATION OF HOW THE MASKS CAN BE MEASURED TO PRODUCE THE SCATTER PLOT
#This shows how the blue (release) and green (detectors) particles are proccessed separately.
#There are no teal particles; objects that are overlapping are discarded implicitly.

results=np.zeros([Labelbluemask[1]+Labelgreenmask[1],2])

#
i=0
maxDim=len(IR[0])-1
for j in range(1,Labelbluemask[1]):
    currentObject=(Labelbluemask[0]==j)
```

```
    currentObjectPoints=np.nonzero(currentObject)
    currentObjectPointsAdjusted=(np.clip(currentObjectPoints[0],0,maxDim),np.clip(curren-
tObjectPoints[1],0,maxDim))
    results[i,0]=np.mean(IG[currentObjectPointsAdjusted])
    results[i,1]=np.mean(IB[currentObjectPointsAdjusted])
    i=i+1
for j in range(1,Labelgreenmask[1]):
    currentObject=(Labelgreenmask[0]==j)
    currentObjectPoints=np.nonzero(currentObject)
    currentObjectPointsAdjusted=(np.clip(currentObjectPoints[0],0,maxDim),np.clip(curren-
tObjectPoints[1],0,maxDim))
    results[i,0]=np.mean(IG[currentObjectPointsAdjusted])
    results[i,1]=np.mean(IB[currentObjectPointsAdjusted])
    i=i+1


plt.scatter(results[:,0],results[:,1])

# <codecell>

redobjects=measureRedObjectsFromMask(IR,Labelgreenmask)
plt.hist(redobjects)
redobjects=measureRedObjectsFromMask(IR,Labelbluemask)
plt.hist(redobjects)

# <codecell>

#DEMONSTRATION OF HOW THE MASK IS USED TO PROCESS A RED IMAGE
for i in range(len(fileList[:,0])):
    #LOAD THE IMAGES
    IR=loadBinBGFile(fileList[i,0], 0)
    IG=loadBinBGFile(fileList[i,1], 1)
    IB=loadBinBGFile(fileList[i,2], 2)
    #MAKE THE MASK
    #A mask is created by thresholding the image, all pixels above the value specified
    # are set as 1 while those bellow are 0
    gthresh=30
    bthresh=240
    mask = np.logical_or((IG > gthresh),(IB > bthresh))
    tealmask= np.logical_and((IG > gthresh),(IB > bthresh))
    greenmask = mask-(IB > bthresh)
    bluemask =  mask-(IG > gthresh)
    tealmask=processMask(tealmask)
    Labeltealmask=scipy.ndimage.label(tealmask)
    greenmask=processMask(greenmask)
    Labelgreenmask=scipy.ndimage.label(greenmask)
    bluemask=processMask(bluemask)
    Labelbluemask=scipy.ndimage.label(bluemask)


    fileList[i,3]=np.average(measureRedObjectsFromMask(IR,Labelgreenmask))
    fileList[i,4]=np.average(measureRedObjectsFromMask(IR,Labelbluemask))
    print(fileList[i,:])


# <codecell>

np.savetxt("160425_release_detect_summary.csv", fileList, fmt="%s", delimiter=",")

# <codecell>

fileList
```

```
#begin 160424 Amplifier circuit on surface green particles - Fig 2- 2.
# -*- coding: utf-8 -*-
# <nbformat>3.0</nbformat>

# <codecell>

#import packages to find the filenames and format the list
import glob
import numpy as np
#get a list of tiff files with green fluorescence data
fileListG=glob.glob('./160424*/*F2*')
#get a list of tiff files with red fluorescence data
fileListR=glob.glob('./160424*/*F3*')
#format the list and add a column of zeros to be replaced with average intensity value
fileList=np.transpose(np.array([fileListG,fileListR,np.zeros(len(fileListG))]))

# <codecell>

#PRELIMINARY LOADING OF ALL OF THE DEPENDENCIES
import skimage.io as ski
import scipy
import matplotlib.pyplot as plt
from skimage import morphology as mski
from skimage.morphology import disk
import glob
%matplotlib inline

#MAKE A FUNCTION TO LOAD, BIN, BACKGROUND SUBTRACT THE IMAGE
def AVG_pixel(Im): #function bins an image by summing every 2x2 pixel block
    row,col = np.shape(Im)
    x = np.floor((row-50)/2) #not that we cut off the bottom 50 pixels to remove time/date
stamp
    y = np.floor(col/2)
    new_Image = np.zeros([int(x),int(y)],dtype=float)

    for i in range(1,int(x)):
        for j in range(1,int(y)):
            new_Image[i-1,j-1] = float(Im[2*i-1,2*j-1])+float(Im[2*i-2, 2*j-2])+float(Im[2*i-
1,2*j-2])+float(Im[2*i-2,2*j-1])
    return new_Image

def loadBinBGFile(fileName, color):
    I=ski.imread(fileName) #read in a file
    I = AVG_pixel(I[:,:,color]) #bin the file using the above function
    A = np.size(I)
    Red_list = np.reshape(I,[1,A])
    #The channel intensities are sorted in an acending list
    Red_list = np.sort(Red_list)
    #The background is subtracted by calculating the 10th percentile intensity
    min_back_red = Red_list[0,np.floor(0.1*A)]
    I = I-min_back_red
    I = np.clip(I,0.,Red_list[0,-1])
    return I

# <codecell>

#DEMONSTRATE HOW A MASK IS CONSTRUCTED FROM THE GREEN IMAGE

#Load the initial green image
I=loadBinBGFile(fileList[2,0], 1)
#MAKE THE MASK
# A mask is created by thresholding the green image.
# All pixels above the value specified
# are set as 1 while those bellow are 0
mask = (I > 25) #threshold is set heuristically at 25 based on inspection;
                #threshold is used consistently for the remaining files
#the mask is refined by removing holes, small objects (20 pixels or less) and smoothed
mask = mski.remove_small_objects(mask, min_size=20)
mask = mask-mski.remove_small_objects(mask, min_size=1900)
mask = mski.opening(mask, disk(3))
mask = mski.closing(mask, disk(3))
```

```
#the mask is then labeled so that each disconencted object is set to a unique value
LabelMask=scipy.ndimage.label(mask)

# SHOW THE RESULTS
fig, axes = plt.subplots(ncols=2, figsize=(10, 5), sharex=True, sharey=True, subplot_kw={'ad-
justable':'box-forced'})
axes[0].imshow(I, cmap=plt.cm.gray)
axes[0].set_title('Image')

axes[1].imshow(mask, cmap=plt.cm.gray)
axes[1].set_title('mask')

for ax in axes:
    ax.axis('off')
plt.show()

# <codecell>

#DEMONSTRATION OF HOW THE MASK IS USED TO PROCESS A RED IMAGE

#load the red image that corresponds to the mask
I2=loadBinBGFile(fileList[0,1], 0)
#make an array with the proper length to hold the average intensity of each object
results=np.zeros(LabelMask[1])


t0, t1 = (0,0)
maxDim=len(I2[0])-1
#for each object in the mask
for j in range(1,LabelMask[1]):
    currentObject=(LabelMask[0]==j) #get the pixels that correspond to that object
    currentObjectPoints=np.nonzero(currentObject) #get a list of the pixel coordinates
    #get a list of the pixel intensities for all of the pixels in that object
    currentObjectPointsAdjusted=(np.clip(currentObjectPoints[0]+t0,0,maxDim),np.clip(curren-
tObjectPoints[1]+t1,0,maxDim))
    results[j]=np.mean(I2[currentObjectPointsAdjusted]) #average those pixel intensities and
add to the array

results #show the array for the sample image

# <codecell>

#REPEAT THE ABOVE DEMONSTRATION FOR EACH FILE IN THE LIST
for i in range(len(fileList[:,0])):
    #LOAD THE INITIAL GREEN IMAGE AND VISUALLY SHOW HOW THE MASK WILL BE MADE
    I=loadBinBGFile(fileList[i,0], 1)
    #MAKE THE MASK
    #A mask is created by thresholding the image, all pixels above the value specified
    # are set as 1 while those bellow are 0
    mask = (I > 25)
    mask = mski.remove_small_objects(mask, min_size=20)
    mask = mask-mski.remove_small_objects(mask, min_size=1900)
    mask = mski.opening(mask, disk(3))
    mask = mski.closing(mask, disk(3))
    LabelMask=scipy.ndimage.label(mask)

    I2=loadBinBGFile(fileList[i,1], 0)
    #make an array with the proper length to hold the average intensity of each object
    results=np.zeros(LabelMask[1])

    t0, t1 = (0,0)
    maxDim=len(I2[0])-1
    #for each object in the mask
    for j in range(1,LabelMask[1]):
        currentObject=(LabelMask[0]==j)
        currentObjectPoints=np.nonzero(currentObject)
        currentObjectPointsAdjusted=(np.clip(currentObjectPoints[0]+t0,0,maxDim),np.clip(cur-
rentObjectPoints[1]+t1,0,maxDim))
        results[j]=np.mean(I2[currentObjectPointsAdjusted])
```

```
    fileList[i,2]=np.mean(results)
    print(fileList[i,1], fileList[i,2])


# <codecell>

#save the array of averages to a text file with comma separated values
np.savetxt("160424_DZ_summary.csv", fileList, fmt="%s", delimiter=",")

# 160427 Green particles OSD Reaction LOD calculation - Figure 2- 3
# -*- coding: utf-8 -*-
# <nbformat>3.0</nbformat>

# <codecell>

#import packages to find the filenames and format the list
import numpy as np
import glob
#get a list of tiff files with red (F3), green (F2), and blue (F1) fluorescence data
fileListR=glob.glob('./160427_Multiplex_GreenC*/*F3*')
fileListG=glob.glob('./160427_Multiplex_GreenC*/*F2*')
fileListB=glob.glob('./160427_Multiplex_GreenC*/*F1*')
#format the list and add columns of zeros to be replaced with average intensity value
fileList=np.array([fileListR,fileListG,fileListB,np.zeros(len(fileListR)),np.ze-
ros(len(fileListR)),np.zeros(len(fileListR))])
fileList=np.transpose(fileList)
[fileList[0,:]]

# <codecell>

#PRELIMINARY LOADING OF ALL OF THE DEPENDENCIES
import skimage.io as ski
import scipy
import matplotlib.pyplot as plt
from skimage import morphology as mski
from skimage.morphology import disk
import glob
%matplotlib inline

#MAKE A FUNCTION TO BIN AND BACKGROUND SUBTRACT THE IMAGE
def AVG_pixel(Im): #function bins an image by summing every 2x2 pixel block
    row,col = np.shape(Im)
    x = np.floor((row-50)/2) #note that we cut off the bottom 50 pixels to remove time/date
stamp
    y = np.floor(col/2)
    new_Image = np.zeros([int(x),int(y)],dtype=float)

    for i in range(1,int(x)):
        for j in range(1,int(y)):
            new_Image[i-1,j-1] = float(Im[2*i-1,2*j-1])+float(Im[2*i-2, 2*j-2])+float(Im[2*i-
1,2*j-2])+float(Im[2*i-2,2*j-1])
    return new_Image

#Read and bin an image
def loadBinBGFile(fileName, color):
    I=ski.imread(fileName)      #read in a file
    I = AVG_pixel(I[:,:,color]) #bin the file using the above function
    A = np.size(I)
    Red_list = np.reshape(I,[1,A])
    #The channel intensities are sorted in an acending list
    Red_list = np.sort(Red_list)
    #The minimum background is removed from the image by taking the first 10% value
    min_back_red = Red_list[0,np.floor(0.1*A)]
    I = I-min_back_red
    I = np.clip(I,0.,Red_list[0,-1])
    return I

#this function processes a mask by removing holes, small
#objects (50 pixels or less) and smoothing the edges
def processMask(mask):
    mask = mski.remove_small_objects(mask, min_size=50)
```

```
    mask = mski.opening(mask, disk(3))
    mask = mski.closing(mask, disk(3))
    mask = mski.dilation(mask,disk(3))
    return mask

#This function takes an image and a labeled mask (created later with scipy.ndimage.label)
#it resurns a list of the average intensity of each object in the mask
def measureRedObjectsFromMask(I2, LabelMask):
    results=np.zeros(LabelMask[1])
    maxDim=len(I2[0])-1
    for j in range(1,LabelMask[1]):
        currentObject=(LabelMask[0]==j)
        currentObjectPoints=np.nonzero(currentObject)
        currentObjectPointsAdjusted=(np.clip(currentObjectPoints[0],0,maxDim),np.clip(curren-
tObjectPoints[1],0,maxDim))
        results[j]=np.mean(I2[currentObjectPointsAdjusted])
    return results

# <codecell>

#LOAD THE INITIAL GREEN IMAGE AND VISUALLY SHOW HOW THE MASK WILL BE MADE
IB=loadBinBGFile(fileList[0,2], 2)
IG=loadBinBGFile(fileList[0,1], 1)
IR=loadBinBGFile(fileList[0,0], 0)
#MAKE THE MASK
#A mask is created by thresholding the image, all pixels above the value specified
# are set as 1 while those bellow are 0
gthresh=40
bthresh=150
mask = np.logical_or((IG > gthresh),(IB > bthresh))
tealmask= processMask(np.logical_and((IG > gthresh),(IB > bthresh)))
greenmask = processMask(mask-(IB > bthresh))
bluemask =  processMask(mask-(IG > gthresh))

#SHOW THE RESULTS
fig, axes = plt.subplots(ncols=5, figsize=(20, 10), sharex=True, sharey=True, subplot_kw={'ad-
justable':'box-forced'})
axes[0].imshow(IB, cmap=plt.cm.gray)
axes[0].set_title('BImage')

axes[1].imshow(IG, cmap=plt.cm.gray)
axes[1].set_title('Gimage')

axes[2].imshow(tealmask, cmap=plt.cm.gray)
axes[2].set_title('Tmask')

axes[3].imshow(greenmask, cmap=plt.cm.gray)
axes[3].set_title('Gmask')

axes[4].imshow(bluemask, cmap=plt.cm.gray)
axes[4].set_title('Bmask')

for ax in axes:
    ax.axis('off')
plt.show()

# <codecell>

#DEMONSTRATE THE PROCESSING OF A SINGLE IMAGE (fileList[1])
for i in range(1): #set file 1
    # LOAD THE INITIAL GREEN IMAGE AND VISUALLY SHOW HOW THE MASK WILL BE MADE
    IB=loadBinBGFile(fileList[i,2], 2)
    IG=loadBinBGFile(fileList[i,1], 1)
    # MAKE THE MASK
    # A mask is created by thresholding the image,
    # all pixels above the value specified
    # are set as 1 while those bellow are 0
    gthresh=40   #thresholds are set heuristically based on inspection;
    bthresh=150  #thresholds are used consistently for the remaining files
    mask = np.logical_or((IG > gthresh),(IB > bthresh))
    tealmask= np.logical_and((IG > gthresh),(IB > bthresh))
```

```
    greenmask = mask-(IB > bthresh)
    bluemask =  mask-(IG > gthresh)
    tealmask=scipy.ndimage.label(processMask(tealmask))
    greenmask=scipy.ndimage.label(processMask(greenmask))
    bluemask=scipy.ndimage.label(processMask(bluemask))

    I2=loadBinBGFile(fileList[i,0], 0)
    fileList[i,3]=np.average(measureRedObjectsFromMask(I2,tealmask))
    fileList[i,4]=np.average(measureRedObjectsFromMask(I2,greenmask))
    fileList[i,5]=np.average(measureRedObjectsFromMask(I2,bluemask))
    print(fileList[i,:])

# <codecell>

#PROCESS ALL IAMGES (fileList[all])
for i in range(len(fileList[:,0])):
    #LOAD THE INITIAL GREEN IMAGE AND VISUALLY SHOW HOW THE MASK WILL BE MADE
    IB=loadBinBGFile(fileList[i,2], 2)
    IG=loadBinBGFile(fileList[i,1], 1)
    #MAKE THE MASK
    #A mask is created by thresholding the image, all pixels above the value specified
    # are set as 1 while those bellow are 0
    gthresh=40
    bthresh=150
    mask = np.logical_or((IG > gthresh),(IB > bthresh))
    tealmask= np.logical_and((IG > gthresh),(IB > bthresh))
    greenmask = mask-(IB > bthresh)
    bluemask =  mask-(IG > gthresh)
    tealmask=scipy.ndimage.label(processMask(tealmask))
    greenmask=scipy.ndimage.label(processMask(greenmask))
    bluemask=scipy.ndimage.label(processMask(bluemask))

    I2=loadBinBGFile(fileList[i,0], 0)
    fileList[i,3]=np.percentile(measureRedObjectsFromMask(I2,tealmask),80)
    fileList[i,4]=np.percentile(measureRedObjectsFromMask(I2,greenmask),80)
    fileList[i,5]=np.percentile(measureRedObjectsFromMask(I2,bluemask),80)
    print(fileList[i,:])

# <codecell>

np.savetxt("160427_green_LOD_top50.csv", fileList, fmt="%s", delimiter=",")

#Begin 160426 Multiplex OSD reaction, scatter plot and orthogonality - Fig5
# -*- coding: utf-8 -*-
# <nbformat>3.0</nbformat>

# <codecell>

#import packages to find the filenames and format the list
import numpy as np
import glob
#get a list of tiff files with green fluorescence data
fileListR=glob.glob('./160426_Multiplex*/*F3*')
fileListG=glob.glob('./160426_Multiplex*/*F2*')
fileListB=glob.glob('./160426_Multiplex*/*F1*')
#get a list of tiff files with green fluorescence data
fileList=np.array([fileListR,fileListG,fileListB,np.zeros(len(fileListR)),np.ze-
ros(len(fileListR)),np.zeros(len(fileListR))])
fileList=np.transpose(fileList)
[fileList[0,:]]

# <codecell>

#PRELIMINARY LOADING OF ALL OF THE DEPENDENCIES
import skimage.io as ski
import scipy
import matplotlib.pyplot as plt
from skimage import morphology as mski
from skimage.morphology import disk
import glob
%matplotlib inline
```

```
#MAKE A FUNCTION TO LOAD, BIN, BACKGROUND SUBTRACT THE IMAGE
def AVG_pixel(Im):
    row,col = np.shape(Im)
    x = np.floor((row-50)/2) #note that we cut off the bottom 50 pixels to remove time/date
stamp
    y = np.floor(col/2)
    new_Image = np.zeros([int(x),int(y)],dtype=float)

    for i in range(1,int(x)):
        for j in range(1,int(y)):
            new_Image[i-1,j-1] = float(Im[2*i-1,2*j-1])+float(Im[2*i-2, 2*j-2])+float(Im[2*i-
1,2*j-2])+float(Im[2*i-2,2*j-1])
    return new_Image

def loadBinBGFile(fileName, color):
    I=ski.imread(fileName)
    I = AVG_pixel(I[:,:,color])
    A = np.size(I)
    Red_list = np.reshape(I,[1,A])
    #The channel intensities are sorted in an acending list
    Red_list = np.sort(Red_list)
    #The minimum background is removed from the image by taking the first 10% value
    min_back_red = Red_list[0,np.floor(0.1*A)]
    I = I-min_back_red
    I = np.clip(I,0.,Red_list[0,-1])
    return I

def processMask(mask):
    mask = mski.remove_small_objects(mask, min_size=50)
    mask = mask-mski.remove_small_objects(mask, min_size=1900)
    mask = mski.opening(mask, disk(3))
    mask = mski.closing(mask, disk(3))
    mask = mski.dilation(mask,disk(3))
    return mask

def measureRedObjectsFromMask(I2, LabelMask):
    results=np.zeros(LabelMask[1])
    maxDim=len(I2[0])-1
    for j in range(1,LabelMask[1]):
        currentObject=(LabelMask[0]==j)
        currentObjectPoints=np.nonzero(currentObject)
        currentObjectPointsAdjusted=(np.clip(currentObjectPoints[0],0,maxDim),np.clip(curren-
tObjectPoints[1],0,maxDim))
        results[j]=np.mean(I2[currentObjectPointsAdjusted])
    return results


#DEMONSTRATE HOW A MASK IS CONSTRUCTED FROM THE BLUE, GREEN AND TEAL
IB=loadBinBGFile(fileList[0,2], 2)
IG=loadBinBGFile(fileList[0,1], 1)
#MAKE THE MASK
#A mask is created by thresholding the image, all pixels above the value specified
#are set as 1 while those bellow are 0
#thresholds are set heuristically based on inspection;
#thresholds are used consistently for the remaining files
gthresh=40
bthresh=150
mask = np.logical_or((IG > gthresh),(IB > bthresh))
tealmask= processMask(np.logical_and((IG > gthresh),(IB > bthresh)))
greenmask = processMask(mask-(IB > bthresh))
bluemask =  processMask(mask-(IG > gthresh))

#SHOW THE RESULTS
fig, axes = plt.subplots(ncols=5, figsize=(20, 10), sharex=True, sharey=True, subplot_kw={'ad-
justable':'box-forced'})
axes[0].imshow(IB, cmap=plt.cm.gray)
axes[0].set_title('BImage')

axes[1].imshow(IG, cmap=plt.cm.gray)
axes[1].set_title('Gimage')
```

```
axes[2].imshow(tealmask, cmap=plt.cm.gray)
axes[2].set_title('Tmask')

axes[3].imshow(greenmask, cmap=plt.cm.gray)
axes[3].set_title('Gmask')

axes[4].imshow(bluemask, cmap=plt.cm.gray)
axes[4].set_title('Bmask')

for ax in axes:
    ax.axis('off')
plt.show()


#PROCESS THE MASKS IDENTIFIED ABOVE AND
labeltealmask=scipy.ndimage.label(tealmask)
labelgreenmask=scipy.ndimage.label(greenmask)
labelbluemask=scipy.ndimage.label(bluemask)
results=np.zeros([labelbluemask[1]+labelgreenmask[1]+labeltealmask[1],2])

#For each object in the complete list, make an entry in the list of the results
#with the blue and green average intensity for that object to set up the scatterplot.
i=0
maxDim=len(IB[0])-1
for j in range(1,labelbluemask[1]):
    currentObject=(labelbluemask[0]==j)
    currentObjectPoints=np.nonzero(currentObject)
    currentObjectPointsAdjusted=(np.clip(currentObjectPoints[0],0,maxDim),np.clip(curren-
tObjectPoints[1],0,maxDim))
    results[i,0]=np.mean(IG[currentObjectPointsAdjusted])
    results[i,1]=np.mean(IB[currentObjectPointsAdjusted])
    i=i+1
for j in range(1,labelgreenmask[1]):
    currentObject=(labelgreenmask[0]==j)
    currentObjectPoints=np.nonzero(currentObject)
    currentObjectPointsAdjusted=(np.clip(currentObjectPoints[0],0,maxDim),np.clip(curren-
tObjectPoints[1],0,maxDim))
    results[i,0]=np.mean(IG[currentObjectPointsAdjusted])
    results[i,1]=np.mean(IB[currentObjectPointsAdjusted])
    i=i+1
for j in range(1,labeltealmask[1]):
    currentObject=(labeltealmask[0]==j)
    currentObjectPoints=np.nonzero(currentObject)
    currentObjectPointsAdjusted=(np.clip(currentObjectPoints[0],0,maxDim),np.clip(curren-
tObjectPoints[1],0,maxDim))
    results[i,0]=np.mean(IG[currentObjectPointsAdjusted])
    results[i,1]=np.mean(IB[currentObjectPointsAdjusted])
    i=i+1

plt.figure(num=None, figsize=(12, 7), dpi=80, facecolor='w', edgecolor='k')
plt.scatter(results[:,0],results[:,1])


for i in range(len(fileList[:,0])):
    #LOAD THE INITIAL GREEN IMAGE AND VISUALLY SHOW HOW THE MASK WILL BE MADE
    IB=loadBinBGFile(fileList[i,2], 2)
    IG=loadBinBGFile(fileList[i,1], 1)
    #MAKE THE MASK
    #A mask is created by thresholding the image, all pixels above the value specified
    # are set as 1 while those bellow are 0
    gthresh=40
    bthresh=150
    mask = np.logical_or((IG > gthresh),(IB > bthresh))
    tealmask= np.logical_and((IG > gthresh),(IB > bthresh))
    greenmask = mask-(IB > bthresh)
    bluemask =  mask-(IG > gthresh)
    tealmask=scipy.ndimage.label(processMask(tealmask))
    greenmask=scipy.ndimage.label(processMask(greenmask))
    bluemask=scipy.ndimage.label(processMask(bluemask))
```

```
    I2=loadBinBGFile(fileList[i,0], 0)
    fileList[i,3]=np.average(measureRedObjectsFromMask(I2,tealmask))
    fileList[i,4]=np.average(measureRedObjectsFromMask(I2,greenmask))
    fileList[i,5]=np.average(measureRedObjectsFromMask(I2,bluemask))
    print(fileList[i,:])


np.savetxt("160426_multiplex_redo.csv", fileList, fmt="%s", delimiter=",")
```

References

(1) Zhang, D. Y.; Turberfield, A. J.; Yurke, B.; Winfree, E. Engineering Entropy-Driven Reactions and Networks Catalyzed by DNA. *Science* **2007**, *318* (5853), 1121–1125.

APPENDIX B: CHAPTER 3 SUPPORTING INFORMATION

Purification of Single-Stranded DNA by Co-Polymerization with Acrylamide and Electrophoresis

Published in: "Damase, T. R.; Ellington, A. D.; Allen, P. B. Purification of Single-Stranded DNA by Co-Polymerization with Acrylamide and Electrophoresis. BioTechniques 2017, 62 (6), 275–282."

Table B- S1: List of DNA Sequences Used

Name	Description	Sequence
Test template	Test template for demonstrating PCR (75nt)	CACGAATTAC ATGTTGCTCT TACCATACCT TTATATAGAC AATTCTCTGA ATATCCCCAC AAGGAACACGCAAAT
Test Template Primer 1	5′-Fluorescein modified 20nt	5′Fluorescein-ATTTGCGTGTTCCTTGTGGG
Test Template Primer 2	5′-Fluorescein modified 23nt	5′Acrydite-CACGAATTACATGTTGCTCTTAC
Cy5 modified Primer 2	5′-acrydite modified & internal Cy-5 modified 23nt	5′Acrydite-internal Cy5-CACGAATTACATGTTGCTCTTAC
Quench Probe	18nt 3′-modified	CACAAGGAACACGCAAAT-3′Iowa Black Quencher
Aptamer	Clone 1 anti-lysozyme aptamer (80nt)	GGGAATGGAT CCACATCTAC GAATTCATCA GGGCTAAAGA GTGCAGAGTT ACTTAGTTCA CTGCAGACTT GACGAAGCTT
F-Aptamer	Clone 1 anti-lysozyme aptamer-F (80nt)	5′Fluorescein- GGGAATGGAT CCACATCTAC GAATTCATCA GGGCTAAAGA GTGCAGAGTT ACTTAGTTCA CTGCAGACTT GACGAAGCTT
Clone 1 Primer 1	23nt 5′-Fluorescein modified primer for clone 1	5′Fluorescein-AAATACGGGAATGGATCCACATC
AC-clone-1-P_2	23nt 5′-acrydite modified primer for clone 1	5′Acrydite-ATAAGCTTCGTCAAGTCTGCAGT
Clone 1 Biotinylated Primer 2	23nt 5′-biotin modified clone 1 primer	5′biotin-ATAAGCTTCGTCAAGTCTGCAGT
F-DNA*	19nt 3′-FAM modified DNA	GTCTCTGTGCCGCTATAAT-/FAM/
AC-DNA	19nt 5′-acrydite modified DNA	/5Acryd /ATTATAGCGGCACAGAGAC
AC-DNA-F	19nt 5′-acrydite and 3′-FAM modified DNA	/5Acryd /ATTATAGCGGCACAGAGAC/36-FAM/

APPENDIX C: CHAPTER 4 SUPPORTING INFORMATION

Application of the Open qPCR Instrument for the *in Vitro* Selection of DNA Aptamers against Epidermal Growth Factor Receptor and *Drosophila* C Virus

Published in: "Damase, T. R.; Miura, T. A.; Parent, C. E.; Allen, P. B. Application of the Open QPCR Instrument for the in Vitro Selection of DNA Aptamers against Epidermal Growth Factor Receptor and Drosophila C Virus. ACS Comb. Sci. 2018, 20 (2), 45–54."

Table C- S1: Name of sequences

Name	Sequence
N30 pool	CTT ACC TCT TTC TCC CAC CGC [N30] CGC ACA ACA CAC AAC AAT CAA TAT C
P1	CTT ACC TCT TTC TCC CAC CGC
P1-f	5′ Fluorescein CTT ACC TCT TTC TCC CAC CGC
P2-acryd	5′ Acrydite GAT ATT GAT TGT TGT GTG TTG TGC G
CS1-P1	ACACTGACGACATGGTTCTACA CTTACCTCTTTCTCCCACCGC
CS2-P2	TACGGTAGCAGAGACTTGGTCT GATATTGATTGTTGTGTGTTGTGCG
P2-F	5′ Fluorescein GATATTGATTGTTGTGTGTTGTGCG
DCVKM1	CTTACCTCTTTCTCCCACCGC TTACCTTCAATTTGCTCCGTTCTTTATCGC ACAACACACAACAATCAATA
DCVKM2	CTTACCTCTTTCTCCCACCGC ATCCACGTTCTTTATCGCACTGTTCCCTCG ACAACACACAACAATCAATA
DCVKM3	CTTACCTCTTTCTCCCACCGC CCATTCCTTTTTCTACGCCTTCCATTACGC ACAACACACAACAATCAATA
DCVKM4	CTTACCTCTTTCTCCCACCGC CCGATATTCACTTTTACGCTTCCATTACGC ACAACACACAACAATCAATA
NS-DNA	CGACATCT TT AACCTAGC CCTTGTCA GTGCTCTA TGACAAGG TGTGTAGA CGACATCT AACCTAGC
MUT	CTTACCTCTTTCTCCCACCGC AATTGCCTCACTGGTCTAGTTCTCTCTGGA ACAACACACAACAATCAATA
FINNI1	TTTATTTTTGATTTTTTATATTTATCGCAC CGCACAACCCACACCAATCAATATC
FINNI2	ACAATAGATCTAACTTTATATTTATCGCAC CGCACAACACACAACAATCAATATC
FINNI3	TAAACAGCTTTAATTTTATATTTATCGCAC CGCACAACACACAACAATCAATATC
FINNI4	TTATGCTGTAATACTTTATATTTATCGCAC CGCACAACACACAACAATCAATATC
FINNI5	TGTAGAATACACAGTTTATATTTATCGCAC CGCACAACACACAACAATCAATATC
LINN1	CCGCTTTATTGTTAATTAAGTTTTATATTT CGCACAACACACAACAATCAATATC
LINN2	CCGCTTTATTGTTAATTAAGTTTTATATTT CGCACAACACACAACAATCAATATC
LINN3	CCGCTTTATTGTTAATTAAGTTTTATATTT CGCACAACACACAACAATCAATATC
LINN4	TGAATCTTTATTGTTAATTAACATTTATGG CGCACAACACACAACAATCAATATC

Details on background subtraction to generate binding curve of aptamer-DCVKM3 and DCV interaction

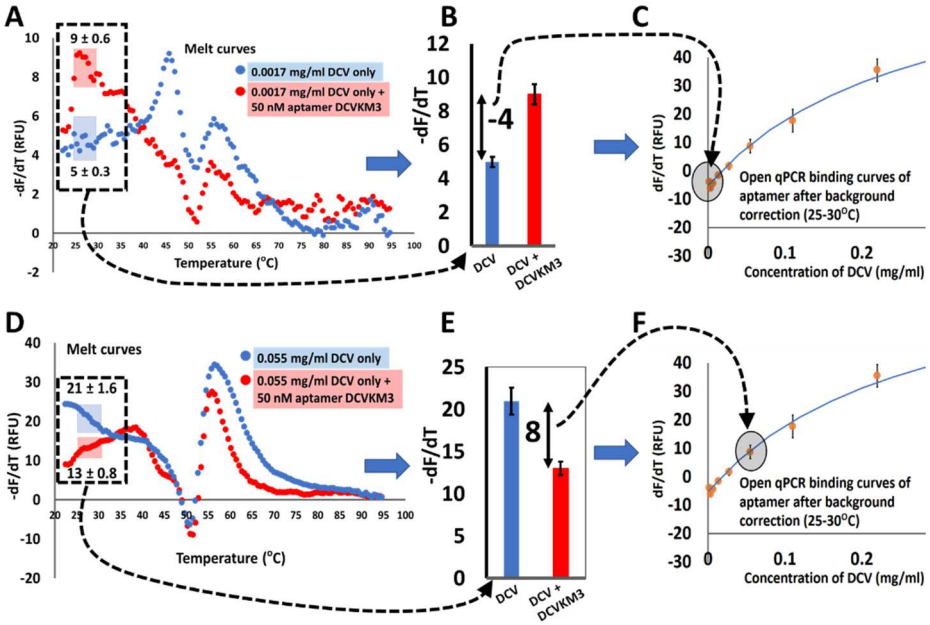

Figure C- S 1: Schematic shows details of background subtraction to generate binding curve of aptamer-DCVKM3 and DCV interaction. (A) Change in fluorescence (-dF/dT) as a function of temperature (°C) graph shows the difference in the thermofluorimetric profiles of background (DCV, 0.0017 mg/ml, blue) and signal (binding interaction of aptamer-DCVKM3, 50 nM, and DCV, 0.0017 mg/ml, red). (B) Bar graph shows -dF/dT data of background (DCV, 0.0017 mg/ml, blue) and -dF/dT data of signal (binding interaction of 0.0017 mg/ml DCV and 50 nM aptamer DCVKM3, red) averaged from 25 °C to 30 °C. (C) Binding curve of aptamer and DCV interaction after background correction. The blue line is the best fit binding isotherm used to determine dissociation constant (K_d) between DCVKM3 and DCV. Arrow indicates that the difference of -4 from the bar graph is plotted at 0.0017 mg/ml. (D) Change in fluorescence (-dF/dT) as a function of temperature (°C) graph shows the difference in the thermofluorimetric profiles of background (DCV, 0.055 mg/ml, blue) and signal (binding interaction of aptamer-DCVKM3, 50 nM, and DCV, 0.055 mg/ml, red). (E) Bar graph shows -dF/dT data of background (DCV, 0.055 mg/ml, blue) and -dF/dT data of signal (binding interaction of 0.055 mg/ml DCV and 50 nM aptamer DCVKM3, red) averaged from 25 °C to 30 °C. (F) Binding curve of aptamer and DCV interaction after background correction. The blue line is the best fit binding isotherm used to determine dissociation constant (K_d) between DCVKM3 and DCV. Arrow indicates that the difference of 8 from the bar graph is plotted at 0.055 mg/ml.

Supplemental Figures

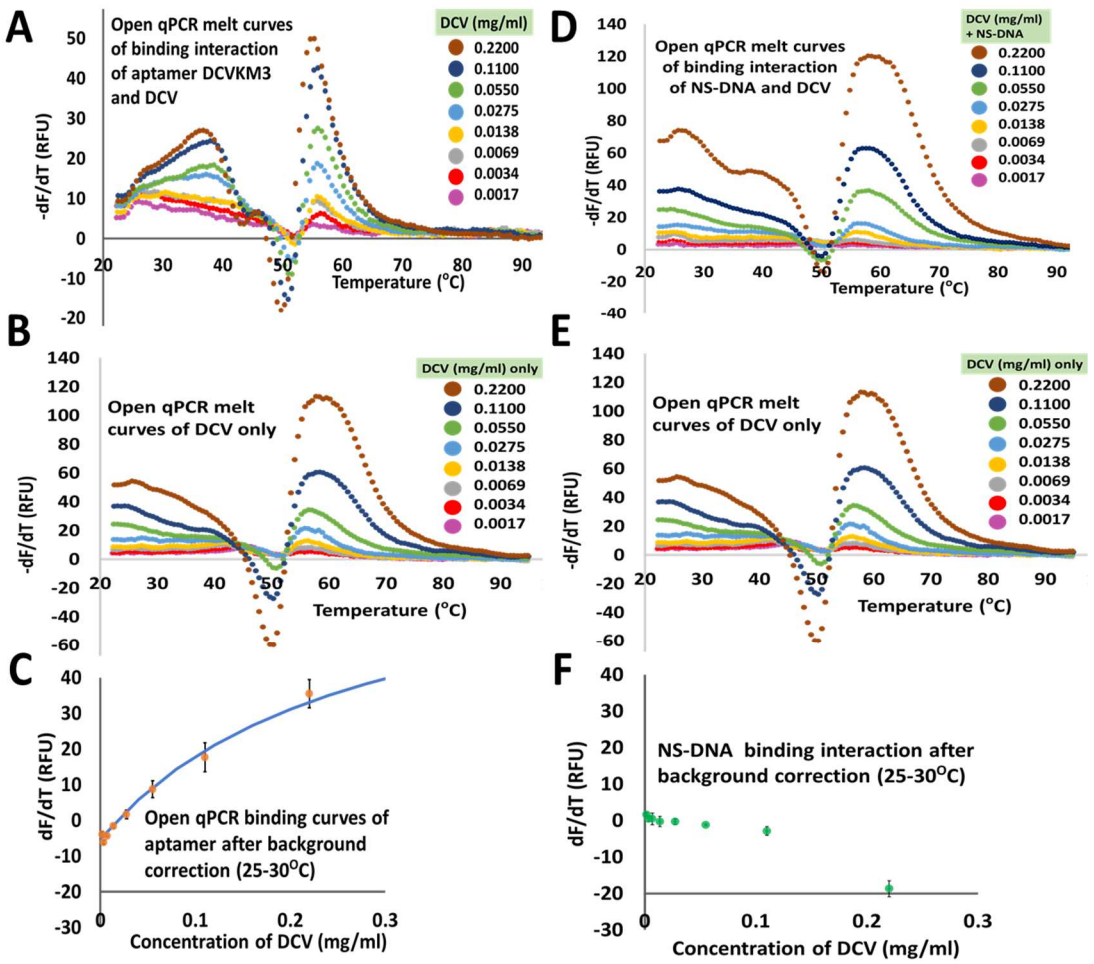

Figure C- S 2: Schematic shows generation of binding curve of aptamer DCVKM3 and non-specific DNA, NS-DNA from melting curve analysis. (A) Thermofluorimetric analysis (TFA) melt curves of binding interaction of aptamer and target DCV using Open qPCR. (B) TFA melt curves of target DCV only. (C) Open qPCR binding curves of aptamer DCVKM3 at 25-30ºC after background correction (A minus B). (D) TFA melt curves of non-specific DNA, NS-DNA, and target DCV. (E) TFA melt curves of target DCV only. (F) NS-DNA binding interaction obtained after background correction at 25-30ºC (D minus E).

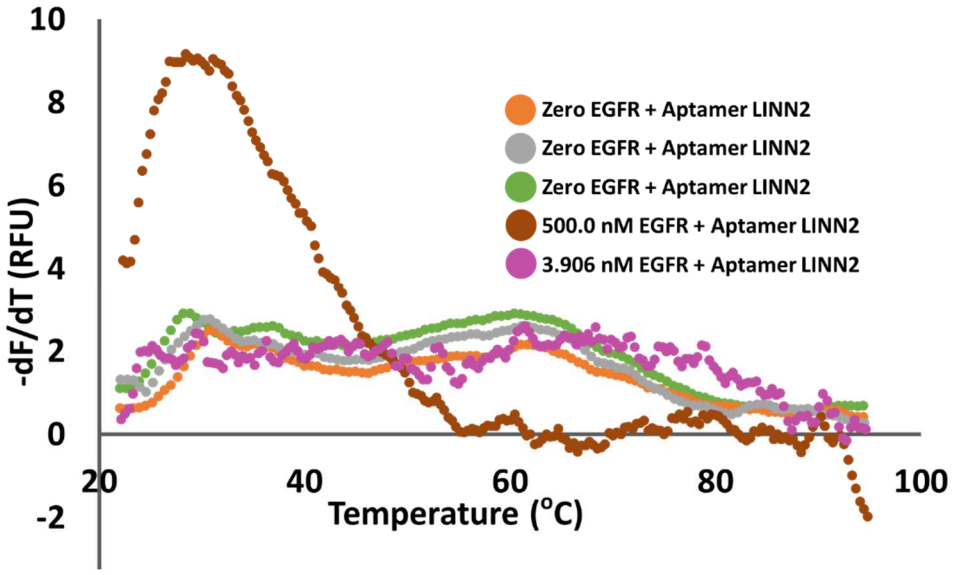

Figure C- S 3: Change in fluorescence (-dF/dT) as a function of temperature (°C) graph shows the difference in the thermofluorimetric profiles of aptamer, LINN2 interaction at high EGFR concentration (500.0 nM, brown), low EGFR concentration (3.906 nM, purple) and zero EGFR concentration (orange, gray and green).

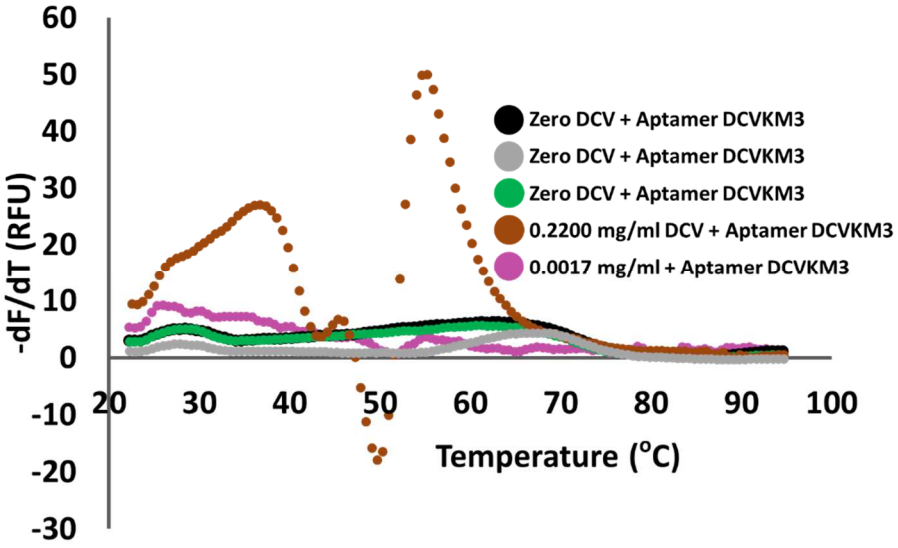

Figure C- S 4: Change in fluorescence (-dF/dT) as a function of temperature (°C) graph shows the difference in the thermofluorimetric profiles of aptamer, DCVKM3 interaction at high DCV concentration (0.2200 mg/ml, brown), low DCV concentration (0.0017 mg/ml, purple) and zero DCV concentration (black, gray and green).

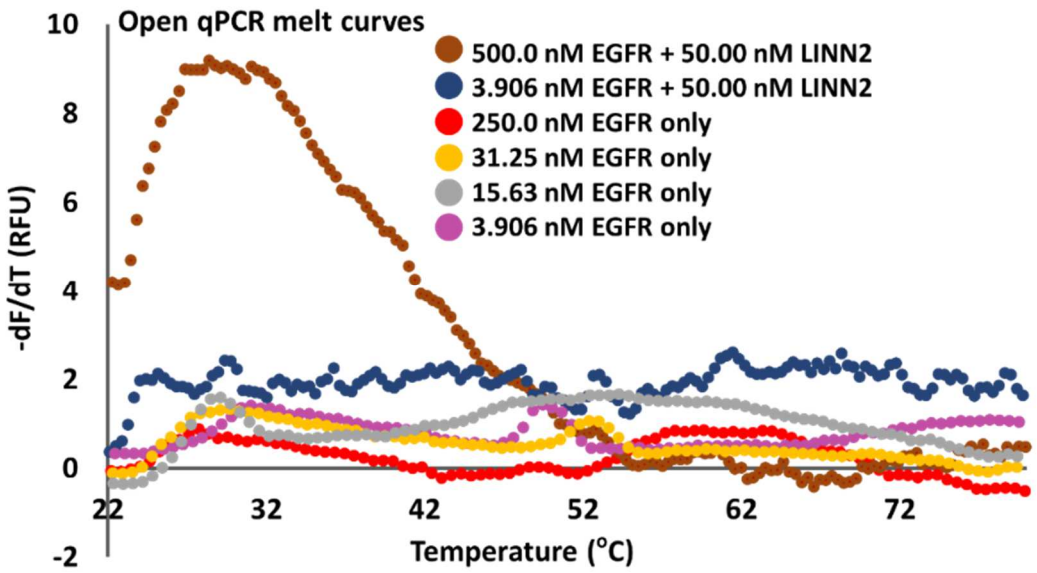

Figure C- S 5: Change in fluorescence (-dF/dT) as a function of temperature (°C) graph shows the difference in the thermofluorimetric profiles of (a) background (EGFR at various concentrations) and (b) signals (interaction of aptamer, LINN2 at high EGFR and low EGFR concentration).

Triplicate Binding Assay by Thermofluorimetric Analysis (anti-EGFR Aptamer)

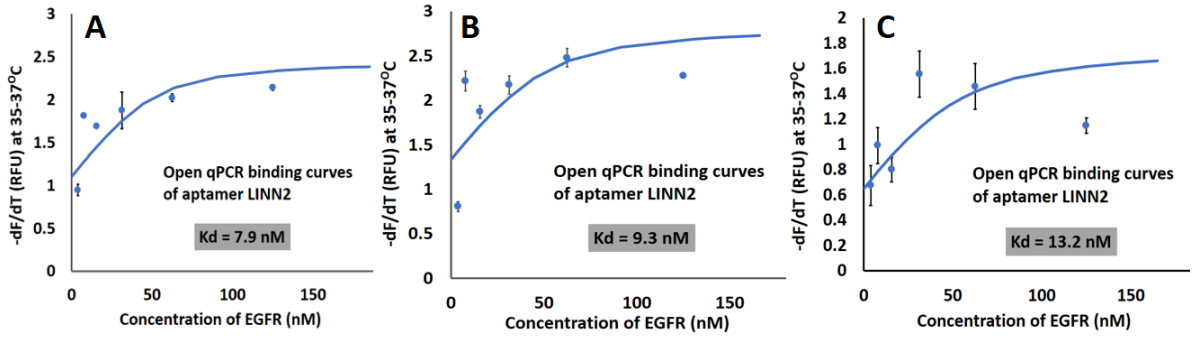

Figure C- S 6: Graph shows triplicate of dF/dT data as a function of EGFR concentration. The blue line is the best fit binding isotherm used to determine dissociation constant (K_d) between LINN2 and EGFR.

Triplicate Binding Assay by Thermofluorimetric Analysis (anti-DCV Aptamer)

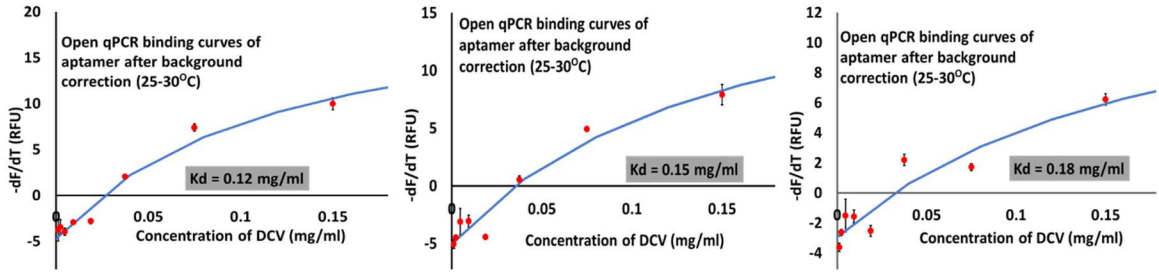

Figure C- S 7: Graph shows triplicate of background-subtracted dF/dT data as a function of DCV concentration for DCVKM3 (red dots). The blue line is the best fit binding isotherm used to determine dissociation constant (K_d) between DCVKM3 and DCV.

k-mer Analysis of anti-DCV aptamer candidate's identification

```
#Python Source Code
#Written in Anaconda, Python 2.7, iPython notebook

from Bio import SeqIO
import re
import numpy as np

#Change to directory containing FASTQ file
cd "C:\Users\Peter Allen\Documents\2016files\aptamer\virus_aptamer_seq"
#open data file and parse it into a list of records
handle = open("Aptamers_R1.fastq", "rU")
records = list(SeqIO.parse(handle, "fasta"))
handle.close()
#define a function that compares two sequences for simple sequence homology
#and a second function that compares a sequence looking for reverse complement
def reduceToVector(inputString, letter):
    outputvector=np.zeros(len(inputString))
    for i in range(0,len(inputString)):
        if (inputString[i] == letter):
            outputvector[i]=1
        else:
            outputvector[i]=0
    return outputvector

def computeComplement(seq1, seq2):
    seq2 = seq2[-1:-1*(len(seq2)+1):-1] #reverse seq2
    complementA = np.correlate(reduceToVector(seq1, "A"),reduceToVector(seq2, "T"), "full")
    complementT = np.correlate(reduceToVector(seq1, "T"),reduceToVector(seq2, "A"), "full")
    complementG = np.correlate(reduceToVector(seq1, "G"),reduceToVector(seq2, "C"), "full")
    complementC = np.correlate(reduceToVector(seq1, "C"),reduceToVector(seq2, "G"), "full")
    return max(complementA+complementT+complementG+complementC)

def computeOverlap(seq1, seq2):
    complementA = np.correlate(reduceToVector(seq1, "A"),reduceToVector(seq2, "A"), "full")
    complementT = np.correlate(reduceToVector(seq1, "T"),reduceToVector(seq2, "T"), "full")
    complementG = np.correlate(reduceToVector(seq1, "G"),reduceToVector(seq2, "G"), "full")
    complementC = np.correlate(reduceToVector(seq1, "C"),reduceToVector(seq2, "C"), "full")
    return max(complementA+complementT+complementG+complementC)

#demonstrate computeOverlap function
print(computeOverlap("ACACAACAATCAATATTA", "ACAACACACAACAATCACTATCAGACCAAGTCAC"))#should be 16



#Make a list of all likely aptamer candidates. This looks for data in the FASTA
#file that have the prefix "DCV1_Round". We gave that name as the label for the
#barcoded primer we used. Illumina precedes our data with this text to
#differentiate it from other samples that were sequenced in the same run.
#The data is then filtered for quality.

index=0
aptamerSeqCandidates=[]
for record in records:
    sequence = str(record.seq) #for each record in the file
    for m in re.finditer('DCV1_Round_8', sequence): #look for text every time it appears
        #NO PRIMERS in random region of the sequence (to filter out primer dimers)
        if                                                                  computeOverlap(se-
quence[(m.start()+47):(m.start()+80)],"ACAACACACAACAATCAATAT")<=11:
            #primer2 sequence after random regions is required
            if                                                                  computeOverlap(se-
quence[(m.start()+68):(m.start()+110)],"ACAACACACAACAATCAATAT")>=17:
                #if conditions are met, add the candidate sequence to the list of candidates
                aptamerSeqCandidates.append(sequence[(m.start()+47):(m.start()+80)])
                if len(aptamerSeqCandidates) <=10:
                    print index, m.start(), sequence[(m.start()+47):(m.start()+100)]
    index=index+1
```

```
print len(aptamerSeqCandidates)
print len(list(set(aptamerSeqCandidates)))

#define a function to list all possible sub-sequences of length k (k-mers)

def listAllKmers(k,sequenceList):
    outputList=[]
    for sequence in sequenceList:
        for i in range(len(sequence)-k+1):
            outputList.append(sequence[i:i+k])
    return outputList
#build a list of all unique k-mers in the aptamerSeqCandidates list
uniqueKmers = list(set(listAllKmers(12,aptamerSeqCandidates)))

#set up to count occurrences of each list
remaining=len(uniqueCandidateList)
index=0

#take each unique k-mer sequence...
for candidateKmer in uniqueKmers:
    count=0
    for aptamerSeq in aptamerSeqCandidates:             #...compare to each candidate aptamer
        count = count + aptamerSeq.count(candidateKmer) #count times it shows up
    if count>=3:                                       #if kmer appears (3+) times in the data
        print count, candidateKmer                      #print the sequence
    if index==10000:                                    #show progress
        print remaining
        index=0
    index=index+1
    remaining = remaining-1

#based on the output of k-mers appearing frequently, process further
#Take a k-mer printed above (e.g. "CTTCCATTACGC") and view all of its occurrences in the data

index=0
for record in records:
    sequence = str(record.seq)
    for m in re.finditer('CTTCCATTACGC', sequence): #look for  seq
        #print "entry: ", index
        #print "found: ", m.start()
        print index, m.start(), sequence[(m.start()-60):(m.start()+50)]
       #print the whole candidate with primer binding sites
    index=index+1


#DCV most common kmer appears 6 times in round 8: GTTCTTTATCGC
#DCVKM1 CTTACCTCTTTCTCCCACCGC TTACCTTCAATTTGCTCCGTTCTTTATCGC ACAACACACAACAATCAATA
#DCVKM2 CTTACCTCTTTCTCCCACCGC ATCCACGTTCTTTATCGCACTGTTCCCTCG ACAACACACAACAATCAATA
#DCV second candidate appears 3 in R8, 1 in R6: CTTCCATTACGC
#DCVKM3 CTTACCTCTTTCTCCCACCGC CCATTCCTTTTTCTACGCCTTCCATTACGC ACAACACACAACAATCAATA
#DCVKM4 CTTACCTCTTTCTCCCACCGC CCGATATTCACTTTTACGCTTCCATTACGC ACAACACACAACAATCAATA.
```

APPENDIX D: CHAPTER 5 SUPPORTING INFORMATION

Idiosyncrasies of Thermofluorimetric Aptamer Binding Assays

Forthcoming in: Biotechniques

Table D- S1: Name of Sequences

Name	Sequence
N30 pool	CTTACCTCTTTCTCCCACCGC [N30] CGCACAACACACAACAATCAATATC
P1	CTTACCTCTTTCTCCCACCGC
P1-F	5′ Fluorescein CTTACCTCTTTCTCCCACCGC
P2-acryd	5′ Acrydite GATATTGATTGTTGTGTGTTGTGCG
CS1-P1	ACACTGACGACATGGTTCTACACTTACCTCTTTCTCCCACCGC
CS2-P2	TACGGTAGCAGAGACTTGGTCTGATATTGATTGTTGTGTGTTGTGCG
P2-F	5′ Fluorescein GATATTGATTGTTGTGTGTTGTGCG
KM1-am	/5AmMC6/CTTACCTCTTTCTCCCACCGCGAATCACCTGGCTTCTAGTGGCCCGCACAACGCACA ACACACAACAATCAATATC
KM2-am	/5AmMC6/CTTACCTCTTTCTCCCACCGCGTCTGACGGCTACCTGCTCGGCCCGCACAACGCACA ACANACAACAATCAATATC
KM3-am	/5AmMC6/CTTACCTCTTTCTCCCACCGCCCTACTTTTTGCCCGCAACACAACGCACACCGCACA ACACACAACAATCAAT
KM4-am	/5AmMC6/CTTACCTCTTTCTCCCACCGCCCCAAACATAATTGGTATACCGCAACACAACGCACA ACACACAACAATCAAT
NS-DNA	CGACATCT TT AACCTAGC CCTTGTCA GTGCTCTA TGACAAGG TGTGTAGA CGACATCT AACCTAGC
MUT-DNA	CTTACCTCTTTCTCCCACCGCAATTGCCTCACTGGTCTAGTTCTCTCTGGAACAACACACAACAA TCAATA
LINN2	CCGCTTTATTGTTAATTAAGTTTTATATTT CGCACAACACACAACAATCAATATC

Selection of DNA aptamers to recognize target EGFR cells:

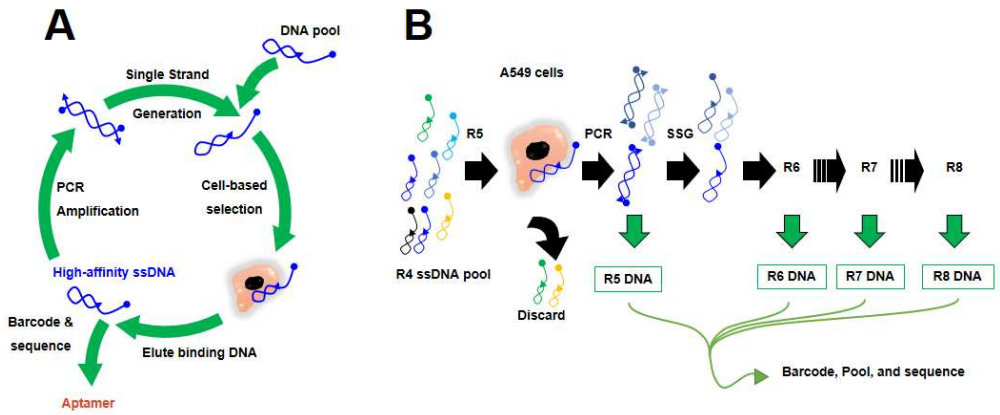

Figure D- S 1: Schematic of Cell-SELEX. If this hybrid SELEX method, round four of a conventional selection against EGFR is used as the input for four rounds of cell SELEX.

We generated a new DNA aptamer against EGFR on the cell surface. Previously, after four rounds of selection against recombinant EGFR from E. coli, we characterized our pool with deep sequencing, screened and characterized the best candidate, LINN2 [1]. LINN2 bound recombinant EGFR but displayed no measurable affinity to the native protein on the surface of mammalian cells (as measured by microscopy and flow cytometry). This serves to highlight the need to select aptamers against a target that is identical to the in vivo target (e.g., glycosylation patterns). To find an aptamer that binds to cell-surface EGFR, we performed cell-SELEX.

Starting at round 5, the further selection was carried out against fixed, EGFR-positive A549 cells. The selection proceeded as above with fixed cells in the place of magnetic particles. This might be considered "hybrid SELEX" [2–4](four rounds of conventional SELEX and four rounds of cell-SELEX). After round eight of selection, the pool was submitted for sequencing. The results were processed by *k*-mer analysis [1,5]and four aptamer candidates (the highest abundance sequences) were synthesized and denoted aptamer candidates KM1, KM2, KM3, and KM4.

Materials and Methods: Aptamer Selection

Pool preparation: A single-stranded DNA N30 pool (30 mer randomized sequence flanked by two primer-binding sites) initially was purchased as a gel-purified oligonucleotide from IDT (Integrated DNA Technologies, Coralville, IA, USA) and was used as received. The pool from round four, R4 done initially was used in this project for Cell-SELEX as the pool. The primers used in the selection (P1, P1-F, P2-F, and P2-acryd) were also synthesized by IDT. See Table D- S1 for sequence information.

Positive Microsphere Preparation using clear microsphere: EGFR, Human Protein, Recombinant (hIgG1-Fc Tag, Active, Sino Biological Life Technologies, CA, USA) was diluted in 50 µl of Protein buffer. The protein buffer is a 1:4 mixture of 5X Py buffer (pH 6.8, 250 mM Na2HPO4, 250 mM NaCl, both from EMD Chemicals, Gibbstown, Germany) and 1X phosphate buffer (pH 8, 50 mM Na2HPO4, 50 mM NaH2PO4, both from EMD Chemicals, Gibbstown, Germany). The resulting concentration of EGFR was 1 µM. Incubation of 50 µl of pre-washed and activated clear microspheres (Carboxylated Polymer Particles, PS- COOH, 2.36 µm, Bangs Laboratories Inc., IN, USA) was carried out with 50 µl of EGFR solution (1 µM) for 2 hours at room temperature by vortexing, followed by washing in selection buffer (1X phosphate buffer, pH 8, 50 mM Na2HPO4, 50 mM NaH2PO4, both from EMD Chemicals, Gibbstown, Germany). The microspheres were resuspended in 50 µl of selection buffer. The microspheres thus prepared were denoted as "positive microspheres."

Positive Microsphere Preparation using magnetic microsphere: The positive microspheres were made similarly (see *Positive Microsphere Preparation using clear microsphere)* with magnetic microspheres (ProMag TM Magnetic Microspheres, 1 HC. COOH, solids 2.53% 0.78 µm, Bangs Laboratories Inc., IN, USA).

Negative Microsphere Preparation using magnetic microsphere: IgG1Fc-coated magnetic microspheres were prepared similarly (see *Positive Microsphere Preparation using clear microsphere)* using magnetic microspheres and IgG1-FC Recombinant Human Protein (Sino Biological Life Technologies, CA, USA) instead of EGFR.

SELEX procedure: Approximately 10-50 pmol (1012 molecules) of DNA pool was annealed in 45 µl of selection buffer. Ten µl of A549 cells (was originally obtained from Dr. Samir Iqbal, University of Texas at Arlington, Texas, USA) were then added to the annealed pool and incubated for 30 minutes by rotating at room temperature. The sample was centrifuged at 12K for 10 minutes in Biofuge fresco, Sorvall (Hyland Scientific, WA, USA) at RT. Unbound DNA was then removed, and fresh buffer was added to the tube. Washing was done four times in the selection buffer. Cells were then resuspended in water, and bound aptamers were eluted after heat treatment (90 °C) for five minutes. The number of PCR cycles required for amplification was then optimized in Open qPCR, and the eluted DNA was amplified by PCR. Single-strand generation [6] was carried out in 5% denaturing 7M urea-PAGE gel. The gel was cast in a horizontal gel rig. The round five (R5) ssDNA pool was generated by extracting a sample from gel followed by ethanol precipitation. Approximately 10-50 pmol of R5 ssDNA pool was used as a pool for the sixth round. Using the same methodology, the selection was carried out up to eight rounds.

Illumina sequencing: The eluted DNA of each round (rounds 5, 6, 7 and 8) was amplified first with CS1-P1 and CS2-P2 and then with barcoded primers. The amplified product was finally purified by 4% non-denaturing PAGE gel and submitted to the Institute for Bioinformatics and Evolutionary Studies sequencing core facility at the University of Idaho for MiSeq sequencing (MiSeq, Illumina, San Diego, CA, USA).

Screening of selected aptamers for EGFR cells:

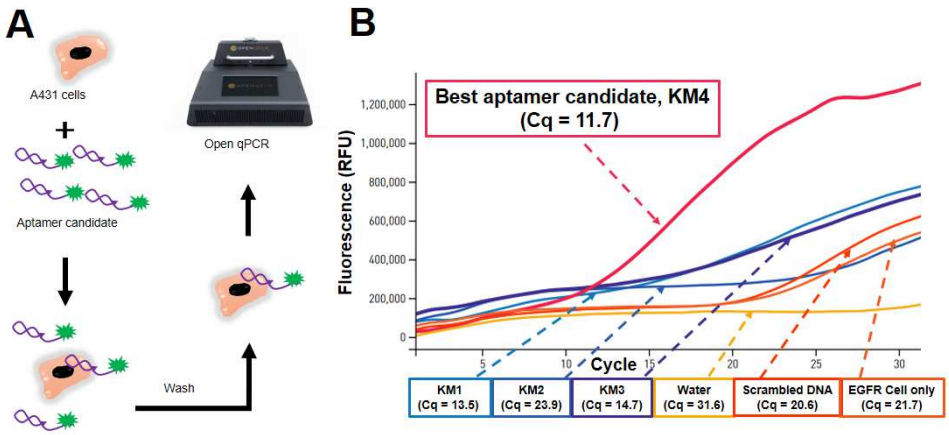

Figure D- S 2: Screening of aptamer candidates. Cells were exposed to the aptamer candidates, washed, and the result was added to a qPCR master mix and analyzed in the Open qPCR. (A) Schematic shows experimental steps of Open qPCR analysis of aptamer candidate binding to A431 cells. (B) Open qPCR amplification curves show fluorescence as a function of PCR cycle count. The results indicate aptamer candidate KM4 binds to cells and is the best aptamer candidate (Cq=11.7).

Materials and Methods: Screening of selected aptamers for EGFR cells

Cell qPCR: Affinity testing was carried out with four possible aptamer candidates (KM1 through KM4) obtained by *k*-mer analysis. The A439 cells (ATCC, VA, USA) were incubated with each aptamer candidate separately for 30 minutes at RT. This process was followed by washing, resuspending in selection buffer and then screened on Beckman Coulter CytoFLEX S and Open qPCR, 95°C-15secs, 64°C-15secs, 69°C-30secs; (CHAI Bio, CA, USA).

Specificity test of aptamer KM4:

To identify the specificity of LINN2, we incubated the KM4 aptamer with positive microspheres (EGFR coated magnetic microspheres) and negative microsphere (Fc-coated magnetic microspheres)

and observed in the fluorescence microscope. The KM4 aptamer incubated with EGFR coated microspheres showed strong fluorescence while the Fc-coated showed significantly less fluorescence as shown in Figure D- S3. We reported from this that our KM4 aptamer is specific.

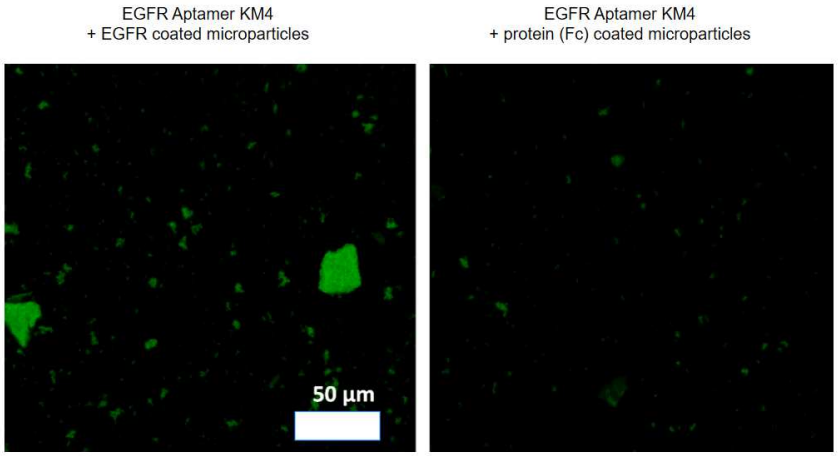

Figure D- S 3: Specificity test of aptamer KM4. Fluorescence micrographs show a specificity test of aptamer KM4 with EGFR coated (left) and Fc-coated (right) microparticles.

Materials and Methods: Specificity test of aptamer KM4

Fluorescence microscopy of KM4 and microparticles: To test aptamer specificity, EGFR coated magnetic microspheres were blocked in superblock for 1 h. The blocked microspheres were washed one time in selection buffer. Two microliters of 35µM of KM4 aptamer candidate (annealed fast in selection buffer) was incubated at room temperature for 30 minutes with 1µL blocked EGFR coated magnetic microspheres plus 8 µL of selection buffer. The incubation was followed by washing, resuspending in 50 µL selection buffer and then observed on the fluorescent microscope (LumaScope 620, EtaLuma, Carlsbad, CA) in the green channel (λex 490 nm). Similarly, incubation of KM4 aptamer with blocked IgG1Fc-coated magnetic microspheres was carried out.

Flow cytometry binding assay for aptamer KM4

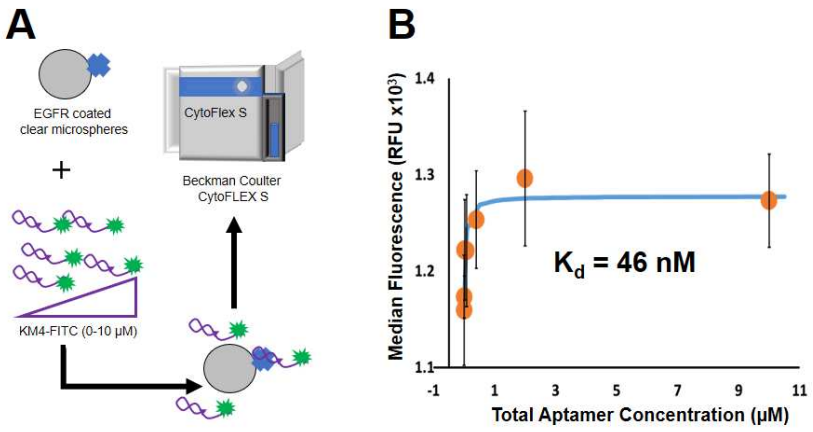

Figure D- S 4: Flow cytometry binding assay for aptamer KM4 to recombinant EGFR. (A) Schematic illustrations of Flow cytometric analysis to report aptamer and target binding. We performed flow cytometric analysis [1,7–10] using EGFR coated clear microspheres to generate a binding curve. (B) Binding curve of RFU vs. total aptamer concentration to calculate K_d. Error bars are standard deviations of triplicate. We take the signal to be proportionate to the quantity of bound aptamer. Despite the high background, we obtained a median fluorescence increase and plateau as a function of aptamer concentration. We fit the curve using nonlinear regression analysis and calculate K_d as 46 nM.

Materials and Methods: Flow cytometry binding assay for aptamer KM4

Flow cytometry binding assay: KM4-am, an amine modified aptamer, was conjugated with FITC (Sigma-Aldrich, MO, USA) to yield KM4-FITC (10 µM, analyzed by Quick drop, Molecular Devices, CA, USA). KM4-FITC (50 µl) was added to the first PCR tube, and then 5-fold serial dilution was carried out across eight tubes in the selection buffer. Five µl of blocked positive microspheres (EGFR-coated clear microspheres) were added to each tube and incubated for 30 minutes. Two µl incubated sample was taken in a vial, and 400 µl selection buffer was added. Particles were finally vortexed to perform flow cytometric analysis using a Beckman Coulter CytoFLEX S.

Secondary structure of aptamers predicted from NUPACK:

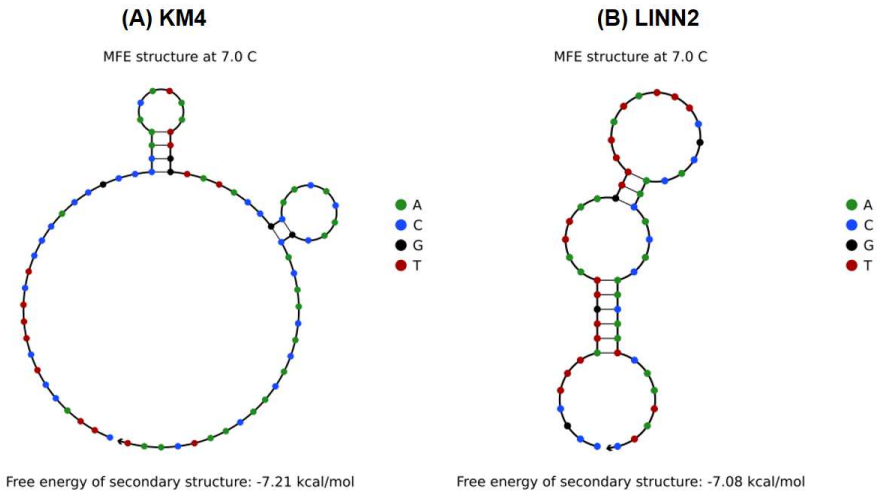

Figure D- S 5: Secondary structure of aptamers predicted from NUPACK [11]. (A) KM4. (B) LINN2.

Comparison of simulation with experimental KM4 melt curve data:

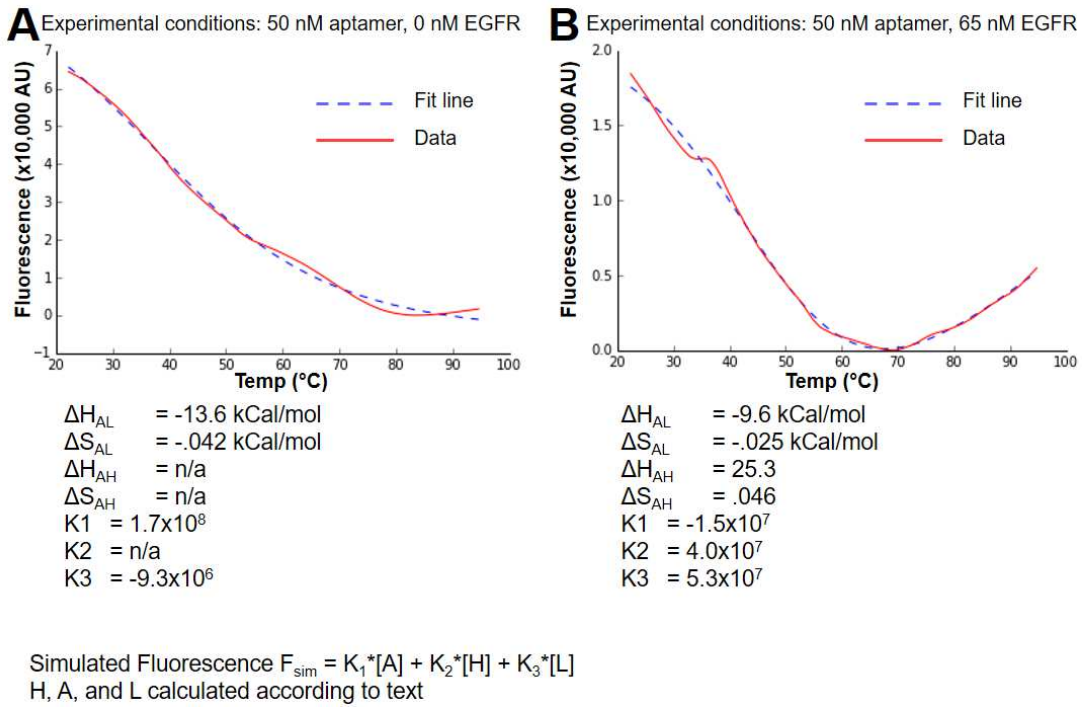

Figure D- S 6: Comparison of simulation with experimental KM4 melt curve data. (A) Fluorescence data as a function of temperature (solid line), fit line from model (dashed line) and extracted parameters with 50 nM aptamer and 0 nM EGFR. (B) Fluorescence data as a function of temperature (solid line), fit line from model (dashed line) and extracted parameters with 50 nM aptamer and 65 nM EGFR.

Python 2.7.14 code to simulate TFA

```
# Source code for Figure 5- 3 and Figure D- S6

#initialize
import numpy as np
import matplotlib.pyplot as plt
import matplotlib.image as mpimg
import math
import sympy
%matplotlib inline

# Demonstrate sympy.solve for getting algebraic solutions to equilibria problems

#A/L=K
#A+L=1

#single equilibrium case, solve for concentrations of A and L given Atot and K

A=sympy.Symbol('A')
L=sympy.Symbol('L')
K=sympy.Symbol('K')
Atot=sympy.Symbol('Atot')
sympy.solve([sympy.Eq(A/L, K), sympy.Eq(A+L, Atot)], [A, L])


#A/L=Kal
#A+L+H=Atot
#A*T/H=Kah
#H+T=Ttot

#solve for the concentration of H, A, L and T

A=sympy.Symbol('A')
L=sympy.Symbol('L')
H=sympy.Symbol('H')
T=sympy.Symbol('T')
Kal=sympy.Symbol('Kal')
Kah=sympy.Symbol('Kah')
Ttot=sympy.Symbol('Ttot')
Atot=sympy.Symbol('Atot')
sympy.solve([sympy.Eq(A/L,     Kal),     sympy.Eq(A+L+H,     Atot),     sympy.Eq((A*T)/H,Kah),
sympy.Eq(T+H,Ttot)], [H,A,L,T])


# Single equilibrium between Apo (folded) and linear (denatured); plot the concentration of Apo
as a function of Temp


T = np.arange(280,360,5)
dH = -16.2
dS = -.0551
dG = dH - T*dS
K=np.exp(-1*(dH - T*dS)/(T* 0.00198588))
Atot=1e-6
A=Atot*K/(K + 1) #consistent with solution from sympy.solve() above


plt.plot(T,A) #plot apo concentration as a function of temperature


# Make a function that returns Holo and Apo concentration, given Atot, Ttot, Kah, Kal

#A/L=Kal
#A+L+H=Atot
#A*T/H=Kah
#H+T=Ttot

def speciationFromThreeStateEquil(Atot, Ttot, Kah, Kal):
#A=sympy.Symbol('A')
```

```
#L=sympy.Symbol('L')
#H=sympy.Symbol('H')
#T=sympy.Symbol('T')
#speciation=sympy.solve([sympy.Eq(A/L, Kal), sympy.Eq(A+L+H, Atot), sympy.Eq((A*T)/H,Kah),
sympy.Eq(T+H,Ttot)], [H,A,L,T], quick=True)
#to speed up execution, use the analytical solution from sympy.solve() above instead of calling
it every iteration
speciation=[(Atot*Kal + Kah*Kal + Kah + Kal*Ttot - np.sqrt(Atot**2*Kal**2 + 2*Atot*Kah*Kal**2
+ 2*Atot*Kah*Kal - 2*Atot*Kal**2*Ttot + Kah**2*Kal**2 + 2*Kah**2*Kal + Kah**2 +
2*Kah*Kal**2*Ttot + 2*Kah*Kal*Ttot + Kal**2*Ttot**2))/(2*Kal), \
(Atot*Kal - Kah*Kal - Kah - Kal*Ttot + np.sqrt(Atot**2*Kal**2 + 2*Atot*Kah*Kal**2 +
2*Atot*Kah*Kal - 2*Atot*Kal**2*Ttot + Kah**2*Kal**2 + 2*Kah**2*Kal + Kah**2 + 2*Kah*Kal**2*Ttot
+ 2*Kah*Kal*Ttot + Kal**2*Ttot**2))/(2*(Kal + 1))\
]
return speciation #returns [Holo, Apo]



# More complex case: use the same constants for DNA melting and add target binding equilibrium
with constant Kd=1uM

T = np.arange(280,360,5)
dH = -16.2
dS = -.0551
dG = dH - T*dS
K=np.exp(-1*(dH - T*dS)/(T* 0.00198588))
Atot=1e-6
A=Atot*K/(K + 1) #consistent with solution from sympy solve

TargetConcentrations=[.1e-6, .5e-6, 1e-6, 5e-6, 10e-6, 0]
apoAtTempTarget=[]
apoHoloAtTempTarget=[]

for eachTtot in TargetConcentrations:
apoAtT=[]
apoHoloAtT=[]
for eachK in K:
speciation=speciationFromThreeStateEquil(1e-6,eachTtot,1e-6,eachK) #[apt], [target], Kd, Kapo-
linear
apoAtT.append(speciation[1])
apoHoloAtT.append(speciation[1]+speciation[0])
apoAtTempTarget.append(apoAtT)
apoHoloAtTempTarget.append(apoHoloAtT)


#plot apo concentration as a function of temperature (blue) and at increasing target concen-
tration (red)
plt.plot(T,apoAtTempTarget[0],'r-',\
T,apoAtTempTarget[1],'r-',\
T,apoAtTempTarget[2],'r-',\
T,apoAtTempTarget[3],'r-',\
T,apoAtTempTarget[4],'r-',\
T,apoAtTempTarget[5],'b-');


#plot apo+holo concentration as a function of temperature (blue) and at increasing target
concentration (red)
plt.plot(T,apoHoloAtTempTarget[0],'r-',\
T,apoHoloAtTempTarget[1],'r-',\
T,apoHoloAtTempTarget[2],'r-',\
T,apoHoloAtTempTarget[3],'r-',\
T,apoHoloAtTempTarget[4],'r-',\
T,apoHoloAtTempTarget[5],'b-');



# Semi-realistic case: use real aptamer-target binding thermodynamic constants

T = np.arange(280,360,5)
dHal = -16.2
dSal = -.0551
```

```
Kal=np.exp(-1*(dHal - T*dSal)/(T* 0.00198588))

#A.S. Potty et al Biopolymers, 91 (2009), pp. 145-156
#Kd=40.5nM  constants of ASSOCIATION  dH = -18.5 kCal/mol   TdS = -8.6 kCal/mol  dG = -10
#strong aptamer, enthalpy driven association
#input DISSOCIATION thermodynamic parameters
dHah = 18.5
dSah = 8.6/297

Kah=np.exp(-1*(dHah - T*dSah)/(T* 0.00198588))


TargetConcentrations=[.5e-6, 1e-6, 3e-6, 5e-6, 10e-6, 0]
apoAtTempTarget=[]
apoHoloAtTempTarget=[]

for eachTtot in TargetConcentrations:
apoAtT=[]
apoHoloAtT=[]
for i in range(len(T)):
speciation=speciationFromThreeStateEquil(1e-6,eachTtot,Kah[i],Kal[i])
apoAtT.append(speciation[1])
apoHoloAtT.append(speciation[1]+speciation[0])
apoAtTempTarget.append(apoAtT)
apoHoloAtTempTarget.append(apoHoloAtT)

#plot apo concentration as a function of temperature (blue) and at increasing target concen-
tration (red)
plt.plot(T,apoAtTempTarget[0],'r-',\
T,apoAtTempTarget[1],'r-',\
T,apoAtTempTarget[2],'r-',\
T,apoAtTempTarget[3],'r-',\
T,apoAtTempTarget[4],'r-',\
T,apoAtTempTarget[5],'b-');

#plot apo+holo concentration as a function of temperature (blue) and at increasing target
concentration (red)
plt.plot(T,apoHoloAtTempTarget[0],'r-',\
T,apoHoloAtTempTarget[1],'r-',\
T,apoHoloAtTempTarget[2],'r-',\
T,apoHoloAtTempTarget[3],'r-',\
T,apoHoloAtTempTarget[4],'r-',\
T,apoHoloAtTempTarget[5],'b-');


# Make up thermodynamics for an aptamer where the association melts at an accessible temperature


T = np.arange(280,360,5)
#input thermodynamic parameters Linear --> Folded
dHal = -16.2
dSal = -.05
Kal=np.exp(-1*(dHal - T*dSal)/(T* 0.00198588))

#made up weak aptamer, enthalpy driven association
#chose based on a Tm close to the Tm of aptamer denaturation
#input DISSOCIATION thermodynamic parameters Holo --> Apo
dHah = 64.4
dSah = .165
Kah=np.exp(-1*(dHah - T*dSah)/(T* 0.00198588))


TargetConcentrations=[.5e-6, .7e-6, 1e-6, 3e-6, 10e-6, 0]
apoAtTempTarget=[]
apoHoloAtTempTarget=[]

for eachTtot in TargetConcentrations:
apoAtT=[]
apoHoloAtT=[]
for i in range(len(T)):
speciation=speciationFromThreeStateEquil(1e-6,eachTtot,Kah[i],Kal[i])
```

```
apoAtT.append(speciation[1])
apoHoloAtT.append(speciation[1]+speciation[0])
apoAtTempTarget.append(apoAtT)
apoHoloAtTempTarget.append(apoHoloAtT)


#plot apo concentration as a function of temperature (blue) and at increasing target concen-
tration (red)
plt.plot(T,apoAtTempTarget[0],'r-',\
T,apoAtTempTarget[1],'r-',\
T,apoAtTempTarget[2],'r-',\
T,apoAtTempTarget[3],'r-',\
T,apoAtTempTarget[4],'r-',\
T,apoAtTempTarget[5],'b-');


#plot apo+holo concentration as a function of temperature (blue) and at increasing target
concentration (red)
plt.plot(T,apoHoloAtTempTarget[0],'r-',\
T,apoHoloAtTempTarget[1],'r-',\
T,apoHoloAtTempTarget[2],'r-',\
T,apoHoloAtTempTarget[3],'r-',\
T,apoHoloAtTempTarget[4],'r-',\
T,apoHoloAtTempTarget[5],'b-');


# Now we fit a curve to real data

#read in the real data
import csv
from scipy.optimize import curve_fit

#cd 'C:\Users\Peter Allen\Documents\IPython Notebooks\CELL-SELEX'

import csv
temp=[]
fluorescence=[]

#with open('qpcr_experiment_20180614_TFA KM4 vs 0 EGFR only.txt.csv', 'rb') as csvfile:
#    csvreader = csv.reader(csvfile)
#    for row in csvreader:
#        temp.append(float(row[0]))
#        fluorescence.append(float(row[1]))

fluorescence=[64439.396,  63949.137,  63459.05,  62968.448,  62368.645,  61741.667,  61046.608,
60350.141,  59646.205,  58912.217,  58170.152,  57445.704,  56658.999,  55855.416,  55014.297,
54138.168,  53249.85,  52318.061,  51324.966,  50312.721,  49269.268,  48177.397,  47129.436,
46099.569,  45063.179,  44001.541,  42915.495,  41802.663,  40611.417,  39427.003,  38310.088,
37246.393,  36192.586,  35220.715,  34302.414,  33388.177,  32529.246,  31691.99,  30888.912,
30070.309,  29254.186,  28476.539,  27707.428,  26931.284,  26178.166,  25432.648,  24637.633,
23827.26,  23031.202,  22193.344,  21449.051,  20795.941,  20263.05,  19770.661,  19383.735,
18974.348,  18606.665,  18218.795,  17833.603,  17443.939,  17050.466,  16619.48,  16157.565,
15696.499,  15253.727,  14782.633,  14305.439,  13821.444,  13316.908,  12757.529,  12207.092,
11630.435, 11064.708, 10454.928, 9852.044, 9249.444, 8627.563, 8011.862, 7411.528, 6819.851,
6242.033,  5672.19,  5067.491,  4527.038,  4016.712,  3528.964,  3054.276,  2620.873,  2227.588,
1841.854, 1492.374, 1200.981, 953.65, 723.871, 553.576, 386.415, 248.918, 170.62, 79.26, 19.149,
9.577, 32.195, 36.381, 91.052, 138.229, 211.126, 284.557, 361.467, 458.386, 589.641, 710.169,
811.916, 946.344, 1071.33, 1191.186, 1302.731, 1441.228, 1576.401, 1698.752]
temp=[22.195, 22.809, 23.423, 24.037, 24.651, 25.264, 25.878, 26.492, 27.106, 27.72, 28.334,
28.948, 29.562, 30.175, 30.789, 31.403, 32.017, 32.631, 33.245, 33.859, 34.473, 35.087, 35.7,
36.314, 36.928, 37.542, 38.156, 38.77, 39.384, 39.998, 40.612, 41.225, 41.839, 42.453, 43.067,
43.681, 44.295, 44.909, 45.523, 46.136, 46.75, 47.364, 47.978, 48.592, 49.206, 49.82, 50.434,
51.048, 51.661, 52.275, 52.889, 53.503, 54.117, 54.731, 55.345, 55.959, 56.572, 57.186, 57.8,
58.414, 59.028, 59.642, 60.256, 60.87, 61.484, 62.097, 62.711, 63.325, 63.939, 64.553, 65.167,
65.781, 66.395, 67.009, 67.622, 68.236, 68.85, 69.464, 70.078, 70.692, 71.306, 71.92, 72.533,
73.147, 73.761, 74.375, 74.989, 75.603, 76.217, 76.831, 77.445, 78.058, 78.672, 79.286, 79.9,
80.514, 81.128, 81.742, 82.356, 82.969, 83.583, 84.197, 84.811, 85.425, 86.039, 86.653, 87.267,
87.881, 88.494, 89.108, 89.722, 90.336, 90.95, 91.564, 92.178, 92.792, 93.406, 94.019, 94.572]

FluorSmall=np.divide(fluorescence, 10000)
plt.plot(temp,FluorSmall, 'r-')
```

```
def fluorescenceSimulated(T, dHal, dSal, dHah, dSah, K1, K2, K3, Atot, Ttot):
#[dHal, dSal, dHah, dSah, K1, K2, K3, Atot, Ttot]=params
T=np.add(T,273) #convert temp to kelvin
Kal=np.exp(-1*(dHal - T*dSal)/(T* 0.00198588))
Kah=np.exp(-1*(dHah - T*dSah)/(T* 0.00198588))

fluorAtT=[]

for i in range(len(T)):
speciation=speciationFromThreeStateEquil(Atot,Ttot,Kah[i],Kal[i])
H=speciation[0]
A=speciation[1]
L=Atot-speciation[0]-speciation[1]
fluorAtT.append(A*K1 + H*K2 + L*K3)

return fluorAtT


#[dHal, dSal, dHah, dSah, K1, K2, K3]
#[  -9.64469562e+00    -2.51831235e-02     2.53131320e+01     4.55983131e-02    -1.52122735e+07
4.02030868e+07   5.34588036e+07]

def fluorSimNoTarget(T, dHal, dSal, K1, K3):
return fluorescenceSimulated(T, dHal, dSal, 18.5, 8.6/297, K1,   0, K3, 5e-8, 0)

fluorSim=fluorSimNoTarget(temp, -16.2,  -.0551, 2e8, 1e5)
plt.plot(temp,fluorSim, 'b--')


from scipy.optimize import curve_fit


popt, pcov = curve_fit(fluorSimNoTarget, temp, FluorSmall, p0=[-16.2, -.0551, 1.8e8, 1e6])
fluorSim=fluorSimNoTarget(temp, *popt)
plt.plot(temp,fluorSim,'b--',\
temp,FluorSmall,'r-',\
) ;


print '[dHal, dSal, K1, K3 ]\n', popt


# Try to fit the 64 nM EGFR curve with the above Kal parameters to get the Kah

fluorescence=[]
temp=[]

#with open('qpcr_experiment_20180614_TFA KM4 vs 62 EGFR only.txt.csv', 'rb') as csvfile:
#    csvreader = csv.reader(csvfile)
#    for row in csvreader:
#        temp.append(float(row[0]))
#        fluorescence.append(float(row[1]))

fluorescence=[18450.516,  18124.923,  17799.328,  17469.678,  17139.866,  16806.481,  16439.631,
16066.346,  15692.182,  15315.509,  14970.491,  14632.94,  14321.878,  14030.004,  13734.038,
13448.864,  13195.826,  12963.295,  12820.672,  12762.864,  12757.452,  12785.954,  12805.405,
12712.567, 12461.868, 12125.651, 11715.92, 11220.412, 10733.951, 10280.781, 9798.21, 9365.705,
8976.057,  8543.676,  8114.36,  7749.479,  7334.715,  6929.647,  6607.757,  6277.533,  5956.69,
5659.731,  5366.783,  5032.988,  4760.684,  4458.2,  4162.931,  3882.938,  3630.707,  3349.329,
3064.382,  2706.854,  2361.519,  2044.325,  1788.32,  1556.334,  1409.52,  1301.639,  1178.735,
1061.563,  998.578,  945.404,  861.789,  790.969,  730.099,  644.611,  578.628,  501.786,  439.918,
373.733,  262.761,  193.862,  155.61,  109.603,  28.639,  24.807,  7.807,  13.821,  59.134,  122.862,
214.758,  290.447,  391.498,  498.757,  632.281,  764.625,  895.828,  1009.936,  1098.396,  1176.31,
1238.812,  1307.535,  1372.552,  1451.974,  1548.394,  1644.606,  1740.917,  1862.216,  1999.613,
2124.219,  2270.908,  2443.357,  2611.523,  2748.106,  2920.655,  3092.254,  3214.438,  3358.281,
3518.25,  3648.641,  3778.574,  3948.51,  4118.834,  4312.435,  4555.674,  4804.416,  5025.713,
5271.878, 5490.537]
temp = [22.38, 22.994, 23.608, 24.222, 24.836, 25.45, 26.064, 26.678, 27.292, 27.906, 28.519,
29.133, 29.747, 30.361, 30.975, 31.589, 32.203, 32.817, 33.431, 34.045, 34.659, 35.273, 35.887,
36.501, 37.115, 37.729, 38.343, 38.957, 39.571, 40.185, 40.799, 41.413, 42.027, 42.641, 43.254,
```

```
43.868, 44.482, 45.096, 45.71, 46.324, 46.938, 47.552, 48.166, 48.78, 49.394, 50.008, 50.622,
51.236, 51.85, 52.464, 53.078, 53.692, 54.306, 54.92, 55.534, 56.148, 56.762, 57.376, 57.989,
58.603, 59.217, 59.831, 60.445, 61.059, 61.673, 62.287, 62.901, 63.515, 64.129, 64.743, 65.357,
65.971, 66.585, 67.199, 67.813, 68.427, 69.041, 69.655, 70.269, 70.883, 71.497, 72.111, 72.724,
73.338, 73.952, 74.566, 75.18, 75.794, 76.408, 77.022, 77.636, 78.25, 78.864, 79.478, 80.092,
80.706, 81.32, 81.934, 82.548, 83.162, 83.776, 84.39, 85.004, 85.618, 86.232, 86.846, 87.459,
88.073, 88.687, 89.301, 89.915, 90.529, 91.143, 91.757, 92.371, 92.985, 93.599, 94.213, 94.766]

FluorSmall=np.divide(fluorescence, 10000)
plt.plot(temp,FluorSmall,'r-')


#possible starting values
#[delta-H Apo-lin, delta-S Apo-lin,  K1, K3 ]
#[ -1.32890860e+01  -4.24777078e-02   1.70443492e+08  -9.32043684e+06]

def fluorSimWithTarget(T, dHah, dSah, K2):
#[dHal, dSal, dHah, dSah, K1, K2, K3, Atot, Ttot]=params
return fluorescenceSimulated(T, -1.3e+01, -4.2e-02, dHah, dSah, 1.7e8, K2, -9.3e6, 50e-9, 62e-
9)

fluorSim=fluorSimWithTarget(temp, 35, .13, 1e3)
plt.plot(temp,fluorSim,'b--',);


popt, pcov = curve_fit(fluorSimWithTarget, temp, FluorSmall, p0=[45.4, .165, 1e3])


fluorSim=fluorSimWithTarget(temp, *popt)
plt.plot(temp,fluorSim,'b--',\
temp,FluorSmall,'r-',\
) ;

print 'dHah, dSah, K2 \n'
print popt
[dHah, dSah, K2] = popt
T=298
Kah=np.exp(-1*(dHah - T*dSah)/(T* 0.00198588))
print Kah


# Fit All the things for the 65 nm EGFR case

fluorescence=[]
temp=[]

#with open('qpcr_experiment_20180614_TFA KM4 vs 62 EGFR only.txt.csv', 'rb') as csvfile:
#    csvreader = csv.reader(csvfile)
#    for row in csvreader:
#        temp.append(float(row[0]))
#        fluorescence.append(float(row[1]))

fluorescence=[18450.516,  18124.923,  17799.328,  17469.678,  17139.866,  16806.481,  16439.631,
16066.346,  15692.182,  15315.509,  14970.491,  14632.94,  14321.878,  14030.004,  13734.038,
13448.864,  13195.826,  12963.295,  12820.672,  12762.864,  12757.452,  12785.954,  12805.405,
12712.567, 12461.868, 12125.651, 11715.92, 11220.412, 10733.951, 10280.781, 9798.21, 9365.705,
8976.057,  8543.676,  8114.36,  7749.479,  7334.715,  6929.647,  6607.757,  6277.533,  5956.69,
5659.731,  5366.783,  5032.988,  4760.684,  4458.2,  4162.931,  3882.938,  3630.707,  3349.329,
3064.382,  2706.854,  2361.519,  2044.325,  1788.32,  1556.334,  1409.52,  1301.639,  1178.735,
1061.563,  998.578,  945.404,  861.789,  790.969,  730.099,  644.611,  578.628,  501.786,  439.918,
373.733,  262.761,  193.862,  155.61,  109.603,  28.639,  24.807,  7.807,  13.821,  59.134,  122.862,
214.758,  290.447,  391.498,  498.757,  632.281,  764.625,  895.828,  1009.936,  1098.396,  1176.31,
1238.812,  1307.535,  1372.552,  1451.974,  1548.394,  1644.606,  1740.917,  1862.216,  1999.613,
2124.219,  2270.908,  2443.357,  2611.523,  2748.106,  2920.655,  3092.254,  3214.438,  3358.281,
3518.25,  3648.641,  3778.574,  3948.51,  4118.834,  4312.435,  4555.674,  4804.416,  5025.713,
5271.878, 5490.537]
temp = [22.38, 22.994, 23.608, 24.222, 24.836, 25.45, 26.064, 26.678, 27.292, 27.906, 28.519,
29.133, 29.747, 30.361, 30.975, 31.589, 32.203, 32.817, 33.431, 34.045, 34.659, 35.273, 35.887,
36.501, 37.115, 37.729, 38.343, 38.957, 39.571, 40.185, 40.799, 41.413, 42.027, 42.641, 43.254,
43.868, 44.482, 45.096, 45.71, 46.324, 46.938, 47.552, 48.166, 48.78, 49.394, 50.008, 50.622,
51.236, 51.85, 52.464, 53.078, 53.692, 54.306, 54.92, 55.534, 56.148, 56.762, 57.376, 57.989,
```

```
58.603, 59.217, 59.831, 60.445, 61.059, 61.673, 62.287, 62.901, 63.515, 64.129, 64.743, 65.357,
65.971, 66.585, 67.199, 67.813, 68.427, 69.041, 69.655, 70.269, 70.883, 71.497, 72.111, 72.724,
73.338, 73.952, 74.566, 75.18, 75.794, 76.408, 77.022, 77.636, 78.25, 78.864, 79.478, 80.092,
80.706, 81.32, 81.934, 82.548, 83.162, 83.776, 84.39, 85.004, 85.618, 86.232, 86.846, 87.459,
88.073, 88.687, 89.301, 89.915, 90.529, 91.143, 91.757, 92.371, 92.985, 93.599, 94.213, 94.766]

FluorSmall=np.divide(fluorescence, 10000)
plt.plot(temp,FluorSmall,'r-')

def fluorSimWithTarget(T, dHal, dSal, dHah, dSah, K1, K2, K3,):
#[dHal, dSal, dHah, dSah, K1, K2, K3, Atot, Ttot]=params
return fluorescenceSimulated(T, dHal, dSal, dHah, dSah, K1, K2, K3, 5e-8, 62e-9)

fluorSim=fluorSimWithTarget(temp,  -1.32890860e+01,  -4.24777078e-02,  45.4,  .165,  1.70e+08,
9.32043684e+06, 1e3)

plt.plot(temp,fluorSim,'b--',\
) ;


popt, pcov = curve_fit(fluorSimWithTarget, temp, FluorSmall,\
p0=[-1.3e+01, -4.2e-02, 64, .165, 1.70443492e+08,  0, 1e3])

fluorSim=fluorSimWithTarget(temp, *popt)
plt.plot(temp,fluorSim,'b--',\
temp,FluorSmall,'r-',\
) ;


print '[dHal, dSal, dHah, dSah, K1, K2, K3]'
print popt
[dHal, dSal, dHah, dSah, K1, K2, K3] = popt
T=298
Kah=np.exp(-1*(dHah - T*dSah)/(T* 0.00198588))
print Kah
```

References

(1) Damase, T. R.; Miura, T. A.; Parent, C. E.; Allen, P. B. Application of the Open QPCR Instrument for the in Vitro Selection of DNA Aptamers against Epidermal Growth Factor Receptor and Drosophila C Virus. *ACS Comb. Sci.* **2018**, *20* (2), 45–54.

(2) Parekh, P.; Kamble, S.; Zhao, N.; Zeng, Z.; Portier, B. P.; Zu, Y. Immunotherapy of CD30-Expressing Lymphoma Using a Highly Stable SsDNA Aptamer. *Biomaterials* **2013**, *34* (35), 8909–8917.

(3) Hicke, B. J.; Marion, C.; Chang, Y. F.; Gould, T.; Lynott, C. K.; Parma, D.; Schmidt, P. G.; Warren, S. Tenascin-C Aptamers Are Generated Using Tumor Cells and Purified Protein. *J. Biol. Chem.* **2001**, *276* (52), 48644–48654.

(4) Sun, H.; Zhu, X.; Lu, P. Y.; Rosato, R. R.; Tan, W.; Zu, Y. Oligonucleotide Aptamers: New Tools for Targeted Cancer Therapy. *Mol Ther Nucleic Acids* **2014**, *3* (8), e182.

(5) Hoon, S.; Zhou, B.; Janda, K. D.; Brenner, S.; Scolnick, J. Aptamer Selection by High-Throughput Sequencing and Informatic Analysis. *BioTechniques* **2011**, *51* (6), 413–416.

(6) Damase, T. R.; Ellington, A. D.; Allen, P. B. Purification of Single-Stranded DNA by Co-Polymerization with Acrylamide and Electrophoresis. *BioTechniques* **2017**, *62* (6), 275–282.

(7) Wang, D.-L.; Song, Y.-L.; Zhu, Z.; Li, X.-L.; Zou, Y.; Yang, H.-T.; Wang, J.-J.; Yao, P.-S.; Pan, R.-J.; Yang, C. J.; et al. Selection of DNA Aptamers against Epidermal Growth Factor Receptor with High Affinity and Specificity. *Biochemical and Biophysical Research Communications* **2014**, *453* (4), 681–685.

(8) Shangguan, D.; Li, Y.; Tang, Z.; Cao, Z. C.; Chen, H. W.; Mallikaratchy, P.; Sefah, K.; Yang, C. J.; Tan, W. Aptamers Evolved from Live Cells as Effective Molecular Probes for Cancer Study. *PNAS* **2006**, *103* (32), 11838–11843.

(9) Zhang, P.; Zhao, N.; Zeng, Z.; Feng, Y.; Tung, C.-H.; Chang, C.-C.; Zu, Y. Using an RNA Aptamer Probe for Flow Cytometry Detection of CD30-Expressing Lymphoma Cells. *Laboratory Investigation* **2009**, *89* (12), 1423–1432.

(10) Dunaway, A. B.; Sullivan, R. S.; Siegel, K. J.; Milam, V. T. Evaluating the Dual Target Binding Capabilities of Immobilized Aptamers Using Flow Cytometry. *Biointerphases* **2015**, *10* (1), 019015.

(11) Zadeh, J. N.; Steenberg, C. D.; Bois, J. S.; Wolfe, B. R.; Pierce, M. B.; Khan, A. R.; Dirks, R. M.; Pierce, N. A. NUPACK: Analysis and Design of Nucleic Acid Systems. *Journal of Computational Chemistry* **2011**, *32* (1), 170–173.

APPENDIX E: CHAPTER 6 SUPPORTING INFORMATION

Thioflavin-T as a Fluorogenic Small Molecule Reporter for an Enzyme-Free Catalytic DNA Amplifier

Table E- S1: Sequences of all DNA

Name	**Sequences (5′ ⟶ 3′)**
GQplex	GAGGAGGAGGAGGAGAGGGTAGGGCGGGTTGGG
BeaconAnalyte	GCAAGCGACGACAACGAGGAGGAGG
TFTBeacon	TCTCCTCCTCCTCCTCGTTGTCGTCGCTTGCGAGGAGGAGGAGGAGAGGCGGGTTGGG
Part A	CGCGCTTC TAGCAACT AGAGGCGGGTTGGG
Part B	GAGGAGGAGGAGG AGTTGCTA GAAGCGCG
Spine	TCTCCTCC TCCTCCTC TTTTC TGAATAAGAAGAAGAA TCTCCA
Block	TTCTTCTTCTTATTCA GAAAA
TFTSignal	GAGGAGGA GGAGGAGA GGCGGGTTGGG
EDAAnalyte	TGGAGA TTCTTCTTCTTATTCA
Fuel	TTCTTCTTCTTATTCA GAAAA GAGGAGGA GGAGGAGA
TFTSignal 35_1235	GGTGAGGA GAGGAGGA GGAGGAGA GGCGGGTTGGG
TFTSignal 24_123	GGTGAGGA GAGGAGGA GGAGGAGA
TFTSignal 27_235	GAGGAGGA GGAGGAGA GGCGGGTTGGG
TFTSignal 16_12	GGTGAGGA GAGGAGGA
TFTSignal 19_35	GGAGGAGA GGCGGGTTGGG
TFTSignal 16_23	GAGGAGGA GGAGGAGA
TFTSignal 14_23	AGGAGGA GGAGGAG
TFTSignal 12_23	GGAGGA GGAGGA
TFTSignal 10_23	GAGGA GGAGG
TFTSignal 8_23	AGGA GGAG
ssDNA	AAAAAAAACATACGGCAATTCGGCGGAGGGAAGGAAGGGAGAGGTGGGATAATAGGCTGGAATAAAGGAGGA
dsDNA	Sequence1: TCCTCCTTTATTCCAGCCTATTATCCCACCTCTCCCTTCCTTCCCTCCGCCGAATTGCCGTATGTTTTTTT Sequence2: AAAAAAAACATACGGCAATTCGGCGGAGGGAAGGAAGGGAGAGGTGGGATAATAGGCTGGAATAAAGGAGGA

Origin of TFTSignal Sequence (domains 2-3-5)

Domains	2	3	4	5
PW17			GGTAGG	GCGGGTTGGG
GQplex	GAGGAGGA	GGAGGAGAG	GGTAGG	GCGGGTTGGG
TFTSignal	GAGGAGGA	GGAGGAGAG		GCGGGTTGGG

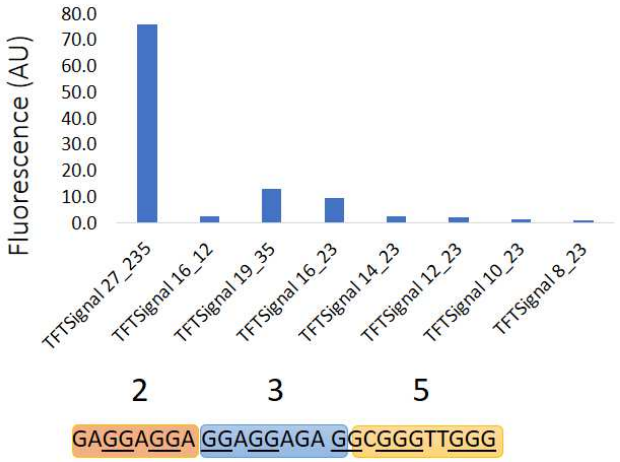

Figure E- S 1: Determinations of domains critical for thioflavin-T (TFT) fluorescence enhancement.

TFTSignal (domains 2-3-5) DNA was originally designed to be one half of a split version of PW17 (designed to become fluorescent when combined with 4-3*-2*). Surprisingly, TFTSignal (2-3-5) resulted in greater fluorescence emission in the presence of TFT than GQplex (2-3-4-5) which contained the full version of PW17 (4-5). We characterized oligonucleotides to determine which combinations of the domains were critical for this activity. The TFTSignal sequence (2-3-5) enhances TFT fluorescence more than other combinations. Removing or shortening the any domain resulted in reduced fluorescence.

The fluorescence emission of each TFTSignal oligonucleotide (500 nM) was measured in the presence of 5 µM of TFT in Tris buffer (20 mM Tris, 50 mM NaCl, 10 mM KCl, 1mM EDTA, pH7) using an excitation wavelength of 440 nm and emission wavelength 510 nm.

APPENDIX F: COPYRIGHT PERMISSION

SPRINGER NATURE

Title: Biomimetic Molecular Signaling using DNA Walkers on Microparticles
Author: Tulsi Ram Damase et al
Publication: Scientific Reports
Publisher: Springer Nature
Date: Jun 22, 2017

Title: Application of the Open qPCR Instrument for the in Vitro Selection of DNA Aptamers against Epidermal Growth Factor Receptor and Drosophila C Virus

Author: Tulsi Ram Damase, Tanya A. Miura, Christine E. Parent, et al

Publication: ACS Combinatorial Science

Publisher: American Chemical Society

Date: Feb 1, 2018

LOGIN

If you're a copyright.com user, you can login to RightsLink using your copyright.com credentials.

Already a RightsLink user or want to learn more?

PERMISSION/LICENSE IS GRANTED FOR YOUR ORDER AT NO CHARGE

This type of permission/license, instead of the standard Terms & Conditions, is sent to you because no fee is being charged for your order. Please note the following:

- Permission is granted for your request in both print and electronic formats, and translations.
- If figures and/or tables were requested, they may be adapted or used in part.
- Please print this page for your records and send a copy of it to your publisher/graduate school.
- Appropriate credit for the requested material should be given as follows: "Reprinted (adapted) with permission from (COMPLETE REFERENCE CITATION). Copyright (YEAR) American Chemical Society." Insert appropriate information in place of the capitalized words.
- One-time permission is granted only for the use specified in your request. No additional uses are granted (such as derivative works or other editions). For any other uses, please submit a new request.

BACK CLOSE WINDOW

Copyright Clearance

CHAPTER 3: PURIFICATION OF SINGLE-STRANDED DNA BY CO-POLYMERIZATION WITH ACRYLAMIDE AND ELECTROPHORESIS

Need Copyright permission for thesis

JM

Joseph Martin <j.martin@futuremedicine.com>
Thu 10/11, 8:28 AM
Damase, Tulsi (dama9796@vandals.uidaho.edu)

Inbox

Dear Tulsi,

Thank you for your email.

I can confirm that it is fine to use in your dissertation provided you acknowledge the *BioTechniques* paper (https://www.future-science.com/doi/10.2144/000114557).

If there is anything else I can help you with, please do let me know.

Kind regards,

Joseph Martin
Managing Editor - *BioTechniques*

part of future science group
+44 (0)20 8371 6090 | www.future-science.com

Future Medicine Ltd, Unitec House, 2 Albert Place, London, N3 1QB, UK (registered in England & Wales, No: 4059017); VAT No: GB 833 0029 67